THESE DE DOCTORAT DE

L'UNIVERSITE DE NANTES
COMUE UNIVERSITE BRETAGNE LOIRE

ECOLE DOCTORALE N° 596
Matière, Molécules, Matériaux
Spécialité : Constituants élémentaire et physique théorique

Par
Sophys Gabriel

Formation of Quark-Gluon-Plasma:
Understanding the energy and system size dependence

Thèse présentée et soutenue à Nantes, le 23 Octobre 2018
Unité de recherche : SUBATECH UMR6457
Thèse N° : 145257

Rapporteurs avant soutenance :

Matthew Nguyen	Chargé de Recherche titulaire d'un HDR, Laboratoire Leprince-Ringuet
Nicolas Borghini	W2 Professor, Fakultät für Physik Universität Bielefeld

Composition du Jury :

Président :	Ginés Martinez	Directeur de Recherche, SUBATECH
Examinateurs :		
	Sarah Porteboeuf-Houssais	Maitre de conférences, Laboratoire de Physique Corpusculaire de Clermont-Ferrand
	Ginés Martinez	Directeur de Recherche, SUBATECH
	Elena Bratkovskaya	Professor, Goethe University Frankfurt and GSI Darmstadt
	Matthew Nguyen	Chargé de Recherche titulaire d'un HDR, Laboratoire Leprince-Ringuet
	Nicolas Borghini	W2 Professor, Fakultät für Physik Universität Bielefeld
Dir. de thèse :	Klaus Werner	Professeur d'université, Université de Nantes

2

Formation of a Quark-Gluon-Plasma : understanding the energy and system size dependence

---

Formation du Plasma de Quark et de Gluon : compréhension de la dépendance en énergie et de la taille du système

Gabriel Sophys

SUBATECH – Nantes (France) – 2015-2018

Soutenance de Thèse : 23 Octobre 2018

CONTENTS

REMERCIEMENTS

Avant de commencer, j'aimerais remercier rapidement toutes les personnes qui m'ont accompagné lors de ma thèse. Bien sûr je commence par Klaus, un très bon directeur de thèse toujours à l'écoute et gardant toujours son sourire dans toutes les situations, que je fasse les choses bien ou non. Ensuite, je tiens à remercier les rapporteurs de mon manuscrit de thèse: Nicolas Borghini et Matthew Nguyen qui ont dû souffrir pour lire ce manuscrit mais qui ont su me guider pour corriger quelques parties écrites à la hâte. Je remercie mon jury de thèse: Gines Martinez, Elena Bratkovskaya et Sarah Porteboeuf-Houssais avec qui ma soutenance s'est très bien passée et qui m'ont posé des questions pertinentes pour la suite de mon parcours mais également quelques travaux de finalisations pour cette thèse.

Je remercie doublement Sarah pour avoir été un membre exemplaire de mon comité de suivi de thèse (ou individuel avec le changement de nom) qui m'a suivi pendant ces trois ans, me demandant si j'avais besoin d'aide et étant le plus possible à mon écoute et disponible à mes besoins. Je remercie Joerg Aichelin en tant que second membre de mon comité de suivi de thèse avec qui j'ai pu avoir de grandes discussions sur la physique et avec qui j'ai toujours eu une bonne entente. Je remercie également tous les membres du groupe Théorie de Subatech que je trouve bon vivant et de bons conseils de toute sorte.

Je remercie finalement tous les thésards que j'ai fortement côtoyé ces trois dernières années, en voici une petite liste : Martin Rohrmoser, Erwann Masson, Loic Virone, Loic Le Meur, Alexandre Subercaze, Alexandre Parent du Châtelet, Quentin Mouchard, Ophélie Bugnon, Chloe Therreau, Audrey Francisco, Benjamin Audurier, Kevin Micheneau, Dennys Arrebato Villar, Maria Stefaniak, Delorme Stéphane, Etienne Nigron, Flavien Ralite, David Hénaff, Manuel Guittière, etc .... Bien sûr je remercie le sang-méléclown David Fasou (Fuseau) qui a été un très bon partenaire avec qui on a pu faire des parties de flennis, où on a pu être défié et le meilleur des Alsaciens avec Manon Delarue. Finalement je remercie mon partenaire de bureau (si on néglige la fin où tu m'as lâchement abandonné pour les States) Docteur Florian Cougoulic, le croate avec qui j'ai partagé trop de choses pour le synthétiser ici mais que j'espère recroiser lors de certaines conférences ou autour d'un tacos XL (Plus jamais !).

Je sors du laboratoire pour remercier des contacts plus anciens mais avec qui je garde toujours de très bons contacts et que je suis heureux de toujours pouvoir compter pour eux comme Manon Nirrengarten, Fanny Gilles, Marie-France Malcher, Quentin Mahuet et bien d'autres ! Je remercie mes amis de la Fac avec qui j'ai pu partagé quelques années de Licence et avec qui je compte partager de grands moments et des vacances lors des années qui suivront: Alexis, Nico et Damien. Je remercie fortement Nico pour avoir lu et relu et relu cette longue thèse et qui a pu corriger les nombreuses fautes que j'ai pu écrire. Je remercie Damien pour m'accompagner avec Cougoulic pour des clochettes endiablées pour faire le max de score et terminer le plus rapidement possible ces events.

Ensuite je remercie ma famille pour s'être intéressé à ce que je fais même si c'est totalement en dehors de vos domaines de vie. Je remercie ma soeur pour avoir compris la globalité de mon message lors de ma répétition, je remercie mes parents et mon frère pour avoir pu participer à ma soutenance de thèse et me voir parler en anglais limite pour la première fois alors que j'ai boudé cette langue jusqu'au début du Master ...

Et bien sûr je termine par Morgane Monsimier qui est la personne avec qui je compte continuer ma vie à ce jour. Je ne sais pas ce que l'avenir nous réserve mais j'espère qu'il sera accompagné de ta personne. Tu as pu me supporter alors que je travaillais sans relâche pour sortir des derniers résultats, préparer des slides pour des conférences, écrire jusque très tard ce manuscrit... Cette période est derrière nous et je te remercie pour être à mes côtés. Maintenant, nous allons plus profiter de nous et de cette vie.

INTRODUCTION

How to start my PhD thesis? That is one big question I have asked to myself for a long time. I think that I must explain that my thesis has no purpose to do a revolution of the world or physics. My thesis wants to higlight a very functionnal event generator and try to increase its action field, this event generator is EPOS. EPOS takes its name by Energy conserving multiple scattering Partons, parton ladders, and strings Off-shell remnants Saturation (EPOS), it is an event generator dedicated to the study of proton-proton and heavy ion collisions.

The context of this thesis is in Quantum ChromoDynamics (QCD), which describes the interaction between partons (nuclear matter's degrees of freedom). These partons are usually confined into hadrons, however QCD predicts that a new state of matter exists where partons are deconfined from hadrons: the Quark Gluon Plasma (QGP).

The QGP is formed in high energy heavy ion collisions. QGP study is exciting and theoretically challenging research field mainly because instead of partons inside the plasma, only hadrons are observed in the final state. In this thesis, I study anisotropies in the azimuthal angle of particle production, which is directly related to the fluid's anisotropy. The fluid anisotropy is the response of the system to some initial space anisotropy and provides information on the properties of the QGP and its expansion. As in heavy ion (AA) collisions at high energies of Relativistic Heavy Ion Collider (RHIC) and Large Hadron Collider (LHC), "flow-like" effects are hinted at Beam Energy Scan (BES) low energies. Very recently, unexpected "flow-like features" have also been observed in small systems like proton-proton (pp). In this thesis, I try to answer the following question:

> Is there a "collectively expanding plasma" in all systems: big (PbPb) or small (pp), from BES low energies to LHC higher energies?

To answer this question, I will start this manuscript by an introduction of the QGP story and the heavy ion collision physics. I will introduce the different probes of the QGP and the physics of the BES program. This program was created in order to study the phase diagram of QCD using Au-Au collisions at different energies in function of the temperature and the density. The BES has three main goals: i) Can we see evidence of a Critical Point?, ii) Can we see evidence of a phase transition? iii) What is the evolution with $\sqrt{s_{NN}}$ of the medium that we produce?

I will describe the tool that I used everytime during my Ph.D in order to answer its problematic. I will start by the description of the general event generators. Then I will describe the different theories which inspire the main theory in EPOS: the Parton-Based-Gribov-Regge Theory (PBGRT). I will describe how an event is generated in EPOS to understand different analysis points in the fifth chapter.

The third chapter will describe the different methods to study the anisotropic flow. All anisotropic flow analysis will be done using the event generator EPOS, dedicated to the study of proton-proton and heavy ion collisions. We analyze all kinds of systems (pp, AA) and energies (LHC, RHIC BES), for all kinds of flow “probes”. In particular, we investigate different methods of anisotropic flow. Using the Event Plane method, we calculate the anisotropy with respect to an event plane angle. In the Scalar Product method, anisotropic flow is usually assumed to be the only or dominant source of correlation in azimuth between particles. However, there are other sources of two particle correlations called “nonflow” correlations. In order to minimize these contributions, we use Event Plane where we cut in different pseudorapidity ranges, called the eta-sub method. Another way of reducing non-flow is to employ multi-particle correlations: The Q-cumulants method, where multi-particle cumulants are constructed. We can also reduce the nonflow effects using both ways: Q-cumulants with cuts in phase space, if we have a very large multiplicity. A complex observable which connects different orders of anisotropy, called the Symmetric Cumulants, is also studied.

The next chapter will be dedicated to the different results on my Ph.D. We analyze all kinds of systems (pp, AA) and energies (LHC, RHIC BES), for all kinds of flow “probes”. I will describe the different results of the integrated and differential flows versus different variables: transverse momentum, pseudorapidity, multiplicity, centrality ...

Finally, I will conclude this manuscript with an outlook and the different perspectives of this Ph.D work.

The different appendix will give some explanation about technical points of methods to calculate anisotropic flow or the possibility to use EPOS with the future accelerator. The final appendix is an abstract in French of this manuscript.

Appendix B will give details on the framework that I have developed specifically for several methods to calculate the anisotropic flow. I will describe also the different tools used towards the release of EPOS like the centralization of particle’s characteristics like mass, charge, width decay, identification etc ...

The main goal of this Ph.D is not to have a complete analysis of the different results and have a complete physical interpretaion. The main goal is to have a "snapshot" of a huge number of results and prepare the future by this synthesis.

CHAPTER 1

HIGH ENERGY PHYSICS - MATTER - QUARK-GLUON-PLASMA

Contents

This part is the compulsory part of each Ph.D thesis on high energy physics. This is the part where we want to explain easily what we are doing. The main concept of this Ph.D is the formation of the QGP, consequently I will introduce the most important concepts about QGP formation in particle physics.

This part is important before talking about the event generation of collisions with own theoretical model to know which part of particle physics we want to investigate. The main observable that we will investigate during this thesis is the anisotropic flow which plays the role of (soft) probe about the formation of the QGP. This chapter will introduce the main difference of anisotropic probes and other ones.

In this chapter, I will introduce what we study at very high energy in particle physics. To do that, we will travel around fundamental particles and their fundamental interactions within the Standard Model (SM) of Physics. We will do few steps to explain how the matter is composed, what we know (or not) now about all elementary constituent particles in the world. The next step is a little story of theory which tries to explain interactions between elementary particles. Then, we will talk about one of the most important types of matter in particle physics: the quark soup or the Quark Gluon Plasma (QGP). Therefore, we will see how we can explain and discover the QGP with particle accelerators. Finally, we will see few programs that we created to study the Quark Gluon Plasma with particle colliders and the connexion to my Ph.D work.

1.1 Standard Model describes the known matter

I am pretty sure that 90% of particle physicists know, what the Standard Model is and how this model can explain elementary interactions between elementary particles. This is a powerful tool but the SM explains three fundamental interactions: electromagnetic, strong, and weak. We cannot use the SM to explain how the gravitational interaction between particles works.

1.1.1 Description of the Standard Model

The SM is one of the very huge theories of particle physics since 50 years by Murray Gell-Mann and George Zweig, who introduced the idea of quarks [1–4]. Afterwards in 1973, the quantum field theory of strong interaction is formulated: this is QCD. Quarks are determined to be real particles and carrying the color charge. Gluons are quanta of the strong interaction field. This strong interaction theory was suggested by Harald Fritzsch and Murray Gell-Mann [5]. Like the biologists, we want to classify all particles and interactions in one tree with different branches. The elementary particles are characterized by their mass and quantum numbers like electric charge (Q), color charge, spin (S) ... We define within the SM that all particles with integer spin are *bosons* and all particles with half-integer spin are *fermions*.

Formal Aspects of the Standard Model

One formal aspect of the SM is a Quantum Field Theory (QFT) that can be formulated as a gauge theory, since it obeys the internal symmetries of the unitary product group $SU(3)_C \times SU(2)_L \times U(1)_Y$. The strong interaction is related with the symmetry group: $SU(3)_C$ and the electroweak interaction (grouping of weak and electromagnetic interactions) by the way of the symmetry group: $SU(2)_L \times U(1)_Y$.

We can describe the SM with its Lagrangian, not important to recall here. However, I can say that this equation explains all the dynamics of all elementary known particles with all interactions. But these dynamics depend on 19 parameters whose numerical values are established by experiments. The parameters are summarized in the following table[1]:

Symbol	Description	Value
m_e	Electron Mass	511 KeV
m_μ	Muon Mass	105.7 MeV
m_τ	Tau Mass	1.78 GeV
m_u	Up Quark Mass	1.9 MeV
m_d	Down Quark Mass	4.4 MeV
m_s	Strange Quark Mass	87 MeV
m_c	Charm Quark Mass	1.32 GeV
m_b	Beauty or Bottom Quark Mass	4.24 GeV
m_t	Truth or Top Quark Mass	172.7 GeV
ω_{12}	CKM 12-mixing angle	13.1 °
ω_{23}	CKM 23-mixing angle	2.4 °
ω_{13}	CKM 13-mixing angle	0.2 °
δ	CKM CP-violating Phase	0.995
g'	U(1) gauge coupling	0.357
g	SU(2) gauge coupling	0.652
g_s	SU(3) gauge coupling	1.221
θ_{QCD}	QCD vacuum angle	≈ 0
v	Higgs vacuum expectation value	246 GeV
m_H	Higgs Mass	$\approx$ 125.36 GeV

Table 1.1: 19 parameters in Standard Model [6]

We can add seven other parameters because neutrinos possess mass. The seven parameters are [6]:

- mass of electron neutrino $<$ 2.5 eV
- mass of muon neutrino $<$ 170 KeV
- mass of tau neutrino $<$ 18 MeV
- three other mixing angles of CKM due to their mass (like ω_{12})
- another CKM phase due to their mass (like δ)

The huge number of free parameters gives us one indication that the SM is not the fundamental theory for every particle in physics, we also see a wide range in mass for elementary particles. Why is there such a wide spectrum of masses among the building blocks of matter?

A lot of theoretical and experimental researches try to extend the SM into a Unified Field Theory or a Theory of Everything. They want to find a complete theory explaining all physical phenomena including all constants.

[1] CKM means Cabibbo Kobayashi Maskawa (CKM) due to the authors of this matrix

Interactions and particles in the Standard Model

SM of particle physics is the theory construct to describe the three fundamental forces in the universe.

These three interactions are called:

- **electromagnetic**: called sometimes Quantum ElectroDynamics (QED), where all charged particles can interact by exchanging a photon
- **weak**: called sometimes Quantum FlavourDynamics (QFD), where quarks and leptons can change their flavour by exchanging a W^+, W^-, Z^0 (called weak bosons)
- **strong**: called sometimes Quantum ChromoDynamics (QCD) where partons (identified as quarks or gluons) can change their colour charge by exchanging a gluon

There are two types of elementary particles:

Fermion is the first type of elementary particles. Paul Dirac [7] calls these particles fermions in respect of Enrico Fermi [8]. All fermions have half-integer spin. Therefore, they are characterized by the statistics of Fermi-Dirac. It means that fermions follow the Pauli exclusion principle: two fermions cannot occupate the same quantum state.

All particles which induce the interaction are called **bosons**. Induce means that the four vector bosons (spin=1) for the SM are: photons for QED, gluons for QCD and weak bosons for QFD. All bosons have integer spin. The name 'bosons' of this particle type is dedicated to the memory of Satyendra Nath Bose [9]. All bosons follow the Bose-Einstein statistics. It means that bosons do not follow the Pauli exclusion principle: two bosons can occupate the same quantum state.

Since 50's, the SM gives very powerful prediction about characteristics of particles. In 60's, we predicted theoretically the existence, mass and width decay of the Ω^- [10] but this particle has three quarks in the same quantum state. However, the quarks are also fermions, that means that they contradict the Pauli exclusion principle! Indeed, the Ω^- can contain one spin up and one spin down quark, but it is not possible to introduce a different spin for the third quark. To save the Pauli exclusion principle, we include the notion of colour charge.

The colour index is another quantum number taken by each elementary particle who takes place in the QCD. This is not the colour that we can see in the spectra of visible light. For quarks, we can take three colours: red, green and blue. Each anti-quark can take another colour: cyan, magenta or yellow.

To conclude basics notions of colour, when we merge all colours or anti-colours, we have one colourless object. We can also refer to a colourless composite as a white object. We cannot observe experimentally a colour object, we observe in each case a colourless object. All particles that we can measure are white like protons, neutrons or electrons.

Now we want to know: how do we build the structure of the Standard Model? How many types of bosons or fermions? Do we have classify all of that?

The architecture of the Standard Model

As I explained before, we have fermions with colour like quarks. However, we have other, colourless types of fermions, which we can **measure directly**, like electrons. Thus, there exist two types of fermions: The first one with colour, which participates in strong interactions, and the other one, without colour, which participates only in electroweak interactions (the unification in SM of electromagnetic and weak interactions).

We have also two types of bosons. We know that each boson has integer spin (unlike fermions) but some bosons do not have spin. We call those particles: scalar bosons. Now, when we talk about gauge bosons, that means that we talk about bosons with integer spins (spin $\neq 0$). The gauge bosons are the force carriers of each elementary interaction.

I summarize by constructing the architecture of the SM as follows:

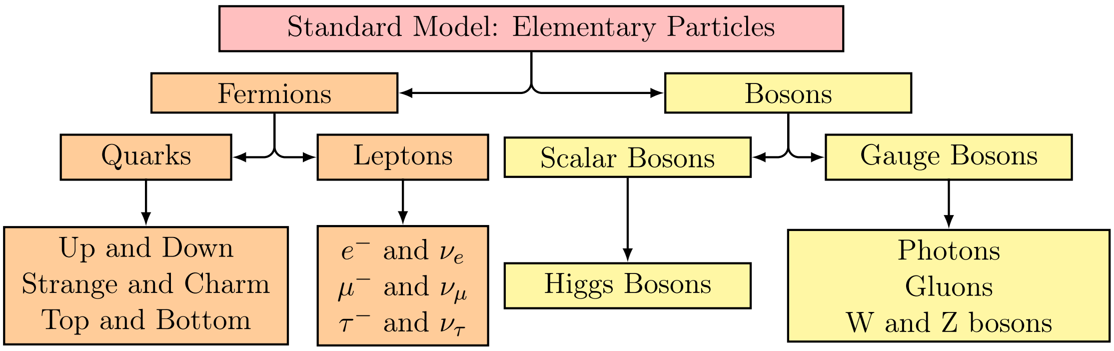

Figure 1.1: Tree structure of the Standard Model

To simplify and for a better visualisation I do not write anti-particles of matter. But for each fermion, we have also a correponding anti-particle. This is a beautiful and simple model and at the end of the 19^{th}, we thought that we knew all of the matter. But the SM has few limitations. These limitations tell us that the SM is not the Theory of everything. I will show a list of few limitations in the next section.

1.1.2 Limitations of the Standard Model

Even though the Standard Model can explain a lot of things about particle physics, we can find few limitations to this model:

- The model does not explain gravitation, we are waiting for a confirmation of the theoretical particle known as graviton. The SM does not explain the usual theory of gravitation, the general relativity, in terms of quantum field theory for particles. For now, nothing connects these two theories. The graviton is not observed experimentally and undiscovered.

- The fact that we have 19 numerical unrelated constants is inelegant [6]. In the same context, the SM can explain that neutrinos have a mass but this is not an obligation so that the theory works [6].

- Experimental observations in cosmology tell us that the SM explains just 5% of the energy present in the universe. Approximately 25 % should be dark matter, another matter not discovered yet. The rest should be dark energy, explained by a constant energy density for the vacuum. If the SM tries to explain the dark energy in terms of vacuum energy, we have a mismatch of 120 orders of magnitude [11].

- As previously stated, neutrinos can be massless in the SM. But neutrino oscillation experiments have shown that neutrinos have a mass. We add by hand the mass terms in SM but this is not explicitly included in this theory.

- Another one is the matter-antimatter asymmetry. The SM predicts that matter and antimatter should have been created approximately in equal amounts from the initial conditions of the universe. The SM does not explain the matter-antimatter asymmetry, but we measure it experimentally [12].

- We can say other things like the emerging Standard Model of Cosmology or the hierarchy problem with the Higgs mechanism and new physics.

Theoretical and experimental researches have attempted to extend the Standard Model into a Unified field theory or a Theory of everything, a complete theory explaining all physical phenomena including constants.

1.1.3 Beyond the Standard Model

To overcome the limitations of the Standard Model, some physicists try to create "better" and more elementary models. We go Beyond the Standard Model (BSM). I will explain two of them a little bit. I will start with one of the most popular extensions of the SM: the Supersymmetry (SUSY).

Supersymmetry

The SUSY is very well known by experimental and theoretical physicists. The creation of SUSY can be attached to B. Zumino and J. Wess with their paper in 1974 [13]. The idea is: each fermion with half-integer spin is associated with one superpartner who posses an integer spin: a sboson. The same idea exists for bosons: each one with integer spin is associated with one sfermion with half-integer spin.

This idea is simple but it is very complicated to include that mathematically. As it was the case for Quantum Physics, we have to create new operators, groups of symmetry, new mathematical laws or rules. We call this algebra: ***the superalgebra*** [14].

The idea of a (super)symmetry between mesons and baryons was proposed for the first time by Hironari Miyazawa in 1966, but his works were ignored at that time [15–17].

In 1971-1972, three independent groups rediscovered the SUSY in the context of Quantum Field Theory: J. L. Gervais and B. Sakita [18], Yu. A. Golfand and E. P. Likhtman and D. V. Volkov and V. P. Akulov [19]. But Julius Wess and Bruno Zumino in 1974 introduced the SUSY with applications to/in particle physics. Since then, we can successfully apply SUSY to nuclear physics [20, 21], quantum mechanics and statistical physics. The Minimal Supersymmetric Standard Model is one of the realistic SUSY versions and was proposed in 1977 by Pierre Fayet [22–24].

To give a simple idea in mathematical terms, we use a generator Q which transforms one fermion in one boson like:

$$Q\,|\text{fermion}\rangle = |\text{boson}\rangle \qquad Q\,|\text{boson}\rangle = |\text{fermion}\rangle \tag{1.1.1}$$

We notice one particularity of this generator: If it is applied twice on the state of a system, this system state remains invariant.

One property of this symmetry is that all superpartners must poss the same mass but we know that is wrong. Experimentally, it is easy to identify the electron. If the superpartner of the electron, the selectron, possesses the same mass, it must be easy to discover, but we never discovered one superpartner for now. The conclusion is: we have the obligation to break the symmetry to have two different masses [10, 25].

Finally, many versions of SUSY predict that the lighter superparticle must be stable and electrically neutral. This particle must interact weakly with particles in the SM. These are exactly a few characteristics of Dark Matter. The SUSY gives us one candidate of particle to the Dark Matter: WIMPs or Weakly Interacting Massive Particles [26]. The Standard Model does not give any particle candidate for the Dark Matter.

String Theory

To be short, one of the big problems in subatomic physics is that we cannot unify the gravity with particles. The framework of the force of gravity is the theory of relativity by Albert Einstein. The framework of particles is the quantum field theory. These two frameworks proved their efficacity by comparisons with experiments.

But, the theory of relativity is within the "classical" physics whereas other forces are in the quantum physics. To unify these two frameworks, we need to create the quantum gravity. But we have a lot of difficulties to use prescriptions of the quantum theory for relativity [27].

The string theory attempts to solve all of these problems. The string theory started by the idea that the point-like particles can be modeled as one-dimensional objects called strings. These strings can interact with each other. We have two types of strings: open one and closed one. A closed string has no end-points, it can be viewed like a circle. An open string has two end-points and is equivalent to a line, see Figure 1.2.

The string can vibrate. These vibrations give the properties of particles: mass, charge etc ... One point of view is to see different elementary particles by vibrating strings. We can say that the theory allows for quantum gravity, because one of the vibrational states of the string corresponds to a graviton [28].

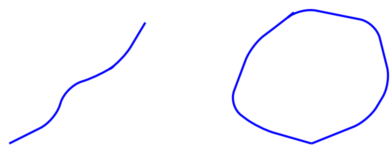

Figure 1.2: Open string at the left and closed string at the right side

The string theory solves a lot of problems like the SUSY that I will not explain in this Ph.D thesis. Also, as was the case for SUSY, there exist a lot of different string theories with different formalisms and parameters. However, we cannot prove the string theory experimentally unlike the SUSY, even if we have not found any superparticles yet (in 2018).

1.1.4 Summary

The Standard Model proved its efficacity with a lot of results. But we find a few limitations that can prove us that the SM cannot explain everthing in subatomic physics. We try to cure these limitations using new theories like the SUSY and the string theory. For now, these theories are not universally accepted.

A very important thing of this part is that all partons (quarks and gluons) are confined into hadrons. We do not have any knowledge about the hadronization of partons. We try to understand the hadronization since decades without success.

In this Ph.D thesis, we work on one matter predicted by the SM since ≈ 40 years. This matter takes a lot of attention by physicists and I will show why in the next part. The name of this matter is: The Quark Gluon Plasma (QGP). This matter is very interesting because this is a matter where all partons are deconfined!

1.2 One of the first kinds of matter in the Universe

In the normal matter, particles are not free, we cannot see one quark or one gluon independently. One of the first kinds of matter in the Universe created a few millionths of a second after the Big Bang is the QGP or quark soup [29]. This is a hot and dense soup made of particles moving near the speed of light. This soup or mixture contains quasi-free quarks and gluons. All partons can move freely in the QGP, this is the reason why we call this matter a "plasma".

The questions that will arise in this section are:

- Why is this matter important for physicists?
- How do we create this matter experimentally?
- How do we study this matter theoretically?
- How can we be sure to create this matter experimentally? Do we have probes? Different types of probes?
- What are the different projects that which study this matter?

1.2.1 Asymptotic Freedom

To recall the subsection 1.1.1, within the framework of the SM, the theory of strong interaction is the Quantum ChromoDynamics. This is a Quantum Field Theory which works with the symmetry group $SU(3)_c$[2]. The boson of the strong interaction: the gluon, has non-zero colour charge. Consequently gluons can interact with one another..

One of the most important parameters of QCD is the coupling constant α_s. In contrast to QED with the Sommerfeld's constant α, α_s is not really constant. It characterizes the strength of the strong interaction. We cannot see one parton alone, the coupling constant is too strong, we call this the **confinement**. The QCD evolution is characterized by the Dokshitzer Gribov Lipatov Altarelli Parisi (DGLAP) equations [10] (from the authors of these equations) as shown in Fig. 1.3. The coupling constant α_s varies with the momentum transfer Q of the interaction.

[2] c represents the colour

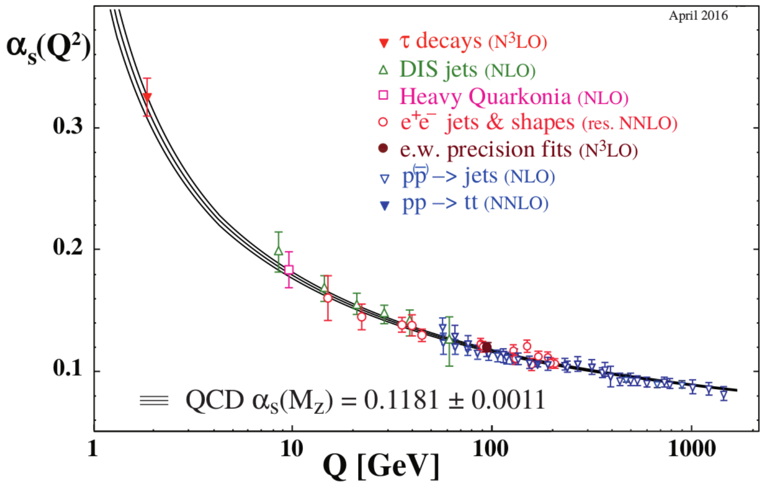

Figure 1.3: Summary of measurements of α_s as a function of the energy scale Q. The respective degree of Quantum ChromoDynamics perturbation theory used in the extraction of α_s is indicated in brackets (NLO: next-to-leading order; NNLO: next-to-next-to leading order; res. NNLO: NNLO matched with resummed next-to-leading logs; N^3LO: next-to-NNLO) [10]

The exact dependence of α_s with the momentum transfer is giving by the following equation:

$$\alpha_s(Q) = \frac{12\pi}{(11N_c - 2N_s)\ln\left(\frac{Q^2}{\Lambda^2_{QCD}}\right)} \tag{1.2.1}$$

where Λ^2_{QCD} is the scale of QCD. This is an infrared cutoff to keep the possibility to use pertubative theory in QCD. With the DGLAP equations, we can see two things:

- at small momentum transfer Q, we can see that the coupling increases. We know that the potential energy between two partons increases linearly with the distance between them. This is not sufficient to explain the **confinement** of partons.
- at high momentum transfer Q, we can see that the coupling decreases. If we have a very high momentum Q, we can find $\alpha_s \to 0$. This condition is known as **asymptotic freedom**.

But we can have another scenario like the picture in the next page [30]:

In this scenario, the asymptotic freedom is not with $\alpha_s \approx 0$ but we poss a $\alpha_s =$ constant after a given μ. It shows that asymptotic freedom can be traded for *asymptotic safety* while leaving the fundamental properties of QCD untouched. Therefore, it becomes crucial to test the high energy behaviour of strong interactions. The final asymptotically safe value, to be reached below the Planck scale, does not have to be large. This theory is in disagreement with the possibility to have a QGP at high energy.

If we take the general scenario with a high momentum transfer Q, we have:

$$\lim_{Q\to+\infty} \alpha_s(Q) \approx 0 \tag{1.2.2}$$

With this property, we can use at the accelerators physics the perturbative theory called the perturbative Quantum ChromoDynamics (pQCD). The asymptotic freedom

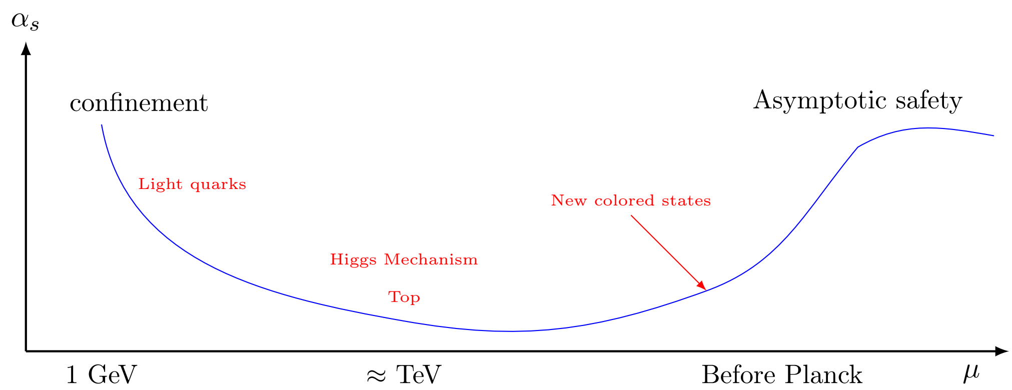

Figure 1.4: Asymptotically safe scenario of Quantum ChromoDynamics expressed in terms of the running of α_s

of QCD was discovered in 1973 independently by David Politzer [31] and David Gross and Frank Wilczek [32]. This is just before the idea of a type of matter, where partons can be free, without hadrons.

1.2.2 The beginning of Quark-Gluon Plasma in physics

The idea that quarks and gluons could exist in a state where they could move freely within a given volume was proposed by T. D. Lee in 1974 [33] . Quickly, it was suggested that heavy nuclei collisions could create this matter at high energy density [34]. We call this matter **"the Quark Gluon Plasma"** [34]. To study the QGP, the European Organization for Nuclear Research (CERN) built the Super Proton Synchrotron (SPS) [35]. Then, we created more powerful installations to try to produce the QGP like at the Brookhaven National Lab (BNL) with the RHIC [36] and at CERN with the LHC.

1.2.3 Phases of nuclear matter

The nuclear or QCD matter is describe by different phases. We want to create experimentally the QGP by following the transition phase of the nuclear matter. Like the water or other well known matter, the phase changes with two state variables: the Temperature and the Density.

With the SPS, RHIC or LHC, we want to move on the QGP phase diagram increasing the temperature (see Fig 1.5). At low temperature and low density, quarks and gluons are confined into hadrons. The coupling is too strong, the matter can be described as an hadronic gas. At low temperature and high density, the matter is a gas of neutrons, an object with enough large density can be the core of a neutron star. At higher density and same temperature, the quarks begin to form pairs and a color superconducting state is expected to be formed [37].

When the temperature is high, $T >> \Lambda_{QCD}$[3], due to asymptotic freedom the QGP is highly expected [38, 39].

The condition of high temperature and vanishing baryon density can be found at the early universe a few microseconds after the Big Bang. We reproduce these conditions by colliding heavy ions in particle accelerators. We will discuss this in the next section.

[3] $\Lambda_{QCD} >> 200$ MeV is one of the main parameter of the QCD [10]

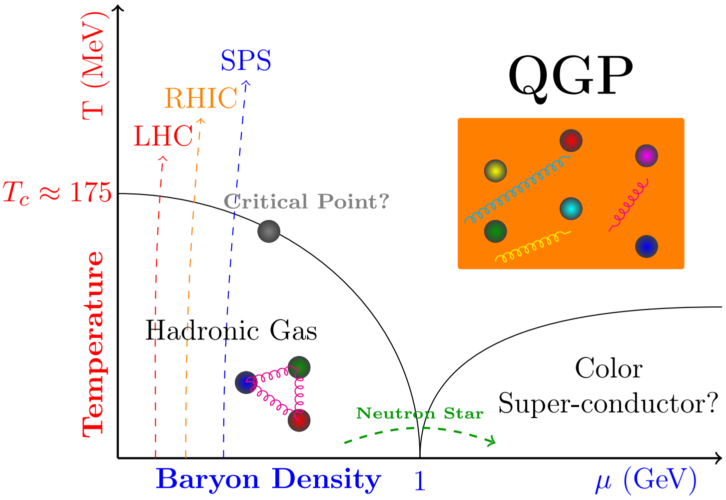

Figure 1.5: Phase Diagram of nuclear matter

1.2.4 Heavy Ions Collisions

To produce the QGP in experiment, we make collisions between heavy ions in particle accelerators. the collisions are performed in an Alternating Gradient Synchrotron (AGS) with Gold-Gold (Au-Au) collisions at energy collision ($\sqrt{s_{NN}}$) equal to 11.5 GeV [4] and by means of RHIC with gold, uranium and copper ions at $\sqrt{s_{NN}} = 7.7$ to 200 GeV per nucleon pair [40]. At CERN, we do now heavy ions collisions with the LHC between Lead-Lead (Pb-Pb) with $\sqrt{s_{NN}} = 2.76$ TeV in Run I [41] and $\sqrt{s_{NN}} = 5.02$ TeV in Run II [42].

When two nuclei collide, the participating nucleons leave behind a system out of equilibrium. If the energy and density attained by the system are bigger than the critical energy density (1 GeV/fm^3), we can create a QGP or a QGP-like. The evolution of the system created by heavy ions collisions is modelized by the Bjorken scenario [43].

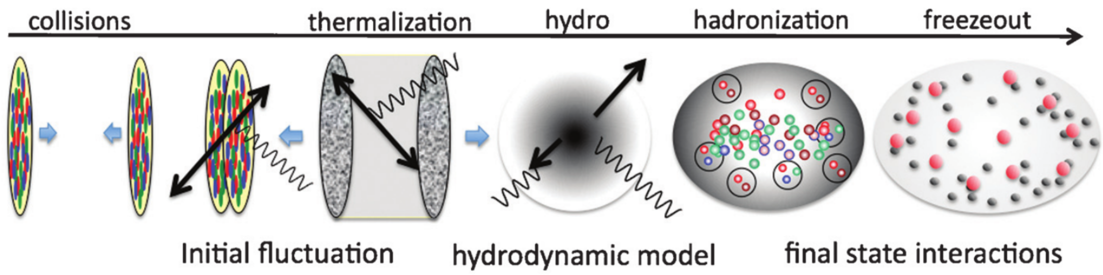

Figure 1.6: Time evolution of heavy ions collision [44]

The Bjorken scenario gives us the space-time evolution of the heavy ions collision. If we follow the evolution of the initial state, the matter evolves according to these steps (see also Fig 1.7 and Fig 1.6):

[4] 1 eV $= 1.602 \times 10^{-19}$ J

1. **Pre-equilibrium** ($0 < \tau < 1$ fm/c): If we say that the collision of the nuclei begins at $\tau = 0$, the duration of this step cannot be measured directly, but we can approximate this one by 1 fm/c [43]. The pre-equilibrium phase is created by multiple interactions/scatterings of partons. These partons do another scattering and begin a thermalization of the system. The large energy density produces fluctuations in the initial shape of the collisional region.

2. **QGP or hydrodynamic phase** ($1 < \tau < 10$ fm/c): The fluctuations (Fig 1.6) generate pressure gradients. That gives us geometrical or momentum anisotropies, I give more details in the section 1.3.1 but later we will find anisotropic flow of particles due to the pressure. If the energy density of the system is high enough, the system turns out like a fluid. We can describe this fluid by hydrodynamic model with different **E**quations of **S**tate and we call this fluid: the **QGP**. First measurements tell us that the fluid must be perfect but the LHC results [41] give us that the fluid has viscous effects.

3. **Mixed state** ($10 < \tau < 20$ fm/c) The pressure gradient between the very high density and the vacuum expands the QGP. This is a hydrodynamic expansion. Subsequently, it cools down at a mixed phase from deconfined to confined matter. The system then begins propagating particles outward where particles production begins to take over. These new particles along with some of the original particles from the colliding nuclei can interact with the created medium. Finally, when the temperature drops below a critical temperature, all partons hadronize.

4. **Hadronic Gas** ($\tau > 20$ fm/c) The hadronization of partons consists of two steps: the fragmentation of partons gives us a shower of quarks and gluons. Therefore, the second step begins, when all of the partons inside the mixed phase and in showers recombine into hadrons. The system can be described by an expanding hadronic gas.

5. **Freeze Out** (At the end) This step contains two different substeps.

   Chemical Freeze out: in this step, all inelastic collisions cease. The number of hadrons is approximatively fixed (we can produce few hadrons by decays).

   Kinetic Freeze out: in this step, all elastic collisions cease too. It is at this moment that all detectors detect hadrons.

Before the run II of LHC, we thought (generally) that the pp collisions[5] were just a reference system, where no QGP is formed[6]. If the QGP is not formed, the collision must just be a freeze-out into a hadron phase. We can compare all properties of the produced particles between AA[7] and pp system to give us a baseline of a production of QGP. Currently, the question of collectivity in pp collisions is in discussion that is one fundamental question of this Thesis. Personally, I think that nothing can just be a reference but some things must be simpler than others. It is possible that we created some things like a QGP in pp collisions if we have enough energy or density. But in this Thesis, we will prove that we have some collectivity effects in pp collisions. It can be important to do more investigations in this part of physics.

[5]pp collisions is for proton-proton collisions

[6]this is not rigorously accurate but the general observations on pp collisions are the idea of a reference.

[7]AA is for nuclei-nuclei

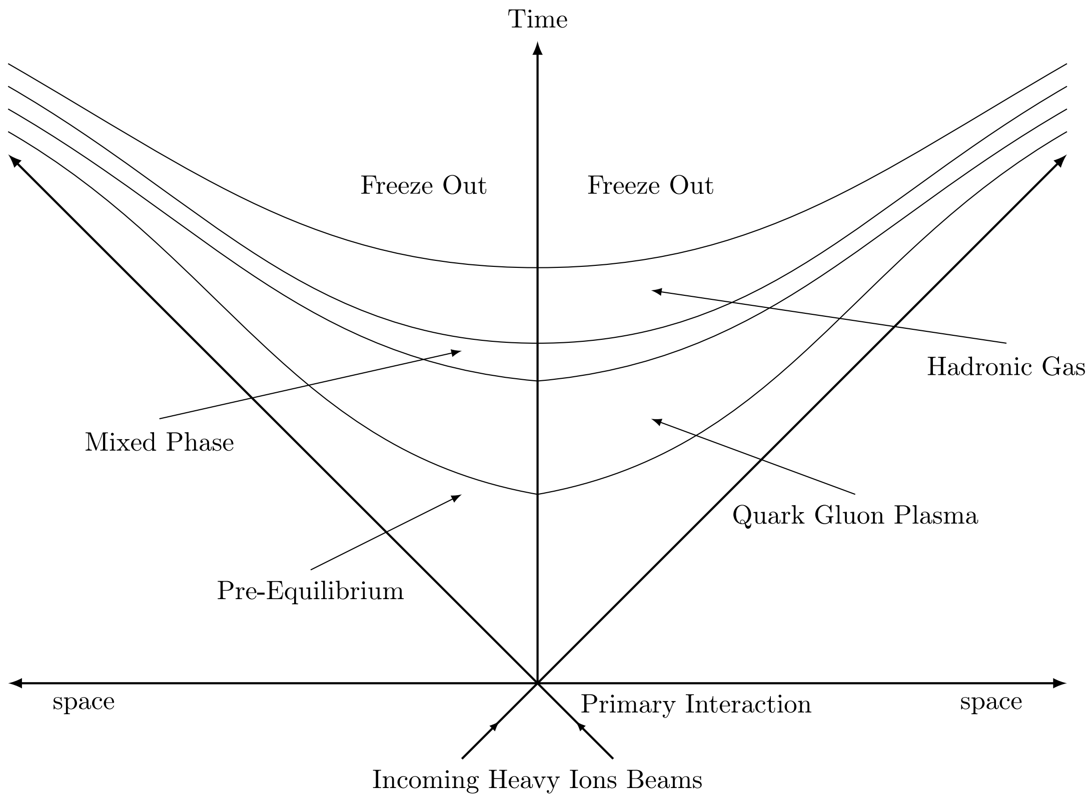

Figure 1.7: Space time evolution of heavy nuclei collision

1.2.5 Summary

One of the first type of matter after the Big Bang is an equivalent to the Quark Gluon Plasma. The QGP is a hot, dense liquid of quarks and gluons. We want to produce the QGP experimentally with particle colliders. The life time of the QGP is too tiny to be measured directly.

However, the detected final hadrons store some information about the evolution of the system. We can find some experimental probes to study the different phases of the system created in heavy ions collisions.

We know that the QGP can be formed by soft partons (with low momentum) and by hard partons (with high momentum). All soft probes give characteristics of the relativistic fluid, like its viscosity, its expansion etc ... Hard partons are produced at the beginning of heavy ions collisions. They pass through the QGP and lose energy in the process ⇒ give us information about the system.

We will see more details about probes that we use to study the Quark Gluon Plasma and its properties in the next section.

1.3 Studies of the Quark Gluon Plasma

We cannot observe directly the QGP due to its tiny life time and due to the confinement property of the strong interaction, but we can detect all final particles. When the QGP cools down and expands, constituents of the system hadronize in two types of particles: *soft* and *hard* [31, 32]. The distinction of soft particles or hard particles comes from the momentum transferred in a collision. Generally, we use the transverse momentum (p_T) to characterize physics of high energy collisions.

Hard particles are created by hard partons scattering at early time of the collision while soft particles are created when the medium has expanded and cooled down [10,45].

1.3.1 Soft Probes

Soft probes come usually from thermal QCD. The majority of particles produced in heavy ions collisions has a momentum lower than 2 GeV/c [38]. Therefore, the information given by soft processes reflects the size, the dynamics, the temperature, and the composition of the QGP [38].

Photons

In heavy ions collisions, we create different types of photons: direct and indirect. Direct photons are not originating from hadronic decays. Unlike hadrons, we have different sources of direct photons in AA collisions. Direct photons are produced at early stages of the collision and escape from the hot nuclear matter basically unaffected. They deliver direct information on the conditions at the time of production. We can plot the spectrum of *inclusive* photons. This is a spectrum with all photons:

- *prompt* photons which are produced in initial hard QCD processes, early in the collision. These photons emerge exactly by hard processes or by bremsstrahlung in hard QCD processes.
- *decay* photons are decay products of hadronic resonances. They can be either produced in hard QCD processes or at the end of the thermal evolution of the system.
- *thermal* photons which are emitted in the collisions of partons in the QGP phase [46] or by radiation of the medium or in scattering of hadronic resonances in hot matter. The spectrum of thermal photons is exponentially damped at large enough energy.
- *direct* photons are the sum of prompt and thermal photons.

To give a simple example: The photon produced by a quark or a gluon, with Compton process, annihilation process and fragmentation process is defined as prompt photon. However, the photon from hadron decay is not defined as prompt photon. As photons do not participate in strong interactions, we can access all information between the beginning and the end of the collisions.

Direct Photons

Direct photons were predicted to exist by C.O. Escobar in 1975 [47] but we observed them for the first time at CERN in 1976 by WA48 Collaboration in S-Au (200 AGeV) and Pb-Pb (158 AGeV) collisions at SPS [48] and other experiments [49–57]: details in Table 1.2. All QCD calculations for direct photons production are easier than other processes. Direct photons have been used to test predictions of pQCD. Pioneering High Energy Nuclear Interaction eXperiment (PHENIX)[8] measured direct photons in pp collisions at $\sqrt{s_{NN}} = 200$ GeV [58]. This is a success for the pQCD, we can describe the direct photon cross section for $1 < p_T < 20$ GeV/c. Must precise measurements are effectuated with Tevatron and LHC accelerators.

[8]Detector of RHIC more details in section 1.4

Results with LHC give us that direct photons produced in the QGP constitute at most about 50 % of all photons. The photon production in the QGP is dominated by early phase and is localized in the center of the QGP where the flow [9] is still low.

Accelerator	Collisions	Experiments	Years	$\sqrt{s_{NN}}$ [GeV]	p_T [GeV/c]
SPS	p+p	NA24	1987	23.8	3.25 - 6.0
$Sp\bar{p}S$	p+$\bar{p}$	UA1	1988	546 and 630	17 - 46 and 90
SPS	p+p	WA70	1988	22.9	4.11 - 5.7
ISR	p+p	R110	1989	63	4.5 - 10.0
ISR	p+p	R806	1989	63	4.75 - 10.36
$Sp\bar{p}S$	p+$\bar{p}$	UA2	1992	630	15.9 - 82.3
Tevatron	p+$\bar{p}$	CDF	1995	1800	12.3 - 114.7
FNAL	Fixed p	E704	1995	19.4	2.5 - 3.8
Tevatron	p+$\bar{p}$	D0	1996	1800	10.5 - 72.0
SPS	p+p and $p+\bar{p}$	UA6	1998	24.3	4.1 - 7.7
Tevatron	Fixed p	E706	2004	31.6 and 38.7	3.5 - 12.0

Table 1.2: Measurement of Prompt photon in many experiments

Thermal Photons

At low p_T spectrum of direct photons, thermal photons take large contribution. This is the thermal photons of the thermal radiation of the QGP. We consider at RHIC and LHC energies that direct photons with p_T between 1-3 GeV/c are considered as thermal photons [59]. By taking the slope of the p_T spectra of the thermal photons averaged over the space-time evolution of the collision, the temperature of QGP formation can be estimated [60]. With the p_T distribution of thermal photons, we can also find some characteristics of flow and chemical composition of the medium [46]. Using thermal photons, we find that the temperature of the medium in LHC is approximately 300 MeV while 220 MeV in RHIC.

Baryon enhancement

One thing that we want to know is: what is the particle production in the medium? To know that, we can measure the baryon/meson ratio in heavy ions collisions. Very quickly, they saw that we have an enhancement of baryon at intermediate p_T compared for AA to pp collisions. They can interpret this as evidence that the dominant mechanism of particles production in the thermal medium is not vacuum fragmentation.

They measured the enhancement of baryons by different ways. In 2006, with the Solenoidal Tracker At RHIC (STAR) detector [61], they measured the ratio of p/π^+ and $\bar{p}/pi^-$ by different heavy ions collisions. Results are shown in Fig. 1.8. In this figure, we have results of p/π ratios from d-Au [62, 63] and Au-Au collisions at $\sqrt{s_{NN}} = 200$ GeV. They have also the results of this ratio from light quarks jets in $e^+ + e^-$ collisions at $\sqrt{s_{NN}} = 91.2$ GeV shown in dotted-dashed line [64]. The shaded boxes represent the systematic uncertainties in the top 12% central Au+Au collisions. The systematic uncertainties for 60-80% Au-Au collisions are similar. The dotted and dashed lines are model calculations in central Au-Au collisions [65, 66].

[9] Flow refers to how energy, momentum, and number of particles vary with direction more details in subsection 1.3.1

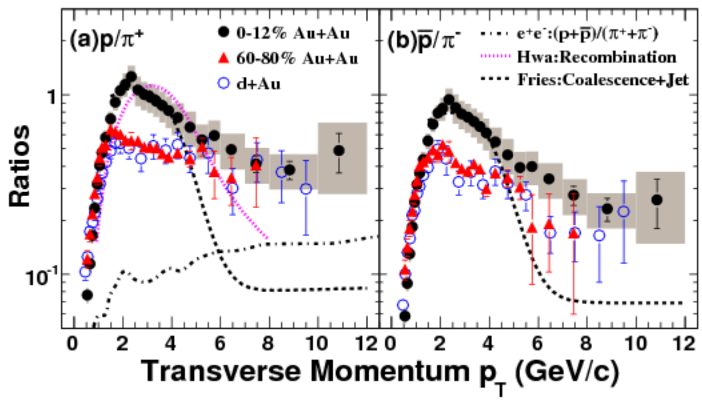

Figure 1.8: Ratio of p/π^+ and $\bar{p}/\pi^-$ take on [61]

Protons and antiprotons are less suppressed than pions at intermediate p_T. At $p_T > 6$ GeV/c, both mesons and baryons are strongly suppressed. We see that in $e^+ + e^-$ collisions, we do not reproduce the enhancement of baryons.

The baryon enhancement is reproduced for other particles than protons and at energy of LHC with A Large Ion Collider Experiment (ALICE) detector [67, 68]. The baryon enhancement figure was taken from [67].

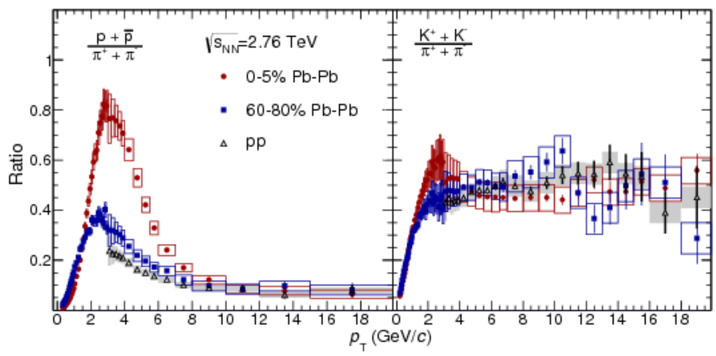

Figure 1.9: (Color online). Particle ratios as a function of p_T measured in pp and Pb-Pb collisions. Statistical and systematic uncertainties are displayed as vertical error bars and boxes, respectively.

We can see in Fig 1.9 an evidence of the baryon enhancement at intermediate p_T for different centralities with the $\frac{p+\bar{p}}{\pi^+ + \pi^-}$ ratio at Pb-Pb collisions but not at p-p collisions at $\sqrt{s_{NN}} = 2.76$ TeV.

For other particles than protons, we reproduce also the baryon enhancement at intermediate p_T for different centralities with the λ/K_s^0 ratio at Pb-Pb collisions at $\sqrt{s_{NN}} = 2.76$ TeV in Fig 1.10. However, the excess of baryons is not very relevant in pp collisions at the center-of-mass energy up to $\sqrt{s_{NN}} = 0.9$ or 7 TeV [69]. The excess of baryons is relevant at RHIC in Au+Au collisions at $\sqrt{s_{NN}} = 200$ GeV [70]. Some comparisons with hydrodynamic model [71–73], a recombination model [74] and EPOS event generator [75] are done. The following figure was taken from [68].

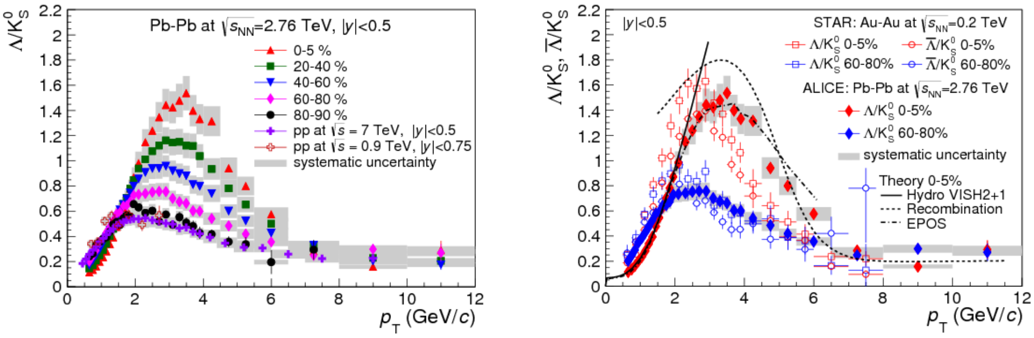

Figure 1.10: (Color online). Left: ratios as a function of p_T for different event centrality intervals in Pb–Pb collisions at $\sqrt{s_{NN}} = 2.76$ TeV and pp collisions at $\sqrt{s_{NN}} = 0.9$ and 7 TeV. Right: Selected ratios as a function of p_T compared with ratios measured in Au–Au collisions at $\sqrt{s_{NN}} = 200$ GeV and different models.

We understood the baryon enhancement in the intermediate transverse momentum region as hadronization through recombination of quarks in the medium [76]. The recombination model assumes that particles production occurs from quarks which are near each other in space and relative velocity. We mean by in recombination that the hadron momentum is the sum of partons momentum that recombine. In the Fig 1.11, we see that the quark distribution falls with increasing p_T, this figure was taken from [77] :

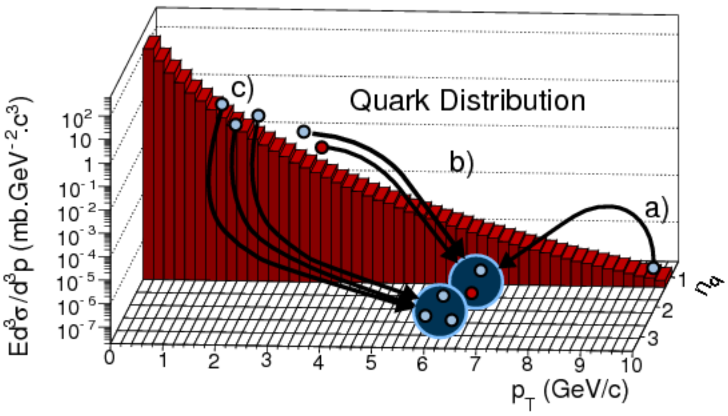

Figure 1.11: Illustration of the possible competition between fragmentation and coalescence in the intermediate p_T range with: a) corresponds to a high p_T quark fragmentation into a meson, whereas b) and c) show respectively the creation of a meson and a baryon via quark recombination

Transverse energy

To explain what is the transverse energy, we start by the transverse momentum. This is the momentum of an object transverse to the beam. We define the transverse energy for an object with mass m and transverse momentum p_t by:

$$E_T = \sqrt{m^2 + p_t^2} \tag{1.3.1}$$

The mean transverse energy per unit pseudorapidity $\langle dE_T/d\eta \rangle$ gives a measure of the amount of longitudinal energy of the colliding nuclei which is carried off by particles produced in the transverse direction [78,79]. Consequently, we can find information about the energy densities, centrality dependence and both thermal and chemical equilibrium of the system [80].

In the reference [80], they measured $\langle dE_T/d\eta \rangle$ at midrapidity in Pb-Pb collisions at $\sqrt{s_{NN}} = 2.76$ TeV using four differents methods. They find similar results or conclusions than previous measurements at RHIC [78, 79, 81]. Otherwise, the observable increases in mean energy per particle and not with increased particle productions which was seen at lower $\sqrt{s_{NN}}$ energies [80]. $\langle dE_T/d\eta \rangle$ can be independent at very high energy of the particle productions, we see a saturation of $\langle dE_T/d\eta \rangle$.

ALICE concluded: if we assume that the formation time τ_0 is 1 fm/c, the energy density is estimated to be approximately: 12.3 ± 1.0 GeV/fm^3 in 0-5 % central Pb-Pb collisions at $\sqrt{s_{NN}} = 2.76$ TeV. This is twice the amount that was observed in 0-5 % central Au-Au collisions at $\sqrt{s_{NN}} = 200$ GeV. The energy density at the core of the collisions exceeds 21 ± 2 GeV/fm^3, but the energy density for all participants is above 1.0 GeV/fm^3 to produce the QGP, indicating that the QGP can be formed in peripheral collisions.

Anisotropic Flow

This section is just an introduction to the anisotropic flow. Further descriptions of this type of flow and approaches to measure it will be discussed in Chapter 3.

The azimuthal flow characterizes the fact that azimuthal distributions of produced particles are not uniform. Indeed, in heavy ions collision, the dense overlap region looks like an ellipse [82]. This is, rather, one of the tools we use to investigate collectivity.

Generally we reproduced the picture given in Fig 1.12. The pressure gradient is larger in the direction of the reaction plane rather than orthogonal to it. The differences in the pressure gradient imply that more particles move along the directions of the reaction plane. Spatial deformations in the initial state give us an anisotropic momentum distribution in the final state. It is generally this anisotropy that we measure experimentally [82]:

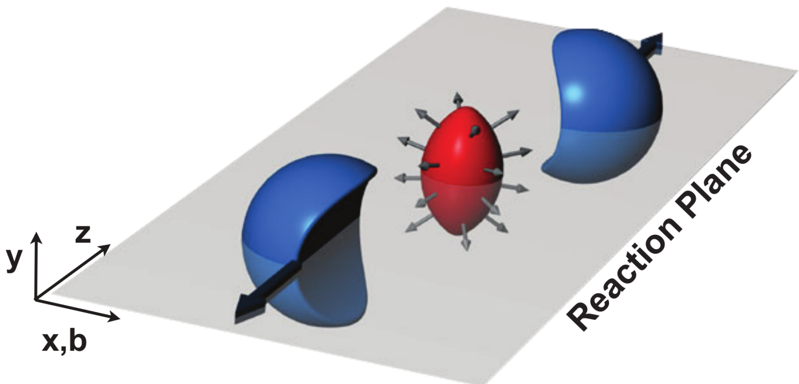

Figure 1.12: Almond shaped interaction volume after a non-central collision of two nuclei. The spatial anisotropy with respect to the x-z plane (reaction plane) translates into a momentum anisotropy of the produced particles (anisotropic flow).

Flow signals multiple interactions between the constituents of the medium in the collision (like the QGP). If we have more interactions, we have a larger magnitude of the flow. Then, the system is closer to thermalization. Consequently, we say that the flow, or more specifically, the magnitude of the flow is a probe of the level of thermalization.

Experimentally, we measure directly the anisotropic flow which is the anisotropy in particle momentum distributions correlated with the reaction plane, see Fig 1.12. We say that the anisotropy is a probe of QGP, by the fact of collective expansion of the medium. This is a signal that partons are strongly interacting with the QGP. The final state particle yield or the azimuthal angle of emission with respect of the reaction plane can be expressed with a Fourier series, given by the following equation:

$$E\frac{d^3N}{d^3p} = \frac{1}{2\pi}\frac{d^2N}{p_T dp_T dy}\left(1 + \sum_{n=1}^{\infty} 2v_n \cos(n(\phi - \Psi_{RP}))\right) \tag{1.3.2}$$

with E the energy of the particle, p its momentum, p_T its transverse momentum, ϕ its azimuthal angle, Ψ_{RP} the reaction plane angle and y its rapidity[10].

We use this equation to describe the kinematics of one particle relative to the beam axis. The amplitude of the asymmetry is characterized by the coefficients v_n. We call these coefficients, the **anisotropic flow**. These are the coefficients that we want to measure experimentally. I represent in the two following pictures how we can represent the anisotropic flow and the strengh of the asymmetry with two different values of v_n.

Figure 1.13: To represent different coefficients v_n, functions $f(\phi) = 1 + 2v_n \cos(n\phi)$ for $n = 1, 2, 3, 4$ are plotted with $v_n = 0,1$. $\Psi_{RP} = 0$ for simplicity.

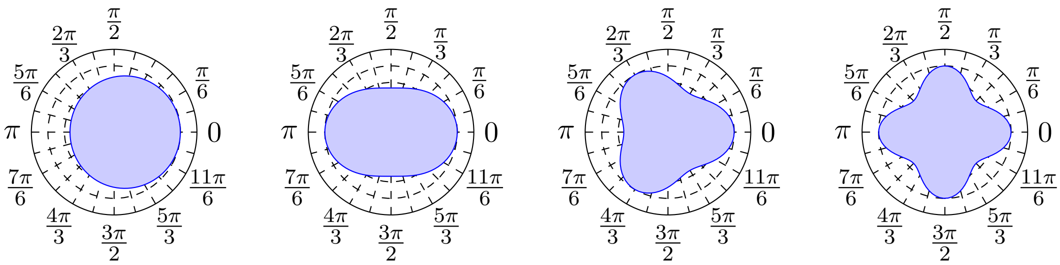

(a) $n = 1$ (b) $n = 2$ (c) $n = 3$ (d) $n = 4$

Figure 1.14: To represent different coefficients v_n, functions $f(\phi) = 1 + 2v_n \cos(n\phi)$ for $n = 1, 2, 3, 4$ are plotted with $v_n = 0,3$. $\Psi_{RP} = 0$ for simplicity.

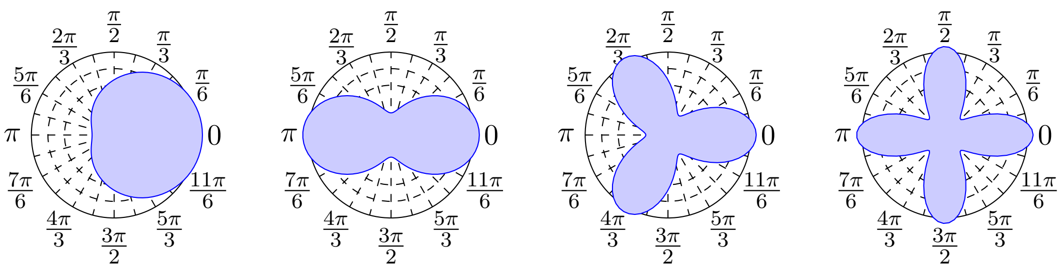

(a) $n = 1$ (b) $n = 2$ (c) $n = 3$ (d) $n = 4$

[10]Maybe it is useful to introduce the expression of the rapidity: $y = \frac{1}{2}\ln\left[\frac{(E+p_z)}{(E-p_z)}\right]$

Because v_n are Fourier coefficients, we can calculate with:

$$v_n(p_t, y) = \langle \cos(n(\phi(p_T, y) - \Psi_{RP})) \rangle \tag{1.3.3}$$

where the angular brackets represent the average over all particles, summed over all events. The anisotropic flow is dependent of the transverse momentum and the rapidity. In this Fourier decomposition, the coefficients v_1 and v_2 are known as **directed** and **elliptic** flow, respectively. We can describe the first two coefficients by first approximation:

$$\begin{aligned} v_1 &= \langle \frac{p_x}{p_T} \rangle \\ v_2 &= \langle \left(\frac{p_x}{p_T}\right)^2 - \left(\frac{p_y}{p_T}\right)^2 \rangle \end{aligned} \tag{1.3.4}$$

To describe and understand the flow, we use hydrodynamic or microscopic transport models. The definition of flow is different in these two cases. In the transport framework, flow depends on the opacity of the medium, if it partonic or hadronic. We can see in Ultrarelativistic Quantum Molecular Dynamics (UrQMD) that the second order of anisotropy fails for $\sqrt{s_{NN}} \geq 17$ GeV and for third order it essentially fails everywhere, see Fig 1.15 taken from [83]. The third order is supposed to be more sensitive to the presence of the fluid phase in the evolution [83]. There is a similar story with other transport models (not all of course), but generally speaking it indicates that the mean free path in the dense medium should be small (i.e. close to an ideal fluid). The hydrodynamic model allows for a description of the system with macroscopic quantities. We use the equation of state of the matter to describe the QGP.

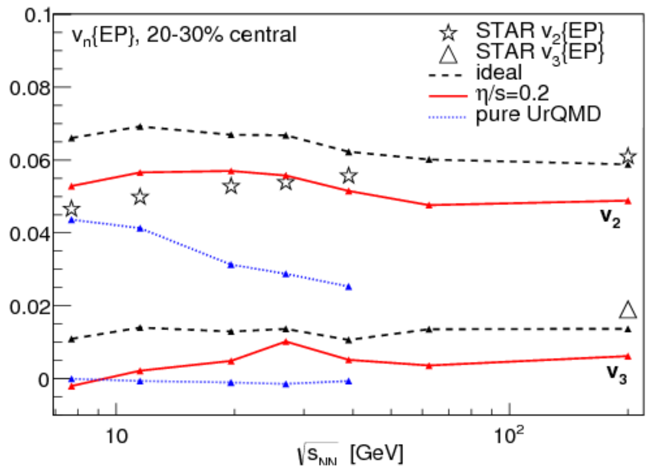

Figure 1.15: Pure UrQMD transport model fails at third order of anisotropy.

The magnitude of flow agrees with hydrodynamic models with an equation of state [82], therefore we can say that the anisotropic flow is a probe of the level of thermalization of the medium. It also can characterize the number of interactions. At the beginning of the study of anisotropic flow, all hydrodynamic models cannot reproduce data with $p_T > 2$ GeV/c [84,85]. We said that is because we cannot reproduce exactly the viscosity of the medium. Eventually, after ten years of work, we can try to reproduce data with $p_T > 2$ GeV/c [86].

We do not forget that after $p_T = 2$ GeV/c, we do not have just hydrodynamic evolution of the medium but we also have jets[11] contributions. It is obvious that before incrementing all jet contributions, we could not reproduce experimental data. This is important because I will not include the jet matter interaction during the different collisions for the results obtained with this Ph.D.

An important point of view, that will be discussed in the fourth Chapter and the chapted dedicated to the flow, is the possibility of an anisotropic flow in pp collisions. This is an important feature and recent observations because the collectivity was previously a specificity of heavy ion collisions.

We have finished with soft probes, to do a better description of probes of QGP, we continue with descriptions of hard probes.

1.3.2 Hard Probes

All previous probes did not need generally a high energy. Usually, energetic particles are created early in the collisions through hard partons scattering. If these particles have enough energy, they can survive through the entire collision and can be used as probes of the medium. If we transfer a large momentum, we call the process a hard process [87].

Quarkonia

Firstly, what are quarkonia and why can they be a (hard) probe of the QGP? Quarkonia can be excited states of a flavorless meson composed of a heavy quark and its own heavy anti-quark. To give few and common examples, we have the J/Ψ (a pair of quark c and antiquark $\bar{c}$) and the Υ mesons (bottom and antibottom pair). We call quarkonia like heavy flavor quark pairs due to their large mass. We talk about charmonium when the bound state is $(c\bar{c})$ and about bottomonium when the bound state is $(b\bar{b})$. Charmonium states are usually used as probes of the formation of the QGP [88, 89]. They can be created in the primary nucleon nucleon collisions, thus before the creation of the QGP. Consequently, these bound states can interact with the medium and give us information. They are created by fusion of gluons. It was predicted that the formation of QGP must suppress different states of quarkonia as a function of the temperature of the medium.

We say that the quarkonium production rates in heavy ions collisions can be used to probe the formation of the QGP because their formation time is very tiny. Exactly, the pre-resonant state is produced while the QGP is formed, but the bound states are formed in coexistence with the QGP and may decay out of it [90]. In the presence of QGP, the color screening would prevent the binding of the quarkonium [88]. But, recently we saw that we have another mechanism due to the production of the QGP: *the regeneration* of the quarkonium [91, 92]. The theory of the mechanism is simple, if we create a "small" QGP, we must have a given number of quark Q and antiquark $\bar{Q}$. If the QGP is bigger, the number of quark Q and antiquark $\bar{Q}$ grows. Consequently, the number of bound states increases. The regeneration is in competition with the color screening. When the radius of the screening drops below the binding radius of the quark system, the quarkonia can melt and the binding force can no longer hold the quarks together [88]. The suppression of states is determined by the deconfinement temperature T_c and their binding energies. This suppression of quarkonia states was seen by Compact Muon Solenoid (CMS) detector to be consistent with the sequential melting scenario as described by [93].

[11] Collimated beam of particles, more details in 1.3.2

To conclude, we can say that the quarkonia suppression serves as direct evidence of deconfinement since the binding potential between the constituents of the quarkonium state should experience color charge screening by the surrounding light quarks and gluons. I summarize the suppression and the regeneration in these two following pictures:

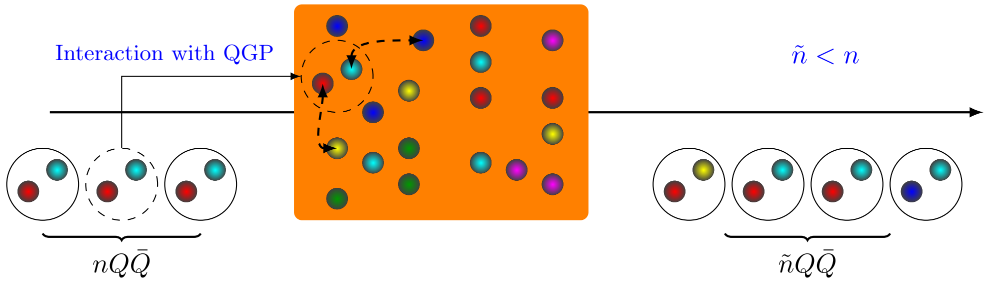

Figure 1.16: Illustration of the suppression mechanism with QGP.

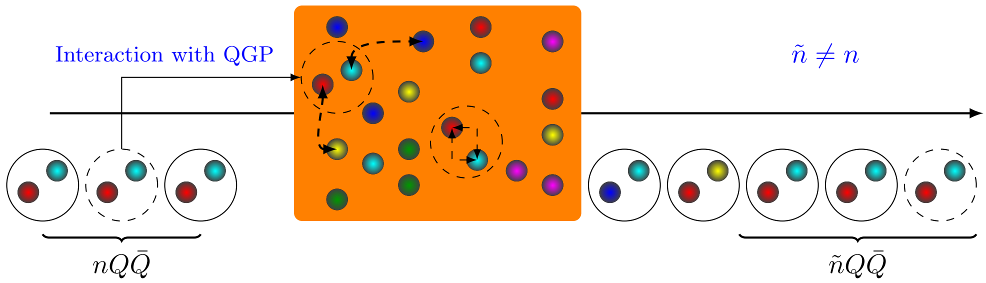

Figure 1.17: Illustration of the suppression and recombination mechanisms with QGP.

Jet Quenching

In an elastic or inelastic scattering of two partons, each of the colliding nuclei results in the production of two or more particles in the final state. If we assume to be in hard processes, all final particles must have large transverse momentum. All final partons must fragment into final state hadrons. The collimated spray of final hadrons formed from the fragmentation of a hard outgoing parton is called a **jet**.

We can see a jet by many hadrons included in a cone with the most hard particle in the center, however this is not necessary, jets come in all kind of different patterns. Hard partons are created at the beginning of the heavy ions collision, then they can fragment in the vacuum or by interaction(s) with the medium (QGP). When partons which form jets interact with the medium, they lose energy. Therefore, the energy loss provides information about thermodynamical or transport properties of the medium. We call the mechanism of interaction between hard partons and QGP: **the jet quenching**. The process of jet quenching is shown in Fig 1.18 taken from [94]:

In this picture, we can see a collision at high energy between nuclei. We have a hard scattering between two quarks and one of them goes directly into the vacuum where it radiates a few gluons and hadronizes. The other one goes inside the vacuum and does interactions, consequently it loses energy by gluon radiation.

There are two primary ways to lose energy when a parton pass through the medium. The first one is where partons undergo collisions and continue to do scattering(s). This mechanism dominates at low energy [95]. At high energy, this is the gluon radiation in

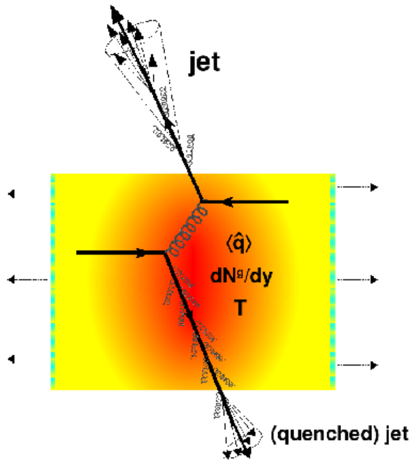

Figure 1.18: Jet Quenching in a head-on heavy-ion collision.

the form of gluon bremsstrahlung [96,97]. The magnitude of energy loss is a characteristic of the density of the medium.

One of the most impressive results of jet quenching was obtained from the measurements of correlations between hadrons that were emitted back-to-back [98], with high momenta. Some sample results are shown in Fig 1.19 taken from [98]. We observe the suppression of two-particle azimuthal distributions at $\phi = \pi$ in the case of central Au-Au collisions compared to pp or d-Au collisions at $\sqrt{s_{NN}} = 200$ GeV. We can also see results with ALICE [99] and CMS [100] in the LHC.

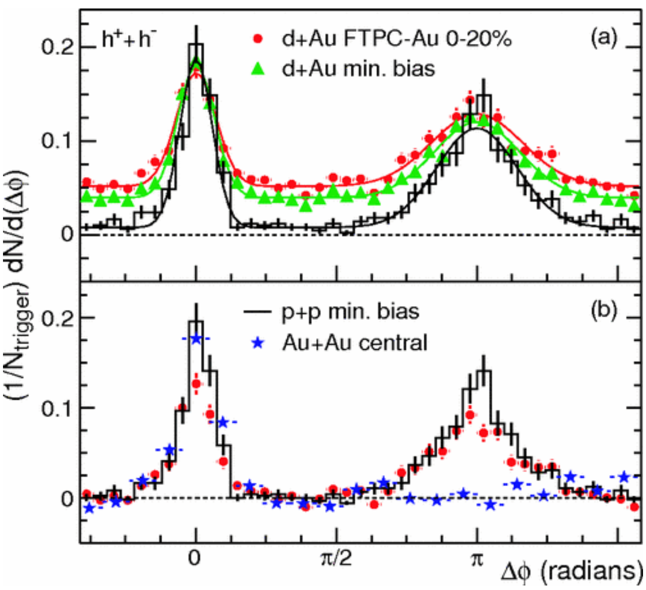

Figure 1.19: (a) Efficiency corrected two-particle azimuthal distributions for minimum bias and central d-Au collisions, and for pp collisions, (b) Comparison of two-particle azimuthal distributions for central d-Au collisions to those seen in pp and central Au-Au collisions

Nuclear Modification Factor

We see that hard probes come from hard scatterings, and can lose energy via gluon bremsstrahlung or multiple collisions within the medium. Consequently, this can lead to a suppression of the number of particles, which is estimated by the nuclear modification factor R_{AA}. R_{AA} compares nucleus-nucleus collisions to proton-proton collisions. This is the ratio between the particle yield in heavy ions collisions divided by the particle yield in pp collisions, normalized by the average number of binary nucleon-nucleon collisions. Mathematically, we can express the R_{AA} by:

$$R_{AA} = \frac{1}{N_{coll}} \frac{\sigma_{AA}}{\sigma_{pp}} = \frac{1}{N_{coll}} \frac{\left.\frac{dN}{dp_t}\right|_{AA}}{\left.\frac{dN}{dp_t}\right|_{pp}} \tag{1.3.5}$$

where σ_{AA} and σ_{pp} are the invariant cross sections and $\left.\frac{dN}{dp_t}\right|_{AA}$ and $\left.\frac{dN}{dp_t}\right|_{pp}$ are the p_T distributions for a given process in AA collisions and pp collisions, respectively [101–103]. N_{coll} is the average number of nucleon-nucleon collisions in the AA collisions. We have three indications by the value of R_{AA}:

- if $R_{AA} \approx 1$, we have not difference between AA and pp collisions for the production of particles
- if $R_{AA} < 1$, some mechanisms do suppress some particles in AA collisions
- if $R_{AA} > 1$, some mechanisms do enhance some particles in AA collisions

The nuclear modification factor has been measured at RHIC and SPS. We can see a comparison between the nuclear factor for Au-Au collisions and d-Au collisions in different detectors of RHIC in the Fig 1.20. We just have to remove AA by the collision in the formula 1.3.5. We see a really big attenuation between AA collisions and dA collisions [98, 104–106].

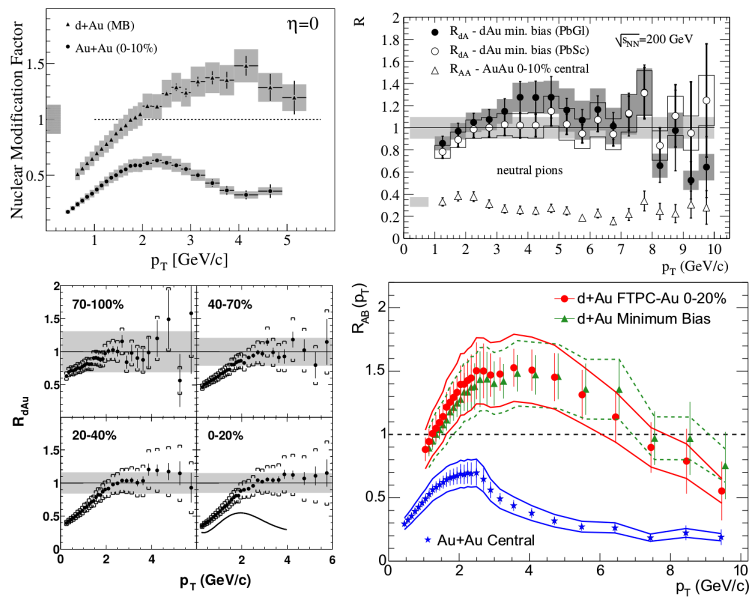

Figure 1.20: Comparison of different nuclear modification factors of hadrons in different detectors at RHIC, take on [107]

We see a huge suppression of hadrons for Au-Au collisions, thus, we can say that we have a QGP. Something happens to suppress more particles than for small collisions like pp or d-Au collisions. The results of the LHC give us approximately the same type of results: we see a large suppression effect in the following figure taken from [108]:

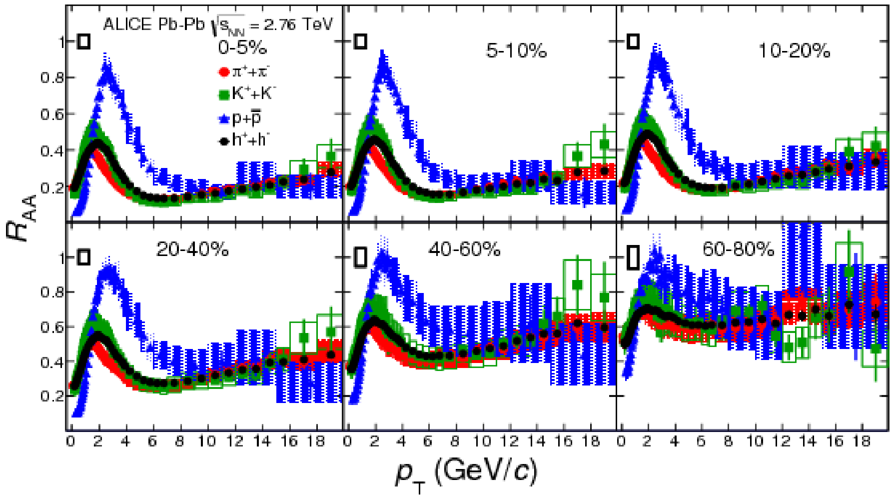

Figure 1.21: (Color online). The nuclear modification factor R_{AA} as a function of p_T for different particle species. Results for different collision centralities are shown. Statistical and systematic uncertainties are plotted as vertical error bars and boxes around the points, respectively. The total normalization uncertainty (pp and $PbPb$) is indicated in each panel by the vertical scale of the box centered at p_T = 1 GeV/c and R_{AA} = 1.

The suppression at the LHC is stronger than at RHIC, meaning that the QGP is hotter than at RHIC energies. Above $p_T \approx 6$ GeV/c, R_{AA} is similar for all particles [108] indicating that the suppression may be a partonic effect and not a collectivity or QGP effect. It appears that heavy quarks have a similar level of suppression than light and strange quarks [108].

The R_{AA} of quarkonia is also studied at the LHC, to compare with the results of RHIC. Surprisingly, we found less suppression of particles than for RHIC energies, see Fig 1.22 taken from [109]. This is the reason why we talk about recombination effects at very high energy with a hotter and bigger QGP than RHIC energies.

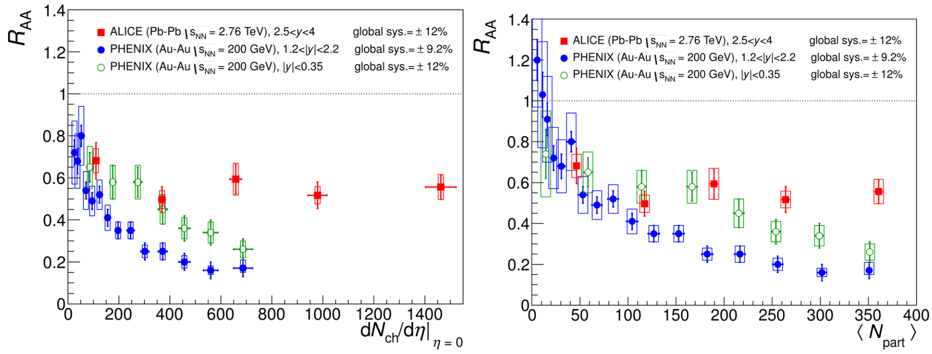

Figure 1.22: Inclusive J/ψ R_{AA} as a function of the mid-rapidity charged-particle density (left) and the number of participating nucleons (right) measured in Pb-Pb collisions at $\sqrt{s_{NN}}$ = 2.76 TeV compared to PHENIX results in Au-Au collisions at $\sqrt{s_{NN}}$ = 200 GeV at mid-rapidity and forward rapidity.

1.3.3 Summary

In this part, we summarize a few probes of the medium: Quark Gluon Plasma. We have many probes that can give us information about QGP. We classify these probes in two cases: soft probes and hard probes. Hard probes are obtained from harder scatterings with larger transverse momenta or higher p_T of particles.

With soft probes, we generally find information about the temperature, density or collectivity effect of the QGP. Photons are excellent probes because they can give us information on each step of the heavy ions collisions. We found a lot of proper characteristics of QGP like the baryon enhancement or the anisotropic flow. We can estimate also the energy density of the QGP with the measurements of transverse energy.

Generally, hard probes are created via hard scatterings at the beginning of the heavy ions collisions. We have information about the medium because the probes traverse it. Quarkonia give us information about color screening and the size of the QGP by (example) measurement of their nuclear modification factor. The nuclear modification factor R_{AA} tells us explicitely if we create a medium or not. Jet Quenching can give us the magnitude of energy loss. This is a characteristic of the density of the medium, the mean free path traveled, the energy and type of particle in question. We can also study the geometry of the medium with hard probes.

Now that we know how we can study the QGP, how we generate some energy to use these tools or probes at RHIC, or LHC, we will see in the following section complex accelerators and what we want to study exactly at different energies.

1.4 Physics on particle accelerators

We are using particle accelerators since a long time ago. Van de Graaf, during 1929, created a generator called by his name [110], that was the started point to create particle accelerators.

Particle accelerators have many applications in nuclear physics, medical field or military domain. Outside the research, we can use particle accelerators for: sterilization, electronic, medical imaging, radiotherapy etc ... In research, we use particle accelerators to: study the elementary matter, in material physics, chemistry, biology, condensed matter, nuclear physics, atomic physics etc ... In particles physics, we use a lot of variables and we have proper languages to explain the matter, we start by explaining it in this section.

1.4.1 Kinematics in accelerators

To understand the kinematics in particle accelerators, we generally use different variables. I will present those that will be important to understand all results of this Ph.D thesis or experimental data.

Transverse Momentum

The transverse momentum (p_T) is the component of momentum transverse (i.e. perpendicular) to the beam line. We can define the p_T mathematically by:

$$p_T = p\cos\theta \mathrel{\widehat{=}} \sqrt{p_x^2 + p_y^2} \tag{1.4.1}$$

With p the momentum of the particle and θ its azimuthal scattering angle.

When particles whose momenta are very far from the beam line direction, we say that we have a hard collision. This is a high p_T event. The reason of the importance of p_T is because each collision event is a short distance collision and because it is Lorentz invariant with respect of all frame. We can calculate characteristics of the collisions using the pQCD.

Rapidity and Pseudorapidity

Before defining the rapidity and the pseudorapidity, it is more common to define the light cone. No particle can travel faster than the speed of light. One can describe this property by a light cone. The light cone is inside a space time reference and each point of the space time describes all enable trajectories of particles. We can define the light cone schematically as follows:

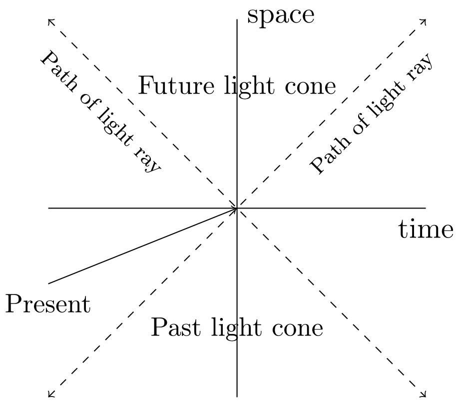

Figure 1.23: Schematic representation of the light cone

We use time coordinates on the light cone x^+ and x^- and spatial coordinate $x_\perp$. With Minkowski's coordinates, coordinates of light cone can be defined like:

$x^0 = t$	$x^1 = x$	$x^2 = y$	$x^3 = z$	Minkowski's coordinates
$x^+ = x^0 + x^3$	$x^- = x^0 - x^3$	$x_\perp = [x^1, x^2]$		light cone coordinates

The notion of **rapidity** can be established when we consider a Lorentz boost within the coordinates of light cone. We can use the rapidity to measure the velocity of a particle in the following way:

$$y = tanh^{-1}\, v$$

We generally use this parameter because it is additive under Lorentz transformation. However, experimental particle physicists often use a modified definition of rapidity relative to a beam axis:

$$y = tanh^{-1}\frac{|p|}{E} = \frac{1}{2}\ln\left(\frac{E+|p|}{E-|p|}\right) \approx \frac{1}{2}\ln\left(\frac{E+|p_z|\times c}{E-|p_z|\times c}\right) \tag{1.4.2}$$

This is the rapidity of the boost along the beam axis which takes an observer from the lab frame to a frame in which the particle moves only perpendicular to the beam. Subsequently, we define the **pseudorapidity** by:

$$\eta = -\ln\left(\tan\frac{\theta}{2}\right) \tag{1.4.3}$$

With θ the angle between the momentum of the particle and the beam. We can define the pseudorapidty in terms of momentum by:

$$\eta = \frac{1}{2}\ln\left(\frac{|p| + p_z}{|p| - p_z}\right) \tag{1.4.4}$$

The pseudorapidity is often used in experimental particle physics because it is easily measured and we can describe the angle of one particle by its pseudorapidity with the following equation:

$$\eta = -\ln\left[\tan\left(\frac{\theta}{2}\right)\right] \tag{1.4.5}$$

where θ is the the angle between the momentum and the beam. When the polar angle approaches zero (particles almost in the beam direction) the pseudorapidity tends toward infinity, while as the polar angle approaches 90 degrees (particles transverse to the beam) the pseudorapidity goes to zero. The region where pseudorapidity is around zero is commonly referred to midrapidity.

Centrality and impact parameter

What about the centrality of collisions? We often speak of centrality or impact parameter in a collision but what is it? We can explain easily what it is with the Fig 1.24. In this picture, we have two circles, each one represents one particle. The distance between the center of each particle is represented by b: **the impact parameter**. One characterizes every heavy ion collision by its degree of centrality or by its impact parameter. A central collision has a small impact parameter. A peripheral collision has a large impact parameter.

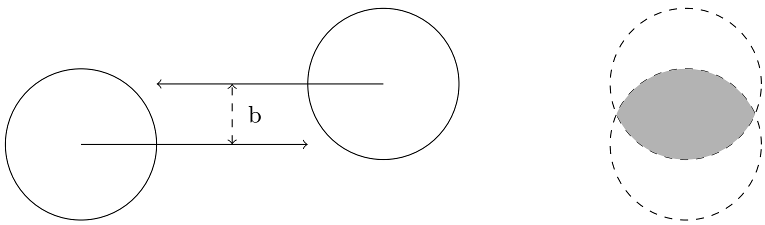

Figure 1.24: Representation of particles collision

We generally use the average multiplicity[12] to estimate the centrality of a collision[13]. Indeed, a central collision produces more particles than a peripheral collision due to a larger overlap region (in gray in the Fig 1.24) with a little impact parameter. Later, we will talk about centrality in percentile, when the collision is the most central, we say that the centrality is equal to 0-5 %.

[12]number of particles detected in an event or collision
[13]We use the Glauber model to estimate the centrality of a collision.

Luminosity

When we want to characterize the performance of a particle accelerator, we usually use the beam energy and the luminosity. The energy available for the production of new effects is one of the most important parameters in particle physics experiments. To have the most new effects, we require large center of mass energies even if this include a larger lost energy. Then, we want to have the most useful interactions or events. When we want to produce Higgs bosons or other rare events, we must optimize the energy and the number of interactions.

The ability of a particles accelerator to produce a number of interactions is called the **luminosity**. The luminosity is characterized by the number of events per second $\frac{dN}{dt}$ and the cross section[14] σ:

$$\frac{dN}{dt} = \mathcal{L} \times \sigma \tag{1.4.6}$$

N is the number of events and σ is the cross section of studied reaction. The unit of luminosity is in cm^{-2} s^{-1}. Simply, we say that the luminosity gives a measure of how many collisions are happening in a particle accelerator.

We cannot observe the same particle physics with different luminosities or beam energies. In this thesis, we want to reconstruct a very large number of anisotropic flow results at wide range of energy obtained by different detectors. Consequently, I will present these different detectors and results that we can find at different energies.

1.4.2 Very high energies

When we talk about very high energy with particle accelerators, we think directly about the Large Hadron Collider (LHC). This is the largest and most powerful particles accelerator ever built in the world. It is currently operating, since 2009 and it is the latest addition to CERN's accelerator complex [111–114]. It is situated at CERN (Geneva in Switzerland), 175m underground at its deepest point, and it is 27 km long. The accelerator complex is a succession of machines that accelerate particles to increasingly higher energies see Fig 1.25 and is designed with eight interaction points. This whole complex contributes to letting the beams reach the desired energy for each collisions. As it has been said, the LHC is a ring of 27 kilometers, it contains superconducting magnets with a number of accelerating structures to boost the energy of the particles all along the LHC. The LHC consists of three main components: the beam pipes to hold particles, the accelerators to move them and the magnet system to manage the direction of them. Of course, the beam pipes must be kept at ultra high vacuum to not get contamination and particle beams travel in opposite direction to the beam pipes at velocities very close to the speed of light until they collide.

In LHC, we collide two types of particles: protons or nuclei (lead of xenon for example). We start by extracting the protons from a hydrogen bottle by an electric field, then we accelerate these by linear machines and boosters. After all linear machines, the protons are accelerated up to 25 GeV by the Proton Synchrotron (PS), then 450 GeV by SPS before coming to final stage: the LHC. To do Pb-Pb collisions at the LHC, we purify lead ions which are heated to over 500 ° Celsius. All ions are accelerated in different accelerators up to 72 MeV per nucleon in the Lower Energy Ion Ring, up to 5.9 GeV per

[14]this is the quantity to express the likelihood of an interaction event

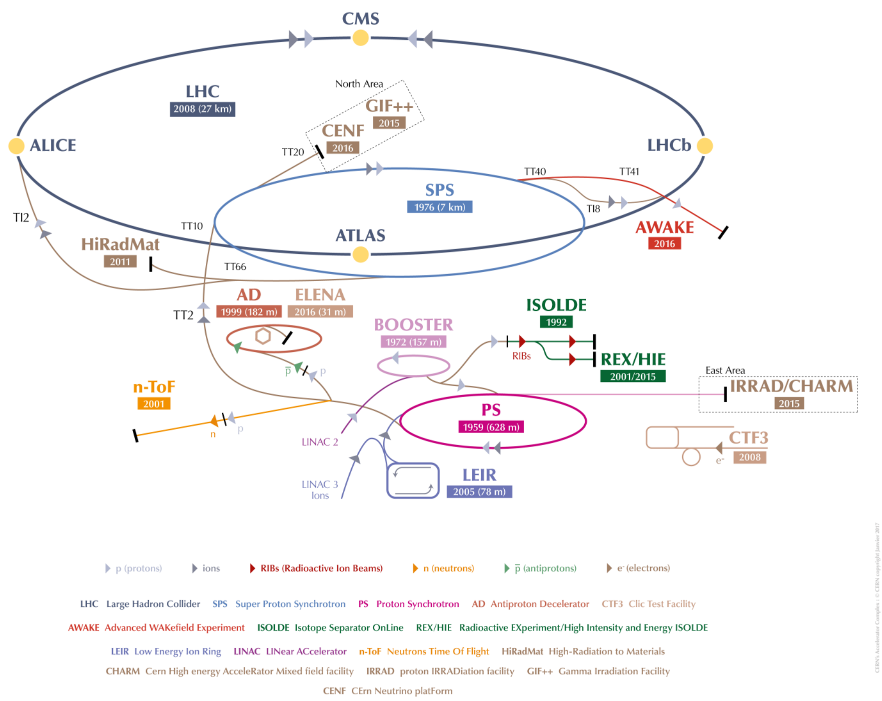

Figure 1.25: The CERN accelerator complex

nucleon in the PS, then up to 177 GeV per nucleon by SPS before the final stage: the LHC.

We have now two high energy particles beams which travel in opposite directions in separate ultra high vacuum beam pipes with the required energy. The beam collide in four interaction points in the LHC, where four particles detectors are located: A Toroidal LHC ApparatuS (ATLAS) [115], Compact Muon Solenoid (CMS) [116], A Large Ion Collider Experiment (ALICE) [117] and Large Hadron Collider beauty (LHCb) [118].

The main physics goals of the LHC is the discovery of the Higgs boson (done!), searches of the matter anti-matter asymmetry, of course QGP studies and searches for supersymmetric particles. To try to discover all of the goals, each detector has special abilities.

I will talk in detail about ALICE, ATLAS and CMS because they can give us results about the medium of this Ph.D Thesis: the QGP. But I cannot forget LHCb. The Large Hadron Collider beauty (LHCb) is created for the study of the matter anti-matter asymmetry, by measuring particles containing a beauty/bottom quark. This is not a cylindric detector unlike other ones, all LHC subdetectors are mainly situated in the forward direction to detect forward particles. We will not work on heavy quark physics in this Ph.D Thesis, consequently, even if this detector is also extraordinary to detect beauty particles, we will not talk a lot about it.

ALICE experiment

ALICE is the acronym of **A** **L**arge **I**on **C**ollider **E**xperiment. ALICE comprises approximately 1500 physicists and engineers from 154 universities and laboratories in 37 countries . This is a detector dedicated to the study of heavy ion resonances. The main goal of ALICE is to study the physics of the QGP by studying strongly interacting matter in ultra relativistic heavy ions collisions at extreme values of temperature and energy density. Of course, the detector can also perform measurements in pp and p-Pb collisions to use them as reference data [119].

I show the ALICE detector in the Fig 1.26 taken from [119]. This detector is located 50 m underground and weighs over 10 000 tons, is 16 m wide, 16 m high and 26 m long [119]. All subdetectors of ALICE are optimized to provide high momentum resolution as well as excellent Particle Identification (PID subdetector) over a broad range of momenta. [120]

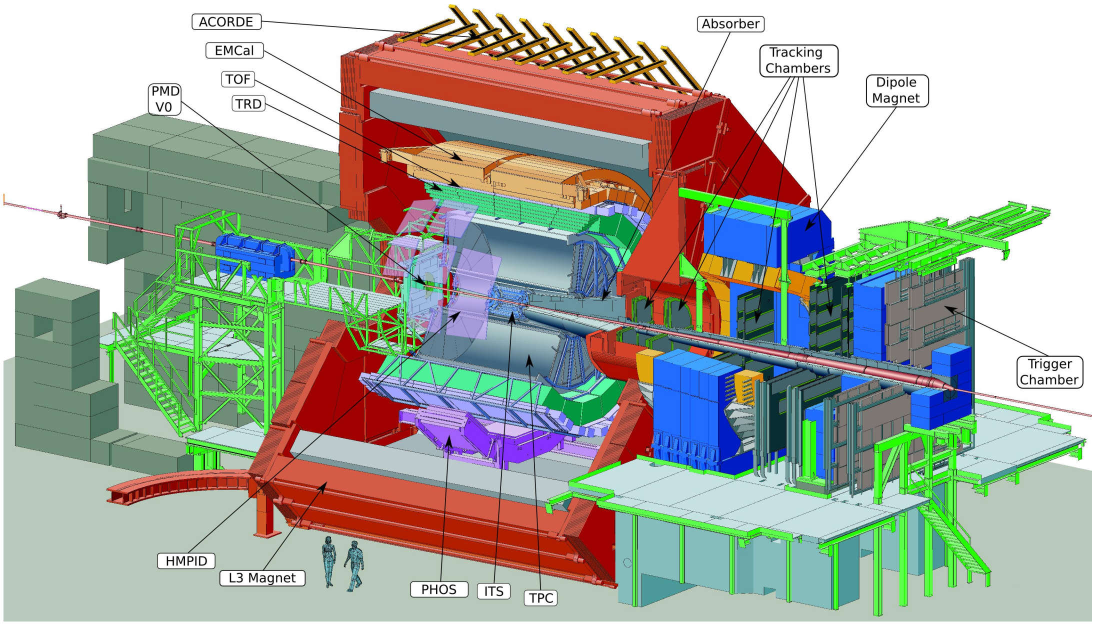

Figure 1.26: Representation of the ALICE detector

To describe the detector, we have three main parts. The central barrel detectors cover $|\eta| < 0.9$. A magnet of 0.5 T surrounds the central detectors. This part of detector is in charge of tracking and identifying charged particles with a lot of subdetectors (TOF, TPC, ITS, TRD, TOF, HMPID) or photons with EMCAL and PHOS. The second main part is global detectors like ZDC, VZERO, TZERO, FMD and PMD, they are forward, central and trigger detectors to provide event characterization like multiplicity, centrality, event plane, luminosity or energy measurements. The last part of the detector is the Muon Spectrometer with a pseudorapidity range of $-4 < \eta < -2.4$ at small angles with dipolar magnetic field of 3 T. This detector provides muon tracking and triggering down to zero transverse momentum.

ATLAS experiment

ATLAS is the acronym of **A** **T**oroidal **L**HC **A**pparatu**S**. ATLAS comprises approximately 3000 physicists and engineers from 182 institutions in 38 countries. It is one of the largest collaborative efforts ever attempted in science. This detector is not really dedicated to one subject in particle physics alone. ATLAS explores a range of physics topics like: study of elementary particles, researches about the antimatter, detection of dark matter, study of the QGP, researches about new physics and supersymmetric particles or anything else.

I show the ATLAS detector in the Fig 1.27 which was taken from [121]. This detector is also 100 m underground and weighs over 7 000 tons, is 46m long and has a diameter of 25m [122]. The ATLAS detector has a large superconducting toroidal magnet. The detector, like ALICE and CMS, surrounds entirely the collision point with an enclosed detector. It is not really specific with regard to one topic in physics alone. Rather, it is created and studied to investigate a wide range of physics.

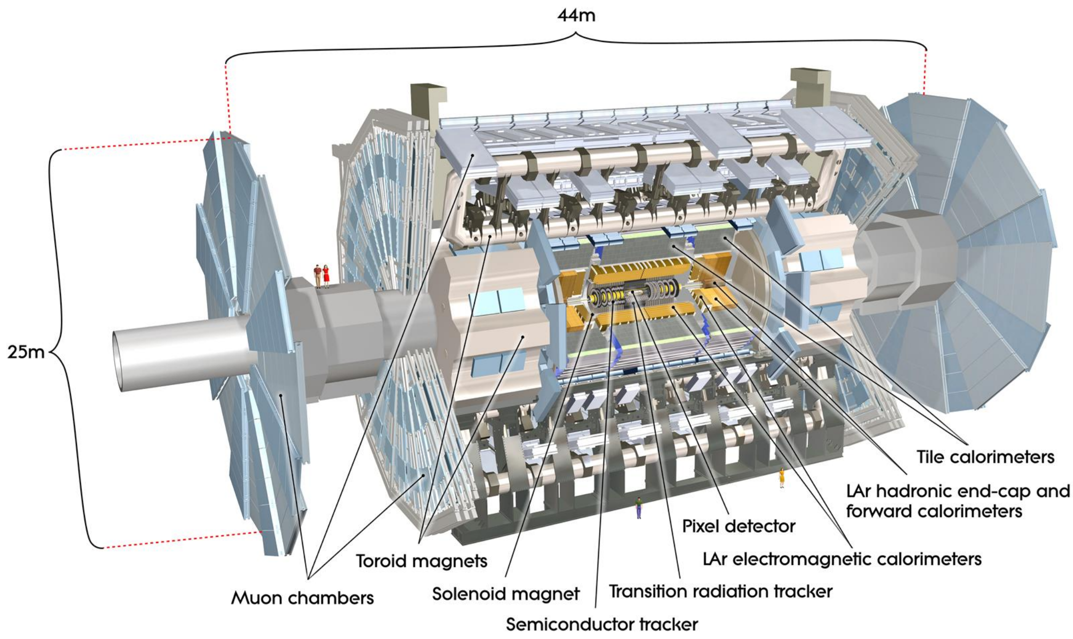

Figure 1.27: Representation of the ATLAS detector

The ATLAS detector consists of four main parts: the inner detector, calorimeter, muon spectrometer and the magnet system. The inner tracking system covers the pseudorapidity range $|\eta| < 2.5$, and consists of a silicon pixel detector, a silicon microstrip detector, and, for $|\eta| < 2.0$, a transition radiation tracker. A magnetic field of 2 T surrounds the inner detector along the beam detector. We detect charged particles (like protons, electrons or muons etc ...) in the inner detector. All electromagnetic particles and hadrons are stopped in the calorimeter unless muons. The calorimeter system covers the pseudorapidity range of $|\eta| < 4.9$. We identify muons and measure their momentum with muon spectrometer. The muon spectrometer tracks muon for $|\eta| < 2.7$

CMS experiment

CMS is the acronym of the **C**ompact **M**uon **S**olenoid. CMS comprises approximately 4000 physicists and engineers from around 200 institutions from more than 40 countries. It is the second general purpose detector at the LHC. This detector is also not really dedicated to one particularity of the particle physics (like the QGP for ALICE). It is also an enclosed detector. Finally, it has the same physics goals as the ATLAS experiment like: study of elementary particles, researches about the antimatter, detection of dark matter, study of the QGP and researches about physics Beyond the Standard Model like supersymmetric particles or anything else.

I show the CMS detector in the Fig 1.28 which was taken from [123]. This detector is 100 m underground and weighs over 14 000 tons, takes 21 m long, 15 m wide and 15 m in height. It is twice smaller than ATLAS.

The CMS detector is designed to detect muons very accurately and it has the most powerful solenoid magnet ever made. The CMS detector surrounds entirely the collision point with an enclosed detector.

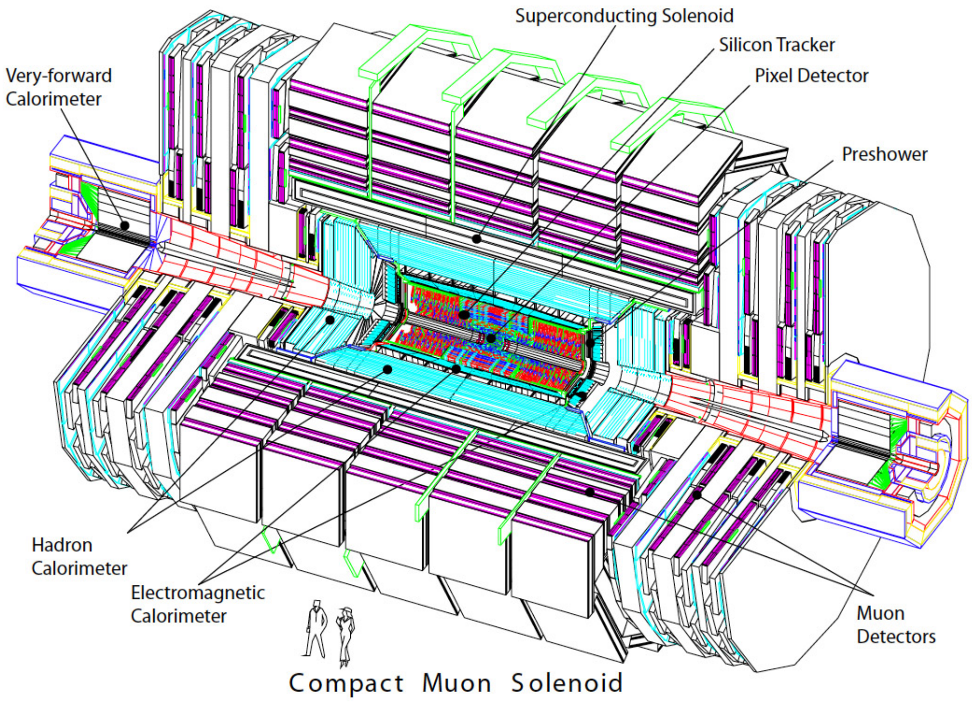

Figure 1.28: Representation of the CMS detector

The CMS detector consists of five main parts: tracking system, electromagnetic calorimeter, hadronic calorimeter, superconducting solenoid and the muon system. The different subdetectors except the muon system are arranged in an onion structure. The tracking system is designed to reconstruct charged particles close to the interaction point. The tracker system covers the pseudorapidity range $|\eta| < 2.5$. All the electromagnetic calorimeters cover the pseudorapidity range $|\eta| < 3$. The electromagnetic calorimeter is designed to measure photons and electrons with a very high precision. The hadronic calorimeter surrounds the electronic calorimeter, consequently, it covers the pseudorapidity range $|\eta| < 3$. It is designed to measure the energy of strong particles like quarks, gluons and neutrinos by measuring the direction of particle jets and missing transverse energy. We measure hadronic particles with the hadronic calorimeter. We can easily measure muons with the muon system detector. This muon system covers the pseudorapidity range $|\eta| < 2.4$.

We can conclude by the fact that each detector in LHC is a great experiment. With all detectors, we can try to understand a very wide range of particle physics. We can better understand the physics around partons with the creation of QGP, we can try to create the dark matter by very high density and very high energy collisions, we try to find new particles Beyond the Standard Model and many things in particle physics. We had already discovered the Higgs bosons with CMS and ATLAS together and we must find other exciting results. The interest observable if this thesis is the anisotropic flow in my Ph.D Thesis and these three detectors can provide a lot of results that we can try to reproduce with our own event generator. During all this thesis, I will show results of these three detectors.

1.4.3 Beam Energy Scan energies

One of the main goals of my Ph.D work is to try to understand the energy and system size dependence of the formation of a Quark Gluon Plasma. To understand the energy dependence, we investigate the BES program and want to reproduce its data and conclusion for the particle physics.

A major goal of heavy ions collisions is to determine the whole phase diagram for matter that interacts via strong nuclear force. In the section 1.2.3 with the Fig 1.5, we talk about the phase diagram. The Lattice QCD tells us that we have the quark-hadron transition at the temperature around 154 MeV for $\mu_B = 0$ [124–126]. Other QCD models predict a first-order transition and the existence of the critical point at high μ_B [127, 128]. However, the locations of the phase boundary and the exact localisation of the critical point are not verified experimentally. We access properties of the matter by studying its evolution, which undergoes phase transitions. By means of the LHC and RHIC experiments, we explore this diagram by raising the Temperature of the matter and keeping close to $\mu_B = 0$. We want to verify the first order transition at higher μ_B.

In order to study experimentally the phase diagram as a function of the temperature and the density, the proposed solution is a scan over beam energies. This is the Beam Energy Scan used at RHIC, we can see a representation of each collision in the phase diagram in the Fig 1.29 taken from [129]. We do several collisions at different energies to create systems with different T and μ_B. The goal is to reduce the temperature and grow the density. We hope to find the critical point or the first-order phase transition by creating systems in a wide range of energy.

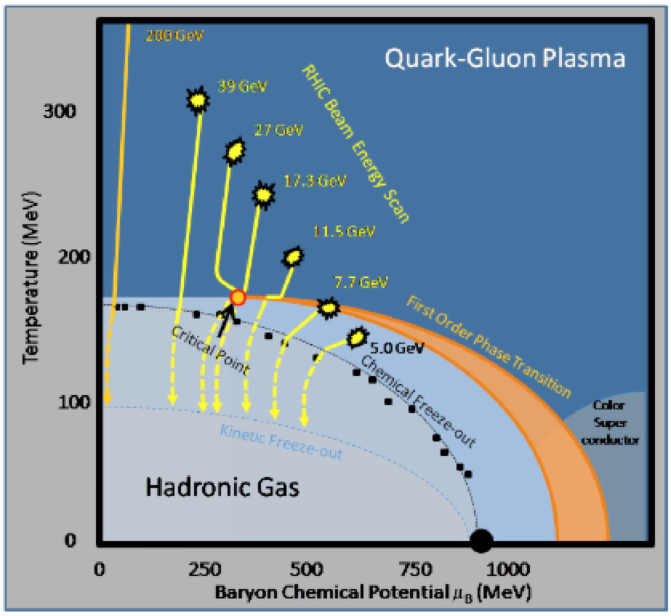

Figure 1.29: Phase diagram of the BES program

We can say that the BES program has three main goals:

1. Can we see evidence of a Critical Point (CP)?
2. Can we see evidence of a phase transition?
3. What is the evolution with $\sqrt{s_{NN}}$ of the medium that we produce? i.e. how do the results that indicate the presence of the sQGP turn off as $\sqrt{s_{NN}}$ is reduced

We can have access to a large range of values of the density μ_B, I summarize all estimations of baryon chemical potential in the following table taken from [130]:

Beam Energy in GeV	Baryon Chemical Potential in MeV	Year of Data Taking	Event Statistics in Millions	Beam Time in Weeks
200	20	2010	350	11
62.4	70	2010	67	1.5
39	115	2010	130	2.0
27	155	2011	70	1.0
19.6	205	2011	36	1.5
14.5	260	2014	20	3.0
11.5	315	2010	12	2.0
7.7	420	2010	4	4.0

Table 1.3: Overview of Baryon Chemical estimation with the BES program

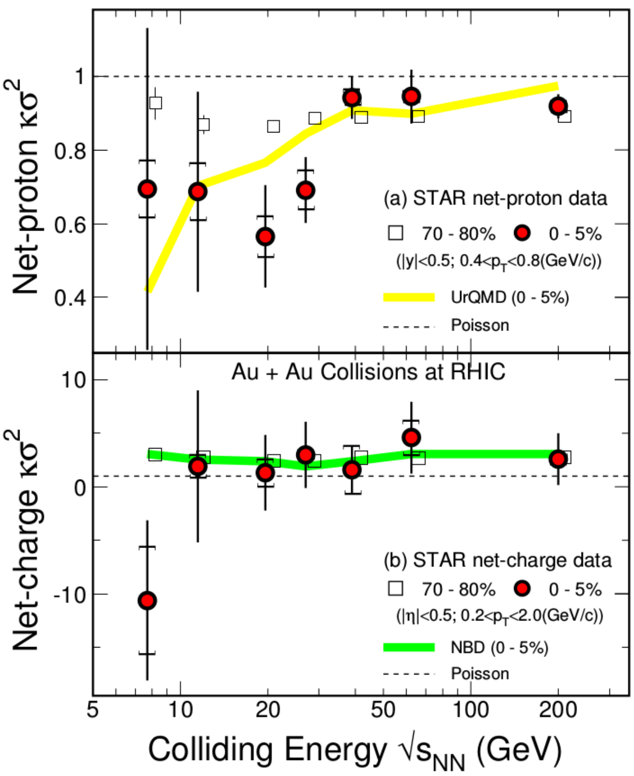

Figure 1.30: Collision energy dependence of net-proton (top panel) [131] and net-charge (bottom panel) [132] $\kappa\sigma^2$ from Au+Au collisions at RHIC.

Search for the Critical Point: We search the critical point of the QCD matter because some thermodynamic principles suggest us that we have a point where the first order phase transition ends and the transition becomes a crossover [124, 133]. One of the experimental signature of the QCD critical point is a large fluctuation in event-by-event multiplicity distribution of conserved quantities like net-charge, net-baryon number ...

STAR in the BES program has studied the kurtosis times and variance ($\kappa\sigma^2$) of net-proton (approximatively the same thing from net-baryon) and net-charge distributions to search the critical point [131, 134]. Some hadron resonance gas models [135] suggest that $\kappa\sigma^2$ must be close to unity in the absence of a critical point.

All measures of $\kappa\sigma^2$ for net-proton and net-charge distributions in Au+Au collisions at midrapidity as a function of colliding energy for two different collision centralities are shown in Fig 1.30. In this figure, the red solid circles correspond to 0-5% central collisions and the open squares represent 70-80% peripheral collisions. The vertical error bars are statistical and the caps correspond to systematic errors. The yellow solid band in the top panel represents 0-5% central Au+Au collision results from UrQMD [136] simulations and the green solid band in the bottom panel is the result where proton and anti-proton distributions follow independent negative binomial statistics. The dashed line in each panel represents the expectation from proton and anti-proton distributions following Poisson statistics. For the net-proton $\kappa\sigma^2$ values for the 0-5% for $\sqrt{s_{NN}} = 19.6$ and 27 GeV, we observe a big deviation from: (a) the values from 70-80% peripheral collisions, that do not show significant bulk properties, (b) the Poisson and hadron resonance gas expectations values close to unity, (c) the transport model UrQMD [136] calculations which do not experience a phase transition. We can say that we have a transition in this range of energy but the large uncertainties preclude a clear definition. We must have more statistics for the next BES program: the BES program II.

Search for the First-order Phase Transition: What is a first-order phase transition? Generally, we say that we have this order of transition when we obtain a discontinuity in one of the state variables. Another characteristic is the presence of an unstable coexistence region. Normally, this region will exhibit a change in compressibility, i.e. a softening of the Equation of State (EoS). Experimentally, to see the softening of the EoS, we measure the directed flow (first coefficient of Fourier decomposition of anisotropy in respect to the reaction plane see 1.3.1) versus beam energy [137, 138]. The results are given by the Fig. 1.31 take on [139] . In this figure, panels (a), (b), and (c) report STAR's measurement for antiprotons, protons, and net-protons, respectively, along with corresponding calculations from the UrQMD hadronic transport model [136] subject to the same cuts and fit conditions. The systematic uncertainties of the measurements are shown as shaded bars. The dashed curves are a smooth fit to guide the eye.

The proton and net proton slopes decrease with energy between 7.7 and 11.5 GeV. The minima are approximatively at 19.6 Gev and the value of the slope of directed flow keeps negative up to 200 GeV. All results of the UrQMD hadronic transport model [136] do not show the same behavior as data. An interpreation of the changing sign can be a change in EoS. Maybe the medium undergoes a first-order parton-hadron phase transition. The program BES motivates to have a lot of precise measurements at $\sqrt{s_{NN}} < 20$ GeV where we can have a transition of the EoS.

The other possible signature of the first-order phase transition is a saturation of the average transverse momentum as a function of collision energy. That is a signature by the relation of temperature and entropy to the average transverse momentum and multiplicity. The signature was proposed by Van Hove in the context of proton-proton collisions [140]. The formation of a mixed phase of QGP and hadrons can be represented by a plateau in the average transverse momentum beyond a certain value of multiplicity. This plateau is described by a first order phase transition scenario.

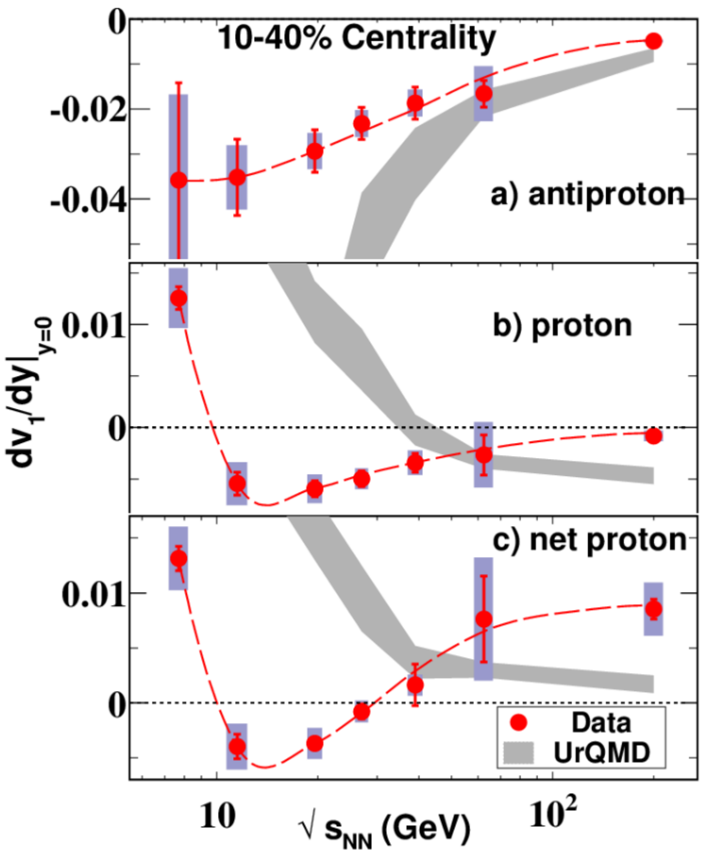

Figure 1.31: Directed flow slope (dv_1 /dy) near mid-rapidity as a function of beam energy for intermediate-centrality (10-40%) Au+Au collisions.

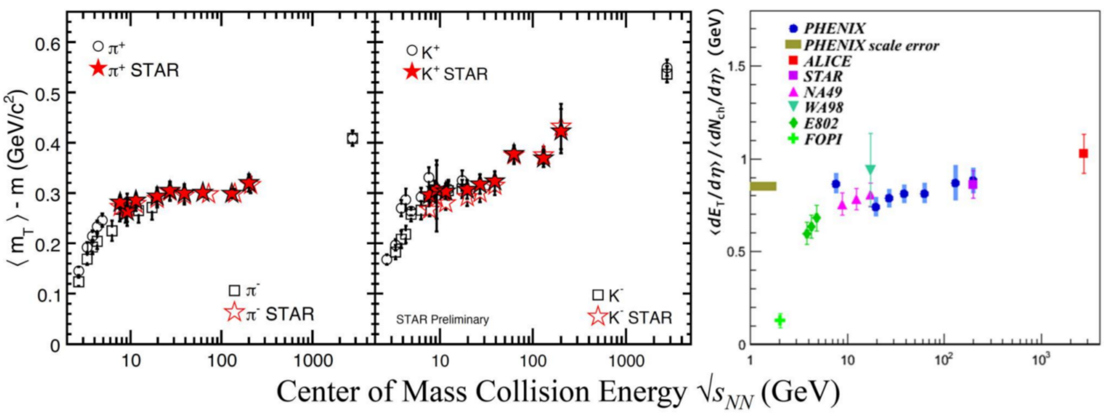

Figure 1.32: Left Panel: Center-of-mass energy dependence of $\langle m_T \rangle - m$ of π and K, in central Au+Au collisions at midrapidity at RHIC and previous experiments. Right panel: The average transverse energy, scaled by the charged particle multiplicity at mid-rapidity, as a function of collision energy observed by the PHENIX and other experiments

I showed in the Fig 1.32 of [139] the dependence of $\langle m_T \rangle - m$ for different particles in central Au-Au collisions at midrapidity at RHIC and AGS [141–146], SPS [147], and LHC [148]. The errors shown are the quadrature sum of statistical and systematic uncertainties. In the Right panel: The average transverse energy, scaled by the charged particle multiplicity at mid-rapidity is shown as a function of collision energy observed by the PHENIX, ALICE, STAR, NA49, WA98, E802, and FOPI Collaborations. We can interpret the $\langle m_T \rangle - m$ like a measure of thermal excitation in the transverse direction. The $\langle m_T \rangle - m$ value increases with $\sqrt{s_{NN}}$ at AGS energies, we must have a plateau for SPS and higher beam energies like RHIC and LHC. We can interpret this result like a characteristic signature of a first order transition of Van Hove [140]. We can see a saturation in $\langle E_T \rangle$ and $\langle m_T \rangle - m$ even if the absolute values of $\langle E_T \rangle$ are much larger.

I explained some researches of the BES program in this section, to explore the range of energy of the BES program, we must present experiments at RHIC energies. I will not introduce all detectors in details in the next sections. I will introduce only the two main detectors which gave us a lot of results that we can try to reproduce with EPOS.

The Relativistic Heavy Ion Collider

We often talk about the Large Hadron Collider, but we do not forget the second most powerful particle accelerator built in the world: The Relativistic Heavy Ion Collider (RHIC). Same as the LHC, this particles accelerator is composed of a succession of machines that accelerate particles to inscreasingly higher energies, see Fig 1.33. It has now been collecting a lot of data for 17 years and it is the first machine which can collide heavy ions at relativistic energies (due its name) and dedicated to study the matter at extreme densities and temperatures. The RHIC is located at Brookhaven National Laboratory on Long Island in New York. The RHIC is a 3.83-kilometer ring in circumference and is designed with six interaction points. The RHIC consists of three main components: the beam pipes to hold particles, the accelerator to move them and the magnet system to manage the direction of them. The beam pipe must be kept at ultra high vacuum to not get contamination and particles beams travel in opposite direction all beam pipes at velocity close to the speed of light until they collide [36].

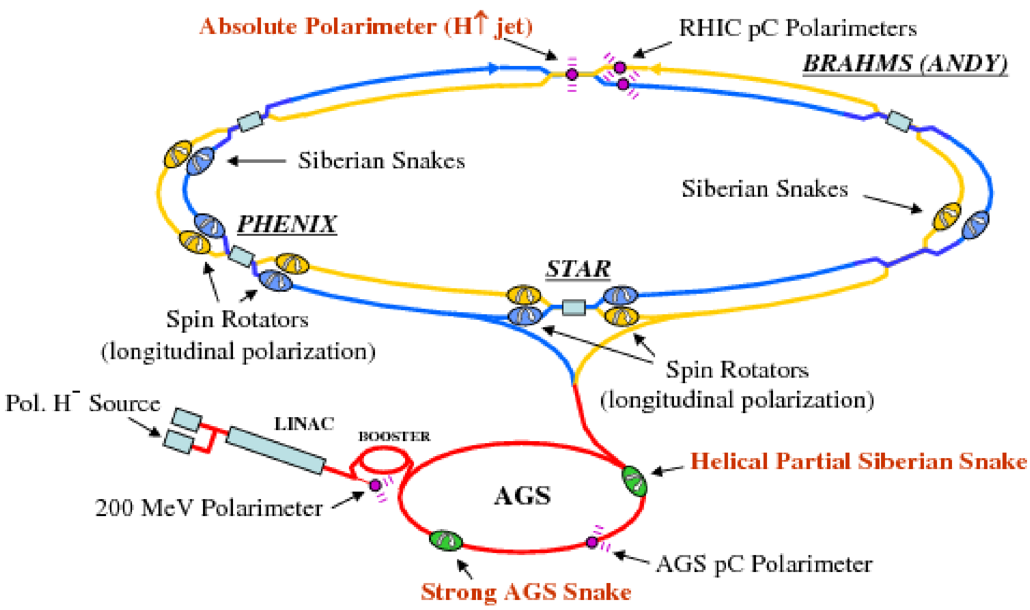

Figure 1.33: RHIC accelerator complex

In the RHIC accelerator, a large number of nuclei are used to do collisions in a wide range of energy. We collide gold, uranium, proton, copper, deuterons, tritons at 7.7 (for copper+copper or gold+gold) GeV at 500 GeV (for protons+protons). We start by accelerating particles with the Tandem Van de Graaff facility from hydrogen to uranium. At this point, particles are travelling at about 5% of the speed of light. Then, particles are accelerated in linear accelerator up the proton beam energy to 200 MeV. In a next step, we include particles in the Alternating Gradient Synchrotron (AGS). The field gradients of the accelerator is composed of 240 magnets successively alternated inward and outward. Each ions entering in the AGS is travelling at $\approx 35\%$ of the speed of light. In the AGS, the velocity of the ions reaches $\approx 99.7\%$ of the speed of light. When we cannot increase the velocity of particles, the ion beam is diverted into another beam line called the AGS to RHIC transfer line. The final step happens in the RHIC [36].

We have now two high energy particle beams which travel in opposite directions in separate high vacuum beam pipes with the required energy. The collisions are done in six interaction points in the RHIC, where four detectors are located: Broad RAnge Hadron Magnetic Spectrometers (BRAHMS) [149], Pioneering High Energy Nuclear Interaction eXperiment (PHENIX) [150], PHOBOS[15] [151] and Solenoidal Tracker At RHIC (STAR) [152]. BRAHMS, PHENIX and PHOBOS are decommissioned and STAR is the last experiment being conducted.

The main physics goals of the RHIC is the creation of the QGP (done!). But all information at RHIC can be applied to nuclear physics like the study of atomic nuclei, particle physics with the study of the partons, also astrophysics with the study of stars and planets, then with the study of condensed matter physics and finally in cosmology with the study of the universe [36].

I will talk in detail about PHENIX and STAR because they can give us results about the QGP for this Ph.D Thesis. But I give some description here of PHOBOS and BRAHMS. To start, PHOBOS is created to study the QCD confinement and vacuum. This detector is designed to examine and analyze a large number of gold-gold collisions. We can have access of the global picture of the consequences of the collision and detailed information about the nuclear fragments ejected from the collision. The PHOBOS detector is a succession of many silicon detectors surrounding the interaction region. We can have access to the temperature, the size and the density of the medium produced in the collision. We can also study the ratios of the particles produced and study the phase transition of the QGP [151]. The BRAHMS experiment was designed to measure charged hadrons over a wide range of rapidity and transverse momentum to study the reaction mechanisms of the relativistic heavy ion reactions at RHIC and the properties of the highly excited nuclear matter formed in these reactions. The experiment took its first data during the 2000 year run and completed data-taking in June 2006.

Phenix experiment

PHENIX is the acronym of **P**ioneering **H**igh **E**nergy **N**uclear **I**nteraction e**X**periment. This detector comprises around 500 members from 69 institutions in 14 countries. It is the largest of the four experiments that have taken data at the RHIC. This detector is an experiment dedicated to the investigation of high energy collisions of heavy ions

[15] Not an acronym. Phobos is a moon of Mars

and protons. Like ALICE of LHC, PHENIX is designed to discover and study the QGP. It detects direct probes of the collisions such as electrons, muons, photons and hadrons. Because photons and leptons are not affected by the strong interaction, they are unmodified during the collisions but they can be produced in each step of the collisions (further information of QGP probes for photons in the section 1.3.1). Of course, the detector can also perform measurements when light particles collide [150].

I show the PHENIX detector in the Fig 1.34 taken from [153]. This detector is bigger than a house with 40 feet wide and four stores high, it weighs over 3000 tons [150]. The PHENIX detector do not surrounds entirely the collision point with an enclosed detector. It is two spectrometer arms than only cover about 180 degrees combined.

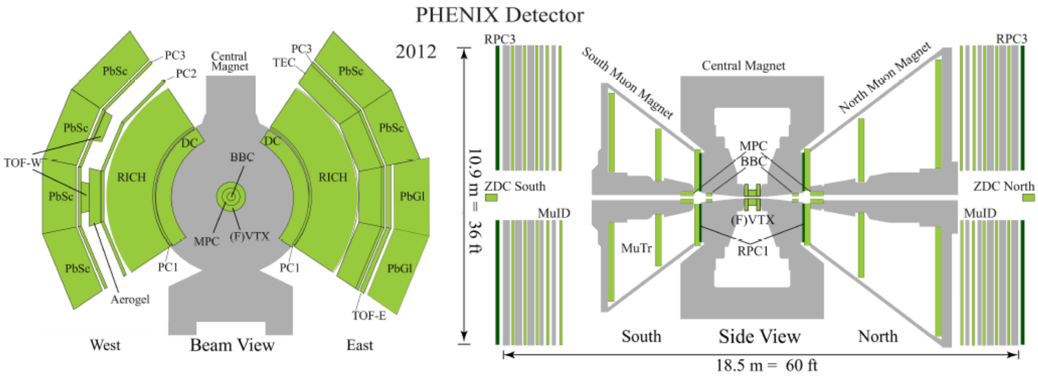

Figure 1.34: Representation of the PHENIX detector

The PHENIX experiments consist of several subsystems which can be classified in three categories: global detectors, central arms and muons arms, it is composed of four instrumented spectrometers and three beam detectors. The global detectors measure time and position of primary vertex of Au+Au collisions and the multiplicity of the events. The two central arms are capable of measuring identified particles like pions, protons and kaons etc ... These arms cover a rapidity range of: $|y| < 0.35$ and cover an azimuthal angle of 90 °. Like ALICE in LHC, the two muon arms focus on the measurement of muon particles. They cover a full azimuthal angle and are positioned at forward positions. The north arms cover a pseudorapidity range of $1.1 < \eta < 2.4$ and the south arm cover a pseudorapidity range of $-1.1 < \eta < -2.2$.

STAR experiment

STAR is the acronym of **S**olenoidal **T**racker **A**t **R**HIC. STAR comprises over 600 collaborators from 63 institutions inside 13 countries. The main goal of STAR is to study the formation and characteristics of the QGP. This experiment can give us many information of the transition phase of QCD by the researches of the program BES [152].

I show the STAR detector in the Fig 1.35 take from [154]. This detector is specialized in tracking particles produced in ions collisions at RHIC. It weighs 1 200 tons and is as large as a house. The detector surrounds entirely the collision point with an enclosed detector.

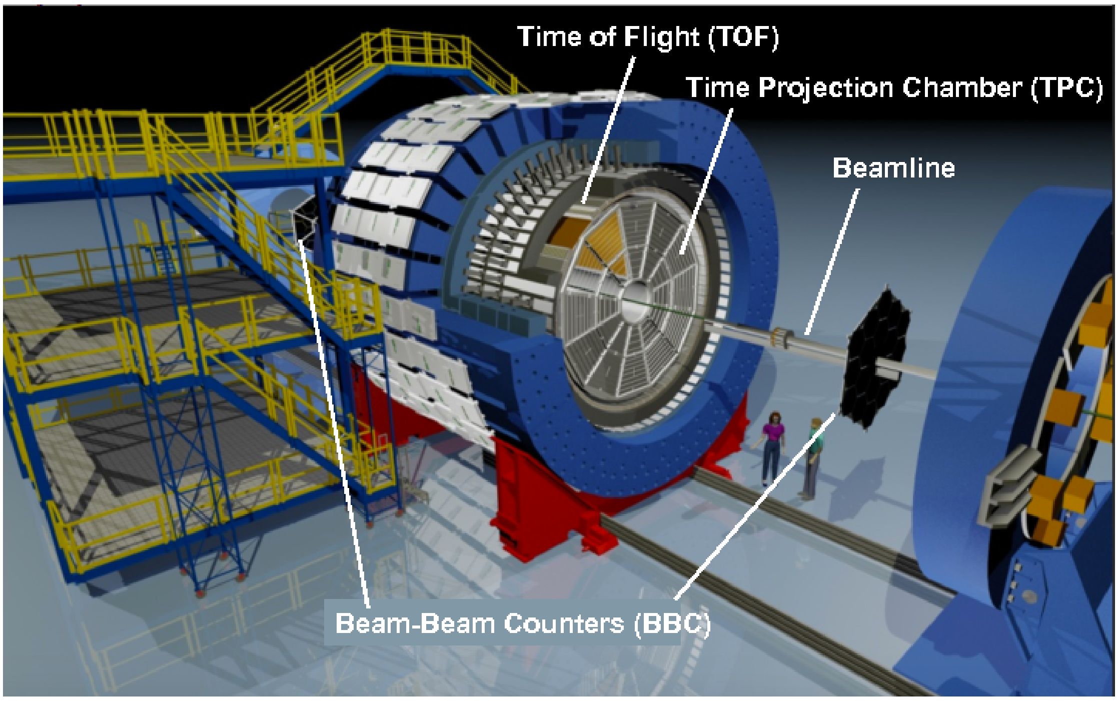

Figure 1.35: Representation of the STAR detector

The main detector of STAR is composed by the Time Projection Chamber (TPC), the Time Of Flight (TOF) and the Electromagnetic Calorimeter (EC). The TPC is the subdetector dedicated to track all charged particles within $|\eta| \leq 1.5$ and covers the full azimuth. It is capable to measure the momentum of charged particles above $p_T \geq 0.1$ GeV/c and can effectuate a first identification of particles via the measurement of energy loss on the subdetector. The TOF can follow all particles within $|\eta| < 0.9$ with full azimuthal coverage. With this subdetector, we can identify the primary vertex positions in collaboration with two Vertex Position Detectors, on either side along the beam line. Using TPC and TOF, STAR can identify particles up to $p_T \leq 3.2$ GeV/c. The last part of subdetectors: the EC, allows fast detection of high energy photons and electrons. It is divided into two components with an acceptance of $|\eta| < 1$ and $1 < \eta < 2$. We have also another subdetector like the Beam-Beam Counters (BBCs) used to put a trigger on events in agreement with the investigated physics.

I have finished with the descriptions of present detectors created to study the QGP or other very interesting physics with particle colliders. But we know that the current colliders will not be powerful enough to understand all the subatomic physics and we must have some ideas for a future collider after the LHC. I will introduce briefly some ideas in the Appendix A.

1.4.4 Summary

I started this part by the most important things to the follow-up of this thesis: some variables that we use with all accelerators. I will talk a lot of times about the transverse momentum: the transverse component of the momentum to the beam line. The rapidity is a way of quantifying how much an outgoing particle has been deflected from the beam direction, the rapidity is zero when a particle is close to transverse to the beam axis. The pseudorapidity is a spatial coordinate describing the angle of a particle relative to the beam axis. Considering that the most central collision is equal to 0-5%. The impact parameter is the distance between the center of each particle, strongly reliable with the centrality. The luminosity is not very important for the rest of this thesis because this is one ability of each experimental detector.

We have two different ranges of energy defined by two different colliders, the LHC and the RHIC. We have some different detectors to measure and identify particles but the analysis are not automatically the same because we want to explore different physics. The very high energy is explored with the LHC with a nominal energy of 13 TeV for a proton-proton collision (for the Run 2) and 5.02 TeV for Lead-Lead collision. The other particle accelerator collider is the RHIC has a lower energy than the LHC but doing also very high energy collisions with a nominal energy of 200 GeV for Gold-Gold collisions.

Another important thing is the program BES, this is one program at RHIC when we try to find evidence of a critical point in the QCD phase diagram, try to find also the phase transition and whether we have an evolution with the energy collision of the QGP.

1.5 Conclusions and Discussions

This is an important chapter because it set up all the context of this thesis. This is really a compulsory part of each Ph.D thesis: explain the context.

My thesis tries to find out ideas about the phase transition of the QCD. We want to see what answers EPOS say to all collisions of the QGP physics into RHIC and LHC. I think that it was important to introduce briefly each detector and important subdetector because I will talk a lot of times about these detectors in the rest of this thesis. To verify the reliability of our event generator, it is important to test it with different system sizes and different energies.

I hope that I have convinced you that the QGP is a very interesting matter, because this a deconfined matter and we can understand a lot of things about our world and understand better the very first time after the Big Bang.

The BES program confirms the interest of researches about the possible critical point of QCD phase transition. This is a very big support for the project of this Ph.D thesis when we want to study (and try to understand) the dependence of energy and system size for the formation of the Quark Gluon Plasma. This is the first time that we study this range of energy, between 7.7 GeV at 62.4 GeV with EPOS.

Maybe now, it is important to explain what is the tool that I have been using during all the thesis and maybe after my Ph.D: EPOS. This is the goal of the next chapter almost exclusively dedicated to this event generator.

CHAPTER 2

PARTICLE PRODUCTION IN THE EVENT GENERATOR EPOS

Contents

The previous chapter explains the physical context of the Ph.D Thesis. This one will present the description of few ways to produce particles in the event generator EPOS. When one talks about event generator, it seems natural to present generalities about them, this is the first section of this Chapter. Contrary to general event generator, EPOS expects to reproduce many aspects of collisions from proton-proton to nucleus-nucleus, including leptons-leptons, the second section will present few differences between EPOS and the other event generators. After the section about the event generator itself, I will present the theory inside EPOS, starting with the Gribov-Regge Theory (GRT) and the parton model. The merge of these two models gives the PBGRT briefly described in the subsection 2.2.4, followed by the description of the string model in EPOS. Finally, I will describe the evolution of EPOS in time thus its history.

2.1 Generalities about event generators

The goal of this section is to explain some generalities about an event generator: what is it? Why do we use an event generator? Who uses an event generator? Then, I will explain the big difference between EPOS and the other theorical models or event generators. I will not compare the results of those models with EPOS because all models do not use the same way to explain the physics of a collision[1]. The equivalence of all results is useless to mention here. Finally, I will introduce the Monte Carlo method which is very used in EPOS but also in general event generator.

2.1.1 What is an event generator?

The most basic thing is that an event generator is an informatic code or software librairies that tries to reproduce the particle production in a particle collision. Consequently, an event generator is a huge tool in subatomic physics, especially in very high energy where one explains the "world" with particle collision.

The goal of a complete event generator is to reproduce the same number of particles produced in an experiment with the same characteristics (anisotropic flow for example). This is a complex challenge but we can reduce the difficulty by choosing a specific collision to reproduce instead of reproducing all collisions like AA or pp collisions[2]. When one creates an event generator, one wants to look at as much data as possible. Another basic thing is the physical nature of an event: **one event is equivalent to one collision**. An event generator is a useful tool because it allows a large flexibility in physical quantities that we can study.

One uses an event generator when we are theorists because we can check our theory directly with data and conclude about different characteristics in particle physics[3]. However, one can use an event generator when we are experimentalists in order to calibrate the detector by studying the detector requirements and imperfections, for example. Consequently, an event generator allows theoretical and experimental studies of complex particle physics. One can treat the event generator like a tool to disseminate ideas from theorists to experimentalists and the other way arround. This is a bridge between theory and experiment.

Experimentally, one can detect only the final particles and one must reconstruct the whole event from these particles from the beginning to the end (initial collisions and final

[1] The EPOS results are not finalised consequently of the other models
[2] not the choice of EPOS
[3] to explain the more general case as possible

particles). This is something interesting but complex. One of the main advantages of an event generator is the fact that one can follow the evolution of a collision from the beginning to the end. Therefore, one can investigate each step of a collision.

Typically the event generator position between an event in the "real life" and in the "virtual reality" can be described with the following way [155]

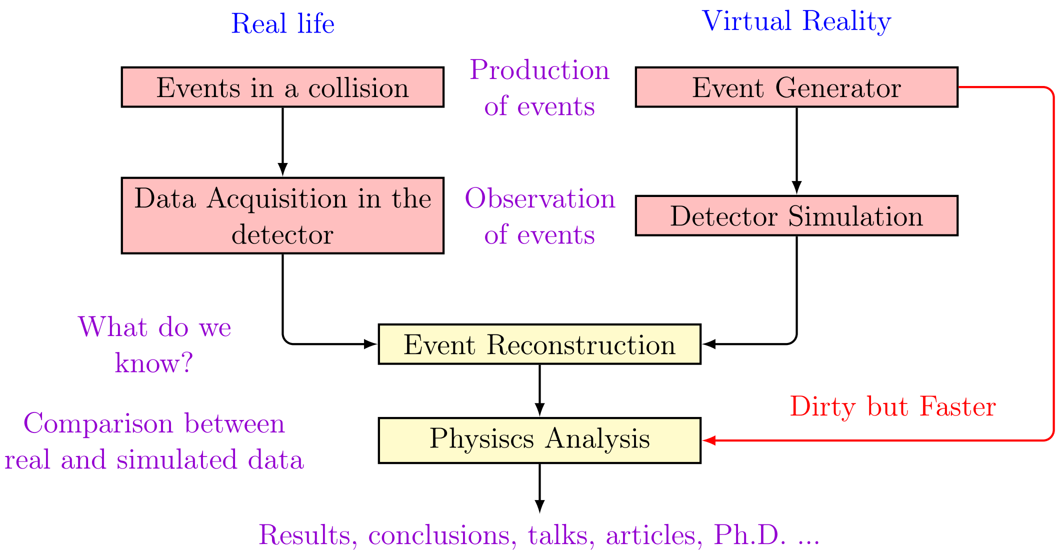

Figure 2.1: How an event generator is usually used in Particle Physics

The last important thing about event generators is that they lie on by the Monte Carlo method and I will explain some generalities about this method in the next section.

2.1.2 Quick introduction about Monte Carlo method

Monte Carlo methods were invented during the development of the atomic bomb in the 1940's and are a class of computational algorithms. Monte Carlo methods consists on repetitif random samplings which provides generally a solution.

Monte Carlo outside particle physics

The Monte Carlo method is very useful in subatomic physics, in particulary when we use an event generator. However one can use the Monte Carlo method in a large number of topics like artificial intelligence for games (recently for the play game: Go [156]), for Finance and business for the risk analysis [157] or to study the climate change [158]!

But what is the Monte Carlo method? Typically the Monte Carlo method is a computational method using randomness to solve a problem that one could not determine the solution by the deterministic way. One of the most famous example about a simple utilisation of the Monte Carlo is to know the superficy of a lake.

In this example, one takes a lake with an unknown superficy or size area. One can know the superficy of the lake by shooting a number of pointlike balls in a known superficy. The higher is the number of balls, the higher will be the accuracy about the superficy of the lake. To know the superficy of the lake, one uses the following equation:

$$S_{\text{lake}} = \frac{N}{X} \times S_{\text{known}} \tag{2.1.1}$$

with N the number of balls in the lake and X the number of balls shot. We can see an illustration of the process in the following figure:

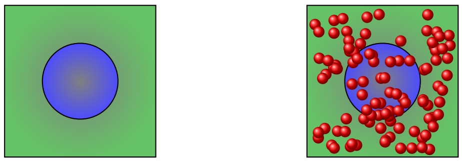

Figure 2.2: Different random shots in a known superficy containing a lake

Overview of the Monte Carlo method

One has the same procedure when a Monte Carlo method is used:

1. One must determine all the statistical properties of the situation, of what we want to calculate;
2. One generates many sets of inputs which follow the previous properties;
3. With each input, one performs a deterministic analysis to have the searched observable;
4. Finally, one must analyze statistically the results.

All statistical errors will decrease when the number of events increases.

For the example of the lake's superficy, one follows this procedure:

1. one has two possibilities, the ball is in the lake or not;
2. one shoots a large number of balls;
3. one uses the equation 2.1.1 to have the lake's superficy;
4. one analyzes the statistical errors of the result.

Generating Distributions

The numerical methods used to construct a Monte Carlo Generator will be briefly explained with an example in the following. The important requirement is the production of points in the phase space that we investigate. One must calculate the density of these points following the probability distribution of the process that we investigate. Ideally, a Monte Carlo uses different random independent variables and identically distributed under the probability distribution.

The generation of a unidimensional variable x distributed in a region $[x_{\min}, x_{\max}]$ with probability distribution proportional to $g(x) \geq 0$ can be done using a uniform random number U in the region $[0, 1]$ as following:

$$\int_{x_{\min}}^{x} g(x')dx' = U \int_{x_{\min}}^{x_{\max}} g(x')dx' \tag{2.1.2}$$

One can estimate the integral of $g(x)$ called $G(x)$, therefore one can solve:

$$G(x) = UG(x_{\max}) + (1 - U)G(x_{\min}) \tag{2.1.3}$$

Now, one just has to know the inverse function G^{-1} to have the generating distribution of x:

$$x = G^{-1}(x) = U \times G^{-1}(x_{\max}) + (1 - U) \times G^{-1}(x_{\min}) \tag{2.1.4}$$

However, the reality is not unidimensional, therefore this is more complicated to generate different variables.

Monte Carlo integration, average and variance

The Monte Carlo method in a multidimensional phase space can be based on the concept of considering an integral as an average. Indeed, one observes that the value of an integral is almost equal as the average of the integrand:

$$I = \int_{x_1}^{x_2} f(x)dx = (x_2 - x_1)\langle f(x)\rangle \tag{2.1.5}$$

The central limit theorem of statistics tells us that if M points are distributed randomly on (x_1, x_2), with unbiased mean value of f on these points reasonable estimator of the integral:

$$I \approx (x_2 - x_1)\frac{1}{M}\sum_{i=1}^{M} f(x_i) \tag{2.1.6}$$

The central limit theorem of statistics works only if M is large enough. Now one powerful aspect of the Monte Carlo method is that the estimated error on this evaluation is given by the variance of f defined as σ:

$$\sigma(f) = \langle (f - \langle f\rangle)^2\rangle \equiv \langle f^2\rangle - \langle f\rangle^2 \Rightarrow \text{Error}(f) = \sqrt{\frac{\sigma(f)}{M-1}} \tag{2.1.7}$$

Consequently, the error of the estimation decreases with the number of points independent of the dimensionality of the integral. Then, developers of Monte Carlo method will play with different tools to reduce the variance of their estimation but I will not explain this game because the purpose of this section is only to introduce few concepts of the Monte Carlo method before applying the utilisation of the Monte Carlo to particle physics. The list of components of Monte Carlo in this Thesis is non-exhaustive, it exists a lot of other characteristics in Monte Carlo like Hit-and-miss, Veto theorem, the problem of pseudo-random number in informatic etc ...

Monte Carlo inside particle physics

Monte Carlo event generators are essential components of almost experimental analysis and are widely used to make theoretical predictions. The Monte Carlo event generator can be used by experimentalists as a *black box* to calculate cross sections or parton distribution function or to treat directly the output data.

A heavy ion or a proton collision is something very complex, one event must contain all the different steps of the collision. The big problem is that one does not know all the components of a collision. Therefore, theorists explain a part of all the steps of a collision by including their theory in the Monte Carlo event generator.

One can decompose the structure of an event into a lot of steps like; i) incoming beams with the parton densities, ii) first hard subprocesses of partons described by matrix elements, iii) some resonance decays correlated with the hard subprocesses, iv) initial state radiation with spacelike parton showers, v) final state radiation with timelike parton showers, vi) other parton-parton (in the incoming beams) interactions with their initial and final state radiation, vii) interaction between beam remnants and other outgoing partons, viii) finally all of these partons are connected by colour confinement (strings or other ...) ix) these strings will produce some primary hadrons, x) which will decay into other hadrons.

And these steps are only for pp collisions! These steps are very complex and one has different ways -or Event Generators- to explain a collision. In the "market" of event generator, one can find some specialized event generator based on the description of one step of a collision, but one needs a General Purpose Monte Carlo event generator to describe the whole a collision.

2.1.3 General Purpose Monte Carlo Generator

A General Purpose Monte Carlo event generators have to purpose -as their names tell- to give a general description of a collision. Generally these event generators divide the process into the following steps:

1. Hard Processes
2. Resonance Decays
3. Parton Shower
4. Hadronization
5. Underlying event
6. Decay of particles

The most famous General Purpose Monte Carlo event generators are: Pythia, Herwig and Ariadne which I will briefly describe in the following.

PYTHIA

Pythia [159, 160] is a general purpose event generator and probably the most used event generator for LHC studies in the world. Pythia is a program for describing high energy collisions between e^+e^-, e^+p, pp or p $\bar{p}$ for 20 years with Large Electron-Positron (LEP), HERA and the Tevatron. However, Pythia is also used as a building block for the heavy ion physics and also cosmic ray physics.

Initially Pythia was written in Fortran 77 with the last version called Pythia 6 but with the LHC era, the usual language is the C++, therefore a new version arises: Pythia 8. The Pythia 7 project [161] is not used as standalone generator like Pythia 8 but becomes a generic structure renamed Toolkit for High Energy Physics Event Generation (ThePEG) [162]. Pythia does not have automatic code generation for new processes: it should be open for all external inputs to accept the largest extent possible.

Pythia is a generator based on the parton model using the Lund Model (more details in section 2.2.5). It was created to reproduce the inclusive cross section of hard processes. Pythia generates a collision by the most harder sub-process and generates an event like following:

1. setting the hard process and reproduction of the inclusive cross section of studied process
2. generate the initial and final radiations with parton showers
3. multiple interaction between remnants and other outgoing partons

4. perform the hadronization via the Lund model

Pythia contains a very extensive list of hard processes: over 200 processes can be chosen and switched on individually. This is one main advantage of Pythia on other event generators because one can reproduce the inclusive cross section of all these processes independently and easily. ThePEG is now used with the general purpose event generator Herwig which I will describe in the next section. These generators calculate hard processes only to leading order accuracy (in the pQCD sense). The modeling of higher order corrections via initial and final state radiation is phenomenological.

Herwig

Currently, Hadron Emission Reactions With Interfering Gluons (HERWIG) [163–165] was replaced by Herwig++ and was developed during the era of LEP. Like Pythia, HERWIG was developped in Fortran before being replaced by a C++ version called Herwig++ firstly for e^+e^- annihilation physics. Herwig++ is a complete event generator used essentially for:

- generation of hard processes with full spin correlations for many BSM models;
- cluster hadronization;
- parton showers
- Multiple partonic interactions (hard and soft)
- hadronic decay models complexe and sophisticate for bottom hadrons;

Herwig++ is distributed as a collection of plugin modules to ThePEG [162]. If we merge the plugins of Herwig++ with ThePEG, one can generate some events for e^+e^-, e^+p and hh collisions. ThePEG is something very impressive because it provides all the infrastructure that is necessary to construct an event generator like tuneable parameter settings, slot for physics implementations for all steps with the generation of an event.

The merging between Herwig++ and ThePEG is configurated as we can change the defaults parameters of Herwig++ using only plain text without recompilations, one can also choose with this plain text the wanted physics analysis. The last general purpose monte carlo event generator presented is Ariadne.

ARIADNE

Ariadne [166] was the first parton shower generator which has implemented a dipole cascade, where gluon emissions are modelled as coherent radiation from two colour-connected partons [167]. It is one of the most successful QCD shower programs proven by the description of final state compared with LEP and HERA.

Like other event generators, Ariadne is currently rewritten in C++ with the era of the LHC. The rewriting in C++ is done using the framework of ThePEG [162] and merging with another shower model called DIPSY [168]. The aim of Ariadne is currently to produce exclusive final states both for pp and AA collisions.

2.1.4 Summary

The event generator is an informatic code created to reproduce the particle production in particle collisions. It is an extraordinary tool both for experimentalists and theorists in particle physics. This is a great ship to navigate between the complex theory and comprehensive results directly comparable with data of experiments. One advantage of an event generator is that one can investigate over each step of a collision contrary to experiments when one detects only the final hadrons produced during the collision.

Generaly, an event generator uses the Monte Carlo method to describe the subatomic physic's world. This is a computational method using randomness to solve a problem that one could not solve by the deterministic way. Approximatively everything can be possible if the process respects all conservation laws. Consequently, the Monte Carlo method seems to be a natural tool to reconstruct physics results theoretically.

Three General Purpose Monte Carlo event generators are convenient frameworks for LHC physic studies: Pythia using the Lund string to describe the hadronization, HERWIG using coherent-shower studies by angular ordering and cluster hadronization and Ariadne, the first parton shower using dipole cascade. I do not use these three General Purpose Monte Carlo event generators in my Ph.D work but I use the event generator EPOS. One legitimate question that one can ask is why do I use EPOS and what is the big difference between EPOS and other event generators? I will answer these questions by describing all theory inside EPOS.

2.2 The theory inside EPOS

I refer to the theory inside EPOS and not theories even if I will describe different theories because I think only about the main theory in EPOS: the Parton-Based-Gribov-Regge Theory. I prefer to describe the precursor theories behind the PBGRT itself. I will describe only few parts crucial for the PBGRT. I will describe some strong and weak points of these theories and how the PBGRT can fix those points. In the Parton-Based-Gribov-Regge Theory, one can read Regge Theory, consequently I will start with this one.

2.2.1 Regge Theory

Before introducing the Regge Theory itself, I will introduce the S-matrix because one inconvenient of the Regge Theory is reliable with the S-matrix. The Regge Theory studies the properties of the S-matrix, the concept of Regge poles has been introduced into nonrelativistic potential theory by Regge [169, 170] in 1959.

The elements if of the S-matrix represent the overlap between the two states $|i\rangle$ and $|f\rangle$. $|i\rangle$ is the initial state composed of free particles at $t \to -\infty$ and $|f\rangle$ is the final state composed of free particles at $t \to +\infty$. Generally, one denotes the S-matrix by:

$$S_{if} = \langle f|i\rangle \tag{2.2.1}$$

The description of the interaction is generally the interesting point of the S-matrix. Consequently we often remove the part where no interaction occurs by separating the matrix in two parts:

$$S_{if} = \delta_{if} + iT_{if} \tag{2.2.2}$$

δ_{if} is the part where no interaction occurs and T_{if} is the part with interaction. The T-matrix can be related to the scattering amplitude $\mathcal{A}_{if}$ with this relation:

$$T_{if} = (2\pi)^4\delta^4\left(\sum_i p_i - \sum_f p_f\right)\mathcal{A}_{if} \tag{2.2.3}$$

where the dirac function explicits the momentum conservation. One can enumerate three important postulates of the S-matrix:

1. The S-matrix is Lorentz-invariant
2. The S-matrix is unitary
3. The S-matrix is analytic in momentum variables

Now, one can talk directly about the Regge Theory itself. This is a non-perturbative theory created before the QCD and the pQCD. The Regge's aim is to study the amplitude's behavior of elastic collision in case of infinite energy. The main idea of Regge is to use the Watson-Sommerfield transformation of elastic collision, consequently, we have a collision $a + b \to c + d$:

$$\mathcal{T}(t,s) = \sum_{j=0}^{\infty} (2j+1)\mathcal{T}(j,s)P_j(z) \tag{2.2.4}$$

$\mathcal{T}$ is the partial-wave amplitude where s, t are the Mandelstam's variables and $P_j(z)$ is the $j-th$ Legendre Polynomial, then $z = \cos\theta$ where θ is the scattering angle. The poles of $\mathcal{T}$ in the complex plane are called the Regge Poles denoted by $\alpha_j(s)$. One correlates the dependence with s with the Regge trajectory. One can exchange the s and t contribution by the following crossing symmetry:

$$\mathcal{T}(t,s,u)_{a+b\to c+d} = \mathcal{T}(s,t,u)_{a+\bar{c}\to\bar{b}+d} \tag{2.2.5}$$

Using the Residue theorem, one can describe the partial-wave amplitude by Regge trajectories, with the limit of infinite energy ($s \to \infty$). This amplitude is related to a measurable cross section via:

$$\mathcal{T}(s,t) \approx s^{\alpha(t)} \qquad \Rightarrow \qquad \frac{d\sigma}{dt} = \frac{1}{s^2}|\mathcal{T}(s,t)|^2 \approx s^{2\alpha(t)-2} \tag{2.2.6}$$

At the beginning of the Regge Theory, one observes an agreement between the measurable cross section and the theory with the linear trajectories:

$$\alpha(s) = \alpha(0) + \alpha' s \tag{2.2.7}$$

One can represent the Regge pole amplitude by a Reggeon exchange:

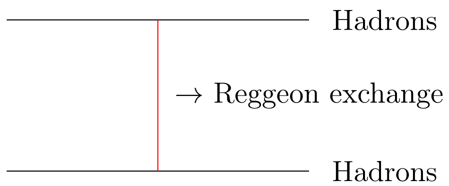

Figure 2.3: Illustration of a Reggeon exchange

The nature of a Reggeon is still to be determinated, however one can calculate the total cross section using the optical theorem. This theorem postulates the fact that the total hadronic cross section is proportionnal to the imaginary part of hadronic elastic scattering amplitude at scattering angle equal to zero. Consequently, the total cross section can be calculated as following:

$$\sigma_{tot} = s^{-1}\Im\left[\mathcal{T}(s,0)\right] \approx s^{\alpha(0)-1} \tag{2.2.8}$$

To explain the data, in particular, the slow growth of σ_{tot} with s, we define two different types of Reggeon:

1. the "normal" Reggeon with $\alpha(0) < 1$, typically around 0.5 denoted by α_R;
2. the "special" Reggeon called the Pomeron with $\alpha(0) \geq 1$, typically around 1 denoted by α_P

Reggeons have the quantum numbers of hadrons but Pomerons must have the quantum numbers of vacuum. Currently, we know that hadrons are not colored particles and the most used particle physics theory to describe the dynamics of elementary particles is the QCD $\Rightarrow$ the exact nature of Pomerons and Reggeons is still undetermined.

Finally, one can obtain good agreement for the cross section of elastic collision between hadrons however the unitarity of the S-matrix is not respected for high energy hh scattering with the case of single Pomeron exchange with an intercept of $\alpha(0) = 1$ by disagreeing with the Froissard limit [171]. The Gribov-Regge Theory will cure the unitarity by multiple Pomeron exchange.

Before introducing the GRT theory, this is time to explain in details what a Pomeron is and how it was introduce in particle physics.

Pomeron:
A Pomeron represents initially an elementary interaction between two hadrons or between partons in the PBGRT. However, the nature of the Pomeron is under to be determinate. It was introduced by Vladimir Gribov in the 60s [172–174] to explain the slow growth of cross sections in hadronic collisions at high energies (see previous paragraphes). The term of Pomeron comes from Isaak Pomeranchuk who demonstrated that pp and p $\bar{p}$ cross section must be equal at sufficiently high energy [175].

2.2.2 Gribov-Regge Theory

The GRT is a multiple scattering theory used to describe soft processes using multiple Pomeron exchange. Even if the nature of Pomeron is unknown, the elastic amplitude $\mathcal{T}$ of a Pomeron exchange can be parametrized by [like the previous section]:

$$\mathcal{T}(s,t) \approx i \times s^{\alpha_0+\alpha' t} = i \times s^{\alpha(t)} \tag{2.2.9}$$

The exchange of several Pomerons in parallel is illustrated in the following picture:

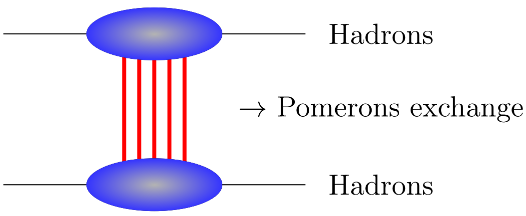

Figure 2.4: Illustration of a multiple Pomeron Exchange

Elastic amplitude:
The unitarity is respected with the formulae of n Pomeron exchanges:

$$\mathcal{T}_n(s,t) \propto \int d^2b \times e^{ikb} - \frac{s \times \omega(s,b)^n}{n!} \tag{2.2.10}$$

with b, the impact parameter, k the transverse momentum of outcoming hadrons, ω is given by:

$$\omega(s,b) \propto \frac{y e^{\alpha_0 - 1}}{R^2 + \alpha' y} \times \exp\left[-\frac{1}{4}\frac{b^2}{R^2 + \alpha' y}\right] \qquad y = \ln\left[\frac{s}{s_0}\right] \tag{2.2.11}$$

with R a free parameter. One can calculate the total elastic amplitude:

$$\mathcal{T}(s,t) = \sum_{n=1}^{\infty} \mathcal{T}_n(s,t) \propto \int d^2b \times e^{ikb} \times y(s,b) \qquad \Rightarrow y(s,b) = 1 - se^{-\omega(s,b)} \tag{2.2.12}$$

One can calculate the total cross section using the total amplitude of Pomeron exchanges:

$$\sigma_{tot} = \int 2\Re\left[y(s,b)\right] d^2b \tag{2.2.13}$$

This equation is in agreement with the Froissard limit [171], consequently, the multiple Pomeron exchange cures the unitarity.

Inelastic amplitude:
The production of particle comes from inelastic collision. Using the amplitude of a Pomeron, we can express the inelastic cross section (thanks to field theory):

$$\sigma_{inel}^{h_1 h_2} = \int d^2b \left\{1 - \exp[-\mathcal{G}(s,b)]\right\} \tag{2.2.14}$$

$\mathcal{G}(s,b)$ is proportionnal to the Fourier transform of $\mathcal{T}(s,b)$ and represents an elementary interaction: a Pomeron exchange.

One can generalize for nucleus-nucleus scattering with more Pomerons and other formulae to calculate the cross section. This cross section gives productive results and a large number of observables were reproduced with Venus [169], the predecessor of NeXuS [176] itself precursor of EPOS.

One important problem of the GRT is about the energy conservation. Indeed, in the particle production treatment, the energy is conserved when the initial energy is shared between the different Pomerons. This procedure is not taken into account during the calculation of cross section: each Pomeron takes the total energy of the incoming hadrons.

Disadvantages : The energy is not conserved during the calculation of cross section and the treatment of particle production and cross section are different.

Another problem is that the first Pomeron is treated differently from other Pomerons without justifications in the particle production treatment.

Summary

The GRT is an effective field theory which describes hadronic interaction using multiple exchange of Pomerons in parallel. Using the field theory, one can calculate cross sections in the terms of variable characterizing the Pomeron.

One of great advantages of GRT is that it cures the unitarity problem of the Regge Theory by interference terms.

However, the approach is inconsistent. The energy shared between Pomerons in case of multiple scattering is well conserved for particle production. But, the energy conservation is not taken into account for the cross section calculations.

Finally, the GRT is only a description of soft processes, consequently I will describe shortly another approach used to describe hard processes: the parton model.

2.2.3 Parton Model

With the Stanford Linear Accelerator Center (SLAC) accelerator etablished in 1962, the possibility to collide two protons with a center of energy higher than 10 GeV arises. These collisions tell that the proton is not an elementary particle. Feynman proposed in 1969 [177] the parton model to explain the proton-proton collisions. The model suggests that the proton is componing by new particles called partons. Feynman decomposes the cross section of pp collision by elementary interaction of partons. Bjorken and Pachos [178] used the parton model to describe the e^+p collisions and identified the partonic distribution function.

I will start by describing the e^+p collision before extending the description for pp collisions.

Electron proton collision

The e^+p collision effectuated with a center of mass energy higher than 10 GeV is called the Deep Inelastic Scattering (DIS). Historically, a electron flux collides with a target of hydrogen. Surprisingly, electrons interact with the protons as an interaction with ponctual charged particles $\Rightarrow$ Feynman and Bjorken introduced partons to solve this new fact.

The parton model describes hadrons as a cluster of partons interacting weakly between them by strong interaction. Some partons must have an electric charge known as quarks or antiquarks while other partons must be neutral, known yet by gluons.

This is the electric charge of quarks that gives the particularity of electron protons collisions. The diagrammatic representation of the DIS is given by the following picture:

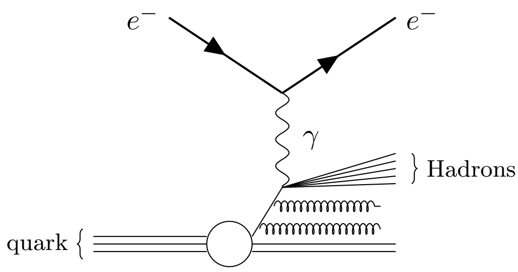

Figure 2.5: Diagrammatic representation of the Deep Inelastic Scattering

In a proton, each parton takes a fraction x of the proton's momentum: x is called the Bjorken variable. If the energy is high enough, one can see the proton as a multitude of ponctual partons $\Rightarrow$ the virtuality of the exchanged photon allows perturbative calculations via the asymptotic freedom [179]. The schematic representation of the proton with an increasing energy is given by:

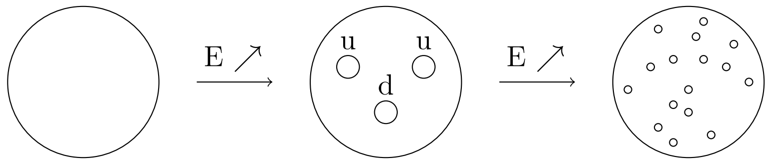

Figure 2.6: Representation of a proton with an increasing energy

Without giving all the details of the QFT treatment of the collisions, the parton model gives the cross section of the e^+p collision by:

$$\frac{d\sigma}{dt}(e^- p \to eX) = \sum_i \int dx f_i(x) \left(\frac{d\sigma}{dt}\right)(e^- q_i \to e q_i') \tag{2.2.15}$$

with σ the cross section, t the Mandelstam variable[4],$f_i(x)$ denotes the partonic distribution functions for a quark with the flavor i inside the proton. $e^- p \to eX$ denotes the collision between an electron and a proton with the remnant productions, finally q_i represents an elastic scattering between an electron and a quark with the flavor i.

Proton Proton collision

The generalization of the e^+p collisions by a pure hadronic collision (here pp) is used to describe all non-elementary interactions. This generalization describes all non-elementary interactions into elementary interactions between partons. The shematic representation of the pp collisions is given as follows:

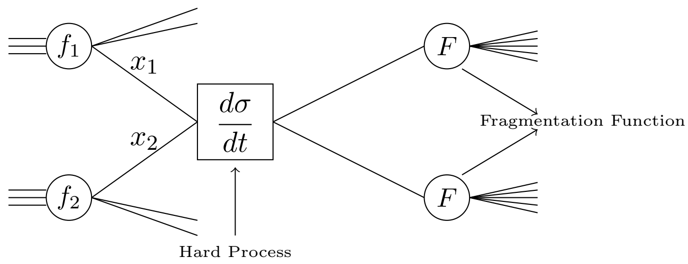

Figure 2.7: Diagrammatic representation of the pp collision

The cross section of the pp collision calculated with the parton model is:

$$\frac{d\sigma}{dt}(pp \to q_3 q_4) = \sum_{q_1 q_2} \int dx_1 dx_2 f_1(x_1, Q^2) f_2(x_2, Q^2) \frac{d\sigma}{dt}(q_1 q_2 \to q_3 q_4) \tag{2.2.16}$$

The cross section $\frac{d\sigma}{dt}(q_1 q_2 \to q_3 q_4)$ can be calculated by the rules of QFT and Feynman diagrams. Then f_1 and f_2 are experimental variables coupled with global fitting depending of the cross section$\Rightarrow$ **We have a lot of Parton Distribution Functions**!

[4]to recall: $t = P_1 - P_3$ with P_1 and P_3 quadrivectors of energy momentum of electrons coming and outcoming respectively

Gluon existence

The decomposition of the structure function of protons by different parton distribution functions is given by the following equation:

$$F_2(x) = 2xF_1(x) = \sum_i e_i \times xq_i(x) \tag{2.2.17}$$

Each parton distribution function of the proton can be decomposed as the following:

$$\begin{aligned} u(x) &= u_v(x) + u_{\text{sea}}(x) \qquad \bar{u}(x) = \bar{u}_{\text{sea}}(x) \\ d(x) &= d_v(x) + d_{\text{sea}}(x) \qquad \bar{d}(x) = \bar{d}_{\text{sea}}(x) \\ & \qquad\qquad s(x) = \bar{s}(x) = s_{\text{sea}}(x) \end{aligned} \tag{2.2.18}$$

Consequently, using the equation 2.2.17, the structure function of the proton is[5]:

$$F_2(x) = \frac{4}{9}\left[u_v(x) + 2u_{\text{sea}}(x)\right] + \frac{1}{9}\left[d_v(x) + 2d_{\text{sea}}(x)\right] + \frac{1}{3}\left[2s_{\text{sea}}(x)\right] \tag{2.2.19}$$

With the experimental determination of the parton distribution function, the number of quarks in the proton can be calculated as following:

$$\int_0^1 dx u_v(x) = 2 \qquad \int_0^1 dx d_v(x) = 1 \qquad \int_0^1 dx s_v(x) = 0 \tag{2.2.20}$$

Now, the calculation of the total momentum fraction carried by all quarks and anti-quarks gives an unexpected result:

$$\int_0^1 dx\, x \sum_i q_i(x) \approx 0.5 < 1! \tag{2.2.21}$$

Consequently, the electric particles carry only half total momentum fraction. That means that, in the proton, it exists a neutral type of particle called the gluon.

Summary

The parton model has been introduced in 1969 by Feynman and changed our point of view about particles. The proton is not an elementary particle! It seems to be partons, that means quark and gluon.

By merging the QFT rules and the parton model vision, we can calculate theoretically the cross section of a lot of processes. I showed the typical calculation of electron-proton and proton-proton collisions but the genereralization with nucleus-nucleus is done. One important object of the parton model is the parton distribution function. Without this object, the theoretical calculation of the cross section will be very complicated.

Using the different parton distribution function, the existence and the nature of the gluon is described in the SM using the parton model.

The calculation of cross section in the parton model is only for hard processes. To calculate the cross section of soft processes, we need to find other solutions. One way to calculate both soft and hard processes cross sections is the theory inside EPOS called the Parton-Based-Gribov-Regge Theory.

[5]To recall, charge of quarks is: $u = \frac{2}{3}$, $d = -\frac{1}{3}$ and $s = -\frac{1}{3}$

2.2.4 Parton Based Gribov Regge Theory

The idea of the Parton-Based-Gribov-Regge Theory comes to study the QGP with its creation's mechanism. The main idea to create this theory is to do a realistic treatment of all processes during a collision. Like its name indicates, the PBGRT consists of a merging approach between the Parton model and the Gribov-Regge Theory. This approach treats in only one formalism the hard and soft processes during a collision, conserving the energy using partons. If we create a realistic interpretation of all processes during a collision, we can reproduce a large number of observables related or not with the QGP. Therefore, the creation of a unified approach[6] must be the main goal of the PBGRT.

This theory must contain a coherent treatment to calculate the cross section and the production of particles taking correctly the energy conservation. The PBGRT has been developed by Drescher, H. J. and Hladik, M. and Ostapchenko, S. and Pierog, T. and my Ph.D supervisor Werner, K. with the main reference [180]. All the details of the PBGRT are given in this reference.

The merging of the GRT and the parton model changes the vision of an elastic collision. Typically, the Fig 2.4 has changed by using partons, consequently this picture changes as:

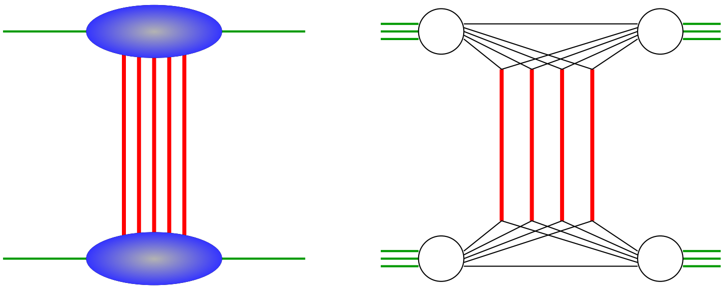

Figure 2.8: Schematic representation of the proton-proton scattering view by the Gribov Regge Theory (left) and the Parton Based Gribov Regge Theory (right)

The thick green lines in the Fig 2.8 are hadrons for the GRT (left) but are partons in the PBGRT (right). The proton was represented as an elementary particle before the introduction of partons in the theory. I will not detail all parts of the PBGRT, only the points more important for the theory itself and my Ph.D thesis. Therefore, I will describe the formalism to conserve the energy and an important tool used in PBGRT: the cut ladder.

Formalism to conserve the energy

The first goal of the PBGRT is to calculate cross sections and particle production in a consistent way. That means that the formalism must be the same and the energy conserved in both calculations. This formalism operates with the Feynman diagrams of the Quantum Field Theory. The main object to describe interaction between particles is the profile function $\mathcal{G}(s, b)$. To define the profile function, let's start by an elastic scattering of two bodies represented by the following picture:

[6] For an event generator, that means we use only one set of parameters for each type of collision

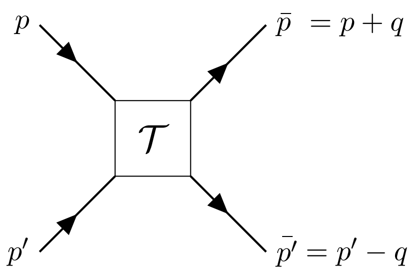

Figure 2.9: Schematic representation of elastic amplitude $\mathcal{T}$ of two bodies

Using the optical theorem, one can express the total cross section with the elastic amplitude $\mathcal{T}$ (with s and t the Mandelstam variables):

$$\sigma_{\text{tot}}(s) = \frac{1}{2s} \times 2\Im\left[\mathcal{T}(s, t = 0)\right] \tag{2.2.22}$$

where $\Im$ represent the imaginary part of the followed function. The profile function is defined using the Fourier transform $\tilde{\mathcal{T}}$ of $\mathcal{T}$ (with $t = -q_\perp$):

$$\tilde{\mathcal{T}}(s, b) = \frac{1}{4\pi^2} \int d^2 q_\perp e^{-i \times \vec{q}_\perp \cdot \vec{b}} \mathcal{T}(s, t) \quad \Rightarrow \quad \mathcal{G}(s, b) = \frac{1}{2s} \times 2\Im\left[\tilde{\mathcal{T}}(s, b)\right] \tag{2.2.23}$$

Consequently, one can verify that:

$$\sigma_{\text{tot}}(s) = \int d^2 b\, \mathcal{G}(s, b) \qquad \text{with b the impact parameter} \tag{2.2.24}$$

which allows an interpretation of $\mathcal{G}(s, b)$ like the probability of an interaction at finite impact parameter b. In the PBGRT, the elementary interaction can be represented as the following picture:

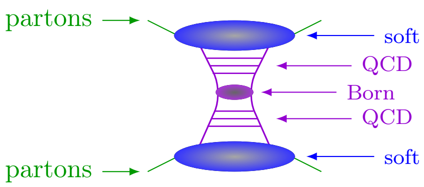

Figure 2.10: Representation of an elementary interaction in the Parton Based Gribov Regge Theory

Green lines are the ingoing and outgoing elementary partons, we called this type of schematic representation a ladder. We see that the elementary interaction is considered as a sum of soft, hard and semi-hard contributions. The soft contribution is non-perturbative where the virtual partons have a virtuality less than the saturation factor Q_s^2. The soft contribution is parametrized and is described by the phenomenological Regge theory. When we approach the center of the diagram, the virtuality increases and $Q^2 > Q_s^2$. Therefore, the contribution becomes much harder. The hard contribution with its respective scattering amplitude is described using the pQCD. The parton's virtuality follows the DGLAP equation, then the center of the ladder is a $2 \to 2$ interaction called the Born process. Finally, the semi-hard contribution for sea-sea, sea-val, val-sea and val-val[7] partons are taken into account to have a complete description of the interaction.

[7]sea is for the case where parton comes from the sea's quark and val is for the case where parton comes from the valence's quark.

This subsection summarizes the formalism used to conserve the energy. This part concerns only the elastic scatterings therefore, I did not explain the particle production in EPOS. This is because the particle production does not come from closed ladder but from cut ones, which will be explained in the next subsection.

Cut ladder

To have a coherent treatment in Quantum Mechanics of the multiple interaction with different ladders, the formalism does not use only elastic and closed ladders but also open ones. Consequently, the schematic representation of AA collision without cut ladder (Fig 2.11) in PBGRT will be changed using also cut ladders (Fig 2.12):

Closed ladders are important for the cross section calculations and the open ones are for the particle production. The schematic view of these two types of ladders are represented in the Fig 2.13 in the next page:

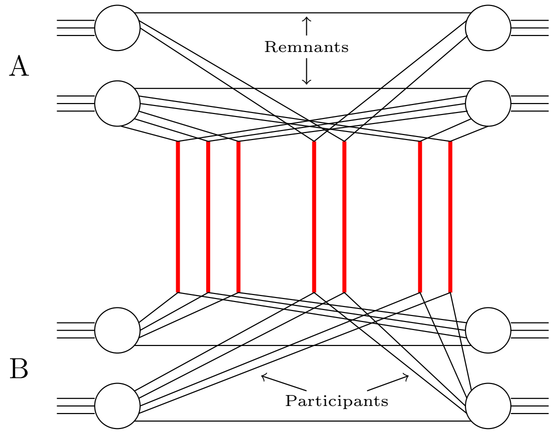

Figure 2.11: Schematic representation of an AA collision in the Parton Based Gribov Regge Theory without cut ladders

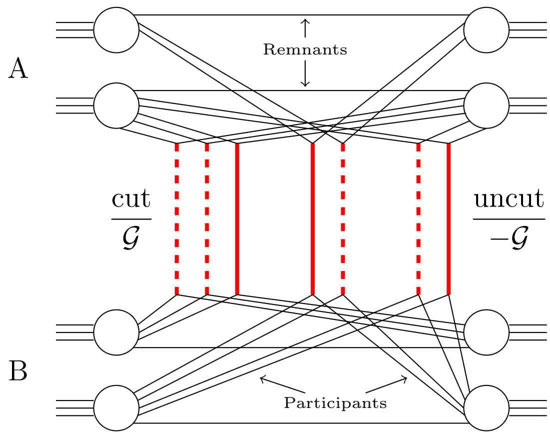

Figure 2.12: Elementary diagrams of an AA collision in the Parton Based Gribov Regge Theory using cut ladders (dashed lines) and uncut (full lines)

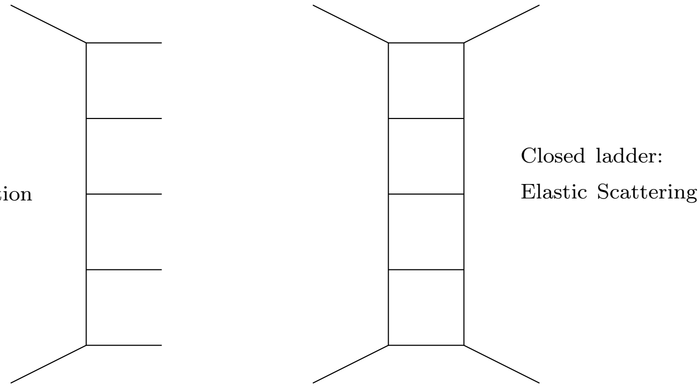

Figure 2.13: Two elementary objects in multiple scattering, right) a closed ladder describes the elastic collision without production of particle, left) an open ladder describes the particle production in the Parton Based Gribov Regge Theory

The great advantage about introducing these two types of ladders in the formalism of PBGRT is that we can calculate the inclusive cross section using exclusive cross section:

$$\sigma_{\text{tot}} = \sum_{cut} \sum_{uncut} \int \tag{2.2.25}$$

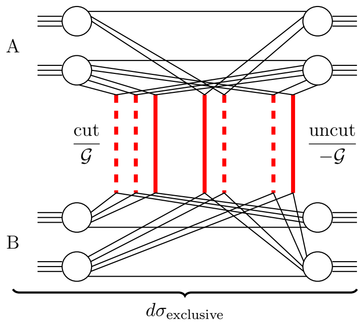

We can calculate both exclusive and inclusive cross sections! Much details are given in the Ph.D. thesis of my predecessors [181, 182].

Summary

The PBGRT tries to be a realistic treatment of all processes during a collision. The collision can be for proton-proton, proton-nucleus and nucleus-nucleus, that means that the theory tries to be a unified formalism for all collisions.

As its name indicates, the Parton-Based-Gribov-Regge Theory is a merging approach between the parton model and the Gribov-Regge Theory. The idea of this theory is to cure the problem of these two approaches by this one. Therefore, this approach treats in only one formalism the hard and soft processes during a collision conserving the energy using partons.

The PBGRT contains a coherent treatment to calculate the cross section and the particle production taking correctly the energy conservation (unlike the GRT). An important point is that we can calculate both exclusive and inclusive cross sections.

The energy is totally conserved by introduction of the profile function which uses the Fourier transform of the collision's amplitude. The elementary interaction is a Pomeron and can be represented as a parton ladder that we can cut to produce the particles.

I will develop the particle production mechanism in the next section which is related to the string model.

2.2.5 String Model

The string model is a phenomenological model [183] created to try to describe the hadronization of partons. The hadronization is something very mysterious for subatomic physicists because we do not have a fundamental theoretical description about how partons become hadrons. We just have different possibilities to describe this process and the string model is one way used by physicists.

The origin of string model comes from the asymptotic freedom where the attraction between partons increases with the distance. The idea is that a string is created between two partons like a colour field. The string does not have a mass and it is colourless. In the Lund Model of string, the string object has a tension of $k \approx 1$GeV which means the energy per distance. The energy in the string increases with the distance between the two partons. If this energy is high enough, the string breaks into few segments where a $q\bar{q}$ pair is created. To keep the flavor conservation, the different color singlet is created like $q_a\bar{q}_b$ and $q_b\bar{q}_a$ with a and b the flavors of quark. The following picture describes the process:

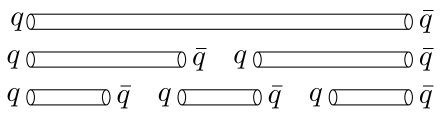

Figure 2.14: Illustration of fragmentations at String Model

Different models are created using strings, for example Pythia and EPOS use differently the string. I will develop only the EPOS part in the following. The way to produce mesons and baryons by the string model will be developed during this chapter but the computational part will be described in the next chapter. I want to separate the theory and the computational interpretation for a better understanding and explain my work purely computational in a separate Appendix (B) of the theory in EPOS. Therefore, to talk about the production of particles, I will start by the string fragmentation and the determination of fragment flavors and masses.

String fragmentation

In order to consider the string breaking in EPOS, the Area law is used to determine the break points of the string. This method is proposed by Artru and Menessier [184] which is based on an extension of the decay law of unstable particles. The decay law of particles gives the probability to decay within a time interval as:

$$dP = \lambda dt \tag{2.2.26}$$

with λ the decay constant. To extend this law on string, the same formula is used by replacing the proper time dt by the proper surface in Minkowski space:

$$dP = \lambda dA \tag{2.2.27}$$

The Monte Carlo method used to find the break points is determinated by the construction of a direct algorithm based on:

$$P_0(A) = e^{-\lambda A} \tag{2.2.28}$$

we see easily the reference about decay law $P(t) = e^{-\lambda t}$, but here P_0 is the probability of having no break points within the Area A. The different surfaces according to $P_0(A)$ are generated as:

$$A_i = -\frac{\log(r_i)}{\lambda} \tag{2.2.29}$$

where r_i are random numbers between 0 and 1. One point about this formula is that it does not say anything about the possible form of the Area. Consequently, this is possible to choose several forms as long as they do not violate causality. In the simple example of string without any gluons, this is considered as placing the surface A_i from left to right such that the break points P_i are the left upper corners of A_{i+1} as shown in the following figure:

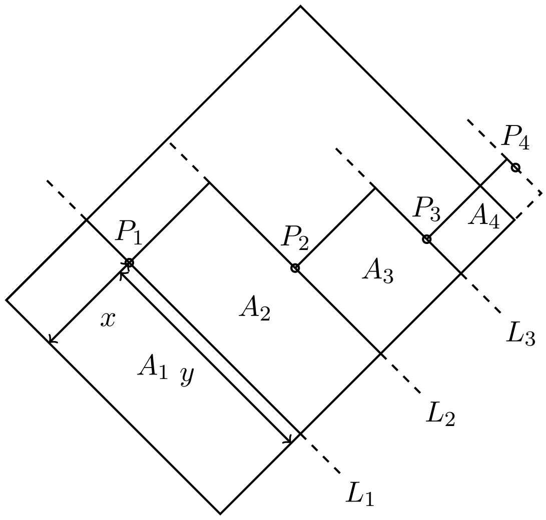

Figure 2.15: Method to determine break points of string

The direct procedure is the following: one takes A_1 defined by the line L_1 where the first break point P_1 is generated randomly on this line. The first break point is used as a contraint for the next one. A_2 is placed in a way to not violate the causality. We continue until the last surface is too large to be placed on the rest of the string. In this case, we stop the procedure and the last break point is rejected.

The great advantage of this method is that no break points are rejected because of causality principle. This one is always obeyed during the whole process. We discussed how the string breaks into small fragments. To create particles, these string fragments have flavors and masses, therefore I will describe the determination of these properties in the next section.

Determination of fragment flavors

A string has a whole flavor determinated by each parton in its extremities. All the small pieces created by break points must respect the colour conservation and flavor conservation of the whole string. The production of mesons is described by the previous formalism with the $q\bar{q}$ fragment of string. We cannot produce baryons with this formalism, consequently we use the diquark formalism in EPOS. The diquark formalism is a hypothetical cluster of two quarks into baryons, this one is considered as a qdq[8] pair. The diquark

[8]dq representing the diquark

has been implemented during the break point proccess. The string fragmentation given by the fig 2.14 changes including diquarks as following:

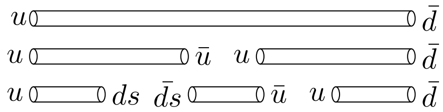

Figure 2.16: Illustration of fragmentations at String Model including diquark

To explain briefly: the whole string has different flavors and additional flavors are created by the different fragments of $q\bar{q}$ or $dq\bar{dq}$. The probability to have a certain flavor is a free parameter of the model used to reproduce the data. In case of quark-antiquark pair, we define the parameter p_{ud}, which gives the probability to have a flavor u or d. Consequently, the probability to have a s flavor is given by $1-2p_{ud}$ which must be smaller than p_{ud} because of its larger mass. The corresponding probability p_{dq} is created for the probability to have a $dq\bar{dq}$ pair fragments.

We have the flavor of our fragment, then we must determine the mass of each string fragment.

Determination of fragment masses

In the following, I will show how to determine the masses of string fragments using the break points.

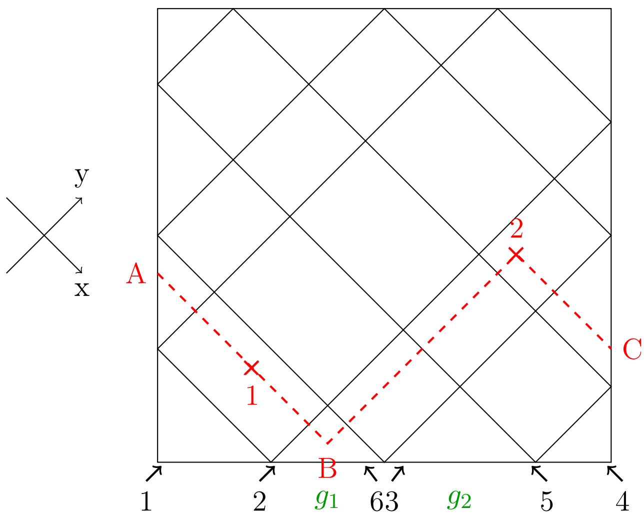

Figure 2.17: Representation of method to calculate the mass of a sub-string

In my exemple, the Fig 2.17 shows an example of two break points (1 and 2) for a string with 2 inner kinks (gluons in green). The momentum bands and the regions of their overlaps are shown: we have two R-bands (2,3) and two L-bands (5,6). The bands at the extremities (1,4) are considered like double bands.

The full string momentum is given as:

$$p_{\text{string}} = \int_{\mathcal{C}} \left[\dot{x}d\sigma + x'd\tau\right] \tag{2.2.30}$$

where $\mathcal{C}$ is an arbitrary curve from one border ($\sigma = 0$) to the other ($\sigma = \pi$) in the parameter space.

Consequently, the string momentum is:

$$p_{\text{string}} = \frac{1}{2}\int_{\mathcal{C}} \left(g(\sigma+\tau)+g(\sigma-\tau)\right) d\sigma + \frac{1}{2}\int_{\mathcal{C}} \left(g(\sigma+\tau)-g(\sigma-\tau)\right) d\tau \tag{2.2.31}$$

Therefore, the momenta of the bands are by definition:

$$p_i = \begin{cases} \frac{1}{2}\int_{band\ i} g(\sigma-\tau)d\sigma - \frac{1}{2}\int_{band\ i} g(\sigma-\tau)d\tau & \text{if R-band} \\ \frac{1}{2}\int_{band\ i} g(\sigma+\tau)d\sigma + \frac{1}{2}\int_{band\ i} g(\sigma+\tau)d\tau & \text{if L-band} \end{cases} \tag{2.2.32}$$

where one integrates along an arbitrary curve from one border of the band to the other. This leads to important property of these equations: an integration path parralel to a band provides zero contribution. One has to be careful for the bands at the extremities: the integration only along $\tau = 0$ represents only half the band. Therefore, the sum of momentum fragments gives the full string momentum:

$$\sum_i p_i = p_{\text{string}} \tag{2.2.33}$$

This leads to the momenta of the bands are related to the corresponding parton momenta as:

$$p_i = \begin{cases} \frac{1}{2}p_{\text{parton}} & \text{if inner band} \\ p_{\text{parton}} & \text{if outer band} \end{cases} \tag{2.2.34}$$

I recall that the outer bands at the extremities are represented in two bands. For the example of Fig 2.17, we have:

$$p_1 = p_q \quad p_2 = p_6 = \frac{1}{2}p_{g1} \quad p_3 = p_5 = \frac{1}{2}p_{g2} \quad p_4 = p_{\bar{q}} \tag{2.2.35}$$

And, summing over the bands, we get the total string momentum:

$$\sum_{i=1}^{6} p_i = p_q + p_{g1} + p_{g2} + p_{\bar{q}} = p_{\text{string}} \tag{2.2.36}$$

The definition of the momentum of string fragment is given as:

$$p_{\text{frag}} = \frac{1}{2}\int_{\mathcal{C}'} (g(\sigma+\tau)+g(\sigma-\tau))d\sigma + \frac{1}{2}\int_{\mathcal{C}'} (g(\sigma+\tau)-g(\sigma-\tau))d\tau \tag{2.2.37}$$

where the path of the integration $\mathcal{C}'$ is an arbitrary curve between two break points or between a break point and a boundary. We can decompose the previous equation where p_R and p_L represent sums of momenta of R-bands and L-bands, respectively:

$$\begin{aligned} p_R &= \frac{1}{2}\int_{\mathcal{C}'} g(\sigma-\tau)d\sigma - \frac{1}{2}\int_{\mathcal{C}'} g(\sigma-\tau)d\tau \\ p_L &= \frac{1}{2}\int_{\mathcal{C}'} g(\sigma+\tau)d\sigma + \frac{1}{2}\int_{\mathcal{C}'} g(\sigma+\tau)d\tau \end{aligned} \tag{2.2.38}$$

We can now describe the Fig 2.17. In this example, we have two break points and two inner kinks. I will describe first the path $1 \to 2$ to have the string fragment between the break points 1 and 2. We decompose for simplicity the path $1 \to 2$ by $1 \to B$ and $B \to 2$. The first path is parallel to all L-bands, therefore only R-bands contribute and the second one is parallel to all R-bands, therefore only L-bands contribute.

Consequently, the momenta of $1 \to B$ and $B \to 2$ paths is:

$$\begin{aligned} p_{1\to B} &= x_1 p_1 + (1-x_2)p_2 \\ p_{B\to 2} &= (1-y_1)p_6 + p_5 + y_2 p_4 \end{aligned} \tag{2.2.39}$$

In this example, we follow the red line between $1 \to B$, we see that we pass through on: a part (x_1) of the band 1, a part $(1-x_2)$ of the band 2. For the path $B \to 2$, we see that we pass through on: a part $(1-y_1)$ of the band 6, the total band 5 and a part (y_2) of the band 4. We can treat all string fragments with the same procedure. Consequently, we can calculate all paths to integrate all the string, the first path corresponds as $A \to 1$, the second one is $1 \to 2$ and the last one is $2 \to C$. Finally, the momenta of the three string fragments are:

$$\begin{aligned} p_{A\to 1} &= (1-x_1)p_1 + y_1 p_6 \\ p_{1\to 2} &= x_1 p_1 + (1-x_2)p_2 + (1-y_1)p_6 + p_5 + y_2 p_4 \\ p_{2\to C} &= x_2 p_2 + p_3 + (1-y_2)p_4 \end{aligned} \tag{2.2.40}$$

We can verify that the sum of the three sub-strings gives the total momentum of the string:

$$\begin{aligned} p_{A\to 1} + p_{1\to 2} + p_{2\to C} &= (1-x_1)p_1 + y_1 p_6 + x_1 p_1 + (1-x_2)p_2 \\ &\quad + (1-y_1)p_6 + p_5 + y_2 p_4 + x_2 p_2 + p_3 + (1-y_2)p_4 \\ &= p_1 + p_2 + p_3 + p_4 + p_5 + p_6 = \sum_{i=1}^{6} p_i = p_{\text{string}} \end{aligned} \tag{2.2.41}$$

Finally, the mass of each string fragment can be calculated by the following equation:

$$\boxed{m_{\text{frag}}^2 = p_{\text{frag}}^2} \tag{2.2.42}$$

For example, we can find the mass of the third fragment:

$$m_{2\to C}^2 = p_{2\to C}^2 = 2 \times \left[x_2 p_2 p_3 + x_2(1-y_2)p_2 p_4 + (1-y_2)p_3 p_4\right] \tag{2.2.43}$$

where we use the advantage of the light-cone variable of the momenta: $p_i^2 = 0$. Finally, we have determined the flavor and the mass of each string fragment. Then, we can determine the hadrons by a table using the flavor and the mass, I will develop in the next chapter with the informatic EPOS description. The approach of this section must be corrected for the fragment masses but I will not describe this one because I have already described the main process to product particles.

Summary

This section explains important points about the string model in EPOS. The string model is a phenomenological model used to describe the hadronization of partons. Different string models are used in event generators and I described few parts of the model used in EPOS.

The string fragmentation or the string breaking in EPOS is done according the Area law. The Monte Carlo is used to construct a direct algorithm to define different break points on the string. Now we must define the flavor and the mass of the different string fragments. Finally, to have particles from string, we define the fragmentation algorithm as following:

1. For a given string, we generate several break points;
2. For each break point, we define the flavor and the transverse momentum;
3. For each break point, we calculate the masses of the two neighbouring substrings;
4. We modify the localization of the break point to get exactly the mass. If this is not possible, we reject this break point and restart the step 3;
5. If the mass of a sub-string is bigger than the upper limit in the mass table, we fragment this sub-string (consequently, go to step 1).

In this way, everything can be done using the kinematic variables and kinematic constraints. Generally, the break points are rejected when the transverse momentum is too high which results on a mass becoming negative. In this case, we look at another break point until a valid configuration is found.

I defined several parts of the formalism used in EPOS to describe an interaction (elastic or inelastic) with the merging of GRT and parton model called PBGRT. One of the main goal of this approach is to treat soft and hard models for pp and AA collisions with only one formalism. However, I showed the formalism used for NeXuS and the first version of EPOS. Now, I will describe the evolution of EPOS with the time.

2.3 Evolution of EPOS during the years

In this section, I will develop the history of EPOS since the beginning of Venus until the third version of EPOS.

Everything started with the creation of Venus [169] in 1990, the first ancestor of EPOS. Venus was an event generator based on simple multiple interaction model. This event generator was developed to describe the data of Super Proton Synchrotron (SPS) [35]. The theory behind Venus was the Gribov-Regge Theory, therefore Venus described soft processes. The GRT was not enough to describe all the data of the SPS. Consequently, the merging of QGSJet[9] [185] and Venus was done around the 2000s; a new event generator from the collaboration of Klaus Werner and Sergei Ostapchenko was born: NeXuS. The theory inside NeXuS follows the same picture, this is the merging of Parton model and GRT to give the Parton-Based-Gribov-Regge Theory.

Some collective effects were implemented with (among others) Tanguy Pierog with the new era of energy by new colliders: RHIC and Tevatron and EPOS were born. This was the beginning in 2006 and prior to the LHC era. The ultimate version of EPOS called EPOS 1.99 was born in 2009. This version reproduced all major results of accelerator data (RHIC, SPS, Tevatron, ...) and it was also used in air shower simulation programs like Corsika [186] or Conex [187]. Therefore EPOS can be used to study ultra high energy cosmic rays [188]. The EPOS 1.99 was released in 2009 with an effective flow (parametrized). Between 2010 and 2012, parallel projects were developped at the same time: EPOS 2 and EPOS LHC.

EPOS LHC [189] differs from other versions of EPOS like EPOS 2 and EPOS 3 in that it does not take advantage of the 3D+1 hydrodynamic evolution followed by the hadronic cascade. The release of EPOS LHC was in 2012 with the same parametrized

[9] a parton model based event generator

flow as EPOS 1.99 tuned to fit pp, pA and AA data up to early LHC data. This version is also used to describe the cosmic rays. One of the main reason to have two parallel projects in development it takes one hour for a Pb-Pb central event in EPOS 2 or EPOS 3 while EPOS LHC will generate it in a few minutes. EPOS LHC is not under development, this is a public stable version. EPOS LHC contains more parameters than EPOS 2 or EPOS 3, the consequence is a less predictive power. We cannot use EPOS LHC for a very precise study in heavy ion collisions but we can use it for pp and pA minimum bias analysis.

EPOS 2 is semi-public with the 2.17 version since 2010. EPOS was enhanced to the second version by an implementation of hydrodynamic treatment of the matter evolution (QGP-like) in the collision [190]. The whole hydrodynamic part of EPOS was mainly developed by Iurii Karpenko [191]. The 2.17 version develops the jet-matter and fluid interaction. EPOS 2 presents a 3D+1 ideal hydrodynamic evolution, then using an hadronic cascade with the UrQMD [136]. This version was created to study, with a realistic treatment of the hydrodynamic evolution of ultrarelativistic heavy collision, the collective effects. EPOS 2 is based on the following features:

- initial conditions obtained from the flux tube approach compatible with the string model used in the PBGRT and the color glass condensate picture;
- initial collective transverse flow;
- core-corona separation procedure will be described in the next section;
- event-by-event procedure;
- solve the hydrodynamic equations in 3+1 dimensions, conserving the baryon number, strangeness and electric charge;
- using an Equation of State compatible with lattice gauge results;
- finally, an hadronic cascade procedure from the thermal system at an early stage.

Since 2014, the final important upgrade, leading to EPOS 3 [192] was the inclusion of parton saturation and viscous hydrodynamic [193] interesting for pp and pA, and the inclusion of heavy quark by Benjamin Guiot [181]. In this version, the Pomeron is also identified as a parton ladder composed by a pQCD hard process, with initial and final state linear parton emissions. All nonlinear effects are considered by a new saturation process. The saturation plays a game during the parton evolution by considering individual saturation scales Q_s per Pomeron, depending on energy and number of participants connected to the Pomeron. The heavy quarks are produced during the PBGRT formalism in the same way as light quarks (adding a heavy mass). The fluid evolves according to the equations of relativistic viscous hydrodynamics with a shear viscosity over entropy: $\eta/s = 0.08$ [192].

I recounted almost all the story of the different versions of EPOS until now. Because one goal is to have a public version of EPOS 3 in 2019-2021, in the following section, I give a description of the full procedure followed in EPOS to create an event.

2.4 How is an event generated in EPOS?

In this section, I will describe the procedure applied for pp, pA and AA collisions to create an event in EPOS 3. The whole procedure consists of five steps employed for each event.

2.4.1 Initial conditions

All the basic important things to know on the initial conditions have been already described in the PBGRT section. In addition of this section, the DGLAP parton ladder (comes by Pomeron) using now a saturation scale for each Pomeron, depending of the number of nucleons connected to the Pomeron and its energy.

The parton ladders are identified with flux tubes as explained in the PBGRT section and the main reference [180]. Now, the flux tube will be described by the string phenomenological model. I will explain now the transition between flux tubes and strings with an example of one Pomeron exchange. The color flow of a cut Pomeron is represented by the following picture:

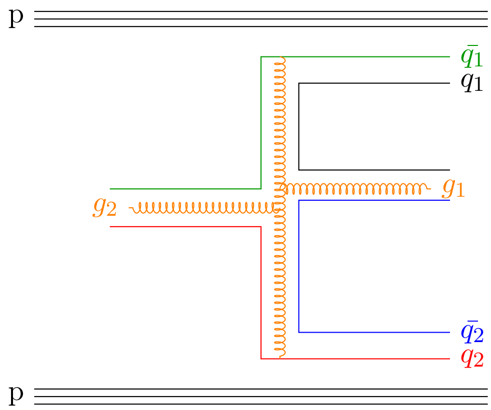

Figure 2.18: Color flow for a single Pomeron exchange, without initial and final state cascade

In this case, the projectile and target remnants stay color neutral, therefore this interaction is between sea quarks. One can follows the color flows between partons by colored lines. We have consequently two flows: $\bar{q}_1 - g_2 - q_2$ and $q_1 - g_1 - \bar{q}_2$. The gluon emission between the two quarks (or antiquarks) gives a "kink" in the flows. Those two parton sequences will be identified as "kinky string". The string picture can be used to describe the color flow with a kink for each gluon emitted. We can see in this simple example, two strings with each a single kink. The pictorial representation of a string at given proper time is drawn as following:

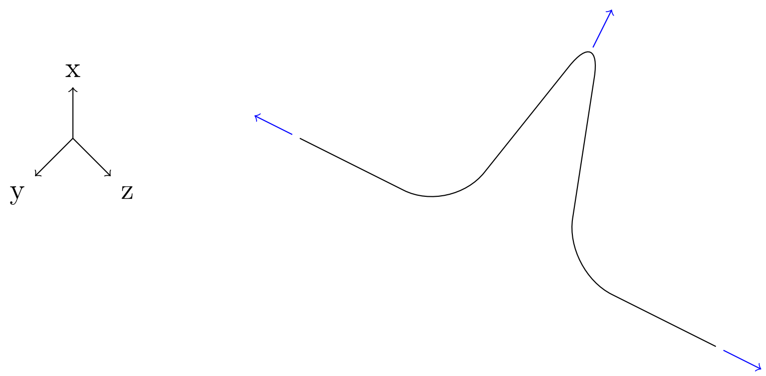

Figure 2.19: Pictorial representation of a flux tube with transversely moving part (kink) in space at given time

The description of parton ladders will be replaced by a relativistic string picture [169], where the dynamic follows a gauge invariant Lagrangian. An important thing is: almost all strings are longitudinal objects because of high transverse momentum partons → the energy is essentially longitudinal.

The string will break following the Area law (viewed in the PBGRT section: 2.2.4 and references [180, 182] via a production of different quarks-antiquarks. These segments will give final hadrons and resonances as the following picture:

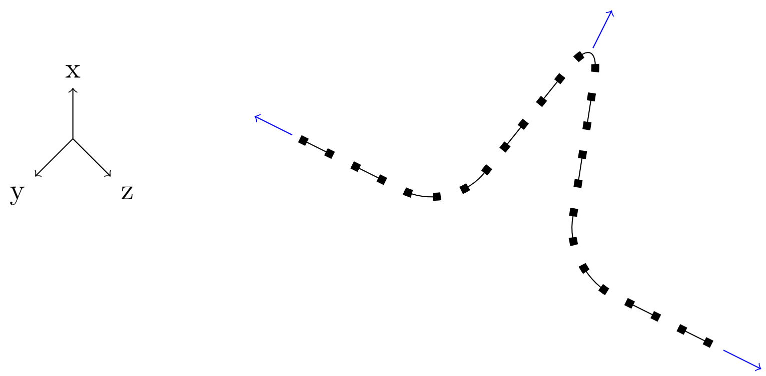

Figure 2.20: Pictorial representation of a flux tube breaking via the Swinger Mechanism via $q - \bar{q}$ production

The phenomenological string model gives the initial state of the following steps: the core corona separation.

2.4.2 Core Corona separation

As I have already said, almost all the hydrodynamic's work has been done by Iurii Karpenko [191]. This is an important part of the core-corona procedure.

In EPOS, the density of strings in high multiplicity events is so high that the strings cannot decay independently as discussed in the PBGRT section 2.2.4. The density of these fragments can be calculated to know the transverse momenta and the density of string fragments at the initial time τ_0 when we start the core corona procedure.

The place where the string density is higher than the critical density ρ_0 is called the *core*: this is the area which constitute the plasma. In this place, partons in string fragments will lost their individual identity in the plasma and constitute only a bulk matter. In the other hand, when the string density is lower than the critical density of ρ_0, we call this place the *corona*. The other opportunity to have string fragments in corona part is to have enough high transverse momenta p_t to escape core part. Consequently, we have two types of matter, the bulk matter which thermalizes and expands hydrodynamically, the core part and the corona where segments will leave the bulk matter to become jets or hadrons.

The central collisions have a huge hydrodynamic part with an important core and less corona part unless the peripheral collisions have a big corona part and a little core part. One of the important part of this procedure is that we can use an hydrodynamic expansion event for AA and pp high multiplicity collisions.

The core corona separation starts by the identification of string fragments in core or corona depending of critical density ρ_0. However, some string fragments of bulk matter can escape the plasma depending of their transverse momenta. To know exactly which fragments escape, we compute for each one:

$$p_t^{new} = p_t - f_{Eloss} \int_\gamma \rho \, dL \tag{2.4.1}$$

where γ is the trajectory of the segment and f_{Eloss} a model parameter using some interpolation. The p^t_{new} can be positive or negative, if the new p_t is positive, the string fragments can escape the bulk matter and can be identified as a corona fragment. In the other case ($p^t_{new} < 0$), the segment cannot escape the plasma, therefore it contributes to the core. In a collision, the core corona process follows these steps:

- all nucleons in a nucleus are distributed by the Wood-Saxon potential;
- during the collision for each interacting parton pair, one Pomeron will be placed midway between them;
- following the above procedure, the core corona separation is done;
- the core will expand hydrodynamically, the corona will hadronize following the Area law.

For example, we can take a p-Pb collisions with 8 Pomerons. In the Fig 2.21 taken from [181], the Pomerons are illustrated in black. Around each Pomeron, the color strings are drawn by a circle. The green circles represent string in corona part, and the red circles represent the string in core part. The blue ellipse is here to guide eyes.

2.4.3 Three other steps

I will not detail the three other steps because they are not important for the complete understanding of my Ph.D manuscript. These three final steps are:

1. **Viscous hydrodynamic expansion:**
   The principle is simple. We do not talk about the corona part in this step of the event procedure, only the core part. Core starts to evolve from τ_0 according to the equations of relativistic viscous hydrodynamics using $\eta/s = 0.08$.

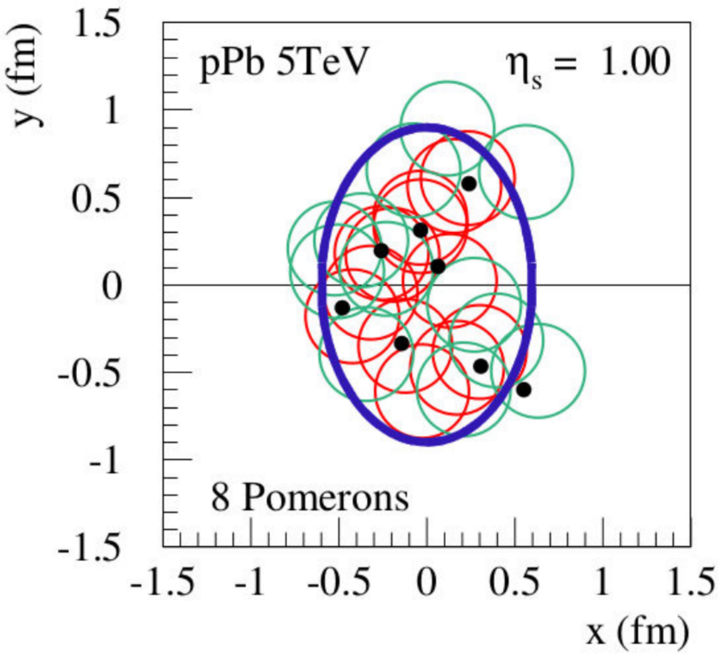

Figure 2.21: Distribution in the transverse plane of colour string. Black points are Pomerons. Around each Pomeron, red circles are string in core part and green circles are string in corona part

2. **Statistical hadronization:**
   The core, which has already evolved, hadronizes using the Cooper-Frye procedure, using equilibrium hadron distribution [194]. The corona part hadronizes using the string phenomenological model described in the 2.2.5.

3. **Final state hadronic cascade:**
   The hadronization is done and the hadron density is big enough to allow hadron-hadron rescatterings. UrQMD [136] model is used to produce the hadron-hadron rescatterings.

2.4.4 Summary

I described the EPOS history and EPOS 3 procedure to generate an event. The birth of EPOS comes from two ancestors: Venus and NeXuS. These two ancestors lay the foundation of the PBGRT and EPOS. Almost all disadvantages are vanished by the work done during years. Different versions of EPOS arise with the implementation of the ideal 3D+1 hydrodynamic (second) and the viscous hydrodynamical evolution and parton saturation (third).

The event procedure to create an event with the last version of EPOS (the third) is in five steps: i) Initial conditions: the PBGRT is employed where the elementary objects (Pomeron) are identified as DGLAP parton ladder using a saturation scale. The parton ladders will be treated as strings. ii) Core-corona approach: one separates fluid (core) and escaping hadron (corona) based on the momenta and the density of string segments. iii) Viscous hydrodynamic expansion: the core part will evolve according to the equation of relativistic viscous hydrodynamics using the shear viscosity over entropy $\eta/s = 0.08$. iv) Statistical hadronization: the core matter will hadronize using the Cooper Frye procedure and the corona will hadronize using the Area law and the Schwinger mechanism. v) Final state hadronic cascade: the hadron density is still big enough to allow hadron-hadron rescattering using UrQMD model.

2.5 Conclusion and Summary

In this chapter, I started by introducing the generalities about event generator: what is it? Why do we use an event generator? Who uses an event generator? The goal of a complete event generator is to reproduce the same number of particles produced in an experiment with the same characteristics. In an event generator, one event is equivalent as one collision. One can treat the event generator like a tool to disseminate ideas from theorists to experimentalists and opposite one. This is a bridge between theory and experiment. One of main advantages of an event generator is the fact that one can follow the evolution of a collision from the beginning to the end.

Then, I introduced the Monte Carlo method and its applications. To resume, the Monte Carlo method is a computational method using randomness to solve a problem that one could not determine the solution by the deterministic way. I introduced in others sections the Monte Carlo integration, average and variance.

In particle physics, we have a lot of General Purpose Monte Carlo in the market and I described few event generators. They are divided (in almost all cases) in the following steps: i) Hard Processes, ii) Resonance Decays, iii) Parton Shower, iv) Hadronization, v) Underlying event, vi) Decay of particles.

Then, I described few points of interests about Regge Theory and Gribov-Regge Theory. The Gribov-Regge Theory is an effective field theory which describes hadronic interaction using multiple exchange of the Pomeron in parallel. However, the approach is inconsistent because the energy conservation is not taken into account for the cross section calculations. After the introduction of the theories using Pomeron exchange, I introduced the parton model which changed our vision of particles with the introduction of partons.

The merging of the parton model and the GRT is called the Parton-Based-Gribov-Regge Theory and it tries to be a realistic treatment of all processes during a collision. This is a unified approach because the collision can be for proton-proton, proton-nucleus and nucleus-nucleus. The PBGRT contains a coherent treatment to calculate the cross section and the particle production taking correctly the energy conservation and calculate both exclusive and inclusive cross sections.

The particle production mechanism is described by the phenomenological string model. The string fragmentation in EPOS is done following the Area law where a direct algorithm is defined to define all characteristics of partons in each string fragment.

Finally I finished this chapter by the description of the EPOS history and the event procedure to create an event with the last version of EPOS.

I described at the most possible the physical point of view of different theories, law, particle production and interesting points for the purpose of this Ph.D thesis. I describe in the Appendix B important points about my computational work to develop EPOS outside physics.

In the next chapter, I will show the different methods used to study the anisotropic flow.

CHAPTER 3

METHODS TO STUDY THE ANISOTROPIC FLOW

Contents

We saw in the previous chapter the tools that I have used during all my Ph.D work. In this chapter, I will show the theoretical methods used to calculate anisotropic flow. Typically, I had some methods in the database of EPOS to calculate easily for developpers and users the anisotropic flow presented in this chapter.

The main observable of this Ph.D is the anisotropic flow that I briefly introduced in the section 1.3.1 of the Chapter 1. This chapter will be dedicated to the history and tacticals to calculate the anisotropic flow. To recall the section 1.3.1 of the Chapter 1, the anisotropic flow characterizes the fact that azimuthal distributions of produced particles are not uniform. For example, the elliptic flow distributions have an azimuthal distribution in almond form.

If we have an anisotropy in spatial space, that gives an anisotropy in the momentum space. The spatial anisotropy comes from the earliest time in the evolution of the collision. As the system expands it becomes more spherical, thus this driving force quenches itself. The momentum anisotropy is sensitive to the early stages of the system evolution [195]. I represent the anisotropy in the two different spaces in the Fig. 3.1. The azimuthal direction of particles produced in the collision is represented with the different arrays:

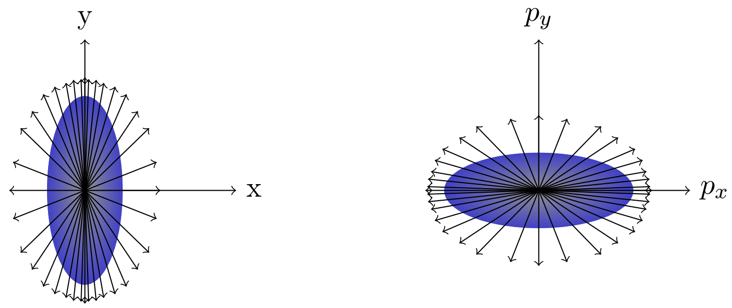

Figure 3.1: Correspondance between the anisotropy of particles production in spatial and momentum spaces

Collective flow observables have been measured experimentally since the 1980's. Over the years, many methods were developed to calculate the anisotropic flow. I will detail them in the different sections of this chapter. We developed a lot of tacticals to calculate the anisotropic flow because each method can be biased by *non-flow* effects. Those effects (nonflow) are not related to the initial geometry of the collision: for example anisotropic from jets, strong interaction, resonance decays... Flow analysis methods available in the early days can be classified into two different categories:

- fit the p_T or rapidity distributions of the particles of interest by assuming a local thermal equilibrium and a hydrodynamical evolution of the system. We can extract some information about the EoS, initial conditions etc ... [196]. This category will not develop more because those approaches are dependent on model assumptions. Our approach is based on reproducing exact experimental condition and methods to limit eventual biais. In addition, we use an unified approach in view of reducing as much as possible additional model inputs.
- study the azimuthal event shapes from data without any models. We have in this category a plentiful tacticals and I will describe in following sections some methods that we implement in EPOS.

The second category of flow analysis methods will be introduced in the following sections. In order to introduce them, I will start by introducing this question: why do we measure anisotropic flow ? To answer this question, we will look at the history of the study of anisotropic flow. Then, we will see the fight of physicists to decrease the contribution of non-flow effects with the first method. The first solution considered by physicists is the Event Plane (EP) method. However, this method is biased by the non-flow effects contributions. On the other hand, we can reduce the contributions of non-flow effects by different processes. We will see some methods to calculate the anisotropic flow after the Event Plane like: scalar products, two cumulant methods and the Lee-Yang-Zeroe method. To conclude this chapter by a discussion about which implementation of tacticals I implemented in EPOS and a conclusion.

3.1 Important definitions for anisotropic flow

The **reaction plane** is spanned by the vector of the impact parameter and the beam direction. The azimuth of the reaction plane is defined by Ψ_{RP}. To have a schematic representation of the nucleus-nucleus collisions with respect to the reaction plane, we can look at the Fig 3.2. I recall the particle azimuthal distribution with respect to the reaction plane. Using an anisotropic distribution, we can expand it into Fourier series [197]:

$$E\frac{d^3N}{d^3p} = \frac{1}{2\pi}\frac{d^2N}{p_T dp_T dy}\left(1+\sum_{n=1}^{\infty}2v_n\cos(n(\phi-\Psi_{RP}))\right) \tag{3.1.1}$$

where E is the energy of the particle, p its momentum, p_T its transverse momentum, ϕ its azimuthal angle, Ψ_{RP} the reaction plane angle, y its rapidity and the set of all v_n is observable of interest: the **anisotropic flow**. We can calculate the anisoptropic flow with:

$$v_n(p_t, y) = \langle\cos(n(\phi-\Psi_{RP}))\rangle \tag{3.1.2}$$

They are used for a quantitative characterization of the event anisotropy. The angle brackets refer to the average over all particles in all events. I do not refer sinus coefficients because we require a symmetry with respect to the reaction plane. As I said in the section 1.3.1, v_1 is referred as **directed flow** and the v_2 is referred as **elliptic flow**. We create two types of anisotropic flow, when v_n coefficients are averaged over transverse momentum and rapidity (or pseudorapidity) we call this flow as **integrated flow**. When the v_n coefficients are in function of pseudorapidity and transverse momentum, we call this flow as **differential flow**. We will try to reproduce both anisotropies in the next chapter.

Sadly, the reaction plane angle cannot be measured directly in high energy nuclear collisions, but fortunately, it can be estimated event-by-event from the particle azimuthal distribution. As I said in the introduction of this chapter, the reconstruction of the different harmonic flow coefficients introduces uncertainties in the analysis. The azimuthal correlations are not determined by the anisotropic flow but have other contributions referred as **non-flow** and quantified by the parameters δ_n.

For example, the equation of the anisotropic flow in function of the two-particle correlations is (with i and j two distinct particles):

$$\langle\cos(n(\phi_i-\phi_j))\rangle = \langle v_n^2\rangle + \delta_n \tag{3.1.3}$$

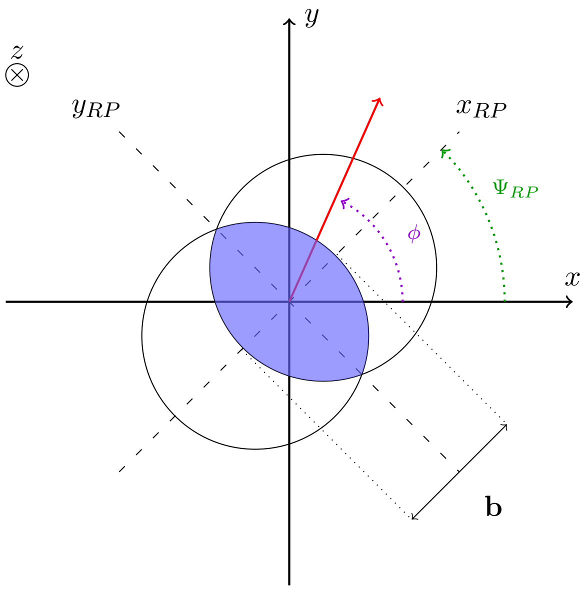

Figure 3.2: Schematic View of a non-central nucleus-nucleus collision

In addition to the non-flow effects, we must be vigilant about the **flow fluctuations**. Effectively, the coefficient of anisotropic flow can fluctuate event to event, both in direction event and in magnitude at fixed impact parameter b. All flow fluctuations are described by:

$$\sigma_{vn}^2 = \langle v_n^2 \rangle - \langle v_n \rangle^2 \tag{3.1.4}$$

One of the most important source of flow fluctuations is the initial geometry of the collisions. The overlapping region (in blue in the Fig 3.2) differs from an event to another one, because to the random nature of the interaction between constituents of the two nuclei. We have two types of particles between a collision like in EPOS. We have participants and remnants particles. The participants are particles which participate to the primary interaction in a collision. We can define a plane which contains just all participants without remnants called the **participant plane**. The participant plane is a little different than the reaction plane, consequently it is important to distinguish the measured flows in these two systems. The values of anisotropic flow in participant plane system are always larger than in reaction plane system. The definitions of both systems are illustrated in the Fig. 3.3.

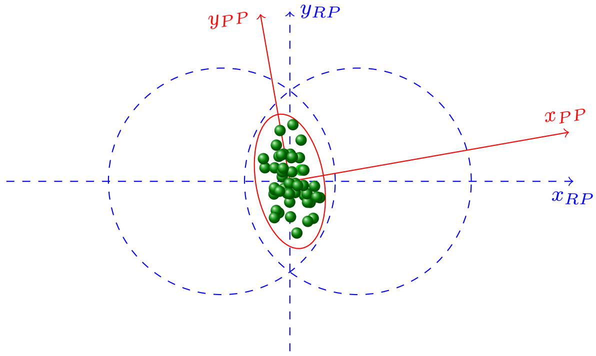

Figure 3.3: Schematic View of a non-central nucleus-nucleus collision

3.2 Why do we measure anisotropic flow?

This is a very interesting question! Why do we measure the anisotropic flow? They are other observables to probe of the QGP, consequently why is this observable crucial for physicists? To answer of this question, let's travel back in time.

Nowadays, it is certain that the anisotropic flow is one of the most informative direction in order to study the nature and properties of matter created at nuclear collisions in very high energy. We have used for a few decades the anisotropies in particle momentum distributions relative to the reaction plane to try to characterize this matter. J. Ollitrault suggested that the elliptic flow is a signature of the collective flow in relativistic nuclear collision [198] and first observed at the AGS [199, 200] and later at the SPS [201]. At the RHIC, we observed a large elliptic flow [202], which led to the concept of the strongly QGP. The large v_2 could be interpreted as the creation of a perfect fluid wihout viscosity at RHIC. In the other hand, first results of LHC tell us that this matter already created at RHIC have a viscosity, consequently this new state of matter is almost but not perfect. In this paper, we find that hydrodynamical model calculations can give a good description of the measurements of elliptic flow for transverse momenta up to 2 GeV/c. The calculation of the higher harmonic anisotropic flow coefficients are calculated for the first time, and the v_3 provides strong constraints on η/s (the viscosity). Currently, it is thought that the fluid has a viscosity also at RHIC [203]. The viscosity is approximatively $\eta/s \approx 0.05 - 0.20$ for the LHC and $\eta/s \approx 0.05 - 0.16$ for the RHIC [204]. In the case of EPOS, we set the viscosity of our fluid at $\eta/s \approx 0.08$.

The main interest in anisotropic flow is its sentivity to the early steps of the evolution of the matter. We saw in the section 1.3.1 of the Chapter 1 that the origin of the anisotropy is related to the initial geometry of the system. We can conclude in first approximation that the anisotropic flow is sensitive at early steps of the evolution of the matter because the matter cools down quickly, consequently the spatial asymmetries decrease with time and exists only in the first fm/c. I think that I convinced you that the anisotropic flow is a unique observable, providing a lot of information about QGP.

In the following of this chapter, I will talk about the methods to calculate the anisotropic flow, we will see there exist a lot of methods for this observable. This is not curious because we have been exploring this observable for a few decades and the method evoluates to remove the maximum of non-flow contributions. We start by the simplest and faster method: the Event Plane method.

3.3 Event plane method: classical but biased

The Event Plane (EP) [200, 205] is the mostly used because even if it is biased by non-flow contributions, this method is faster and simpler than other methods. Fortunately, some variations of the Event Plane method were created to minimize the contribution of non-flow effects. I will introduce in this section all my current knowledge about the EP method and its variations. This is the first method that I implemented in the database of EPOS due to its simplicity.

3.3.1 First ideas to create this method

In the following, I will explain the historical approach to create the EP method. I must step backward and explain how we construct the equation 3.1.2 with the equation 3.1.1. The azimuthal distribution $r(\phi)$ of the total transverse momentum of particles produced in a heavy ions collision is viewed as a periodic quantity, the Fourier expansion of this distribution is:

$$r(\phi) = \frac{x_0}{2\pi} + \frac{1}{\pi}\sum_{n=1}^{\infty}[x_n\cos(n\phi) + y_n\sin(n\phi)] \tag{3.3.1}$$

where:

$$x_n = \int_0^{2\pi} r(\phi)\cos(n\phi)d\phi \qquad y_n = \int_0^{2\pi} r(\phi)\sin(n\phi)d\phi \tag{3.3.2}$$

One can define the corresponding flow harmonics v_n of each pair of Fourier coefficients by the following way:

$$v_n \equiv \sqrt{x_n^2 + y_n^2} \tag{3.3.3}$$

In hadrons collisions, there are two cases: when the two colliding nuclei are either identical or not. In the first case, the symmetry of the system implies that y_n are equal to zero. The symmetry of the collision implies too that all x_n are zero for odd n. For y_n equal to zero, when we look at both Fig 3.2 and 3.3, we can see that we have the same probability of production for particles emitted at direction ψ and $-\psi$. Consequently the equation 3.3.2 becomes:

$$\sin(n\psi) + \sin(n\times -\psi) = \sin(n\psi) - \sin(n\psi) = 0 \tag{3.3.4}$$

For the odd fourier coefficients of x_n, the same reflection can be done as y_n but for particles emitted at direction ψ and $\psi + \pi$. Consequently the equation 3.3.2 becomes:

$$\begin{aligned}\cos(n\psi) + \cos(n\times(\psi+\pi)) &= \cos(n\psi) + \cos(n\psi)\cos(n\pi) - \sin(n\psi)\sin(n\psi)\\ &= \cos(n\psi) + \cos(n\psi)(-1)^n\\ &= \cos(n\psi)\times(1+(-1)^n) = 0 \text{ for odd n}\end{aligned} \tag{3.3.5}$$

The first remark of these characteristics that we can conclude is: when we have a symmetric collision (like p-p, Pb-Pb or Au-Au), the anisotropic flow defined in the equation 3.3.3 is equal to x_n for even n. We can describe v_n with the distribution $r(\phi)$ in the following way:

$$\begin{aligned}\langle\cos(n\phi)\rangle &= \frac{\int_0^{2\pi}\cos(n\phi)r(\phi)d\phi}{\int_0^{2\pi} r(\phi)d\phi}\\ &= \frac{\frac{1}{\pi}\int_0^{2\pi}\cos^2(n\phi)d\phi}{v_0}\\ &= \frac{v_n}{v_0}\end{aligned} \tag{3.3.6}$$

To do the simplification from the first to the second line of the above equation, we have used the orthogonality relationship of the sine and cosine terms:

$$\int_{-\pi}^{\pi} \sin(mx)\sin(nx)dx = \pi\delta_{nm} \tag{3.3.7}$$

$$\int_{-\pi}^{\pi} \cos(mx)\cos(nx)dx = \pi\delta_{nm} \tag{3.3.8}$$

$$\int_{-\pi}^{\pi} \cos(mx)\sin(nx)dx = 0 \tag{3.3.9}$$

where δ_{nm} is the Kronecker symbol. The distribution $r(\phi)$ have been normalized, consequently $v_0 = \int_0^{2\pi} r(\phi)d\phi = 1$ and the Eq. 3.3.6 becomes:

$$v_n = \langle\cos(n\phi)\rangle \tag{3.3.10}$$

This result is not used in the measurement of v_n. One reason is the difficulty to learn about the reaction plane ψ_{RP} with this result. We must also take into account the volume occupied by participants of the collision. We do not take into account the fluctuations in the initial positions of participating nucleons within the created volume [206]. Those fluctuations can generate any type of anisotropy in coordinate space and consequently transferred in the momentum space, where we measure the anisotropic flow v_n. In [207], we rewrite the Fourier decomposition in the Eq. 3.3.1. We will decompose this equation using complex numbers with these idendities:

$$cos(n\varphi) = \frac{1}{2}\left(e^{in\varphi} + e^{-in\varphi}\right) \qquad \sin(n\varphi) = \frac{1}{2i}\left(e^{in\varphi} - e^{-in\varphi}\right) \tag{3.3.11}$$

We insert now these relations in the Eq. 3.3.1:

$$\begin{aligned} r(\varphi) &= \frac{x_0}{2\pi} + \frac{1}{\pi}\sum_{n=1}^{\infty}\frac{1}{2}(x_n - iy_n)e^{in\varphi} + \frac{1}{\pi}\sum_{n=1}^{\infty}\frac{1}{2}(x_n + iy_n)e^{-in\varphi} \\ &= \frac{x_0}{2\pi} + \frac{1}{\pi}\sum_{n=1}^{\infty}\frac{1}{2}(x_n - iy_n)e^{in\varphi} + \frac{1}{\pi}\sum_{n=-\infty}^{-1}\frac{1}{2}(x_{-n} + iy_{-n})e^{in\varphi} \end{aligned} \tag{3.3.12}$$

Then we insert the following equation in the above result ;

$$v_n = \begin{cases} x_n - iy_n, & n > 0 \\ x_n + iy_n, & n < 0 \\ x_0, & n = 0 \end{cases} \tag{3.3.13}$$

and we obtain:

$$r(\varphi) = \frac{1}{2\pi}\sum_{n=-\infty}^{\infty} v_n e^{in\varphi} \tag{3.3.14}$$

We have now a general complex equation of the azimuthal distribution $r(\varphi)$ in function of the anisotropic flow v_n, where v_n is also a complex observable. However, we know and observe that the azimuthal distribution $r(\varphi)$ is real. Therefore, we obtain these characteristics:

$$r(\varphi) = r(\varphi)^* \qquad v_n = v_{-n}^* \tag{3.3.15}$$

Then we insert the above characteristics in the Eq. 3.3.14:

$$\begin{aligned} r(\varphi) &= \frac{v_0}{2\pi} + \frac{1}{2\pi}\sum_{n=1}^{\infty} v_n^* e^{-in\varphi} + \sum_{n=1}^{\infty} v_n e^{in\varphi} \\ &= \frac{v_0}{2\pi} + \frac{1}{2\pi}\sum_{n=1}^{\infty} 2 \times \Re\left[v_n e^{in\varphi}\right] \end{aligned} \tag{3.3.16}$$

We can decompose v_n as each complex number: $v_n \equiv |v_n|e^{-in\psi_n}$ and include this decomposition in the above equation:

$$r(\varphi) = \frac{v_0}{2\pi} + \frac{1}{\pi}\sum_{n=1}^{\infty} |v_n|\ \Re\left[e^{in(\varphi-\psi_n)}\right] \tag{3.3.17}$$

Finally, we take the real part of right part of the above equation and we obtain:

$$r(\varphi) = \frac{v_0}{2\pi} + \frac{1}{\pi}\sum_{n=1}^{\infty} v_n \cos[n(\varphi-\psi_n)] \tag{3.3.18}$$

We see directly that the ψ_n represent the plane of participants, the so called participant plane. The complete anisotropic flow is a generalization of the Eq. 3.3.10 with the participant plane:

$$\boxed{v_n = \langle \cos[n(\varphi-\psi_n)] \rangle} \tag{3.3.19}$$

This is the equation that we need to know for the following development of: **how do we construct the EP method ?** To answer this question, we start with another way to do the Fourier development in the Eq. 3.1.1. Generally, the particle invariant spectrum can be written as:

$$E\frac{d^3N}{dp^3} = \frac{d^3N}{p_t dp_t dy d\phi} = \frac{d^2N}{p_t dp_t dy} \times R(p_t, y, \phi) \tag{3.3.20}$$

we assume that the function $R(p_t, \eta, \phi)$[1] satisfies the normalization condition $\int_0^{2\pi} d\phi\ R(p_t, \eta, \phi) = 1$ and we expand this function in Fourier series:

$$R(p_t, y, \phi) = \frac{1}{2\pi}\left[1 + 2\times\sum_{n=1}^{\infty} Q_x(p_t,\eta,n)\cos(n\phi) + \sum_{n=1}^{\infty} Q_y(p_t,\eta,n)\sin(n\phi)\right] \tag{3.3.21}$$

where $Q_{\{x,y\}}$ plays the same role as $\{x, y\}_n$ of the Eqs 3.3.2:

$$Q_x(p_t,\eta,n) = \int_0^{2\pi} d\phi \times R(p_t,\eta,\phi)\cos(n\phi) \qquad Q_y(p_t,\eta,n) = \int_0^{2\pi} d\phi \times R(p_t,\eta,\phi)\sin(n\phi) \tag{3.3.22}$$

Q_x and Q_y are the components of **Q-vector** or *flow vector* or *event flow vector*. We define the Q-vector in each space phase of p_t and η like following:

$$\vec{Q}(p_t,\eta,n) = \{Q_x(p_t,\eta,n), Q_y(p_t,\eta,n)\} = \{V_n(p_t,\eta), n\Psi_{EP}\} \tag{3.3.23}$$

where EP is for Event Plane. We can rewrite $Q_{\{x,y\}}$ in function of $\{V_n(p_t,\eta), n\Psi_{EP}\}$ as following:

[1] I note that y and η are quasiequal at very high energy, I write η in place of y to remove confusions that we can have with y the rapidity and y the second coefficient of Q-vector

$$Q_x(p_t, \eta, n) = V_n(p_t, \eta)\cos(n\Psi_{EP}) \qquad Q_y(p_t, \eta, n) = V_n(p_t, \eta)\sin(n\Psi_{EP}) \tag{3.3.24}$$

Then, we can put the above conditions in the Eq. 3.3.21:

$$R(p_t, \eta, \phi) = \frac{1}{2\pi}\left\{1 + 2 \times \sum_{n=1}^{\infty} V_n(p_t, \eta)\cos[n(\phi - \Psi_{EP})]\right\} \tag{3.3.25}$$

Finally, we can write the particle invariant spectrum in Eq. 3.3.20 with the new (p_t, η, ϕ) of the above equation:

$$E\frac{d^3N}{dp^3} = \frac{d^2N}{2\pi p_t dp_t dy} \times \left\{1 + 2 \times \sum_{n=1}^{\infty} V_n(p_t, \eta)\cos[n(\phi - \Psi_{EP})]\right\} \tag{3.3.26}$$

We can conclude two things:

1. the big $R(p_t, \eta, \phi)$ plays the same role as $r(\varphi)$ when we compare Eq. 3.3.18 and Eq. 3.3.25: $\Rightarrow$ V_n and v_n are **both** anisotropic flows with respect to different planes: the **participant** and the **event** planes.

2. by comparing Eq. 3.3.26 and Eq. 3.1.1, one can see that **event plane** Ψ_{EP} plays also the same role of **reaction plane** Ψ_{RP}. We can determine an anisotropic flow at the same way of Eq. 3.1.2 and Eq. 3.3.19.

The equation of the anisotropic flow obtained by the Event Plane method is:

$$\boxed{v_n = \langle\cos[n(\phi - \Psi_{EP})]\rangle} \tag{3.3.27}$$

This section is more a theoretical answer of how can we say physically that an event plane has an anisotropic flow equivalent of the reaction plane. However, we never measure the anisotropic flow directly with the particle invariant spectrum. Experimentalist physicists created a simple method to calculate the Event Plane and the anisotropic flow associated to its plane. I will describe this method in the following section.

3.3.2 Practical Method

The standard event plane method [205] estimates the azimuthal angle of the reaction plane from the observed event plane angle determined by the anisotropic flow. We can start the classical method by different ways but I choose to start the description of this method with the event flow vector.

The event flow vector Q_n is defined in the transverse plane by:

$$\begin{aligned} Q_{n,x} &= \sum_{i}^{M} w_i \cos(n\phi_i) = Q_n\cos(n\Psi_n) \\ Q_{n,y} &= \sum_{i}^{M} w_i \sin(n\phi_i) = Q_n\sin(n\Psi_n) \end{aligned} \tag{3.3.28}$$

where the sum is over all particles i used in the event plane calculation within M the multiplicity of the event. ϕ_i is the azimuthal angle of the particles, w_i its weight and Ψ_n the event plane angle.

The weights optimize the event plane resolution. We have a large choice of weights to optimize the resolution: for example, we can choose the transverse momentum of the particles, we can keep $w_i = 1$ or take the transverse energy of the particle. At little value of p_t, $v_n(p_t, y)$ often increase with p_t, consequently the transverse momentum is commonly used at weight up to 2 GeV/c.

We can calculate each order n of Ψ_n with Eq 3.3.28 by the following equation:

$$\Psi_n = \frac{1}{n} \arctan \left(\frac{\sum_i^M w_i \sin(n\phi_i)}{\sum_i^M w_i \cos(n\phi_i)} \right) \tag{3.3.29}$$

And finally, we can calculate the anisotropic flow like the Eq. 3.3.27:

$$v_n^{obs}(p_t, y) = \langle \cos[n(\phi_i - \Psi_n)] \rangle \tag{3.3.30}$$

where brackets denote an average over all particles in all events, ϕ_i their azimuthal angle in a given p_t and rapidity.

Since in each event there is a finite number of particles and because the event plane is an approximation of the reaction plane, this result is biased. To reduce the event-by-event fluctuations, we must include a correction called the **event plane resolution** for each harmonic of event plane. The resolution in classical method of event plane is:

$$\mathcal{R}_n = \langle \cos[n(\Psi_n - \Psi_{RP})] \rangle \tag{3.3.31}$$

where brackets denote an average over all events. The final anisotropic flow of this method is the following equation:

$$\boxed{v_n = \frac{v_n^{obs}(p_t, y)}{\mathcal{R}_n} \equiv \frac{\langle \cos[n(\phi_i - \Psi_n)] \rangle}{\langle \cos[n(\Psi_n - \Psi_{RP})] \rangle}} \tag{3.3.32}$$

This is the faster method to calculate the anisotropic flow for each order of anisotropy. However we took all particles in all events, thus we do not remove the auto-correlation of particles, consequently we include inevitably non-flow effects. The event plane resolution is affected by correlations which do not stem from genuine correlation of all particles with the reaction plane. This is one kind of effect that implies a bias in the estimation of anisotropic flow v_n. In order to reduce those bias, we include alternative approaches to vanish non-flow contributions: i) use gap(s) between different ranges to reduce auto-correlation, ii) use method which does not require the reaction plane estimation event-by-event, iii) use genuine multi-particle correlations (*cumulants*) to suppress systematically the non-flow contributions.

3.3.3 A Way to reduce non-flow effects: Add range gaps

To calculate an estimation of $\langle \cos[n(\Psi_n - \Psi_{RP})] \rangle$, we can define one (or more) independent sub-events with the same multiplicity. There are two general ways to build the sub-events:

- create two η symmetrical planes/ranges/windows: $[\eta_{min}; \eta_{max}]$ and $[-\eta_{max}; -\eta_{min}]$ and add a η gap between these two sub-events.
- separate the total particles randomly into two sub-events with the same multiplicity in each sub-event. We called these events: **random sub-events**

An example the first way is used at STAR [208, 209], they use two sub-events in two ranges of pseudorapidity : one with negative pseudorapidity (A) and another one with positive pseudorapidity (B) to have approximately the same multiplicity. They add a little gap (0.1) between these two planes. Consequently, we reduce the auto-correlation effect.

The event plane resolution changes by:

$$\mathcal{R}_{n,sub} = \sqrt{\langle \cos[n(\Psi_n^A - \Psi_n^B)] \rangle} \tag{3.3.33}$$

The corrected anisotropic flow is calculate by:

$$\boxed{v_n = \frac{v_n^{\text{obs}}}{\mathcal{R}_{n,sub}} = \frac{\langle \cos[n(\phi_i - \Psi_n)] \rangle}{\sqrt{\langle \cos[n(\Psi_n^A - \Psi_n^B)] \rangle}}} \tag{3.3.34}$$

A limitation of this method is we need a large multiplicity if we want to calculate the elliptic flow in more than two ranges with one gap. Another important limitation is the possibility to turn off the collectivity when we increasing too much the gap. Therefore, different new methods were developed over the years to measure the anisotropic flow without these limitations, for example the scalar product.

3.4 Scalar Product method

3.4.1 Introduction of the scalar product method

The EP method offers a direct way to calculate the anisotropic flow, but this method has three principal weaknesses:

1. the contribution of non-flow can be important and difficult to remove
2. all event-by-event fluctuations can bias the final result, we must correct the result by a resolution
3. experimental correction should be implemented to control the non-uniform acceptance correlations

I will talk about the two first weaknesses because the last one is only treated in experimental method as opposed to EPOS that has an uniform acceptance. Two methods are developed to overcome part of the two first weaknesses of the EP method. The first method is the **fitted q-distribution** [197] that I will not talk because we do not implement this one in EPOS. This method have also several serious limitations: we calculate only the integrated flow, we cannot generalize this method to differential flow; this method can be used only for very large multiplicities; consequently we cannot use this method for all detectors, it does not work on detectors with poor acceptance. Another method used is the **Scalar Product (SP)** method [205]. This method follows the idea of the event plane method and takes into account both event-by-event fluctuations and non-flow contributions. This method estimates the anisotropic flow without estimating the reaction plane using unit vector of particle.

3.4.2 Estimation of anisotropic flow

The Scalar Product (SP) [205] is for me an extension of the event plane method bypassing the estimation of the reaction plane. The SP separates each event into two equivalent sub-events with same multiplicity. The event flow vector of each sub-event is evaluated as :

$$\begin{aligned} \vec{Q_n^a}(p_t,\eta,n) &= \{Q_x^a(p_t,\eta,n), Q_y^a(p_t,\eta,n)\} = \{V_n^a(p_t,\eta), n\Psi_n^a\} \\ \vec{Q_n^b}(p_t,\eta,n) &= \{Q_x^b(p_t,\eta,n), Q_y^b(p_t,\eta,n)\} = \{V_n^b(p_t,\eta), n\Psi_n^b\} \end{aligned} \tag{3.4.1}$$

where, the vectors $\vec{Q_n^a}$ and $\vec{Q_n^b}$ are constructed from the sub-events a and b.

We define each sub-event to have approximately the total Q-vector given by :

$$\vec{Q_n} = \vec{Q_n^a} + \vec{Q_n^b} = \{V_n(p_t, \eta), n\Psi_n\} \tag{3.4.2}$$

We define the unit vector u of a particle:

$$\vec{u_n} = \{\cos(n\phi), \sin(n\phi)\} \qquad |\vec{u_n}| = 1 \tag{3.4.3}$$

We can see with the scalar product of each $\vec{u_n}$ (for each particle) and $\vec{Q_n}$ that we can obtain the same v^{obs} than Eq 3.3.30 :

$$\langle \vec{u_n} \cdot \vec{Q_n} \rangle = \langle V_n \cos[n(\phi - \Psi_n)] \rangle = \langle V_n \rangle v_n^{\text{obs}} \tag{3.4.4}$$

Unfortunately, we do not have the exact anisotropic flow, therefore we use one other scalar product whichever is between the two sub-events :

$$\begin{aligned} \langle \vec{Q_n^a} \cdot \vec{Q_n^b} \rangle &= \langle V_n^a V_n^b \rangle \langle \cos[n(\Psi_n^a - \Psi_n^b)] \rangle \\ &\approx \langle V_n^2 \rangle \langle \cos[n(\Psi_n^a - \Psi_n^b)] \rangle \end{aligned} \tag{3.4.5}$$

We can express this average of cosinus with the reaction plane:

$$\begin{aligned} \langle \cos[n(\Psi_n^a - \Psi_n^b)] \rangle &= \langle \cos\{[n(\Psi_n^a - \Psi_{RP}] - [n(\Psi_n^b - \Psi_{RP})]\} \rangle \\ &= \langle \cos[n(\Psi_n^a - \Psi_{RP})] \rangle \langle \cos[n(\Psi_n^b - \Psi_{RP}] \rangle \end{aligned} \tag{3.4.6}$$

The difference between each azimuthal angle of each sub-event and the azimuthal angle of the reaction plane is attributed to event-by-event fluctuations and because the sin terms vanished, one can get the event plane resolution:

$$\begin{aligned} \mathcal{R}_n = \langle \cos[n(\Psi_n - \Psi_{RP})] \rangle &\approx \langle \cos[n(\Psi_n^a - \Psi_{RP}] \rangle \\ &\approx \langle \cos[n(\Psi_n^b - \Psi_{RP})] \rangle \\ &\approx \sqrt{\langle \cos[n(\Psi_n^a - \Psi_n^b)] \rangle} = \mathcal{R}_{n,sub} \end{aligned} \tag{3.4.7}$$

Finally, by combining the Equations 3.4.4, 3.4.5 and 3.4.7, we can obtain the real value of the differential flow:

$$\boxed{v_n^{\text{SP}}} = \frac{v_n^{\text{obs}}(p_T, y)}{\langle \cos[n(\Psi_n - \Psi_{RP})] \rangle} = \frac{v_n^{\text{obs}}(p_T, y)}{\sqrt{\langle \cos[n(\Psi_n^a - \Psi_n^b)] \rangle}} \boxed{= \frac{\langle \vec{u_n} \cdot \vec{Q_n} \rangle}{\sqrt{\langle \vec{Q_n^a} \cdot \vec{Q_n^b} \rangle}}} \tag{3.4.8}$$

We can obtain the anisotropic flow without an estimation of the reaction plane by using two scalar products on two sub-events. One advantage of this method is that the non-flow correlations are removed by using the sub-events. I think that we have same advantages as the eta-sub event plane method about the vanishing of non-flow correlations. The only practical difference is that we calculate the differential flow without an estimation of the reaction plane. The validation of the final results depends on the condition of same multiplicity in each sub-event and some event-by-event fluctuations could be biased. The resolution of the scalar product method can be calculated only if we have large enough statistics (as the event plane method).

We can calculate all n-orders of the anisotropic flow easily and quickly with these two methods: event plane (eta-sub) and scalar product method. Using different sub-events with a pseudorapidity gap, we can reduce a large part of non-flow contribution, but we introduce some effects inducing bias. I will introduce in the following section another method using genuine multi-particle correlations (*cumulants*) to calculate the anisotropic flow and suppress systematically the non-flow contributions.

3.5 Cumulants Methods

Before explaining what is this method, I have one another important concept to define: the differentiation of the **reference particles** and the **particles of interest**. Strictly, the distribution in Eq. 3.1.1 is related to the Particles of Interest (POI), on the other hand, the distribution in Eq. 3.3.26 with a big $V_n(t, \eta)$ is related to the Reference Particles (RP). Effectively, the particles used to determine the event plane in Eq 3.3.29 must be different than the particles that we want to calculate the flow to reduce a collective bias. If we talk in the event plane language, we can say that the particles used to calculate the event plane are the RP and the particles which we want to calculate the flow are the POI. Generally we separate these two concepts of particles with kinematical regions or different types of particles. For example, we can take in RP the charged particles in a pseudorapidity range of -0.8 $< \eta <$ 0.8 and any p_T. Then, we say that the POI are the kaons in a p_T range of 0.2 $< p_T <$ 5 GeV. In particular, we can have particles referenced as **both** POI and RP, here charged kaons in a pseudorapidity range of -0.8 $< \eta <$ 0.8 and a p_T range of 0.2 $< p_T <$ 5 GeV. The differentiation of these two types of particles is very important for the following specifically for **Q-Cumulant** method, but before using it, we must define what is exactly a cumulant.

3.5.1 Where does the cumulant expansion come from?

As mentioned many times above, the methods of flow analysis are sensitive to the non-flow effects. One other problem in using multi-particle correlations is the computing power needed to go over all possible particle multiplets. To remedy these problems, few methods based on the fact that the anisotropic flow is a correlation among all particles in an event whereas non-flow effects originate from a few particle correlations are developed. The cumulant method can measure the anisotropic flow by a cumulant expansion of multi-particle azimuthal correlations [210–214]. One goal of this method is the more we increase the order of the cumulant expansion the more the non-flow effects decrease. I will explain the historical approach written in the different references [210–214] to calculate the different orders of anisotropic flow during the whole section.

To explain where the cumulant expression/framework comes from, I will follow the description of the reference [210]. We call flow, the azimuthal correlations between the outgoing particles and the reaction plane, we can express v_n as a function of the one-particle momentum distribution $f(p) \equiv dN/d^3p$:

$$v_n(\mathcal{D}) \equiv \langle e^{in\phi} \rangle = \frac{\int_{\mathcal{D}} e^{in\phi} f(p) d^3p}{\int_{\mathcal{D}} f(p) d^3p} \tag{3.5.1}$$

where the brackets denote an average over all events and $\mathcal{D}$ represents a phase space window in the (p_T, y) of the detector. Since the particle source is symmetric with respect to the reaction plane for spherical nuclei, $\langle \sin n\phi \rangle$ vanishes and v_n is real.

Two-particle correlations

Same as EP and SP, we measure the relative azimuthal angles between outgoing particles. The standard flow analysis on the measurement of two-particle azimuthal correlations, which involve the two-particle distribution $f(p_1, p_2) \equiv dN/(d^3p_1 d^3p_2)$:

$$\langle e^{in(\phi_1 - \phi_2)} \rangle_{\mathcal{D}_1 \times \mathcal{D}_2} = \frac{\int_{\mathcal{D}_1 \times \mathcal{D}_2} e^{in(\phi_1 - \phi_2)} f(p_1, p_2) d^3p_1 d^3p_2}{\int_{\mathcal{D}_1 \times \mathcal{D}_2} f(p_1, p_2) d^3p_1 d^3p_2} \tag{3.5.2}$$

Taking non-flow correlations effects, we can be written as:

$$f(p_1, p_2) = f(p_1) \times f(p_2) + f_c(p_1, p_2) \tag{3.5.3}$$

where $f_c(p_1, p_2)$ denotes the correlated part of the distribution which the sources are various and not specially about flow correlations. Inserting the equation 3.5.2 in equation 3.5.3, one can find:

$$\langle e^{in(\phi_1-\phi_2)}\rangle_{\mathcal{D}_1\times\mathcal{D}_2} = v_n(\mathcal{D}_1)v_n(\mathcal{D}_2) + \langle e^{in(\phi_1-\phi_2)}\rangle_c \tag{3.5.4}$$

In the last equation, the left-hand side represents the measured two-particle azimuthal correlation, in the right-hand, the first term represents the contribution of flow to this correlation, the last term denotes the contribution of the correlated part f_c. This term corresponds to azimuthal correlations which do not arise from flow, we can call them the **direct** correlations, in opposition to the indirect correlations arising from the correlation with the reaction plane, the **flow**.

Multi-particle correlations and the cumulant expansion

The main idea of the cumulant expansion is to separate the correlated part from the uncorrelated part like the equation 3.5.3 for two-particle correlations. We cannot separate these two parts in standard analysis like EP and SP. The decomposition of the particle distribution into correlated and uncorrelated parts in 3.5.3 can be generalized to an arbitrary number of particles. To have a simplier example of multi-particle correlation, we start by decomposing the three-particle distribution as:

$$\begin{aligned}\frac{dN}{dp_1dp_2dp_3} \equiv & f(p_1,p_2,p_3) = f_c(p_1)f_c(p_2)f_c(p_3) + f_c(p_1,p_2)f_c(p_3) \\ & + f_c(p_1,p_3)f_c(p_2) + f_c(p_2,p_3)f_c(p_1) + f_c(p_1,p_2,p_3)\end{aligned} \tag{3.5.5}$$

Of course, $f_c(p_x) = f(p_x)$, we can express $f_c(p_x, p_y)$ into $f(p_x, p_y)$ with expression 3.5.3 $\rightarrow f_c(p_1, p_2) = f(p_1, p_2) - f(p_1)f(p_2)$. We can represent the equations 3.5.3 and 3.5.5 diagrammatically. In these figures, correlated distributions f_c are represented by enclosed sets of points, they correspond to connected diagrams.

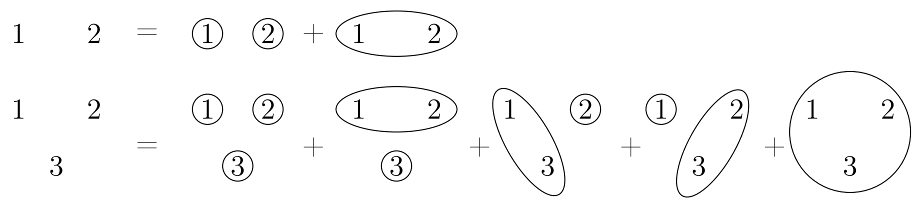

Figure 3.4: Diagrammatic representation of the decomposition of particle distribution into correlated and uncorrelated components

In a more general way, in order to decompose the j-point function $f(p_1, \cdots, p_j)$, one first takes all possible partitions of the set of points $\{p_1, \cdots, p_j\}$. To each subset of points $\{p_{i1}, \cdots, p_{ik}\}$, one can associate the corresponding correlated function $f_c(p_{i1}, \cdots, p_{ik})$. The contribution of a given partition is the product of the contributions of each subset. Finally, $f(p_1, \cdots, p_j)$ is the sum of the contribution of all particles. For example, we can calculate the decomposition of $f(p_1, p_2, p_3)$ as:

$$\begin{aligned} f(p_1,p_2,p_3) = & f_c(p_1,p_2,p_3) + f_c(p_1,p_2)f_c(p_3) + f_c(p_1,p_3), f_c(p_2) \\ & + f_c(p_1)f_c(p_2,p_3) + f_c(p_1)f_c(p_2)f_c(p_3) \\ & = f(p_1)f(p_2)f(p_3) + f(p_3)\left[f(p_1,p_2) - f(p_1)f(p_2)\right] \\ & + f(p_2)\left[f(p_1,p_3) - f(p_1)f(p_3)\right] + f(p_1)\left[f(p_2,p_3) - f(p_2)f(p_3)\right] \\ & + f_c(p_1,p_2,p_3)\end{aligned} \tag{3.5.6}$$

$$\begin{aligned}f(p_1,p_2,p_3) &= f(p_1)f(p_2)f(p_3) + f(p_3)f(p_1,p_2) - f(p_3)f(p_1)f(p_2) + f(p_2)f(p_1,p_3)\\&- f(p_2)f(p_1)f(p_3) + f(p_1)f(p_2,p_3) - f(p_1)f(p_2)f(p_3) + f_c(p_1,p_2,p_3)\\&= f_c(p_1,p_2,p_3) + f(p_3)f(p_1,p_2) + f(p_1)f(p_2,p_3) + f(p_2)f(p_1,p_3)\\&- 2\times f(p_1)f(p_2)f(p_3)\end{aligned}$$

The equations expressing the j-point functions f in terms of the correlated functions f_c can be inverted order by order, so as to isolate the term of smallest magnitude:

$$\begin{aligned}f_c(p_1) &= f(p_1)\\f_c(p_1,p_2) &= f(p_1,p_2) - f(p_1)f(p_2)\\f_c(p_1,p_2,p_3) &= f(p_1,p_2,p_3) - f(p_1,p_2)f(p_3) - f(p_1,p_3)f(p_2) - f(p_2,p_3)f(p_1)\\&+ 2\times f(p_1)f(p_2)f(p_3)\end{aligned} \tag{3.5.7}$$

In the description of the reference [210], they describe the generalization in any orders of the two-particle azimuthal correlations in equation 3.5.3 and the decomposition of all orders in the same way. Finally, with the diagrammatic representation, we can see that the contribution $f_c(p_1,\cdots,p_j)$ can be called the genuine j-particle correlation or the connected part of the correlation or the direct j-particle correlation.

Measuring flow with multi-particle azimuthal correlations

The method developed by N. Borghini et al [210–212] allows the detection of small deviations from an isotropic distribution. With the introduction of this chapter, we can say that there is no flow if the source is isotropic or the reaction plane does not influence the particle distribution. One can measure the j^{th} cumulant of the multi-particle azimuthal correlation, which is of order N^{1-j} if the distribution is isotropic. When a deviation -however tiny- appears, we know that we have flow in our collision. In the rest of this section, we will consider an isotropic particle distribution fast, then introduce a tiny deviation from it.

Firstly, we assume an isotropic particle distribution, thus the flow in equation 3.5.1 vanishes. Therefore, the two-particle azimuthal correlation in equation 3.5.4 reduces to its connected part. As a further consequence of isotropy, only $2j$-particle azimuthal correlation involving j powers of $e^{in\phi}$ and j powers of $e^{-in\phi}$ are nonvanishing because average like $\langle e^{in(\phi_1+\phi_2-\phi_3)}\rangle$ vanish [210]. Now we want to express the cumulant expansion of the correlation $\langle e^{in(\phi_1+\phi_2-\phi_3-\phi_4)}\rangle$, this can be decomposed into:

$$\begin{aligned}\langle e^{in(\phi_1+\phi_2-\phi_3-\phi_4)}\rangle &= \langle e^{in(\phi_1-\phi_3)}\rangle_c\langle e^{in(\phi_2-\phi_4)}\rangle_c + \langle e^{in(\phi_1-\phi_4)}\rangle_c\langle e^{in(\phi_2-\phi_3)}\rangle_c\\&+ \langle e^{in(\phi_1+\phi_2-\phi_3-\phi_4)}\rangle_c\end{aligned} \tag{3.5.8}$$

To obtain this equation, we use the decomposition of particle distribution like (3.5.5) for 4 particles. We keep only $2j$ order on $f_c(p_1,\cdots,p_j)$ and the last term $\langle e^{in(\phi_1+\phi_2)}\rangle_c\times\langle e^{in(-\phi_3-\phi_4)}\rangle_c$ vanishes because this is not a $2j$-particle azimuthal correlation involving j powers of $e^{in\phi}$ and j powers of $e^{-in\phi}$. Then, this equation can decomposed using equations 3.5.7 into:

$$\begin{aligned}\langle e^{in(\phi_1+\phi_2-\phi_3-\phi_4)}\rangle &= \langle e^{in(\phi_1-\phi_3)}\rangle\langle e^{in(\phi_2-\phi_4)}\rangle + \langle e^{in(\phi_1-\phi_4)}\rangle\langle e^{in(\phi_2-\phi_3)}\rangle\\&+ \langle e^{in(\phi_1+\phi_2-\phi_3-\phi_4)}\rangle_c\end{aligned} \tag{3.5.9}$$

The first two terms in the right-hand side of this equation are products of direct two-particle correlations while the last term corresponds to direct four-particle correlations. The last term is called a **cumulant** to order 4 and denoted by $\langle\langle e^{in(\phi_1+\phi_2-\phi_3-\phi_4)}\rangle\rangle$.

One important property to note is the cumulant to order 4 will always be defined by the previous equation even when the source is not isotropic [210]. However, if the source is anisotropic, the cumulant to order 4 $\langle\langle e^{in(\phi_1+\phi_2-\phi_3-\phi_4)}\rangle\rangle$ is not equal to the connected part $\langle e^{in(\phi_1+\phi_2-\phi_3-\phi_4)}\rangle_c$.

Let us consider the small deviation from isotropy, then a flow. The two-particle azimuthal correlation receives a contribution v_n^2 according to equation 3.5.4 and the four-particle azimuthal correlation receives a contribution v_n^4 for same reasons. The cumulant becomes (see Appendix C):

$$\langle\langle e^{in(\phi_1+\phi_2-\phi_3-\phi_4)}\rangle\rangle = -v_n^4 + \mathcal{O}\left(\frac{1}{N^3}+\frac{v_{2n}^2}{N^2}\right) \tag{3.5.10}$$

when N is the total number of emitted particles during the collision. We can conclude that we can calculate the anisotropic flow v_n with different orders of genuine multi-particle correlations (cumulants) when N is huge enough without estimating the reaction plane. This method suppresses systematically the non-flow contributions but we must calculate each order of cumulants.

Two ways are created to calculate/generate each order of cumulants. The first way is using a generating function [210–212] to generate each cumulant and calculate the flow. The second recent way is a direct method using the Q-vector [213, 214] to calculate directly each order of cumulants.

3.5.2 Cumulant by Generating Function

From now, we use cumulant from each order and we can for example define the second order cumulant by:

$$\langle e^{in(\phi_1-\phi_2)}\rangle = \langle e^{in\phi_1}\rangle\langle e^{in\phi_2}\rangle + \langle\langle e^{in(\phi_1-\phi_2)}\rangle\rangle \tag{3.5.11}$$

Cumulants can be expressed without assuming a perfect detector using the formalism of generating functions.

Integrated Flow

This section is different from previous ones. I will write the same physical meaning in two different levels of details. I write twice same results: i) only the idea of the method and the final result, ii) the whole description of the method.

The idea of this method is to use a generating function to calculate all orders of cumulants. The generating function is defined in the 3.5.13 for a perfect detector. To calculate this generating function, some particle distributions function are used. Then, the generating function can be averaged over all events with the same multiplicity. The generating function of integrated cumulants is defined in 3.5.14 using the averaged generating function.

Some interpolation methods are used to compute numerically all the cumulants from their generating function. Finally, the different orders of the integrated flow can be calculated using the different integrated cumulants.

If the detector has full azimuthal acceptance, of if we use an event generator like EPOS, the first three orders are:

$$\boxed{v_n\{2\}^2 = c_n\{2\}} \qquad \boxed{v_n\{4\}^4 = -c_n\{4\}} \qquad \boxed{v_n\{6\}^6 = \frac{c_n\{6\}}{4}} \tag{3.5.12}$$

For the description of the whole method, I will explain how we can estimate the integrated flow over a perfect detector from cumulants of 2-, 4- and 6-particle correlations. For each event, we can define the real-valued function $G_n(z)$, which depends on the complex variable $z = x + iy$:

$$G_n(z) = \prod_{j=1}^{M}\left[1 + \frac{w_j}{M}\left(z\ e^{-in\phi_j} + z\ e^{-in\phi_j}\right)\right] = \prod_{j=1}^{M}\left[1 + \frac{w_j}{M}\left(2x\cos(n\phi_j) + 2y\sin(n\phi_j)\right)\right] \tag{3.5.13}$$

where M represents the number of particles detected in the collision in a single event, w_j is a weight attributed to particle j, as the EP or SP methods, which depends of particle type, transverse momentum or rapidity. Of course, the weight is chosen to maximize the effects of flow relative to statistical fluctuations, for example, I used in my Monte Carlo toy Model the weight of $v_n(p_t, y)$ itself. In practice, z is used as an interpolation point used to estimate the generating function of cumulants $C_n(z)$ as it will be explained.

The generating function can be averaged over events with the same multiplicity M denoted by $\langle G_n(z)\rangle$. The generating function $\langle G_n(z)\rangle$ contains all the information on measured multi-particle azimuthal correlations. Effectively, we use this generating function to define the generating function of the cumulants $C_n(z)$ by:

$$C_n(z) = M\left(\langle G_n(z)\rangle^{1/M} - 1\right) = \sum_{k,l}\frac{z^{*k}z^l}{k!l!}\langle\langle e^{in\phi_1+\cdots+\phi_k-\phi_{k+1}-\cdots-\phi_{k+l})}\rangle\rangle \tag{3.5.14}$$

Cumulants with $k \neq l$ vanish for a perfect detector since the generating function $C_n(z)$ depends only on $|z|$. The interesting cumulants, which are related to the flow, are then the diagonal terms with $k = l$. The denotation of these diagonal terms is:

$$c_n\{2k\} = \langle\langle e^{in(\phi_1+\cdots+\phi_k-\phi_{k+1}-\cdots-\phi_{2k})}\rangle\rangle \tag{3.5.15}$$

To construct $C_n(z)$ in order to calculate $c_n\{2k\}$, we can use interpolation methods to compute numerically the cumulants from their generating functions. If we want to construct the first three cumulants, one may truncate the series to order $|z|^6$ and compute $C_n(z)$ at the following points:

$$z_{p,q} = x_{p,q} + iy_{p,q} \qquad x_{p,q} = r_0\sqrt{p}\cos\left(\frac{2q\pi}{q_{max}}\right) \qquad y_{p,q} = r_0\sqrt{p}\sin\left(\frac{2q\pi}{q_{max}}\right) \tag{3.5.16}$$

for $p = 1, \cdots, k_i$ and $q = 0, \cdots, q_{max} - 1$ where $q_{max} \geq 8$. The parameter r_0 is in principle a small number, since we are interested in the behaviour of the generating functions near the origin, it must be chosen as a compromise between errors due to higher order terms in the power-series expansion, which rapidly increase with r_0, and numerical errors. To conclude, we choose $p = 1, 2, 3$, $q = 0, \cdots, q_{max} - 1$ and $r_0 \simeq 2$.

Now we can evaluate the generating function of cumulants averaged over the phase of z:

$$C_p \equiv \frac{1}{q_{max}} \sum_{q=0}^{q_{max}-1} C_n(z_{p,q}) = \sum_{k=1}^{k_i} \frac{(r_0\sqrt{p})^{2k}}{(k!)^2} c_n\{2k\} \tag{3.5.17}$$

Now, the solution with k_{max}=3 as we chose before is:

$$\begin{aligned} c_n\{2\} &= \frac{1}{r_0^2}\left(3C_1 - \frac{3}{2}C_2 + \frac{1}{3}C_3\right) \\ c_n\{4\} &= \frac{2}{r_0^4}\left(-5C_1 + 4C_2 - C_3\right) \\ c_n\{6\} &= \frac{6}{r_0^6}\left(3C_1 - 3C_2 + C_3\right) \end{aligned} \tag{3.5.18}$$

From the measured $c_n\{2k\}$, one thus obtains an estimation of the integrated flow, which is denoted by $v_n\{2k\}$. If the detector has full azimuthal, or if we use an event generator like EPOS, the first three orders of the integrated flow are (much details in the Appendix C):

$$\boxed{v_n\{2\}^2 = c_n\{2\}} \qquad \boxed{v_n\{4\}^4 = -c_n\{4\}} \qquad \boxed{v_n\{6\}^6 = \frac{c_n\{6\}}{4}} \tag{3.5.19}$$

Now that we calculated the integrated flow for each centrality, we will examine the first three orders of the differential flow for identified particles.

Differential Flow

This section is described as the previous ones. I simplify the description of the method to calculate the differential flow in two times: i) only the idea of the method and the final result, ii) the whole description of the method.

The next step after the measure of the integrated flow is the measure of the differential flow. Like the integrated flow, a generating function of differential cumulants is created using the averaged generating function. This generating function of differential cumulants depends only of $|z|$ and the only nonvanishing terms of this generating function are called the differential cumulants.

Some interpolation methods are used to compute numerically all the differential cumulants from their generating function. The difference between the integrated cumulants is that the nonvanishing terms of the generating function are complex. However, the interpolation to calculate the differential cumulants follows the same procedure than the calculation of reference cumulants. Finally, the different orders of the differential flow can be calculated using the differential cumulants.

If the detector has full azimuthal acceptance, of if we use an event generator like EPOS, the first different orders are:

$$\begin{aligned} &\boxed{v'_{n/n}\{2\} = d_{n/n}\{2\}/v_n\{2\}} \qquad &&\boxed{v'_{n/n}\{4\} = -d_{n/n}\{4\}/v_n^3\{4\}} \\ &\boxed{v'_{2n/n}\{3\} = d_{2n/n}\{3\}/v_n^2\{4\}} \qquad &&\boxed{v'_{2n/n}\{5\} = -d_{2n/n}\{5\}/(2v_n^4\{4\})} \end{aligned} \tag{3.5.20}$$

Let's start the description of the whole method, as I said: the next step after the measure of the integrated flow is the measure of the differential flow. The integrated flow represents the flow of Reference Particles in the phase space of the detector. We calculate generally the differential flow of Particles of Interest in a narrower phase space. I can take again the example of RP the charged particles in a pseudorapidity range of -0.8 $< \eta <$ 0.8 and any p_T. Then, we choose the POI as the kaons in a p_T range of 0.2 $< p_T <$ 5 GeV. The particles referenced as **both** POI and RP, are charged kaons in a pseudorapidity range of -0.8 $< \eta <$ 0.8 and a p_T range of 0.2 $< p_T <$ 5 GeV. Finally, in this cumulant method, we can measure the differential of the POI, we correlate their azimuth ψ with the azimuths of the RP ϕ_j. In the standard flow analysis, if the reaction plane is reconstructed in harmonic n, one may reconstruct not only the corresponding v'_n harmonics but also higher harmonics v'_{mn}, where m is an integer. To construct the interesting cumulants of differential flow $d_{mn/n}\{2k+m+1\}$, we measure the v'_{mn} of POI by using RP in harmonic n, while the number in curly brackets is the order of the correlation: 2k+m RP and 1 POI. Consequently, we want to construct a generating function of the differential cumulants, $D_{mn/n}(z)$:

$$D_{mn/n}(z) \equiv \frac{\langle e^{imn\psi} G_n(z) \rangle}{\langle G_n(z) \rangle} = \sum_{k,l} \frac{z^{*k} z^l}{k!l!} \langle\langle e^{imn\psi + in\phi_1 + \cdots + \phi_k - \phi_{k+1} - \cdots - \phi_{k+l})} \rangle\rangle \tag{3.5.21}$$

Since this quantity depends only on $|z|$, the only nonvanishing cumulants in the previous equation are those with $l = k + m$. Consequently, the denotation of these relevant quantities is:

$$d_{mn/n}\{2k+m+1\} \equiv \Re \left[\langle\langle e^{in(m\psi + \phi_1 + \cdots + \phi_k - \phi_{k+1} - \cdots - \phi_{2k+m})} \rangle\rangle \right] \tag{3.5.22}$$

We use also an interpolation method to calculate the generating function $D_{mn/n}(z)$ in order to calculate the differential cumulants $d_{mn/n}\{2k+m+1\}$. Because $D_{mn/n}(z)$ is complex, we decompose this complex variable into real and imaginary parts with:

$$\begin{aligned} X_{p,q} &\equiv \Re \left[D_{mn/n}(z_{p,q}) \right] = \frac{\langle \cos(mn\psi) G_n(z_{p,q}) \rangle}{\langle G_n(z_{p,q}) \rangle} \\ Y_{p,q} &\equiv \Im \left[D_{mn/n}(z_{p,q}) \right] = \frac{\langle \sin(mn\psi) G_n(z_{p,q}) \rangle}{\langle G_n(z_{p,q}) \rangle} \end{aligned} \tag{3.5.23}$$

In order to isolate the cumulants $d_{mn/n}\{2k+m+1\}$, one computes the multiplication of $D_{mn/n}(z)$ by z^{*m} at the point $z_{p,q}$, obviously one takes the real part and finally one averages over angles:

$$D_p \equiv \frac{(r_0\sqrt{p})^m}{q_{max}} \sum_{q=0}^{q_{max}-1} \left[\cos\left(\frac{m \times 2q\pi}{q_{max}} \right) X_{p,q} + \sin\cos\left(\frac{m \times 2q\pi}{q_{max}} \right) Y_{p,q} \right] \tag{3.5.24}$$

We must take the exact same parameters as the integrated flow, for this analysis, we choose $p = 1, 2, 3$, $q = 0, \cdots, q_{max} - 1$ and $r_0 \simeq 2$. In any case, one must make the interpolation with two different values of r_0 in order to check the stability of the results. The solutions for $m = 1$, the two lowest order cumulants are given by:

$$d_{n/n}\{2\} = \frac{1}{r_0^2} \left(2D_1 - \frac{1}{2} D_2 \right) \qquad d_{n/n}\{4\} = \frac{1}{r_0^4} \left(-2D_1 + D_2 \right) \tag{3.5.25}$$

If one takes $m = 2$, the two lowest order cumulants are given by:

$$d_{2n/n}\{3\} = \frac{1}{r_0^4}\left(4D_1 - \frac{1}{2}D_2\right) \qquad d_{2n/n}\{5\} = \frac{1}{r_0^6}\left(-6D_1 + \frac{3}{2}D_2\right) \tag{3.5.26}$$

These cumulants can give the differential flow, for a perfect detector like EPOS, this flow is given by:

$$\boxed{v'_{n/n}\{2\} = d_{n/n}\{2\}/v_n\{2\}} \qquad \boxed{v'_{n/n}\{4\} = -d_{n/n}\{4\}/v_n^3\{4\}}$$
$$\boxed{v'_{2n/n}\{3\} = d_{2n/n}\{3\}/v_n^2\{4\}} \qquad \boxed{v'_{2n/n}\{5\} = -d_{2n/n}\{5\}/(2v_n^4\{4\})} \tag{3.5.27}$$

Synthesis or strategy to calculate the anisotropic flow:

1. for each particle, calculate the generating function of cumulants in equation 3.5.13;
2. use the generating function in order to obtain the generating function of integrated cumulants with the equation 3.5.14;
3. when one uses interpolation methods to compute numerically the cumulants from their generating function, uses the equation 3.5.17;
4. with the interpolation of the generating function $C_n(z)$, one can estimate the desired orders of integrated cumulants in order to estimate the integrated flow with the equations 3.5.19;
5. now that the integrated cumulant is estimated, one can construct the differential generating function of cumulants with the equation 3.5.21;
6. when one uses interpolation methods to compute numerically the differential cumulants from their differential generating function, uses the equation 3.5.24;
7. with the interpolation of the differential generating function $D_{mn/n}(z)$, one can estimate the desired orders of differential cumulants in order to estimate the differential flow with the equations 3.5.27.

Discussion

The cumulant expansion calculated by a generating function is very useful to measure the anisotropic flow in a heavy ions collision. In the following, I will call this method: the Generating Function Cumulant (GFC). As the standard analysis, one must proceed in two steps. The first step is the reconstruction of the average value of the flow: the **integrated flow** v_n related to the reaction plane resolution in the standard methods. The second step is the measure of the **differential flow** v'_n related to the measure of the anisotropic flow in the standard analysis. One can feature the strong points:

- the cumulant method supresses the non-flow correlations in both integrated and differential flow using a high order of multi-particle azimuthal correlations. The non-flow effects can be removed order-by-order based on the correlation behaviour;
- it also provides several independent estimates of the flow from cumulants of various and higher orders, we do not need to reconstruct any planes;
- finally, this method can be used with detector without full azimuthal coverage.

The limitations of the GFC method to measure the anisotropic flow is that we must satisfy the two following conditions:

- to build the two generating functions $C_n(z)$ and $D_{mn/n}(z)$, we should have the same multiplicity of RP and we must set a small centrality bin size in the analysis. If we do not satisfy this condition, a significant bias arises;
- some approximations can be used if we have a very large multiplicity, the use of higher order cumulants is often limited by statistics.

Finally, we must use a numerical interpolation method to calculate the two generating functions C_p and D_p. We must test the stability of the final results with different values of interpolation variables. Therefore, the problem of the GFC is that we cannot use it if the final results are sensitive with the different values of interpolation variables.

Recently, a new method to measure the anisotropic flow using cumulants has been created [213, 214]: the Q-cumulants (QC) method. This method was built to measure the anisotropic flow faster than the GFC method and to overcome the drawback of the interpolation problem. I will describe in details this method in the following section.

3.5.3 Direct calculation with recent method using cumulants

The Q-cumulants method [213, 214] is an approach when the calculus of cumulants involves any approximations (some bias), which can complicate the interpretation of the results. In this section, I will present the method for a direct calculation of multi-particle cumulants usings the flow vectors. This vector is the central object of this analysis. The Q-vector is defined in equation 3.3.23 but it can be evaluated by this other notation:

$$Q_n \equiv \sum_{i=1}^{M} e^{in\phi_1} \tag{3.5.28}$$

with n the order of the anisotropy, M the multiplicity in an event and ϕ_i the azimuthal angle of the i-th particle.

As in the beginning of this section with the 3.5.1 subsection, I will explain the Q-cumulant method by building the genuine multi-particle azimuthal correlations and the denotation of cumulant in this analysis. When the cumulants are created, I will detail the measure of the integrated and differential flow as in the subsection 3.5.2 and conclude by a small discussion.

Multi-particle azimuthal correlations

I will not explain the generalization to azimuthal correlation in this thesis, I will consider only 2- to 6-particle azimuthal correlations. We do not use only these azimuthal correlations but we use the average of multi-particle azimuthal correlation. The average consists of two steps, the *single-event* average defined by the following way:

$$\begin{aligned}
\langle 2\rangle &\equiv \langle e^{in(\phi_1-\phi_2)}\rangle \equiv \frac{1}{P_{M,2}} \sum_{i,j}' e^{in(\phi_i-\phi_j)} \\
\langle 4\rangle &\equiv \langle e^{in(\phi_1+\phi_2-\phi_3-\phi_4)}\rangle \equiv \frac{1}{P_{M,4}} \sum_{i,j,k,l}' e^{in(\phi_i+\phi_j-\phi_k-\phi_l)}
\end{aligned} \tag{3.5.29}$$

where $P_{n,m} = n!/(n-m)!$, ϕ_i is the azimuthal angle of the i-th particle measured in the laboratory frame and the prime up the sum means that all indices in the sum must be taken different. We take different indices to avoid a trivial and strong contribution of autocorrelations between particles. After calculating the single-event average, the second step is to calculate the *all-event* involving an average over all events:

$$\begin{aligned}\langle\langle 2\rangle\rangle \equiv \langle\langle e^{in(\phi_1-\phi_2)}\rangle\rangle \equiv \frac{\sum_{i=1}^{N}(W_{\langle 2\rangle})_i\langle 2\rangle_i}{\sum_{i=1}^{N}(W_{\langle 2\rangle})_i}\\ \langle\langle 4\rangle\rangle \equiv \langle\langle e^{in(\phi_1+\phi_2-\phi_3-\phi_4)}\rangle\rangle \equiv \frac{\sum_{i=1}^{N}(W_{\langle 4\rangle})_i\langle 4\rangle_i}{\sum_{i=1}^{N}(W_{\langle 4\rangle})_i}\end{aligned} \tag{3.5.30}$$

where double brackets denote an average over all particles and then over all events, N is the number of events. $W_{\langle 2\rangle}$ and $W_{\langle 4\rangle}$ are the event weights. The choice of event weights (contrary of the particle weights) is not arbitrary, they are used to minimize the effect of multiplicity variations in the event sample on the estimates multi-particle correlations. Experimentally, the optimal choice of weights is determined by the multiplicity dependence of v_n but with an event generator or a theoretical model, we know exactly the number of the multiplicity. Therefore we can calculate the weights at fixed M and average over the entire event sample. With EPOS, we want to calculate all observables with the same conditions (except a perfect detector) as the experiment, consequently we never choose a fixed M. Consequently, with v_n independent of multiplicity, we use the event weights:

$$\begin{aligned}W_{\langle 2\rangle} &\equiv M(M-1)\\ W_{\langle 4\rangle} &\equiv M(M-1)(M-2)(M-3)\end{aligned} \tag{3.5.31}$$

The event weight choice corresponds to the number of multi-particle combinations in an event with multiplicity M.

Because the discussion about the introduction about cumulant has been done in the section about cumulant expansion 3.5.1, we can define easily the two first order cumulants $c_n\{2\}$ and $c_n\{4\}$ in the case of perfect detector. We start by using the following equation introduced in the section 3.5.1:

$$\begin{aligned}\langle e^{in(\phi_1-\phi_2)}\rangle_c &\equiv \langle e^{in(\phi_1-\phi_2)}\rangle\\ \langle e^{in(\phi_1+\phi_2-\phi_3-\phi_4)}\rangle_c &\equiv \langle e^{in(\phi_1+\phi_2-\phi_3-\phi_4)}\rangle - \langle e^{in(\phi_1-\phi_3)}\rangle\langle e^{in(\phi_2-\phi_4)}\rangle\\ &+ \langle e^{in(\phi_1-\phi_4)}\rangle\langle e^{in(\phi_2-\phi_3)}\rangle\end{aligned} \tag{3.5.32}$$

Then, we use the notation defined in the equation 3.5.30 and the previous equation, we can find the notation of the two first orders of **reference** cumulant:

$$c_n\{2\} \equiv \langle\langle 2\rangle\rangle \qquad c_n\{4\} \equiv \langle\langle 4\rangle\rangle - 2\times\langle\langle 2\rangle\rangle^2 \tag{3.5.33}$$

I will not show the results for detector without uniform acceptance because we do not use them in our event generator. For completeness, I give the expression of higher order of i^{th}-particle cumulant used in my analysis in the next chapter.

$$\begin{aligned}c_n\{6\} &\equiv \langle\langle 6\rangle\rangle - 9\times\langle\langle 2\rangle\rangle\langle\langle 4\rangle\rangle + 12\times\langle\langle 2\rangle\rangle^3\\ c_n\{8\} &\equiv \langle\langle 8\rangle\rangle - 16\times\langle\langle 6\rangle\rangle\langle\langle 2\rangle\rangle - 18\times\langle\langle 4\rangle\rangle^2\\ &+ 144\times\langle\langle 4\rangle\rangle\langle\langle 2\rangle\rangle^2 - 144\times\langle\langle 2\rangle\rangle^4\end{aligned} \tag{3.5.34}$$

The physical importance of cumulants stems from the fact that all particles produced in a heavy ions collision are correlated to the symmetry plane determined by the geometry of that collision. When we have estimated cumulants from the data, one can estimate flow harmonics. Therefore, we use the reference cumulants to calculate the integrated flow:

$$\begin{aligned} \sqrt{c_n\{2\}} &= \sqrt{\langle\langle 2\rangle\rangle} = v_n \\ \sqrt[4]{c_n\{4\}} &= \sqrt[4]{-\langle\langle 4\rangle\rangle + 2\times\langle\langle 2\rangle\rangle^2} = \sqrt[4]{-v_n^4 + 2v_n^4} = v_n \end{aligned} \tag{3.5.35}$$

where the notation $v_n\{2\}$ is used to denote the reference flow estimated from the second order of the cumulant. Now, I will explain how we can calculate the reference flow using different Q-vectors.

Integrated Flow

We will express all multi-particle cumulants in terms of various expressions depending on Q-vectors: called Q-cumulants. We started by decomposing $|Q_n|^2$ into diagonal and off-diagonal terms:

$$|Q_n|^2 \equiv Q_n Q_n^* = \sum_{i,j=1}^{M} e^{in(\phi_i-\phi_j)} = M + \sum_{i,j}^{\prime} e^{in(\phi_i-\phi_j)} \tag{3.5.36}$$

All summations with a $\prime$ means that all indices are taken distinct.
This equation can be trivially solved to obtain $\langle 2\rangle$ in terms of $|Q_n|^2$:

$$\langle 2\rangle = \frac{|Q_n|^2 - M}{M(M-1)} \tag{3.5.37}$$

Of course, to construct the all-event average of the 2-particle azimuthal correlation, we use the equation 3.5.30. We can use $\langle\langle 2\rangle\rangle$ to calculate the second order cumulant by the equation 3.5.35.

In order to obtain higher orders of i-particle Q-cumulants, we must start by the i-particle correlations in a decomposition of $|Q_n|^i$, for example for the 4-particle correlation:

$$|Q_n|^4 \equiv Q_n Q_n Q_n^* Q_n^* = \sum_{i,j,k,l=1}^{M} e^{in(\phi_i+\phi_j-\phi_k-\phi_l)} \tag{3.5.38}$$

We can see that the sum contains four terms corresponding to four distinct class of combinations: i) they are all different (the exact 4-particle correlation), ii) three are different, iii) two are different and iv) they are all the same (autocorrelation). I will not describe all in details because this is not the main subject of this chapter but if we take all these combinations like the equation 3.5.36 for the 2-particle correlation, we obtain the analytic result for the average 4-particle correlation:

$$\langle 4\rangle = \frac{|Q_n|^4 + |Q_{2n}|^2 - 2\Re[Q_{2n}Q_n^*Q_n^*] - |Q_n|^2\times 4(M-2) - 2M(M-3)}{M(M-1)(M-2)(M-3)} \tag{3.5.39}$$

All details to obtain this result are given in [213]. The first method using the Q-vector to calculate cumulants presented in the previous section 3.5.2 [210–212] was biased because the terms consisting of Q-vector evaluated in different harmonics (for example $\Re[Q_{2n}Q_n^*Q_n^*$ and Q_{2n}) were neglected. We use the exact same strategy to calculate all orders of single-event average i-particle correlation:

- Explicit the i-particle correlation by decomposing the $|Q_n|^i$;
- separate each case of distinct combinations;
- solve the system of coupled equations for multi-particle correlations in the same harmonics in order to obtain $\langle i\rangle$ expressed in terms of combinations of Q-vectors

We can obtain the single event particle correlation for orders 6 and 8:

$$
\begin{aligned}
\langle 6\rangle &= \frac{|Q_n|^6 + 9|Q_{2n}^2|Q_n|^2 - 6\Re[Q_{2n}Q_nQ_n^*Q_n^*Q_n^*] + 4\Re[Q_{3n}Q_n^*Q_n^*Q_n^*]}{M(M-1)(M-2)(M-3)(M-4)(M-5)} \\
&+ \frac{18(M-4)\Re[Q_{2n}Q_n^*Q_n^*] + 4|Q_{3n}|^2 - 12\Re[Q_{3n}Q_{2n}^*Q_n^*]}{M(M-1)(M-2)(M-3)(M-4)(M-5)} \\
&- 9\frac{|Q_n|^4 + |Q_{2n}^2}{M(M-1)(M-2)(M-3)(M-5)} \\
&+ \frac{18|Q_n|^2}{M(M-1)(M-3)(M-4)} - \frac{6}{(M-1)(M-2)(M-3)}
\end{aligned}
\tag{3.5.40}
$$

$$
\begin{aligned}
\langle 8\rangle =& \frac{1}{M(M-1)(M-2)(M-3)(M-4)(M-5)(M-6)(M-7)} \\
&\times[|Q_n|^8 - 12Q_{2n}Q_nQ_nQ_n^*Q_n^*Q_n^*Q_n^* + 6Q_{2n}Q_{2n}Q_n^*Q_n^*Q_n^*Q_n^* \\
&+ 16Q_{3n}Q_nQ_nQ_n^*Q_n^*Q_n^*Q_n^* - 96Q_{3n}Q_nQ_{2n}^*Q_n^*Q_n^* \\
&- 12Q_{4n}Q_n^*Q_n^*Q_n^*Q_n^* - 36Q_{2n}Q_{2n}Q_{2n}^*Q_n^*Q_n^* \\
&+ 96(M-6)Q_{2n}Q_nQ_n^*Q_n^*Q_n^* + 72Q_{4n}Q_{2n}^*Q_n^*Q_n^* + 48Q_{3n}Q_nQ_{2n}^*Q_{2n}^* \\
&- 64(M-6)Q_{3n}Q_n^*Q_n^*Q_n^* + 192(M-6)Q_{3n}Q_{2n}^*Q_n^* - 96Q_{4n}Q_{3n}^*Q_n^* \\
&- 36Q_{4n}Q_{2n}^*Q_{2n}^* - 144(M-7)(M-4)Q_{2n}Q_n^*Q_n^* + 36|Q_{4n}|^2 \\
&+ 64|Q_{3n}|^2|Q_n|^2 - 64(M-6)|Q_{3n}|^2 + 9|Q_{2n}|^4 + 36|Q_n|^4|Q_{2n}|^2 \\
&- 144(M-6)|Q_{2n}|^2|Q_n|^2 + 72(M-7)(M-4)(|Q_{2n}|^2 + |Q_n|^4) \\
&- 16(M-6)|Q_n|^6 - 96(M-7)(M-6)(M-2)|Q_n|^2 \\
&+ 24M(M-7)(M-6)(M-5)]
\end{aligned}
\tag{3.5.41}
$$

Finally, we can obtain the anisotropic flow directly with these average particle correlations by another average over all events with the equations 3.5.30. Then we calculate the i^{th}-particle reference cumulant using 3.5.35 and finally calculate the integrated anisotropic flow by 3.5.19.

Synthesis or strategy to calculate the integrated flow:

1. decompose Q-vector into single event average of particle correlations $\langle i \rangle$ using $|Q_n|^i$;
2. use $|Q_n|^i$ and note all distinct combinations inside sum over particles and use corresponding combinatorial coefficients $\langle k \rangle$ into different Q_m or Q_m^*, solve all equations to finally obtain the $\langle i \rangle$, obviously, we must use only the **reference particles** or RP to calculate the reference flow;
3. use the equation 3.5.30 for each single event average of particle correlations $\langle i \rangle$ in order to obtain the full event average of particle correlations $\langle\langle i \rangle\rangle$;
4. introduce each $\langle\langle i \rangle\rangle$ in equations 3.5.33 and 3.5.34 to calculate the reference cumulants $c_n\{i\}$, these cumulants are called the **Q-cumulants**;
5. finally, use the following equations in order to calculate the integrated flow (details in Appendix C);
6. an optional item but keep in mind or in a corner of table all reference cumulants because we will need them in order to calculate the differential flow.

$$\boxed{v_n\{2\} = \sqrt{c_n\{2\}}} \qquad \boxed{v_n\{4\} = \sqrt[4]{-c_n\{4\}}}$$
$$\boxed{v_n\{6\} = \sqrt[6]{\frac{c_n\{6\}}{4}}} \qquad \boxed{v_n\{8\} = \sqrt[8]{\frac{-c_n\{8\}}{33}}} \tag{3.5.42}$$

In this section, we see a direct way to calculate the integrated flow of a collision, we can calculate it for each centrality or each multiplicity. In contrary to the GFC method, we can calculate the integrated flow in only one loop over data. Even if we need also a large power computing in order to calculate higher orders of anisotropic flow, this method is less greedy in time. However, we do not calculate the anisotropic flow dependent of particle's momentum or particle's rapidity: the differential flow. We will see the direct method to calculate it in the next section.

Reduced multi-particle azimuthal correlation

Once the reference flow has been measured with the previous formalism for the RP, we can proceed to the calculation of the differential flow with the Particles of Interest. But to calculate the differential flow, we must use the reduced multi-particle azimuthal correlation. Reduced azimuthal correlation does mean that we have only one POI in the correlator, restricted in a narrower phase space window. We can start by the single event average reduced 2- or 4-particle azimuthal correlations to explain how to use it:

$$\begin{aligned}
\langle 2' \rangle &\equiv \langle e^{in(\psi_1 - \phi_2)} \rangle = \frac{1}{m_p M - m_q} \sum_{i=1}^{m_p} \sum_{j=1}^{M} e^{in(\psi_i - \phi_j)} \\
\langle 4' \rangle &\equiv \langle e^{in(\psi_1 + \phi_2 - \phi_3 - \phi_4)} \rangle = \frac{\sum_{i=1}^{m_p} \sum_{j,k,l=1}^{M\prime} e^{in(\psi_i + \phi_j - \phi_k - \phi_l)}}{(m_p M - 3m_q)(M-1)(M-2)}
\end{aligned} \tag{3.5.43}$$

where we have: the prime denotes that all indices inside the sum are different, m_p the number of particles labeled as POI, M the number of particles labeled as RP and m_q the number of particles labeled **both** as POI and RP, then ψ_i are the azimuthal angles of particles labeled as POI, finally ϕ_i are the azimuthal angles of particles labeled as RP.

Same as the multi-particle azimuthal correlations, we will calculate the full event average by different event weights for reduced multi-particle azimuthal correlations:

$$\langle\langle 2'\rangle\rangle = \frac{\sum_{i=1}^{N}(w_{\langle 2'\rangle})_i\langle 2'\rangle_i}{\sum_{i=1}^{N}(w_{\langle 2'\rangle})_i} \qquad \langle\langle 4'\rangle\rangle = \frac{\sum_{i=1}^{N}(w_{\langle 4'\rangle})_i\langle 4'\rangle_i}{\sum_{i=1}^{N}(w_{\langle 4'\rangle})_i} \tag{3.5.44}$$

in these equations, the double brackets denote an average over all particles and then over all events, N is the number of events. $w_{\langle 2'\rangle})_i$ $w_{\langle 4'\rangle})_i$ are the event weights. As in the case of the reference flow, each event weight reflects to the number of distinct combinations in an event. In all anisotropic flow analysis by QC in this Ph.D Thesis, I used these event weights:

$$w_{\langle 2'\rangle} \equiv m_p M - m_q \qquad w_{\langle 4'\rangle} \equiv (m_p M - 3m_q)(M-1)(M-2) \tag{3.5.45}$$

We can think that we have all ingredients to calculate the differential flow using reduced multi-particle azimuthal correlations like we used the multi-particle azimuthal correlations to calculate the integrated flow but we must define different new vectors to calculate the differential flow.

Differential Flow

We want to measure the differential flow of POI using also the RP. We can use the same idea of using some flow vectors to calculate the anisotropic flow. Consequently, for the differential flow, we must use a flow vector for POI but also a flow vector for particle in **both** RP and POI. We can start by defining the two new vectors, I use the same definitions all above with p for particles labeled as POI and q for particles labeled **both** as POI:

$$p_n \equiv \sum_{i=1}^{m_p} e^{in\psi_i} \qquad q_n \equiv \sum_{i=1}^{m_q} e^{in\psi_i} \tag{3.5.46}$$

This is to substract the effects of autocorrelations that q-vector is introduced. Same as reference flow, I do not detail all calculations, however we can read the section *differential flow* and the appendix in the article [213] to have more details.

However, we can obtain the single event average reduced multi-particle azimuthal correlations:

$$\begin{aligned}
\langle 2'\rangle &= \frac{p_n Q_n^* - m_q}{m_p M - m_q} \\
\langle 4'\rangle &= \frac{p_n Q_n Q_n^* Q_n^* - q_{2n} Q_n^* Q_n^* - p_n Q_n Q_{2n}^* - 2M p_n Q_n^* - 2m_q |Q_n|^2 + 7 q_n Q_n^*}{(m_p M - 3m_q)(M-1)(M-2)} \\
&= \frac{-Q_n q_n^* + q_{2n} Q_{2n}^* + 2p_n Q_n^* + 2m_q M - 6m_q}{(m_p M - 3m_q)(M-1)(M-2)}
\end{aligned} \tag{3.5.47}$$

Then, we can construct the differential cumulants using full event average reduced multi-particle azimuthal correlations (details in Appendix C):

$$d_n\{2\} = \langle\langle 2'\rangle\rangle \qquad d_n\{4\} = \langle\langle 4'\rangle\rangle - 2\langle\langle 2'\rangle\rangle\langle\langle 2\rangle\rangle \tag{3.5.48}$$

Obviously the previous equations are effective only for detectors with uniform azimuthal acceptance or for perfect detector like EPOS. One can estimate the differential flow v'_n using **both** referential and differential cumulants:

$$\boxed{v'_n\{2\} = \frac{d_n\{2\}}{\sqrt{c_n\{2\}}}} \qquad \boxed{v'_n\{4\} = -\frac{d_n\{4\}}{(-c_n\{4\})^{3/4}}} \tag{3.5.49}$$

One goal by using the reference flow in the measure of the differential flow is also to have good statistics both in numerator and denominator in the previous equation. Effectively, if we only use POI, we never have enough statistics in majority of the cases. This is one reason to take a lot of particles labeled as RP in an analysis of anisotropic flow. As the reference flow, I write a synthesis with each step to calculate the differential flow with the QC method.

Synthesis or strategy to calculate the differential flow:

1. use and decompose Q, p and q-vectors into single event average of reduced multi-particle correlations $\langle i\prime \rangle$;

2. note all distinct combinations inside sum over particles and use corresponding combinatorial coefficients $\langle k' \rangle$ into decomposition of Q, p and q-vectors, solve all equations in order to obtain the $\langle i' \rangle$;

3. use the equation 3.5.47 for each single event average of reduced multi-particle correlation $\langle i' \rangle$ to obtain the full event average of reduced multi-particle correlation $\langle\langle i' \rangle\rangle$;

4. introduce each $\langle\langle i' \rangle\rangle$ and $\langle\langle i \rangle\rangle$ in equations 3.5.48 to calculate the differential cumulants $d_n\{i\}$;

5. finally, use the equation 3.5.49 in order to measure the differential flow.

You can see that the method to calculate the differential flow is almost the same as the method to calculate the reference flow with QC. But one must keep in mind that the differential flow (as its name suggests) is not integrated over p_t or y. Consequently p and q vectors are dependent of p_t or y. Like the GFC method, one strong point of this method is that we can have different independent estimations of reference flow and differential flow but we can calculate these estimations only in one pass over the data.

Discussion

The cumulant expansion calculated by different flow vectors is a very useful method to calculate the anisotropic flow in heavy ions collisions. This method is called the Q-cumulants method. As the standard analysis and the GFC methods, one must proceed in two steps. The first step is the calculation of the **integrated flow** $v_n\{i\}$ and the second step is the measure of the **differential flow** $v'_n\{i\}$. One can feature a list of strong points:

- first we have approximately the same strong points as the GFC formalism: we eliminate the non-flow correlations using high orders of multi-particle azimuthal correlations, the QC method provides several independent estimations of the anisotropic flow in various orders, the method can be used with detector without full acceptance, but we must include some corrections of all equations that I showed;

- unlike the GFC analysis, we can effectuate the complete analysis of the anisotropic flow in a only loop over the data. We can obtain the reference and differential flows in the same step. In the GFC formalism, the first pass is dedicated to the calculation of the reference flow, which then can be used in the second pass to estimate the differential flow;

- unlike the GFC formalism, the cumulants are not biased by intereference between various harmonics;

- one does not use interpolation formulas in the formalism of QC unlike the GFC, that confers a better stability of results;

- we need statistics but we need less statistics than the first cumulant method because we use the event weight as the number of combinations. This choice of event weights minimizes the statistical spread;

- the last strong point is that the method can be used for each order of multi-particle azimuthal correlations. We do not calculate the anisotropic flow only with the multi-particle azimuthal correlations with the same harmonics. This method uses also the multi-particle correlation in mixed harmonics for any number of particles in the correlators.

3.5.4 Direct calculations with gap implementation

The analysis of anisotropic flow using cumulant expansion with GFC and QC methods are useful to remove the non-flow contribution for high order of azimuthal correlation of particles. While, on the other hand, we keep the important contribution of nonflow for two-particle azimuthal correlation. We know that we can reduce the non-flow contribution in anisotropic flow analysis when we include a gap in pseudorapidity between the two phase spaces of particles used in the analysis. Consequently, we can use this method to reduce the contribution of non-flow both for the calculations of the reference flow and differential flow using also Q-cumulant [215].

One talks about the reference flow and the differential flow using 2-particle azimuthal correlation, therefore during all this analysis one talks about only two particles. We introduce a pseudorapidity gap to separate the phase space into two different phase spaces. Therefore, we obtain two different subevents with different number of particles and flow vectors. To simplify the notation, we will talk about the subevent A and B (see Fig. 3.5) with the corresponding multiplicities M_A and M_B, corresponding flow vectors Q_A and Q_B. We start the description of the analysis by the reference flow.

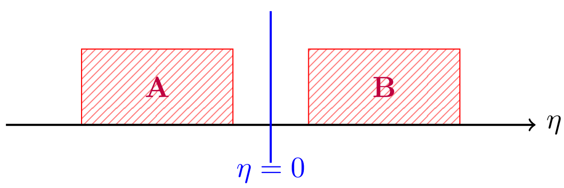

Figure 3.5: Diagrammatic representation of the pseudorapidity gap with 2 subevents in the anisotropic flow analysis

Obviously, the separation of the particle in the subevent A or B is in function of the pseudorapidity of the particle. For example, we define two phase spaces with a pseudorapidity gap of 2 in a detector with a coverage of 6.3 in pseudorapidity. Consequently, we obtain two phase spaces A and B and we include each particle in these phase spaces taking in account its pseudorapidity:

$$-6.3 < \eta_A < -1 \qquad\qquad 1 < \eta_B < 6.3 \tag{3.5.50}$$

We keep the procedure of the classical QC method, therefore we start by calculating the 2-particle azimuthal correlation with a pseudorapidity gap. We select one particle from subevent A and the other from subevent B. We calculate the 2-particle azimuthal correlation as:

$$\langle 2\rangle_{\Delta\eta} = \frac{Q_n^A Q_n^B}{M_A M_B} \qquad \text{with} \quad Q_n^A \equiv \sum_{i=1}^{M_A} e^{in\phi_1} \tag{3.5.51}$$

To have the full event average of the previous equation, we use the event weight defined now as:

$$W_{\langle 2\rangle\Delta\eta} = M_A M_B \qquad \text{in} \quad \langle\langle 2\rangle\rangle_{\Delta\eta} = \frac{\sum_{i=1}^{N}(W_{\langle 2\rangle\Delta\eta})_i \times (\langle 2\rangle_{\Delta\eta})_i}{\sum_{i=1}^{N}(W_{\langle 2\rangle\Delta\eta})_i} \tag{3.5.52}$$

Therefore, the 2-particle Q-cumulant with an eta gap can be given by:

$$c_n\{2|\Delta\eta\} = \langle\langle 2\rangle\rangle_{\Delta\eta} \tag{3.5.53}$$

We can obtain the reference flow using the same equation for each cumulant method 3.5.42. Then, we can calculate the differential flow with a pseudorapidity gap. We can select only RP in one subevent and only POI in the other subevent to not have an overlap of POI and RP. Now the single event average of reduced 2-particle azimuthal correlation is given by:

$$\langle 2'\rangle_{\Delta\eta} = \frac{p_{n,A} Q_{n,B}^*}{m_{p,A} M_B} \qquad \text{with} \quad p_{n,A} \equiv \sum_{i=1}^{m_{p,A}} e^{in\psi_i} \tag{3.5.54}$$

To have the full event average of the reduced 2-particle azimuthal correlation, we use the event weight defined now as:

$$W_{\langle 2'\rangle\Delta\eta} \equiv m_{p,A} M_B \qquad \text{in} \quad \langle\langle 2'\rangle\rangle_{\Delta\eta} = \frac{\sum_{i=1}^{N}(W_{\langle 2'\rangle\Delta\eta})_i \times (\langle 2'\rangle_{\Delta\eta})_i}{\sum_{i=1}^{N}(W_{\langle 2'\rangle\Delta\eta})_i} \tag{3.5.55}$$

Then, we get the differential 2-particle cumulant with:

$$d_n\{2|\Delta\eta\} = \langle\langle 2'\rangle\rangle_{\Delta\eta} \tag{3.5.56}$$

Finally, we can calculate the differential flow from 2-particle cumulant using the same equation for each cumulant method. The only difference is that we use all cumulants containing the eta gap:

$$\boxed{v_n'\{2\} = \frac{d_n\{2|\Delta\eta\}}{\sqrt{c_n\{2|\Delta\eta\}}}} \tag{3.5.57}$$

The method is not really different with an eta gap but these little differences can reduce the non-flow contribution significately in the second order of anisotropic flow.

The description of few cumulant methods is finished. The two main methods were developed and used in different anisotropic flow analysis during the last decade. I will use a lot the Q-cumulants method instead of Generating Function Cumulant method because this method is more used in experimental analysis and we want to reproduce the data of experiment with EPOS using the exactly same methods.

The cumulant method is not an exact method to reduce all the non-flow contribution[2], this one is called the Lee-Yang Zeroes (LYZ) method [216–218]. I will describe how we can evaluate the anisotropic flow and why this method has been created in the next section.

3.6 Lee-Yang Zeroes Method

We are in the context of the beginning of anisotropic analysis using cumulant expansion by GFC method in 2002-2003. The GFC method is used in the different accelerators like SPS at CERN or RHIC at Brookhaven. The non-flow correlations are eliminated at large enough orders of i-particle correlation. The main goal of the GFC method is to isolate the genuine i-particle correlation by substracting the contribution of lower order correlations. But the evaluation of high order is rather tedious and numerically hazardous with the GFC method. N. Borghini et al. [216, 217] created a new way to calculate the anisotropic flow by studying directly the large order behavior of the cumulant expansion, rather than computing explicitly cumulants at a given order by analogy with the theory of phase transitions by Lee and Yang [219, 220].

3.6.1 Why did we create this method ?

Almost seventy years ago, Yang and Lee [219, 220] showed that the locations of the zeroes of the grand partition function in the complex plane can characterize the phase transition. The idea of the LYZ method is to use properties of the theory of Yang and Lee into anisoptropic flow. The creation of the LYZ method is to estimate the anisotropic flow without numeric instabilities and without non-flow contribution. The method uses all orders of azimuthal particle correlations to measure the anisotropic flow in order to vanish (and not reduce) all non-flow effects.

How can be used the Lee-Yang theory into anisotropic flow? Let's start from the Lee-Yang theory about phase transition [219, 220]. They start with the grand partition function:

$$\mathcal{G}(\mu) = \sum_{N=0}^{+\infty} Z_N e^{\mu N/kT} \tag{3.6.1}$$

where Z_N is the canonical partition function for N particles at fixed temperature T in a fixed volume V. We fixe also a reference value of the chemical potential: μ_c. The probability P_N to have N particles in the system at $\mu = \mu_c$ is:

$$P_N \equiv \frac{Z_N e^{\mu_c N/kT}}{\mathcal{G}(\mu_c)} \tag{3.6.2}$$

Now one can define the moment generating function of this probability distribution in terms of the grand partition function:

[2]Still as for infinite multiplicity a nonflow contribution non equal to zero, the nonflow contribution is $\mathcal{O}\left(\frac{1}{M^n}\right)$

$$G(z) \equiv \sum_{N=0}^{+\infty} P_N e^{zN} = \frac{\mathcal{G}(\mu_c + kTz)}{\mathcal{G}(\mu_c)} \tag{3.6.3}$$

with z a complex variable and N the number of particles in a volume V. Now assume that a first order transition occurs at $\mu = \mu_c$. Then, in order to study the liquid-gas transition, the system is a mixture of low density gas phase and high density liquid phase. Therefore, the probability distribution is spread between N_{min} with the gas phase and N_{max} with the liquid phase in the same volume V.

The result of the Lee-Yang theory is that we have a phase transition at $\mu = \mu_c$ only if the zeroes (or minima) of $G(z)$ come closer to the origin $z = 0$ as the volume of the system V increases.

The goal of the LYZ method is to applicate the same idea to anisotropic flow. Correlating a large number of particles is the most natural way of studying a genuine collective motion in the system. Then, the large order behavior is determined by the location of the zeroes of a generating function in the complex plane [216, 217]. The anisotropic flow appears to be the first zero (the closer to the real axis) and appears to be equivalent to a first order transition.

3.6.2 Vanish all non-flow effects ?

As the direct calculations of anisotropic flow using cumulant expansion (QC method), the LYZ method is based on the flow vector. The flow analysis, like the GFC method, proceeds in two successive steps. The first step is the evaluation of the integrated flow (denoted in this section by V_n) by the estimation of how the flow vector is correlated with the true reaction plane. The second step is the evaluation of the differential flow (denoted in this section by v_n) by using the integrated flow as a reference. The exact denotation of both integrated and differential flows evaluated by this method are $V_n(\infty)$ and $v_n(\infty)$ respectively, where the ∞ symbol means that the large order behavior of the cumulant expansion is taken.

Flow vector

The flow vector is the same as previous methods:

$$Q_x = \sum_{j=1}^{M} w_j \cos(n\phi_j) \qquad Q_y = \sum_{j=1}^{M} w_j \sin(n\phi_j) \tag{3.6.4}$$

with M the event multiplicity, ϕ_j the azimuthal angles of the j particle with respect to a fixed direction in the laboratory. One more time, the weight of particle w_j is depending on transverse momentum, particle mass and rapidity, chosen to have the smallest statistical error by increasing the signal. Here, one takes $w_j = 1$ for more simplicity.

Unlike the previous methods where we used the flow vector directly, here one uses the projection of Q on a fixed direction with respect to the x-axis. The denotation of this projection is given by:

$$Q^\theta \equiv Q_x \cos(n\theta) + Q_y \sin(n\theta) = \sum_{j=1}^{M} w_j \cos\left[n(\phi_j - \theta)\right] \tag{3.6.5}$$

with n θ the angle representing the projected direction. All the flow analysis will be performed using this projection of the flow vector in a fixed direction.

Integrated flow

The integrated flow is the average over events of the flow vector projected on the unit vector with angle $n\Phi_R$. To have a physical representation of the $n\Phi_R$ value, the reaction plane corresponds as $n = 1$. The integrated flow is also defined as:

$$V_n \equiv \langle Q^{\Phi_R} \rangle = Q_x \cos(n\Phi_R) + Q_y \sin(n\Phi_R) \tag{3.6.6}$$

The principal difference between the usual integrated flow v_n and the integrated flow V_n used here is the possible dimension of V_n unlike v_n. The usual integrated flow involves a sum over all particles and V_n scales the multiplicity M. Consequently with unit weight, neglecting the multiplicity fluctuations, we can find:

$$V_n = M v_n \tag{3.6.7}$$

where the usual v_n is the integrated flow over the phase space region (typically the used detector). Like the v_n, we cannot measure directly the V_n. One must proceed by an estimation for a given value θ. In the LYZ method, one uses a generating function which depends on the complex variable z, this is the central object of this method. We can define the averaged generating function by two ways:

$$G^\theta(z) = \langle e^{zQ^\theta} \rangle = \langle e^{z\sum_j w_j \cos(n(\phi_j-\theta))} \rangle \quad \tilde{G}^\theta(z) = \langle \prod_j^M [1 + z w_j \cos(n(\phi_j - \theta))] \rangle \tag{3.6.8}$$

with the average done for the number of events: N_{evt} with the same range of centrality. One must compute the generating function for each event for the real positive variable r with $z = ir$ to define the generating function real for real z with few values of θ. For every value of θ, one should estimate the first positive minimum of the modulus $|G^\theta(ir)|$ denoted by r_0. We can find a graphic representation of $|G^\theta(ir)|$ in function of positive value r in different references [217, 221]. The estimation of the integrated flow will be effectuated with the following equation:

$$\boxed{V_n^\theta\{\infty\} \equiv \frac{j_{01}}{r_0^\theta}} \tag{3.6.9}$$

with $j_{01} = 2.40483$ the first zero of the Bessel function J_0. All physical and theoretical reasons of the evaluation of the integrated flow is given in the reference [216, 217]. I will not describe the reason because this is not the purpose of this thesis. I want to describe how we can calculate the anisotropic flow with the LYZ method. Then, we calculate the integrated flow for every θ, thus, one should average all $V_n^\theta\{\infty\}$. I will not describe also all statistical errors because this is not the purpose of this thesis. Once the integrated flow is estimated, one must estimate the differential flow.

Differential flow

The analysis of the differential flow is the estimation of the POI in a definite phase-space. In this section, the differential flow will be denoted by v'_p. The azimuth of the POI will be denoted by ψ. As the previous methods, we will use the estimation of the reference anisotropic flow as a reference to calculate the differential flow. The estimation of v'_p is calculated with p a multiple of n like $p = m \times n$ with m integer.

For a given angle θ (to have the values of r_0^θ therefore $V_n^\theta\{\infty\}$), one can estimate the differential flow v'_{mn} by:

$$\frac{v'^{\theta}_{mn}\{\infty\}}{V_n^\theta\{\infty\}} \equiv \frac{J_1(j_{01})}{J_m(j_{01})}\Re\left(\frac{\left\langle \cos\left[mn(\psi-\theta)\right] e^{ir_0^\theta Q^\theta}\right\rangle}{i^{m-1}\left\langle Q^\theta e^{ir_0^\theta Q^\theta}\right\rangle}\right) \qquad \text{meaning}$$

$$\boxed{\frac{v'^{\theta}_{mn}\{\infty\}}{V_n^\theta\{\infty\}}} \equiv \frac{J_1(j_{01})}{J_m(j_{01})}\Re\left(\frac{\left\langle g^\theta(ir_0^\theta)\frac{\cos(mn(\psi-\theta))}{1+ir_0^\theta w_\psi\cos(n(\psi-\theta))}\right\rangle_\psi}{i^{m-1}\left\langle g^\theta(ir_0^\theta)\sum_j\frac{w_j\cos(n(\phi_j-\theta))}{1+ir_0^\theta w_j\cos(n(\phi_j-\theta))}\right\rangle_{evts}}\right) \tag{3.6.10}$$

with $\langle\cdots\rangle$ denoting an average over events and over all particles in each event in the denominator. The average $\langle\cdots\rangle_\psi$ is over all POI and w_j the weight associated of this type of particle. The denominator denotes the derivative of the generating function at the minimum r_0^θ of LYZ. Of course, one takes the real part of the complex ratio.

Like other methods of anisotropic flow analysis (unlike the QC method), the LYZ has a sign ambiguity because the sign of the integrated flow V_n cannot be reconstructed. Generally, one assumes that $V_n^\theta\{\infty\}$ and r_0^θ are positive. If the true V_n is positive, the estimation of $v'^{\theta}_{mn}\{\infty\}$ has the correct sign, in the other case one should multiply by $(-1)^m$ to have the right estimation of the differential flow.

Synthesis or strategy to calculate the anisotropic flow:

1. for a given centrality bin, one must compute for each event the complex-valued generating function;
2. for every value of θ, one should estimate the first positive minimum of the modulus of the generating function denoted by r_0;
3. use the equation 3.6.9 to estimate the integrated flow;
4. use the estimation of the integrated flow to estimate the differential flow with the equation 3.6.10;

Discussion

One can see that the Lee-Yang theory on phase transition can be used for anisotropic flow analysis. The method can give results similar to high order of cumulant expansions but simpler to implement into experimental analysis. The minimum of the modulus of the generating function is compatible with a zero of the generating function. The LYZ method gives results similar to the cumulant method but simpler than the GFC method.

The Lee-Yang zeroes provide a natural probe of collective behaviour inside heavy ions collisions. Exactly, the existence itself of a zero close to the origin and scaling with the inverse of the system size signals the presence of collective effects. This is the transition with the Lee-Yang theory of phase transition where the zeroes of the partition function come closer to the origin with increasing system size where a phase transition comes from.

The LYZ method has a very well stability but we must make two loops over the data to estimate both integrated and differential flows. The autocorrelation contribution is removed by the factor $e^{ir_0^\theta Q^\theta}$ in the numerator of the equation 3.6.10. Another advantage of the LYZ method is that one does not estimate the cumulant order-by-order, this method returns directly the infinity order of cumulants.

Finally, we will privilege the QC tactical at the LYZ method because we can give an estimation of both integrated and differential flows in one pass over data.

3.7 Symmetric Cumulants or Standard Candles

The last observable about anisotropic flow that I will show you is the Symmetric Cumulants (SC) analysis or **Standard Candles**. This observable has been introduced by the ALICE collaboration in the generic framework for anisotropic flow analysis with multi-particle azimuthal correlations [214, 222] This observable is useful when the magnitudes event-by-event of the flow harmonics fluctuates. We use the corresponding four-particle cumulant given by:

$$\begin{gathered}\langle\langle\cos(m\phi_1 + n\phi_2 - m\phi_3 - n\phi_4)\rangle\rangle_c = \\ \langle\langle\cos(m\phi_1 + n\phi_2 - m\phi_3 - n\phi_4)\rangle\rangle - \langle\langle\cos[m(\phi_1 - \phi_2)]\rangle\rangle\langle\langle\cos[n(\phi_1 - \phi_2)]\rangle\rangle \\ SC(n,m) = \langle v_m^2 v_n^2\rangle - \langle v_m^2\rangle\langle v_n^2\rangle \qquad \text{with } m \neq n\end{gathered} \tag{3.7.1}$$

where the double brackets indicate the average over all particles and all events. Having a non-zero value for $SC(n,m)$ suggests a correlation between the event-by-event fluctuations. A positive value of $SC(n,m)$ suggests a positive value correlation between the event-by-event fluctuation of v_n and v_m, therefore v_n is larger than $\langle v_n\rangle$ enhances the probability to have v_m larger than $\langle v_m\rangle$. A negative value of $SC(n,m)$ suggests a negative value correlation between the event-by-event fluctuation of v_n and v_m, therefore v_n is larger than $\langle v_n\rangle$ enhances the probability to have v_m smaller than $\langle v_m\rangle$. Finally, the SC is equal to zero in the absence of flow fluctuations, or if the magnitudes of the different harmonics v_n and v_m are uncorrelated [214, 222, 223].

We can use the QC method to have an estimation of the different harmonics in the SC observable. Consequently, we use the Q-vector to estimate each order in the 3.7.1 equation. The Q-vector in this section will be denoted by:

$$Q_n \equiv \sum_{j=1}^{M} e^{in\phi_j} \tag{3.7.2}$$

with M the multiplicity detected, and ϕ_j the azimuthal angle of the j-particle. The term of v_n is already known with the section 3.5.3:

$$\langle 2\rangle_n \equiv \frac{|Q_n|^2 - M}{M(M-1)} \tag{3.7.3}$$

but the 4-particle correlation with different harmonics n and m has not been calculated in the section 3.5.3.

The estimation of the 4-particle correlation is:

$$\begin{aligned}\langle 4\rangle_{n,m} &= \frac{|Q_n|^2 \times |Q_m|^2 - 2\Re[Q_{n+m}Q_n^*Q_m^*] - 2\Re[Q_nQ_{n-m}Q_m^*]}{M(M-1)(M-2)(M-3)} \\ &+ \frac{|Q_{n+m}|^2 + |Q_{n-m}|^2 - (M-4)(|Q_n|^2 + |Q_m|^2) + M(M-6)}{M(M-1)(M-2)(M-3)}\end{aligned} \tag{3.7.4}$$

Finally, the last equation to estimate the SC observable is:

$$\boxed{SC(n,m) = \langle\langle 4\rangle\rangle_{n,m} - \langle\langle 2\rangle\rangle_n \times \langle\langle 2\rangle\rangle_m} \tag{3.7.5}$$

One question of this Ph.D thesis will be to calculate the SC of different systems as *pp* collisions and AA collisions and verify if we have the same behavior between these two systems. If these two systems have the same behavior, it will provide a strong evidence of a similar origin of collectivity in small or large hadronic collision systems.

This complex observable can give us more information about the collectivity of the system but we need a lot of statistics to have the estimation of **two different harmonics**.

3.8 Conclusions and Implementation in EPOS

In this chapter, I started by introducing the anisotropic flow itself before introducing different methods to estimate the anisotropic flow. I explained the difference between the integrated flow and the differential flow and the reason of the estimation of this observable: this is a probe about the QGP. The anisotropic flow is sensitive to the early steps of the evolution of the matter at very high energy because it is related to the initial geometry of the system.

Over the years, different methods are created to calculate the anisotropic flow. Different ways are built to remove the non-flow contribution like auto-correlation. I started to describe the Event Plane method and the eta-sub way to reduce the non-flow effects. This method is often used in anisotropic flow analysis because it is fast and simple. This is naturally that we implement the EP method in EPOS.

The eta-sub method can give satisfactory results but it is not perfect, one decreases the non-flow contribution but does not vanish it. One can reduce the non-flow contribution by using method which does not require an estimation of the reaction plane event-by-event. The advantages for this method are: i) the great timeliness to measure the anisotropic flow for any harmonics, ii) the easier possibility to reduce nonflow contributions using a pseudorapidity gap. The disadvantage is that we only have a first approximation about the measurement of the anisotropic flow.

The Scalar Product method fills this part by estimating the anisotropic flow directly using two different sub-events and the scalar product of the Q-vector from these two sub-events. This method is also fast and simple to give an estimation of the anisotropic flow and this is naturally that we implement this one in EPOS. The advantages for this method are: i) also a good timeliness to measure the anisotropic flow for any harmonics, ii) the possibility to measure the anisotropic flow wihtout an estimation of the reaction plane. The disadvantage is that we only have a first approximation about the measurement of the anisotropic flow and the nonflow contribution are not suppress totaly.

Two other methods are created to reduce systematically the non-flow contribution: the Generating Function Cumulant and Lee-Yang Zeroes methods. These methods are very effective and are very accurate to calculate the anisotropic flow. The LYZ suppress totaly the non-flow contribution using Lee-Yang Theory. However, they are not efficient for EPOS because we cannot estimate both integrated and differential flows in one pass over data. These methods need a large statistic and two passes over data will reduce the rapidity of the EPOS analysis.

One of last tacticals to calculate the anisotropic flow is the Q-cumulants method which calculates directly both integrated and differential flows in one pass over data using only Q-vector in multi-particle azimuthal correlation. This complex method has been implemented in EPOS because it is efficient but it needs a large statistic. For algorithm implementation of the QC method, this method is very effective! Indeed, we calculate all different harmonics of anisotropic flow using only one loop over data. This method is also faster and unbiased contrary to the previous cumulants method. The limitation is that we need a lot of statistics and like the GFC method.

Finally, one complex observable called the Symmetric Cumulants can be calculated in order to verify a positive or negative correlation between event-by-event fluctuation. It is very useful to compare different system sizes like pp and AA collisions. As a recall one of main goals of this thesis is to try to answer the following question: Do we really have a “collectively expanding plasma” in all systems, big (PbPb) and small (pp), at high energies and low energies? Consequently this observable is crucial to answer this question, therefore we implement the analysis to calculate the SC observable in EPOS.

In the following chapter, I will present the principal results that I obtained during all the Ph.D about the anisotropic flow or less complex observables like p_T, rapidity and pseudorapidity spectra. I used all methods that I had implemented in EPOS as: EP, eta-sub, SP, QC and calculated the complex observable SC.

CHAPTER 4

ENERGY AND SYSTEM SIZE DEPENDENCE FOR THE FORMATION OF QUARK-GLUON-PLASMA

Contents

I showed in the previous chapter different methods to calculate the anisotropic flow of produced particles during a collision. In this chapter, I show the main results obtained during my Ph.D on the anisotropic flow and also on "basic observables" like yields and spectra. These results will try to answer this following question:

Do we really have a “collectively expanding plasma” in all systems, big (PbPb) and small (pp), at high energies and low energies?

If we find a good agreement between data and theory for all systems (pp to AA) at RHIC and LHC energies, that means that our scenario of an hydrodynamical expansion, based on initial conditions from our Gribov-Regge approach, is supported for each type of collision.

This is the first time that we use EPOS in the BES and LHC Run II energies. I tested own event generator at new energies to know if it can be used in the new range of energy:

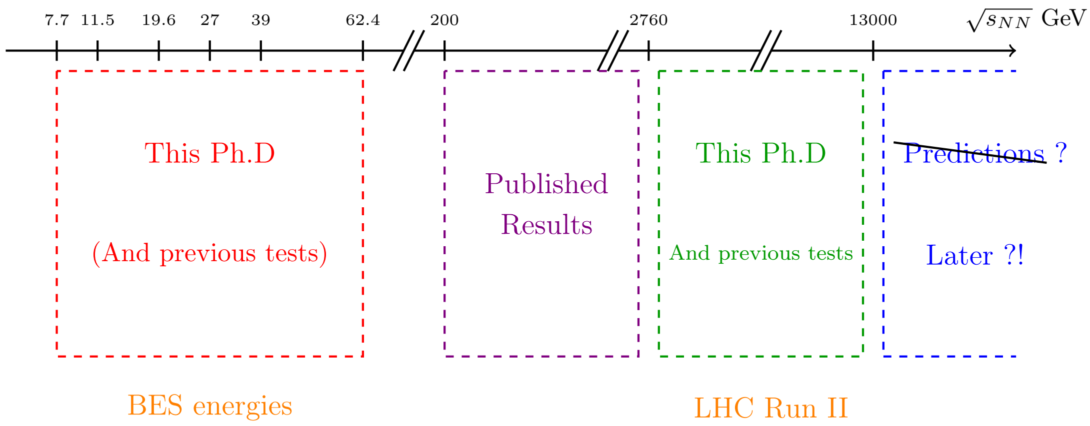

Figure 4.1: Representation of EPOS use after my Ph.D

A lot of systems have been studied during this Ph.D in order to see a global vision of these energies. In the next page, I represent in two dimensions the precedent picture adding the system size dimension in the Fig 4.2.

This chapter is separated in two axes on particle production: dependence of system size and dependence of energy. I start the different analyses by "simple" observables like yields, p_T, rapidity and pseudorapidity spectra before attacking the big part of results on anisotropic flow. I start by the system size dependence because the question is more current: Do we have a collectively plasma in small system at high multplicity? Can we have a droplet of QGP in pp collisions?

4.1 Dependence of system size

The data that we use for this analysis generally comes from Run 2 at the LHC. The recent observation of long-range two-particle azimuthal correlations at large pseudorapidity for high multiplicity pp [224–226] and p-Pb [227–229] collisions at the LHC has not been expected. However, this surprise opens new possibilities to study the dynamics of particle production. We find for pp collisions the most famous feature of the two-particle

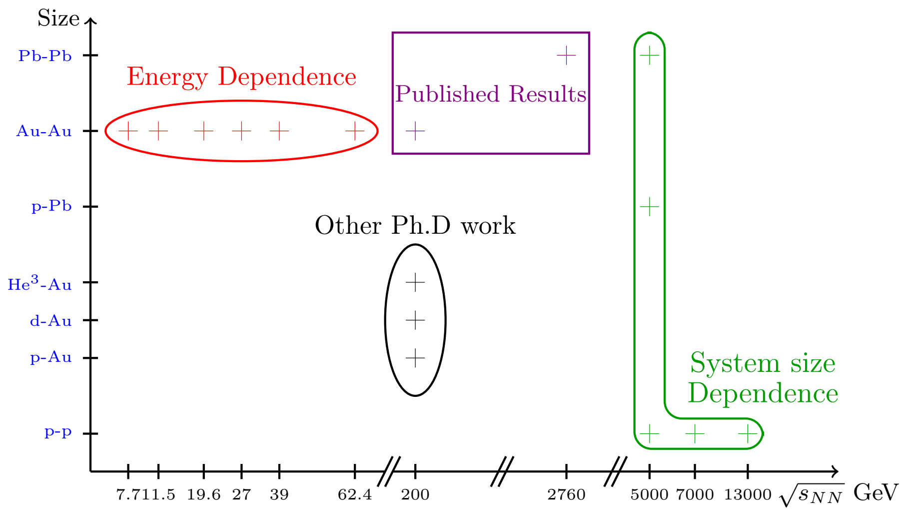

Figure 4.2: System sizes studied during my Ph.D

azimuthal correlations. It is an enhanced structure on the near side of two particle correlation function ($\Delta(\phi) \approx 0$) known as *ridge*. This structure was first observed in AA collisions from RHIC to LHC energies and has been treated as a hydrodynamic collective flow feature of an expanding medium. Fortunately, EPOS was one of first theoretical model which predicted the *ridge* for AA but also pp collisions [230]!

Now, the new definitions to study the pp and pA collisions starts to be "usual"[1]. The pp collisions cannot be considered only as a reference collision to show the hydrodynamic point of view of Pb-Pb and Au-Au collisions. Currently, the small system has a new translation: *system a priori too small to show characteristics of heavy ion physics and however in which we observe them, at least some.*

To answer this question, we use EPOS, which is an hydrodynamic event generator where we can create a little fluid in pp collisions. If we have a good agreement between EPOS and LHC data, that means that the hydrodynamic point of view for pp collisions is supported. In this section, I compare with few observables the differences and similarities between small and large systems. I start by the basic observables to see what is the core (fluid) contribution to the particle production.

4.1.1 Basic Observables

4.1.1.1 Yields of particles

Before comparing results of EPOS with experimental data, I want to see if the fluid contributes strong for each type of collisions (pp, pA and AA). In the following page, I show the minimum bias yield integrated over p_T and η of different particles and antiparticles: π, K, p, Λ, and Ξ produced by the 3.235 EPOS version.

[1] Topic of Quark Matter 2018

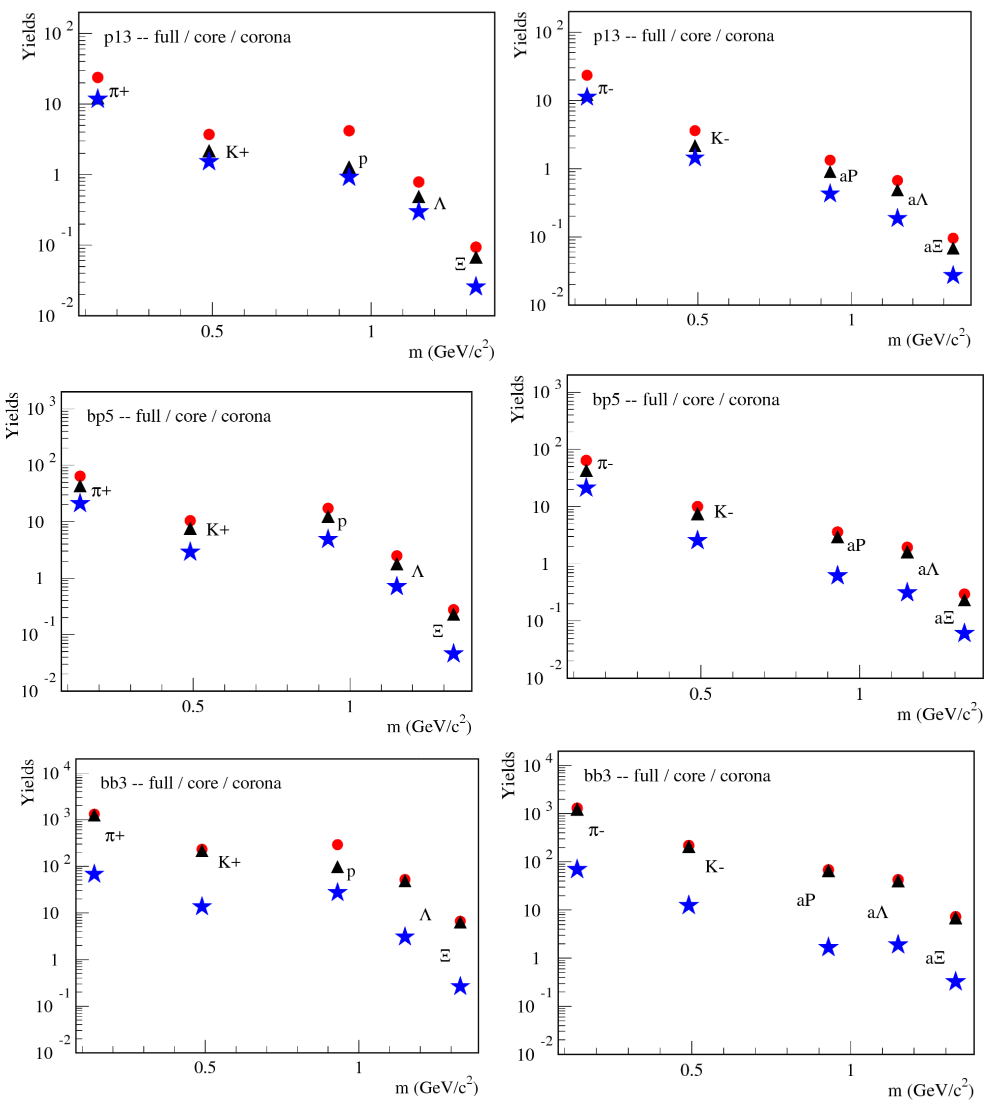

Figure 4.3: Yields of particles (left) and antiparticles (right) generated by EPOS for three collisions: pp at $\sqrt{s_{NN}}$ =13 TeV (up), p-Pb at $\sqrt{s_{NN}}$ =5.02 TeV (middle) and Pb-Pb at $\sqrt{s_{NN}}$ =2.76 TeV (down). The different contributions are plotted in red (full), dashed blue (core) and dotted mauve (corona)

The number of events used to plot yields of particle is almost 1M for pp and 250K for p-Pb and Pb-Pb. I plot yields versus mass of particles with the full contribution in red, the core contribution in dashed blue line and corona part in dotted mauve line. I separate particles and antiparticles for readibility and see if we can see some different characteristics about core-corona contributions.

The first thing that we can see is the same trend of full - core - corona contributions for each system size. That means that EPOS treats each collision in the same way (good for a universal model).

The second thing is that the core part contributes stronger than corona part for each system size. We can also see that each part is important, the corona contribution is not insignificant. If our hydrodynamic model can reproduce experimental data, that is using a lot of core contribution.

The last thing is usual observation, core contributes more for Pb-Pb collision, almost all particles are created by fluid part. More generally, the core contributes more for bigger system sizes than for smaller ones.

4.1.1.2 Spectra of particles

Transverse momenta spectra

The p_t spectra allow us to know the distribution of particles following their p_t. We saw that the core contribution is important for each system size for particle productions. Now I want to see if EPOS can reproduce experimental data for pp, p-Pb and confirm the good results at Pb-Pb collisions.

I plotted the p_T spectra of charged (anti)particles π, K and p because they are the most particles created during a collision. In the same way as the yield section, I want to know the core contribution in p_t spectra of each system size. I want to check if the core contribution is consistent with the previous section (Fig 4.3. To see a possible centrality dependence, some p_t spectra are plotted with different centrality ranges. Consequently, I do not plot the core-corona of each spectra for readibility.

The experimental data are taken on these references: [231–233].

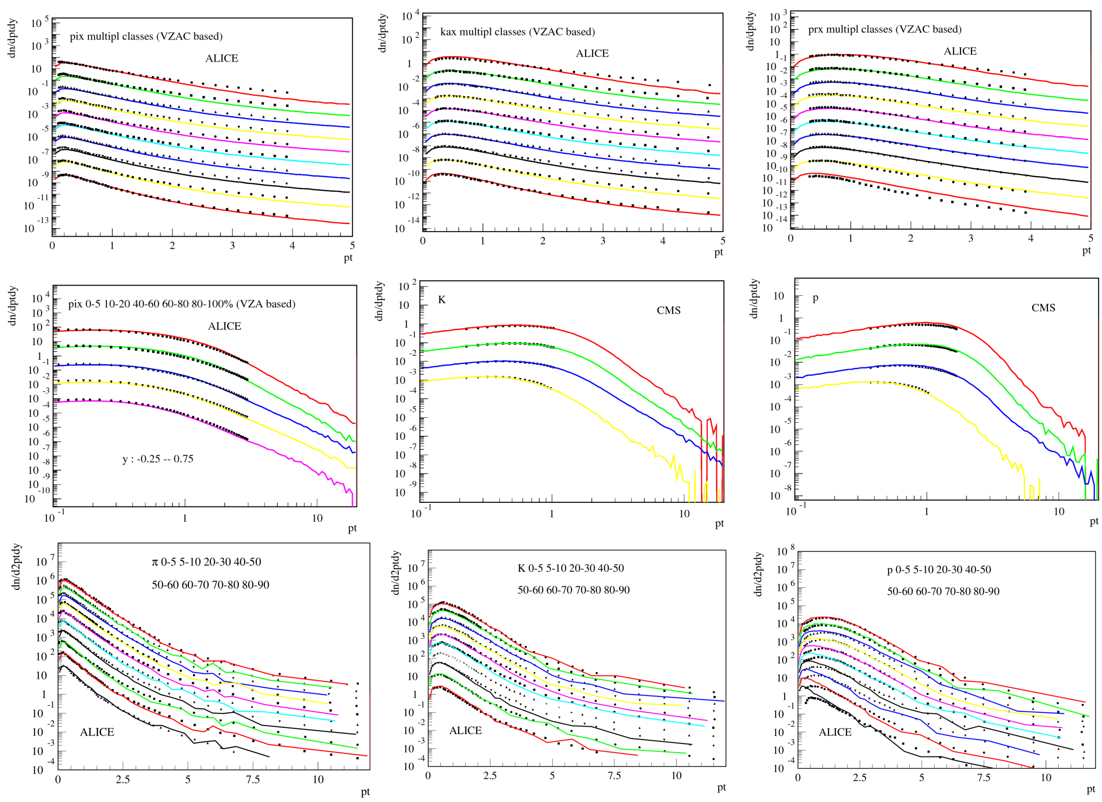

Figure 4.4: Transverse momentum of charged particles: pions (left), kaons (middle) and protons (right) for three collisions: pp at $\sqrt{s_{NN}}$ =13 TeV (up), p-Pb at $\sqrt{s_{NN}}$ =5.02 TeV (middle) and Pb-Pb at $\sqrt{s_{NN}}$ =5.02 TeV (down). The different p_T spectra are plotted with different centrality ranges

The first thing is that we can reproduce p_t spectra from different experiments for each system size. EPOS seems adapted to reproduce Pb-Pb at $\sqrt{s_{NN}}$ = 5.02 TeV at almost same precision than Pb-Pb at $\sqrt{s_{NN}}$ = 2.76 TeV. It is expected because it is assumed that a QGP is created at this energy.

The current version (3.242) cannot reproduce exactly p_t spectra for Proton at low p_t with Pb-Pb $\sqrt{s_{NN}}$ = 5.02 TeV for peripheral collisions.

The experimental data are taken on these references for the following picture: [231, 234, 235].

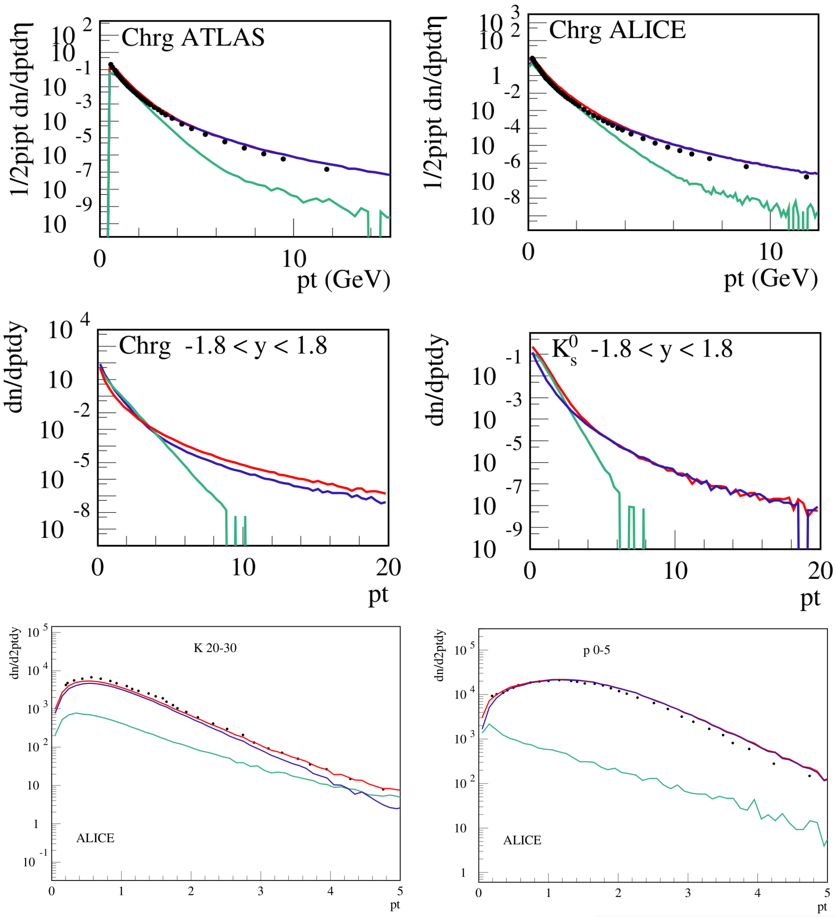

Figure 4.5: Transverse momentum spectra of charged particles (up), kaons and protons (bottom) for three collisions: pp at $\sqrt{s_{NN}}$ =13 TeV (up), p-Pb at $\sqrt{s_{NN}}$ =5.02 TeV (middle) and Pb-Pb at $\sqrt{s_{NN}}$ =5.02 TeV (down). The core part is plotted in green and corona part is plotted in blue.

The second thing is the confirmation that the core contributes more than corona part for big and small system sizes. This is consistent with the results about yields of particles. I put theoretical data for Pb-p to show other particles like K^o_s and show that we have the same behavior for particle production in these collisions.

The p_t spectra with different centrality classes are scaled by different factors for better lisibility. I also want to know if we can reproduce the experimental data for rapidity or pseudorapidity spectra. At the end of the paragraph, we will see what we can say about these results.

Rapidity or pseudorapidity spectra

The y or η spectra allow us to know the distribution of particles following their y or η. We saw that the core contribution is important for each system size for particle productions. Now I want to see if EPOS can reproduce experimental data for pp, p-Pb and confirm the good results at Pb-Pb collisions. Like previous section, I will only show the spectra of charged particles.

The experimental data are taken on these references: [234, 236, 237].

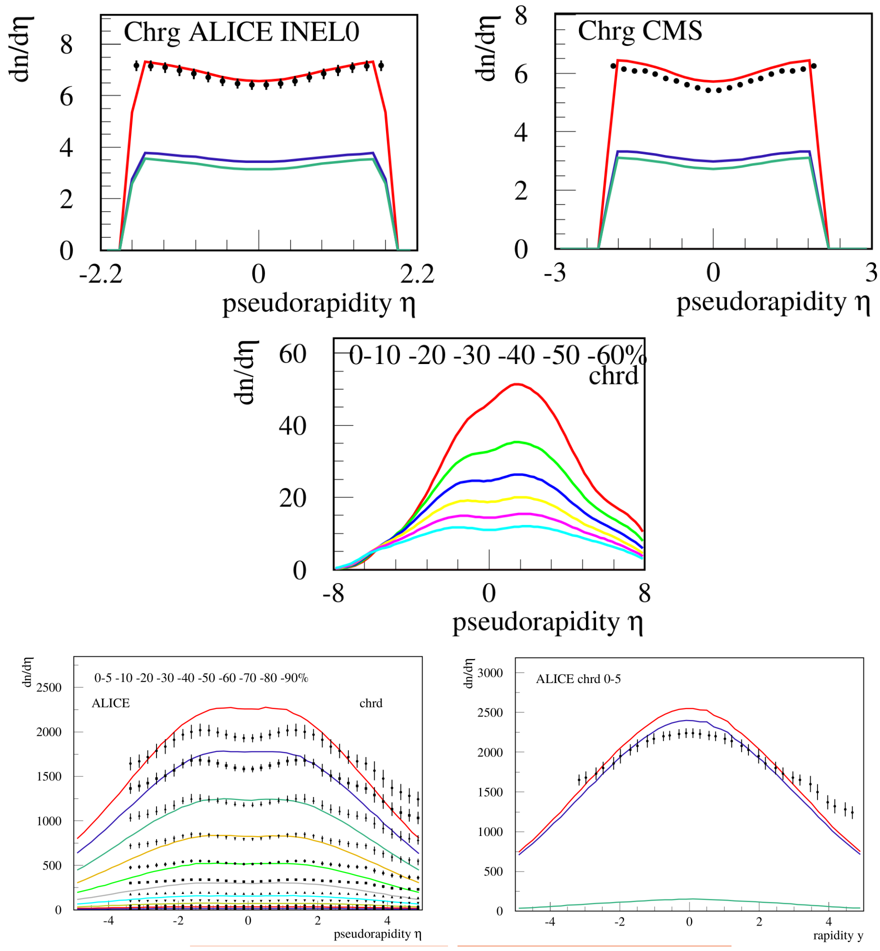

Figure 4.6: Rapidity or pseudorapidity spectra of charged particles for three collisions: pp at $\sqrt{s_{NN}}$ =13 TeV (up), p-Pb at $\sqrt{s_{NN}}$ =5.02 TeV (middle) and Pb-Pb at $\sqrt{s_{NN}}$ =5.02 TeV (down). The core part is plotted only for pp collisions (up) and right side of Pb-Pb collision (bottom) in blue and the corona part is plotted in green.

We have the same observation about core contributions as previous sections. The core contributes stronger than corona part for small and big system sizes. The core contributes also stronger for big system size than small system size.

We do not have a perfect agreement with data however we have the same magnitude as experimental data.

All different spectra on this section do not have the same cuts on transverse momentum, particles, rapidity, multiplicity etc ... Consequently, the idea here is not to compare the different contributions between experiment and spectra but see how our model works with "basic" observables. The results are the same for each observable: **EPOS predicts a strong fluid contribution to describe the experimental data. The EPOS results reasonably agreed with data**, which means that our scenario of an hydrodynamical expansion, based on initial conditions from our Gribov-Regge approach, is supported.

It is too early to say that we have a collectively expanding plasma in all systems at high energies but EPOS seems supported using an expanding plasma for basic observables at all system sizes. Obviously, we can say before reading the next section that we will observe anisotropic flows because we have fluid for each collision (big and small). The question will be if we can reproduce the data without specific tuning at LHC energies and using exactly the same analysis than experiments.

4.1.2 Anisotropic Flow

As previous sections, I will show results for pp or Pb-Pb collisions simutaneously to have the most direct and complete vision.

We are lucky because the science of small system grows up and a lot of data appears for each LHC experiment which works on QGP. For example, *"collectivity at small system"* is now a complete session in Quark Matter 2018 or the subject of different workshops! Consequently, we can do a comparison between experiments and what EPOS says on anisotropic flows. Unfortunately, Quark Matter 2018 started too late to have a complete analysis of small system's results and I do not have a lot of results on anisotropic flow for pp and Pb-Pb collisions.

This section is separates with the contribution of different basic observables on integrated and differential anisotropic flows (remember the Chapter 1).

4.1.2.1 Contributions in transverse momenta

In this section, unfortunately, I do not analyse differential anisotropy on p_T for pp and Pb-p collisions. However, I have the opportunity to do a comparison between Pb-Pb at $\sqrt{s_{NN}}$ =2.76 TeV and $\sqrt{s_{NN}}$ =5.02 TeV. Normally the model must work for high multiplicity Pb-Pb collisions at $\sqrt{s_{NN}}$ =2.76 TeV, a lot of results are already published at this energy. We can do a comparison between these two energies to know if EPOS continues to have a strong power description at $\sqrt{s_{NN}}$ =5.02 TeV. That is the main purpose of this section.

We have access to a lot of data for Pb-Pb at $\sqrt{s_{NN}}$ =2.76 TeV or $\sqrt{s_{NN}}$ =5.02 TeV for charged particles. Consequently, we can also do a comparison between the different methods to calculate the anisotropic flows.

The experimental data are taken on this reference: [238]. In the following picture, I plot only pions and protons for better visibility. The results are obtained using the Scalar Product (SP) method, using a pseudo-rapidity gap of $|\Delta\eta| > 0.9$ between the identified hadron under study and the reference particles.

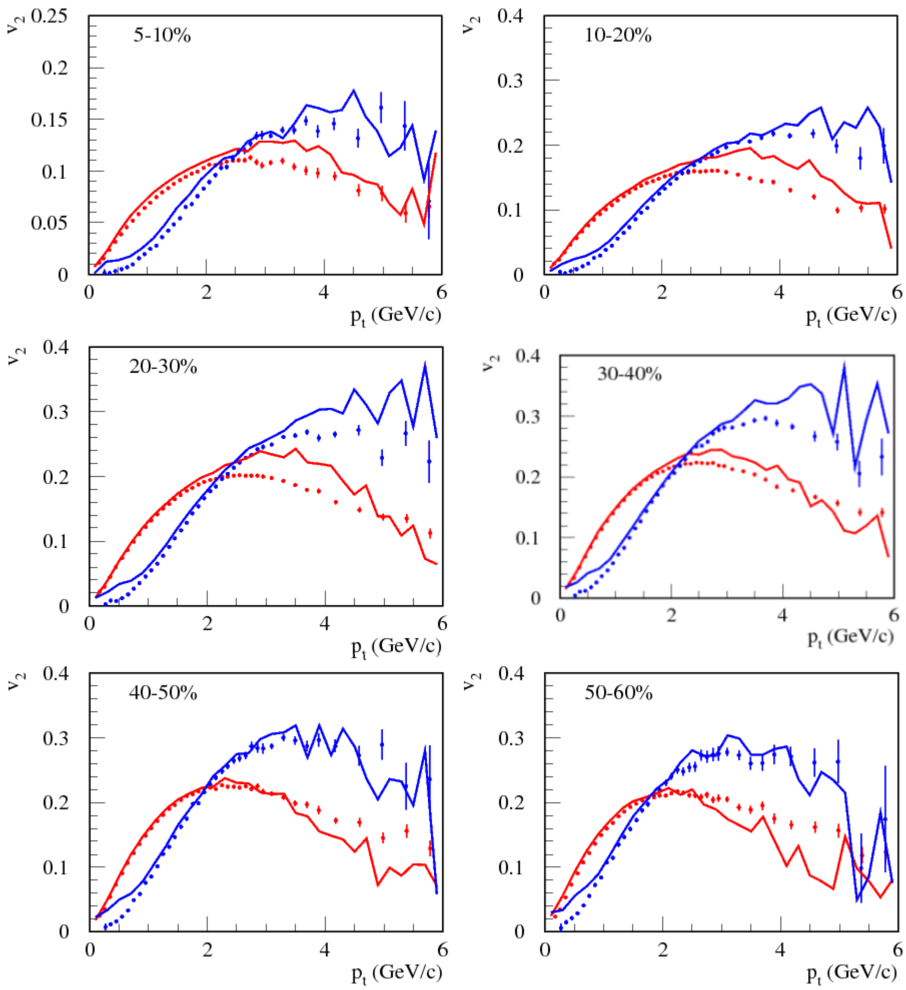

Figure 4.7: Differential flow of protons (blue) and pions (red) for Pb-Pb collision at $\sqrt{s_{NN}}$ =2.76 TeV for different centrality ranges. EPOS results are in full line and experimental in dots.

We see that EPOS can reproduce (not perfectly) the data of mesons (pions) and baryons (protons) for p_t below 2 GeV/c. Above 2 GeV/c, we cannot reproduce the data because the contribution of the hydrodynamic part is leather at these p_T and we do not take in account the jet-matter contribution.

We can take these results (coupled with spectra obviously) to say that EPOS confirms its utility to reproduces the results for Pb-Pb collisions. We can assume later that the results for Pb-Pb at $\sqrt{s_{NN}}$ =2.76 TeV can be considered as good results. This is the starting point to compare results between the two energies (2.76 and 5.02 TeV). In the following, I will compare the results from the Event Plane (EP) and the Q-cumulants (QC) methods. I start by this point because the results for $\sqrt{s_{NN}}$ =5.02 TeV, are recent and obviously to compare with small systems, we use QC (*recent method*) which remove more the nonflow effects.

To compare the two methods, I will follow the [239] reference. In this paper, the anisotropic measurements are performed for charged particles with transverse momenta $0.5 < p_T < 20$ GeV and in the pseudorapidity range $|\Delta\eta| < 2.5$. The experimental data are taken obviously on this reference: [239].

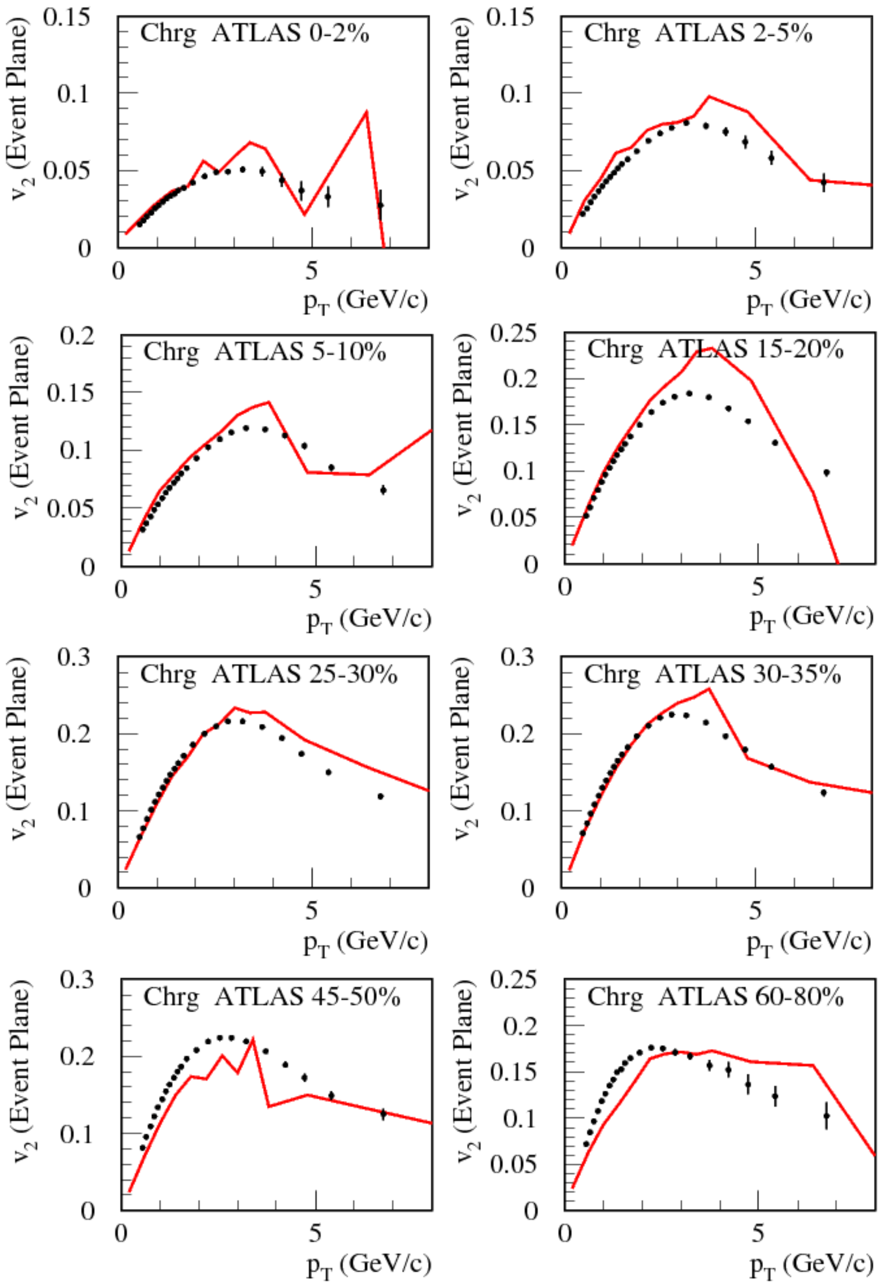

Figure 4.8: Differential flow of charged particles calculated by Event Plane method for Pb-Pb collision at $\sqrt{s_{NN}}$ =2.76 TeV with different centrality ranges. EPOS results are in full line and experimental in dots.

The first thing is that EPOS reproduces approximately well results until p_T = 4 GeV/c for all centrality ranges. The second thing is that the anisotropic flow seems smaller for central collisions. The $v_2\{EP\}$ is measured using a separation between the phase space region where the event plane angle is determined (3.2<$|\eta|$<4.9) and the phase space where charged-particle momenta are reconstructed ($|\eta|$<2.5). Consequently, this elliptic flow may not be too much affected by nonflow effects.

Now let's see how EPOS can reproduce data from QC method!

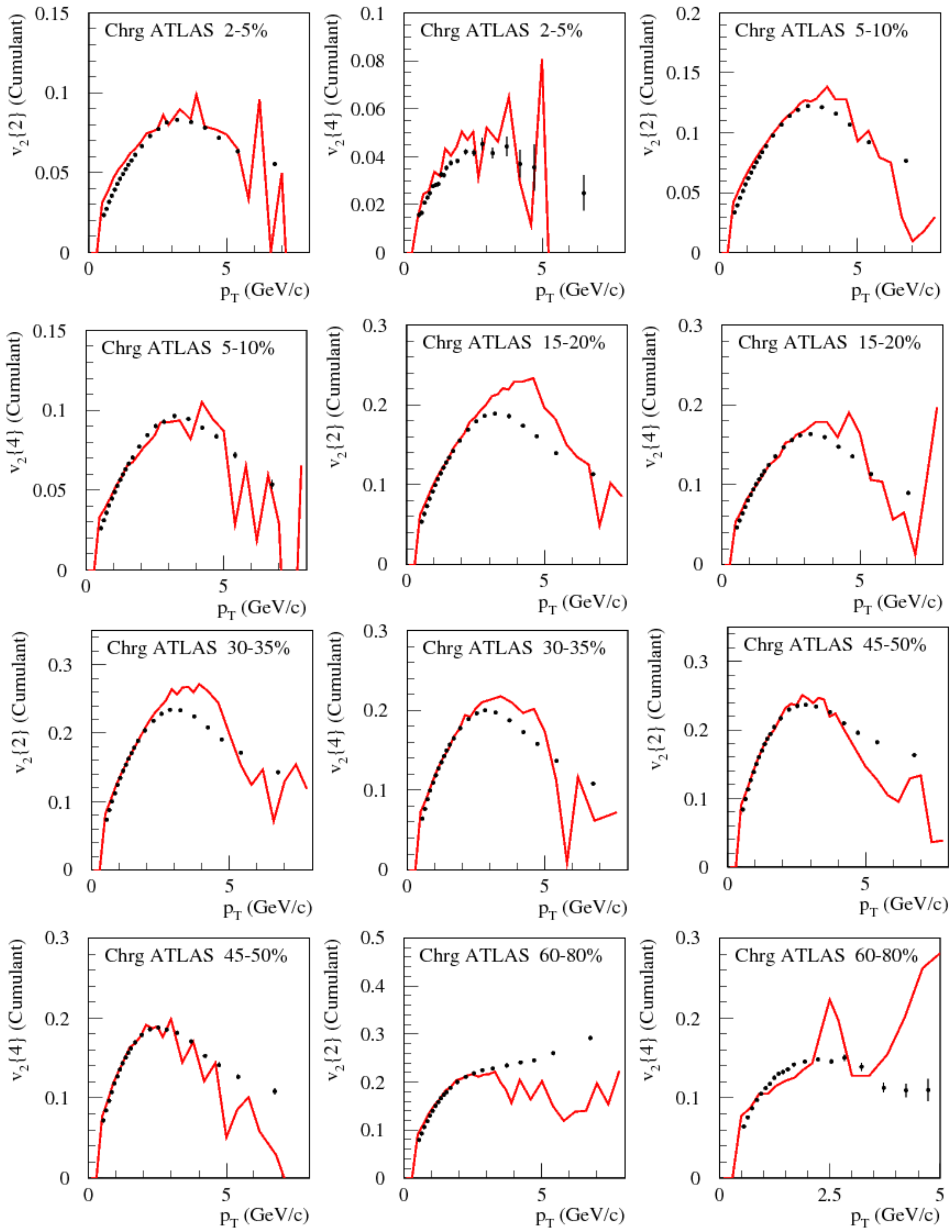

Figure 4.9: Differential flow of charged particles calculated by Q Cumulant method for Pb-Pb collision at $\sqrt{s_{NN}}$ =2.76 TeV with different centrality ranges. EPOS results are in full line and experimental in dots.

We can see that EPOS gives the same behavior between EP and QC results: it reproduces data until $p_T = 3 \backsim 4$ GeV/c for all centrality ranges. Generally, EPOS prediction is higher than experimental data below $p_T = 5$ GeV/c and smaller since $p_T = 5$ GeV/c. The $v_2\{4\}$ is systematically smaller than $v_2\{2\}$, this is consistent with the expected suppression of non-flow effects in v_2 obtained with cumulants of more than two particles.

To do the comparison between the EP and the QC methods, I plot now results of both methods in same canvas.

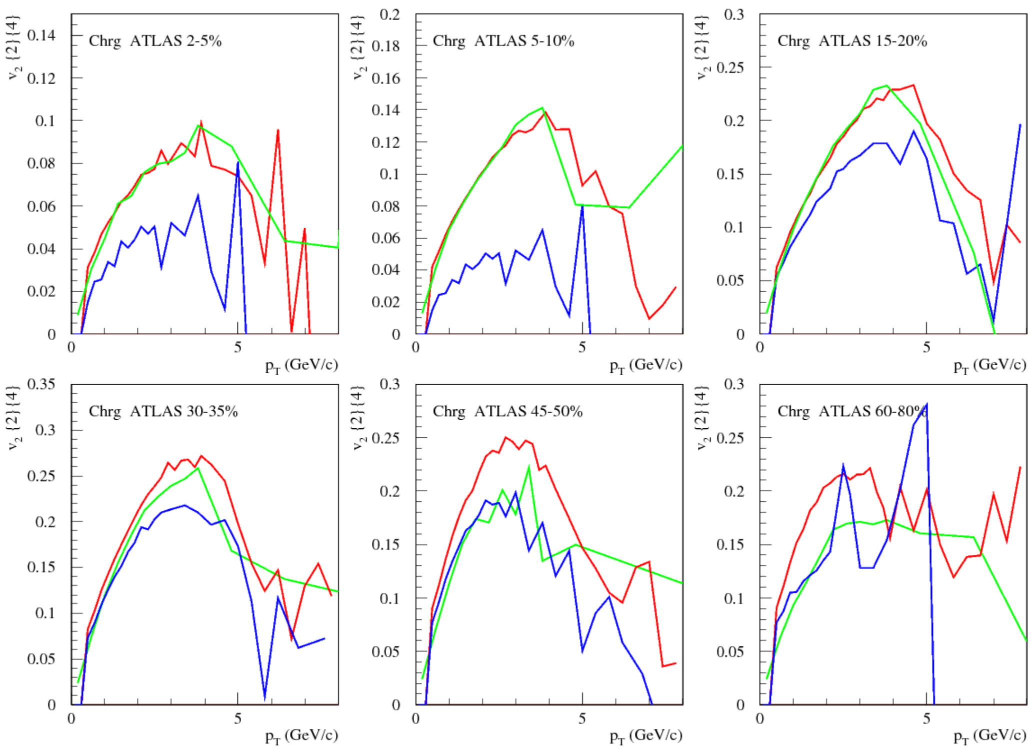

Figure 4.10: Differential flow of charged particles calculated by Q Cumulant (red and green) and event plane (blue) methods for Pb-Pb collision at $\sqrt{s_{NN}}$ =2.76 TeV with different centrality ranges. The anisotropic flow using two-particle correlation is reprensented in red and four-particle correlation in blue.

We see that event plane v_2 is equal to $v_2\{2\}$ for central collisions but it is smaller than $v_2\{2\}$ for peripheral collision since it is less affected by short-range two-particle correlations. This is due from the separation between the phase-space region where the event plane angle is determined (3.2<$|\eta|$<4.9) and the phase space where charged-particle momenta are reconstructed ($|\eta|$ < 2.5). The differences between v_2(EP) and $v_2\{2\}$ can be also attributed to flow fluctuations[2]. The difference between $v_2\{4\}$ is closer to v_2(EP) than $v_2\{2\}$, that indicates that the four-particle cumulants efficiently suppress non-flow correlations.

The last thing that we can say on these plots is that we have the same behavior between both methods: the second flow harmonic first increases with p_T up to 2-3 GeV, then gradually decreases for experimental and our hydrodynamical model. I do not show results for p_T higher than 8 GeV due to significant statistical errors but the v_2 dependence on p_T seems weaker, even nonexistent for p_T higher than 10 GeV.

Now that we know the transverse momenta dependence of the elliptic flow, I will show the transverse momenta dependence of higher orders of harmonics using QC method.

[2] the flow fluctuations can come from the eccentricity fluctuations from one event to the other, fluctuations of impact parameter or fluctuations of the position of participant nucleons

For higher orders of harmonics about the anisotropic flow studies, I find data for Pb-Pb collisions at $\sqrt{s_{NN}}$ =5.02 TeV from this reference: [240].

In this paper, we can find data for ATLAS and ALICE detectors about different harmonics v_2 to v_4 and also an analysis on the centrality dependence about the anisotropic flow using four-particle azimuthal correlation ($v_2\{4\}$). I start by the centrality dependence to have a correlation with the previous results shown in the previous pages but this time with $\sqrt{s_{NN}}$ =5.02 TeV.

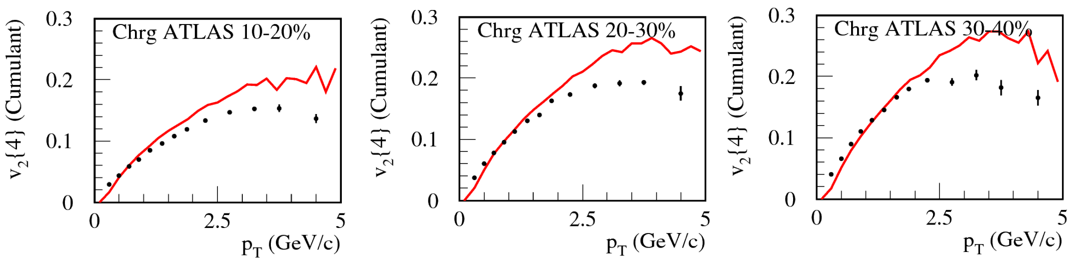

Figure 4.11: Differential flow of charged particles using four-particle azimuthal correlation calculated by Q Cumulant method for Pb-Pb collision at $\sqrt{s_{NN}}$ =5.02 TeV with different centrality ranges.

We see that the anisotropic flow increases at low p_T up to 2-3 GeV, then it saturates until the highest p_T measured. However, we cannot say if the anisotropic flow will gradually decrease at high p_T expected with the precedent analysis. We see that EPOS can reproduce the experimental data with p_T less than 2 GeV, after EPOS overestimates the anisotropic flow using four-particle correlation, fortunately this is the same behavior than previous analysis. Concerning the centrality dependence, we see that the anisotropic flow is higher at mid collision than central collision. This is also the same behavior than precedent analysis.

Now, I show the evolution of anisotropic flow at different harmonics:

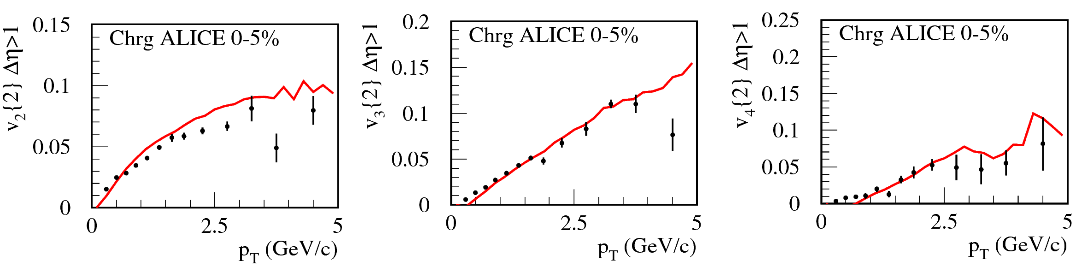

Figure 4.12: Differential harmonic about anisotropic flow of charged particles using two-particle azimuthal correlation calculated by Q Cumulant method for Pb-Pb collision at $\sqrt{s_{NN}}$ =5.02 TeV for central collisions.

We see that, for the 0-5% centrality, EPOS can reproduce the data until 3-4 GeV for each harmonic. At p_T>2 GeV, $v_3\{2\}$ is observed larger than $v_2\{2\}$ and $v_4\{2\}$ for experimental and EPOS data. The triangular flow[3] do not seem saturated with EPOS data in opposition with experimental data. $v_4\{2\}$ seems at the same order than $v_2\{2\}$ within uncertainties at p_T after 2 GeV for experimental data, also for EPOS.

[3]Third order of the anisotropic flow: v_3

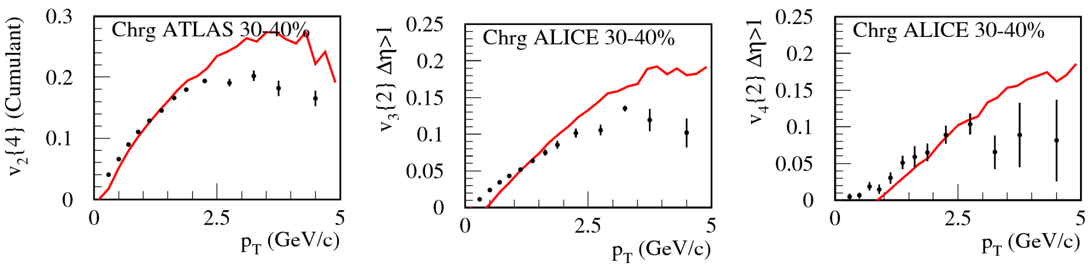

Figure 4.13: Differential harmonic about anisotropic flow of charged particles using two-particle azimuthal correlation calculated by Q Cumulant method for Pb-Pb collision at $\sqrt{s_{NN}}$ =5.02 TeV for mid collisions.

For the 30-40% centrality, we see that EPOS cannot reproduce the data after $p_T = 2$ GeV, after it overestimates the anisotropic flow before to decreasing after $p_T = 4$ GeV. For the experimental data, we do not see some crossing of the different order coefficients. For our hydrodynamic model, we see that elliptic flow seems higher than triangular and quadratic[4] flows. The triangular and quadratic seems similar when p_T>2 GeV.

With these results, we can say that EPOS seems to have a strong power prediction on Pb-Pb collisions at $\sqrt{s_{NN}}$ =2.76 TeV and 5.02 TeV. Our hydrodynamic model can reproduce (of course not perfectly) the experimental results for both energies about the transverse momenta dependence of the anisotropic flow (more precisely elliptic, triangular and quadratic flows).

Now that we know the transverse momenta dependence of the anisotropic flow:

- anisotropic flow increases until $p_T = 2 \backsim 3$ GeV/c
- after the anisotropic flow decreases when we use two-particle azimuthal correlation $v_2\{2\}$ until $p_T = 7 \backsim 8$ GeV/c
- the v_2 dependence on p_T seems weaker higher than 10 GeV/c
- for higher harmonics, the v_n on p_T seems nonexistent since $p_T = 4 \backsim 5$ GeV
- the anisotropy is smaller at central collisions
- the anisotropy seems higher at mid collisions than central and peripheral ones

I will show the (pseudo)rapidity dependence of the anisotropic flow also for QC and EP methods in the next section.

4.1.2.2 Contributions in (pseudo)rapidity

In this section, I show anisotropic flow results of Pb-Pb collisions at $\sqrt{s_{NN}} = 2.76$ TeV calculated by different methods.

[4]Fourth order of the anisotropic flow: v_4

In this reference [239], they calculate different orders of elliptic flow with the EP and QC methods. I separate the EPOS prediction for EP and QC. Like the transverse momenta dependence of anisotropic flow section, I show in same canvas plots for EP and QC later first comparisons between model and experimental data.

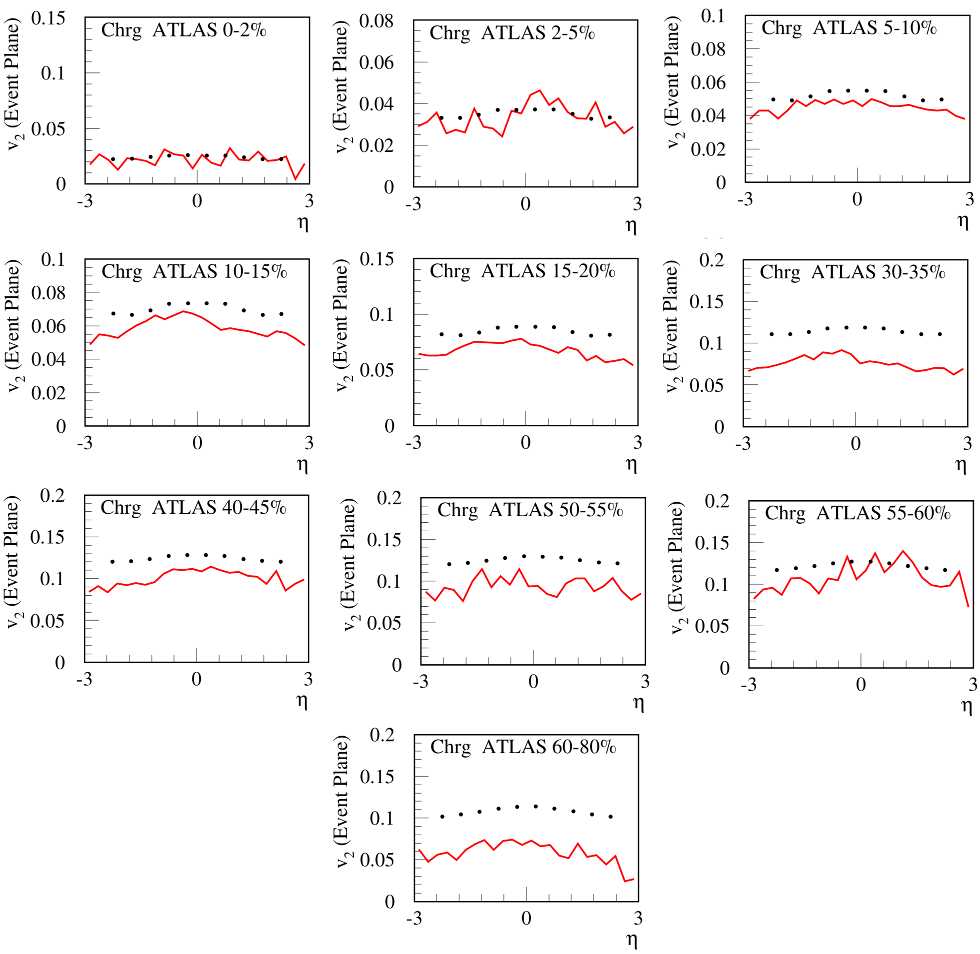

Figure 4.14: Differential flow of charged particles using Event Plane method for Pb-Pb collision at $\sqrt{s_{NN}}$ =2.76 TeV for different centrality collisions.

The anisotropic flow does not depend stronger of the pseudorapidity in the analysis of ATLAS. This is because we take reference particles in the pseudorapidity range of -2.5<η<2.5. We can see that the differential particles have the exact same pseudorapidity range: -2.5<η<2.5. The difference between the two types of particles comes from the accepted transverse momentum of each type of particle, 0.5< p_T<5 (GeV) for reference particles and 0.5< p_T<20 GeV for differential one.

We can see that EPOS cannot reproduce exactly the experimental data for all centralities. Generally EPOS predicts less anisotropic flow at each pseudorapidity. However, in this analysis, the anisotropic flow depends weaker of pseudorapidity experimentally and theoretically than the previous analysis. This observation gives hope for our event generator where we have the same behavior than experimental data.

We can also say that the anisotropic flow is lower for central collision than peripheral collision. This behavior is also respected by EPOS even if it predicts than the anisotropic flow increases slower between the centrality range than experimental data.

Now I show the results from QC method.

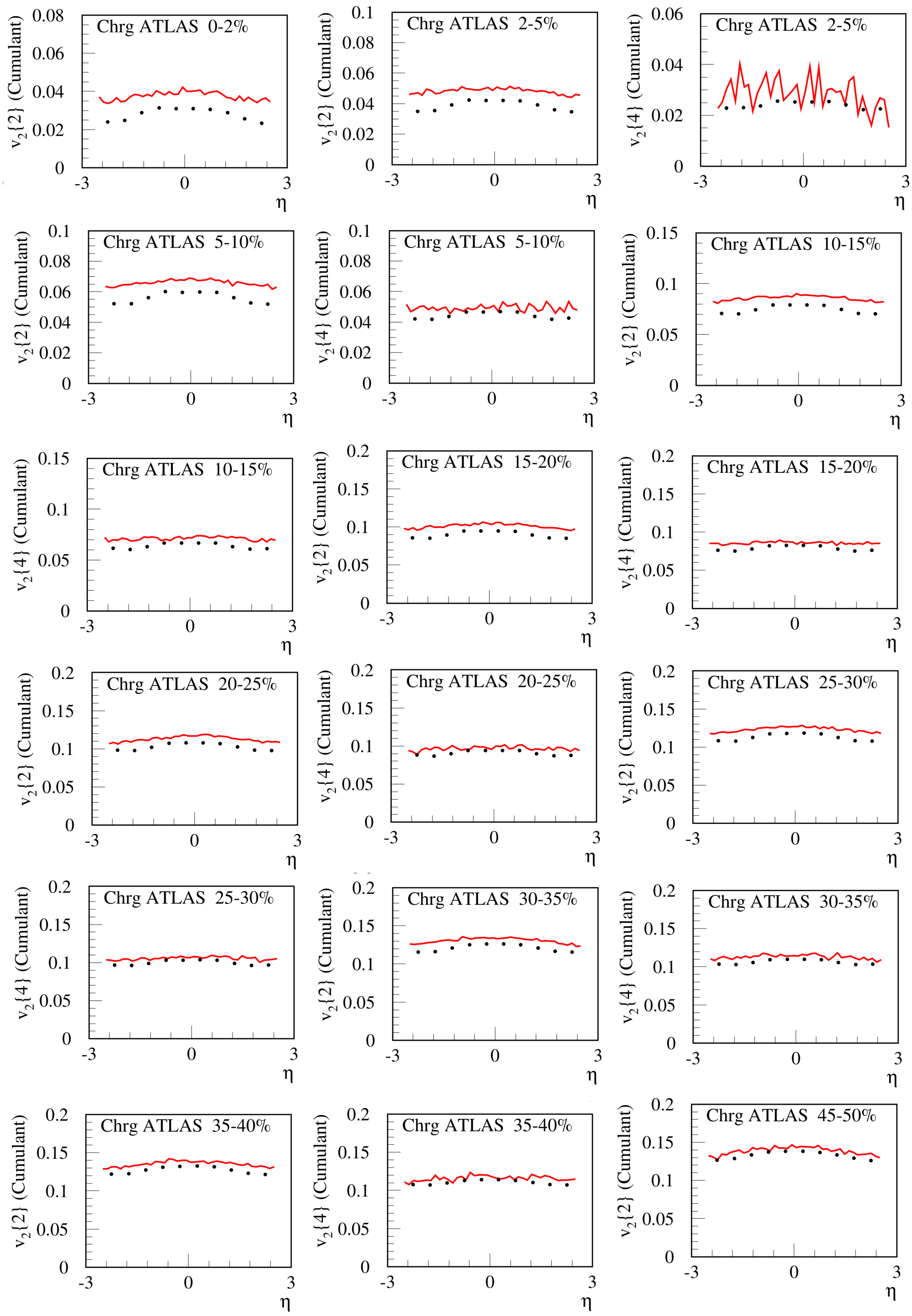

Figure 4.15: Differential flow of charged particles using two or four-particle azimuthal correlation calculated by Q Cumulant method for Pb-Pb collision at the energy collision of $\sqrt{s_{NN}}$ =2.76 TeV for different centrality collisions.

I separate the QC results in two pages for a better readibility.

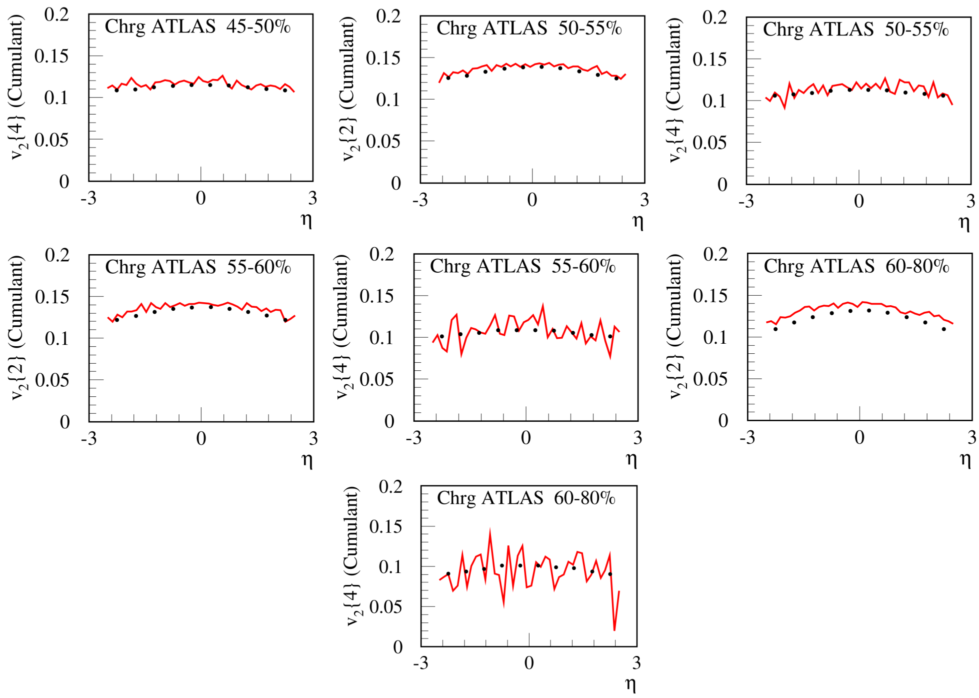

Figure 4.16: Differential flow of charged particles using two or four-particle azimuthal correlation calculated by Q Cumulant method for Pb-Pb collision at the energy collision of $\sqrt{s_{NN}}$ =2.76 TeV for different centrality collisions.

We see that EPOS has the same behavior than experimental data, like results with EP method. However, in contrary to EP results, EPOS overestimates the elliptic flow at central collisions. The model seems to reproduce the data from mid centrality expecially using four-particle azimuthal correlation.

The elliptic flow depends also weakly with cumulants like EP method. It is also higher for peripheral centrality than the central one. An important characteristics is that we have the most of elliptic flow at mid centrality.

For this analysis, we can say that EPOS can reproduce the experimental results with the QC method. I will now compare the results between EP and QC methods to see if we can remark some differences.

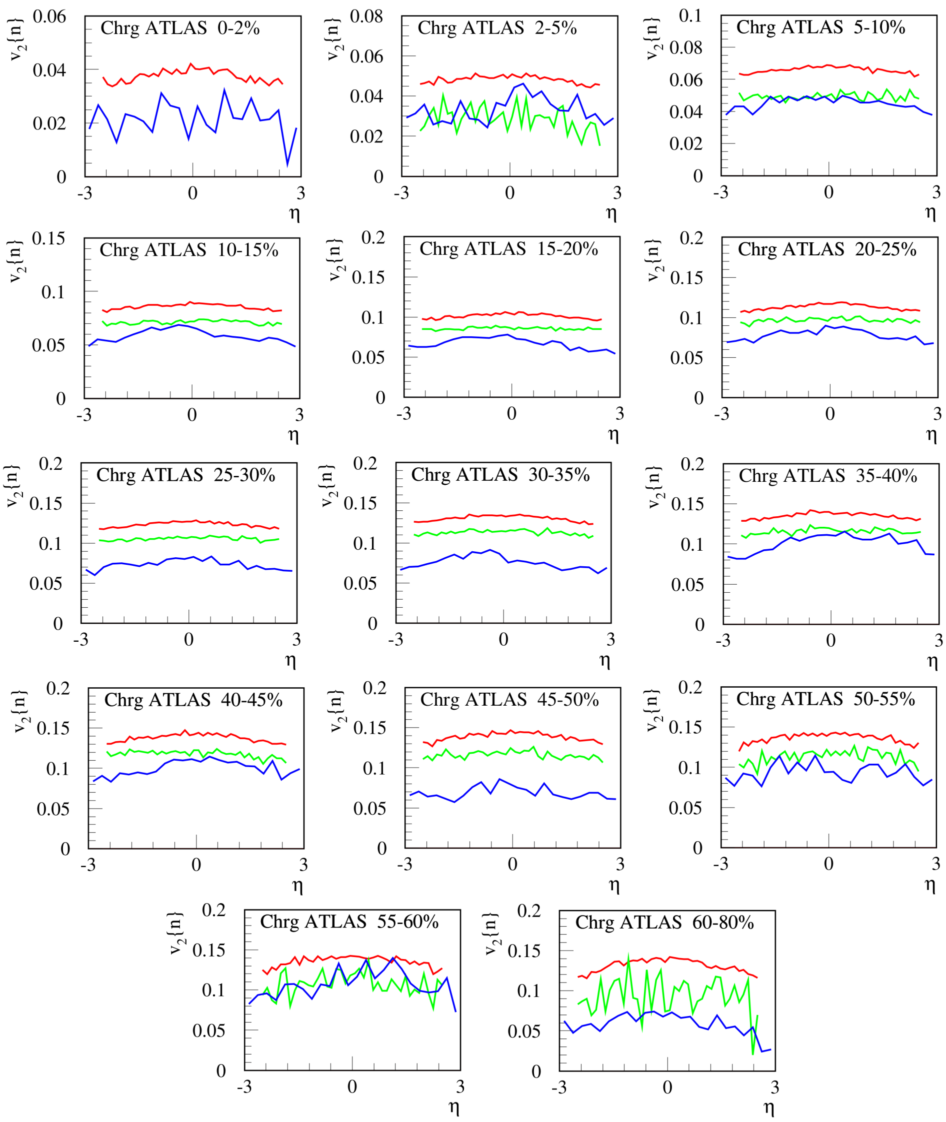

Figure 4.17: Differential flow of charged particles using two (red) or four-particle (green) azimuthal correlation calculated by Q Cumulant (red, green) and Event Plane (blue) methods for Pb-Pb collision at $\sqrt{s_{NN}}$ =2.76 TeV for different centrality collisions.

We see that event plane v_2 (blue) is smaller than $v_2\{2\}$ (red) for all centrality ranges. We can also say that v_2(EP) is smaller than $v_2\{4\}$ (green) for almost all centrality ranges. This is due from the separation between the two phase spaces used to calculate the elliptic flow. This is the **eta-gap method** where we calculate the elliptic flow for particles with the pseudorapidity range equals to: -4.9<η<-3.2 or 3.2<η<4.9. This method creates a separation between the phase-space region where the event plane angle is determined (3.2<$|\eta|$<4.9) and the phase space where charged-particle momenta are reconstructed ($|\eta| < 2.5$). The difference between $v_2\{4\}$ is closer to v_2(EP) than $v_2\{2\}$, that indicates that the four-particle cumulants efficiently suppress non-flow correlations even if we took reference and interested particles in the same pseudorapidity range ($|\eta| < 2.5$).

The last thing that we can say on theses plot is that we have the same behavior between both methods: the anisotropic flow depends weaker of the pseudorapidity for all centrality ranges.

Now that we know the pseudorapidity dependence of the elliptic flow, I will show the pseudorapidity dependence of higher orders of harmonics using EP and QC methods.

Data from higher haronics come from ATLAS reference [239]. I show results from EPOS for v_3 and v_4 vs pseudorapidity. Because one method used to calculate the triangular and quadratic flows is the QC, I can do a comparison between EPOS data and experimental data not only $v_3\{2\}$ and $v_4\{2\}$ but also for $v_3\{4\}$ and $v_4\{4\}$.

The EPOS predictions for the triangular flow are in the following pictures:

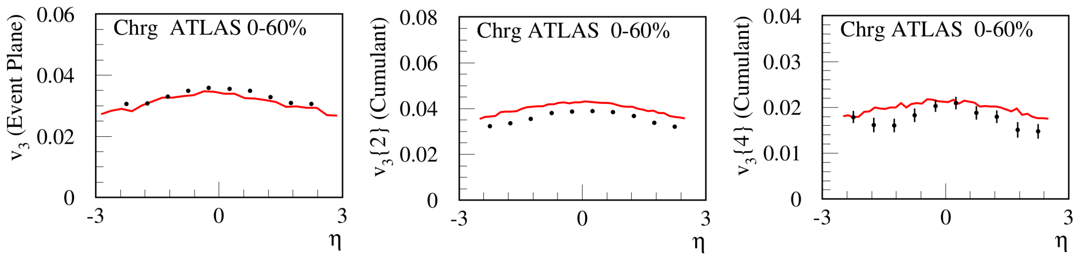

Figure 4.18: Triangular flow of charged particles using two (middle) or four-particle (right) azimuthal correlation calculated by Q Cumulant (middle, right) and Event Plane (left) methods for Pb-Pb collision at $\sqrt{s_{NN}}$ =2.76 TeV.

And we see the strong power prediction of EPOS to calculate the triangular flow of charged particles for EP and QC methods. As the elliptic flow results, EPOS underestimates results for EP method and overestimates results for QC method.

The EPOS predictions for the quadratic flow are in the following pictures:

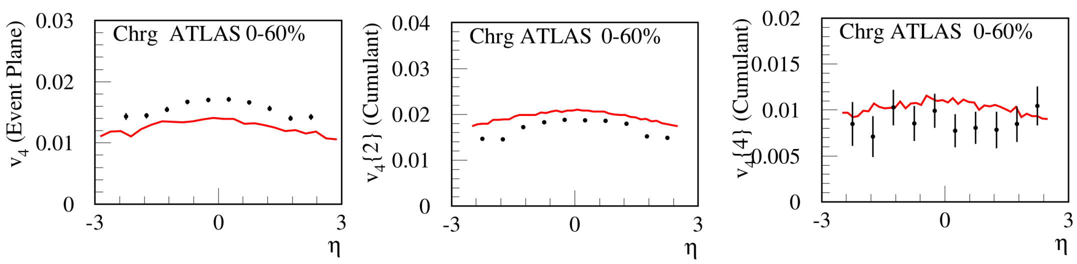

Figure 4.19: Quadratic flow of charged particles using two (middle) or four-particle (right) azimuthal correlation calculated by Q Cumulant (middle, right) and Event Plane (left) methods for Pb-Pb collision at $\sqrt{s_{NN}}$ =2.76 TeV.

We remark the exact same conclusions as triangular flow: EPOS underestimates results for EP method and overestimates results for QC method.

This is the good time to do a comparison between the EPOS results between the two methods. I put in the same canvas the different plots for v_3 and v_4 to have a better readibility.

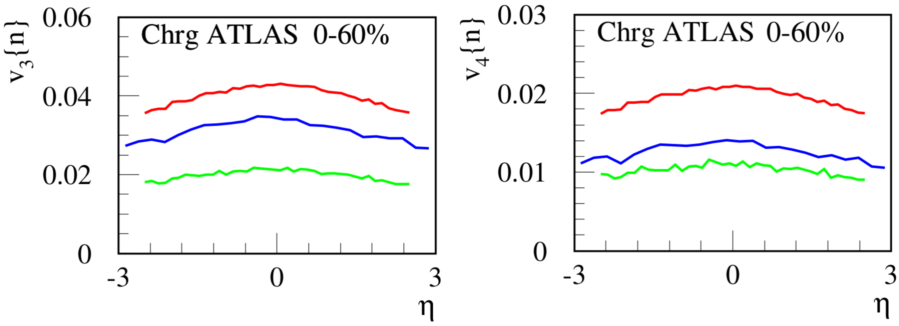

Figure 4.20: Triangular and Quadratic flows of charged particles using two (red) or four-particle (green) azimuthal correlations calculated by Q Cumulant (red, green) and Event Plane (blue) methods for Pb-Pb collision at $\sqrt{s_{NN}}$ =2.76 TeV.

We see that we have the same behavior for Triangular and Quadratic flows: anisotropic flows calculated using two-particle azimuthal correlations are higher than other ones, anisotropic flows calculated using four-particle azimuthal correlations are lower than other ones. The EP can remove some nonflow parts but for this time, QC method seems to remove better nonflow with $v_n\{4\}$.

With these results, we can say that EPOS seems adapted to predict the anisotropic flow observable for all harmonics using two or four-particle azimuthal correlations for Pb-Pb collisions at $\sqrt{s_{NN}}$ =2.76 TeV for all centrality ranges. Our hydrodynamic model can reproduce the experimental results for both EP and QC methods even if this is not perfect.

Consequently, the pseudorapidity dependence for the anisotropic flow is: **anisotropic flow depends weakly of pseudorapidity for all harmonics and for two or four-particle azimuthal correlation orders.** Even if the anisotropic flow depends weakly, we must be careful to not say that it does not depend of the pseudorapidity because we can accentuate this dependence depending of the analysis and different cuts. The anisotropic flow is higher for a pseudorapidity equal to zero, it is what we expected[5]

I will show the multiplicity or centrality dependence of the anisotropic flow using the QC method in the next section. This section will be important because I find some data for all system sizes and I will do a comparison between the anisotropic behavior depending of these system sizes.

4.1.2.3 Contributions in multiplicity/centrality

In this section, I have the opportunity to study the multiplicity dependence of the anisotropic flow for different system sizes. The study of the multiplicity dependence is equivalent to the centrality dependence. Because I have only data for Pb-Pb at $\sqrt{s_{NN}}$ =5.02 TeV to study the centrality dependence of the anisotropic flow, I start by this one. This is the opportunity to see if EPOS can reproduce as expected the integrated flow for Pb-Pb collisions at this energy. We saw that we can reproduce the differencial flow, it seems natural to reproduce the integrated flow and this is what we will see.

The experimental reference which contains the data is this one [240]. The integrated

[5] $\eta = 0$ gives an angle of 90°in the phase space. We assume a little eccentricity in this angle.

flow is calculated with QC method using two, four, six and eight-particle azimuthal correlations. This is also an opportunity to see if we can reproduce the experimental data for high order of particle azimuthal correlations. We have access to experimental results for Pb-Pb at $\sqrt{s_{NN}}$ =2.76 TeV but I do not represent the data/theory comparison for this energy because we already saw that EPOS can reproduce data at this energy and we have already done the comparison between the two energy collisions of Pb-Pb collisions.

The following pictures represent a comparison between EPOS and ALICE data:

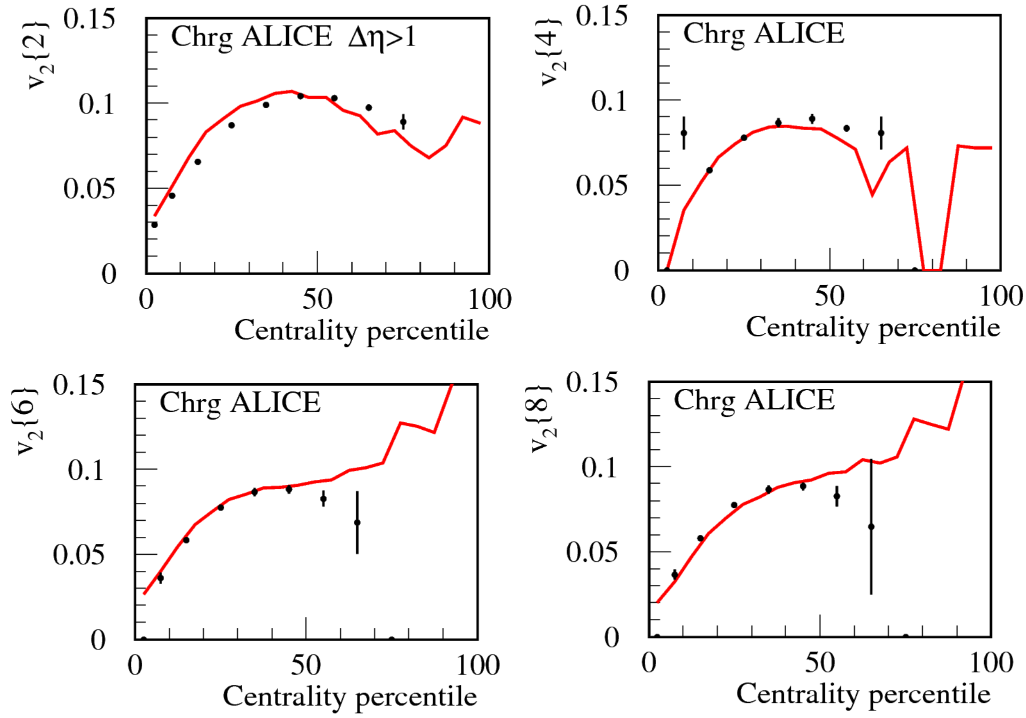

Figure 4.21: Centrality dependence about integrated flow of charged particles using two (above, left), four (above, right), six (below, left) or eight- (below, right) particle (green) azimuthal correlations calculated by Q Cumulant methods for Pb-Pb collision at $\sqrt{s_{NN}}$ =5.02 TeV.

In these plots, the most central collision is where we have 0 % in centrality percentile and the most peripheral collision is where we have 100 % in centrality percentile. We see that we have pretty good agreements between EPOS and ALICE data. The experimental behavior is the same for all particle azimuthal correlation orders: the anisotropic flow increases with the centrality percentile until 50 %. After this value, we can see that the elliptic flow seems to decrease for peripheral collisions.

The main differences between EPOS and ALICE are where the multiplicity is low: at peripheral collisions. EPOS was created for high multiplicity events and it is natural to see that EPOS has more difficulties to reproduce data at low multiplicity. The elliptic flow obtained by the model has the same behavior for two and four-particle azimuthal correlation. We have a little kink at 80 % for $v_2\{4\}$ but this is a problem during the event generation and not EPOS analysis: this is a computational and not a physic problem. However, we do not have the same behavior with peripheral collisions for six and eight-particle azimuthal correlation.

This analysis can already tell us that we will have difficulties to reproduce the integrated flow for pp collisions, because a pp collision is very similar to a peripheral Pb-Pb collision. The conclusion is that **we confirm the strong prediction of EPOS for high multiplicity events but it has difficulties to reproduce data for lower multiplicity.**

The comparison for higher order of anisotropic flow is done in the following pictures:

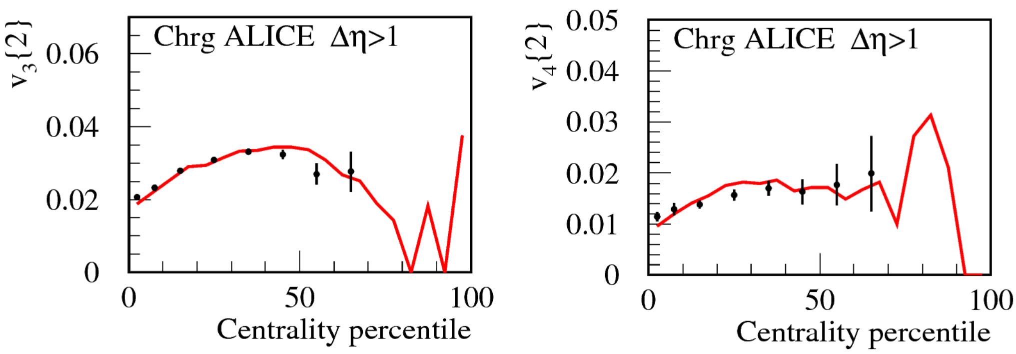

Figure 4.22: Centrality dependence about triangular (left) and quadratic (right) flows of charged particles using two-particle azimuthal correlations calculated by Q Cumulant methods for Pb-Pb collision at $\sqrt{s_{NN}}$ =5.02 TeV.

We have almost the same behavior between the second and third-fourth orders: at central collisions, the anisotropic flow is lower than mid centrality. For the quadratic order, the statistical errors are too large to have a conclusion about the behavior at peripheral collisions. EPOS can reproduce the experimental data until mid centrality. At high centrality, the statistical errors are also too important to have a conclusion about the behavior at peripheral collisions.

Now we can work on the multiplicity dependence of integrated flow for Pb-Pb collisions at $\sqrt{s_{NN}}$ =2.76 TeV found in the ALICE reference [241].

Measurements of multi-particle azimuthal correlations using cumulants for charged particles for p-Pb at $\sqrt{s_{NN}}$ =5.02 TeV and Pb-Pb at $\sqrt{s_{NN}}$ =2.76 TeV are presented in this article.

The pictures are represented in the next page. Something important is the fact that we plot also different orders of reference cumulants to have a direct representation versus the multiplicity.

This is important because the reference cumulants can give us direct information on the correlation: for exemple if $c_2\{4\}$ is negative, that comes from a fluid. We will see if we have a negative $c_2\{4\}$ for the other system size than AA to say if the collectivity comes from fluid or not.

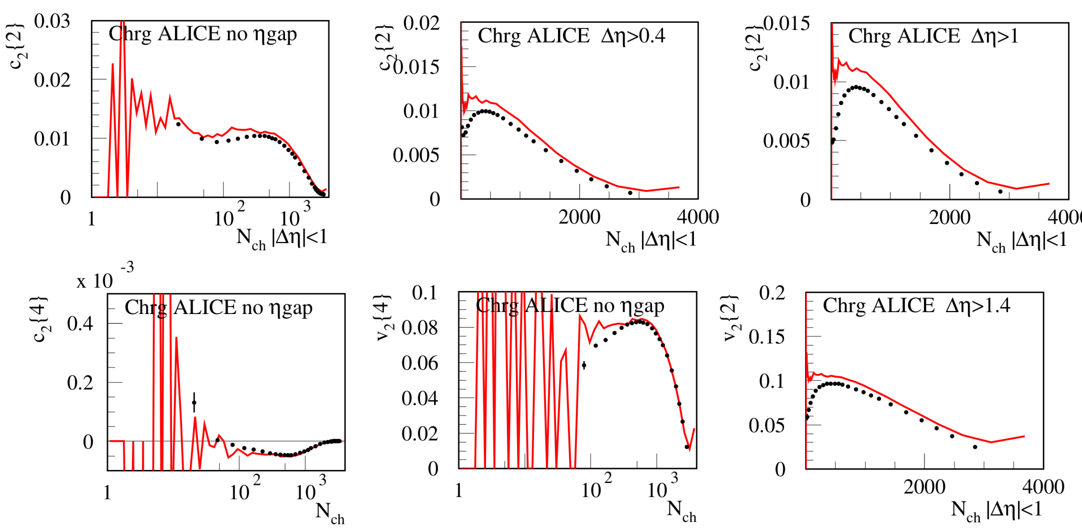

Figure 4.23: Multiplicity dependence about reference cumulants and anisotropic flow of charged particles using two or four-particle azimuthal correlations calculated by Q Cumulant methods for Pb-Pb collision at $\sqrt{s_{NN}}$ =2.76 TeV.

The first thing that we see is that EPOS has more statistical errors at low multiplicity, but this is not a surprise. That seems natural: less multiplicity gives less statistics $\Rightarrow$ more statistical errors.

At high multiplicity, $c_2\{4\}$ is negative for Pb-Pb collision at $\sqrt{s_{NN}}$ =2.76 TeV even for the experimental data and EPOS. This is the expected result: EPOS uses a fluid and can reproduce experimental data for AA collisions at high multiplicity.

In the ALICE reference, they calculate the second order of cumulant with different η gaps to see how we reduce nonflow effects using these gaps. We see that the reference cumulants are less using bigger η gaps.

EPOS can reproduce the data using, or not, an η gap for all orders of reference cumulants and anisotropic flow for very high multiplicity. It seems that our model overestimates results at mid and low multiplicities. It is difficult to have a first conclusion with the too large statistical errors at low multiplicity.

Consequently, we can say that EPOS can reproduce the reference flow at high multiplicity for Pb-Pb collision at $\sqrt{s_{NN}}$ =2.76 TeV as expected. With these results, we can say than our analysis/algorithm is effective to reproduce the reference flow.

This analysis can already tell us that we will have difficulties to reproduce the integrated flow for pp collisions, because a pp collision is very similar to a peripheral Pb-Pb collision, like previous analysis.

Now this is time to see how we can reproduce the same observables for smaller system sizes. The experimental data come from [242] reference.

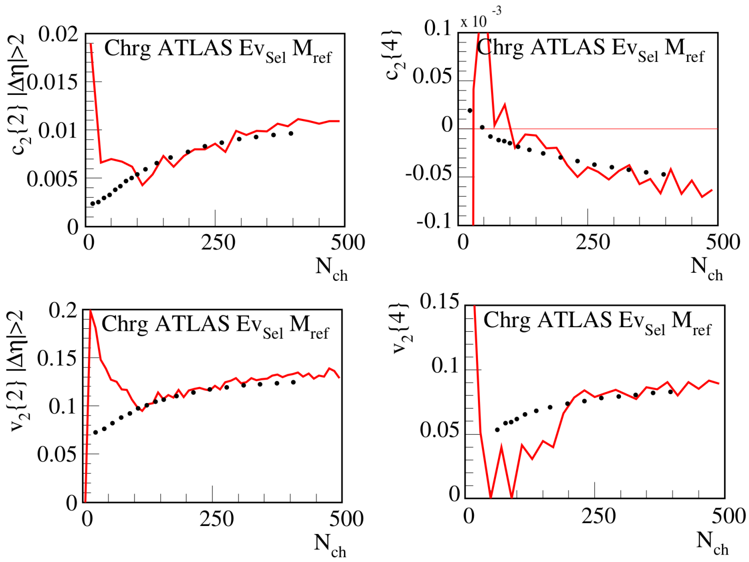

Figure 4.24: Multiplicity dependence about reference cumulants and anisotropic flow of charged particles using two or four-particle azimuthal correlations calculated by Q Cumulant methods for Pb-Pb collision at $\sqrt{s_{NN}}$ =2.76 TeV.

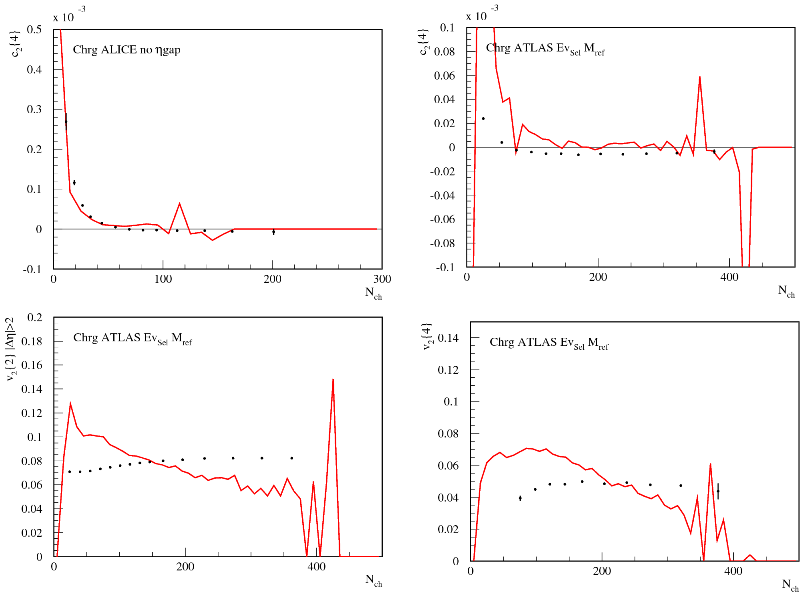

Figure 4.25: Multiplicity dependence about reference cumulants and anisotropic flow of charged particles using two or four-particle azimuthal correlations calculated by Q Cumulant methods for p-Pb collision at $\sqrt{s_{NN}}$ =5.02 TeV.

Starting with the Pb-Pb collisions, we see that we reproduce experimental data at high multiplicity like all previous analysis and this is what we expected. However, EPOS does not reproduce all anisotropic observables at low multiplicity.

For smaller collisions, here p-Pb collisions, EPOS seems to have less difficulties to reproduce experimental data for ALICE [241] and ATLAS [242] results. However, this is important to report that we do not have a negative $c_2\{4\}$. This is directly in conflict with our hydrodynamic model when we use a fluid also to reproduce the experimental data for p-Pb collisions. Concerning the integrated flow directly, we are in contradiction with experimental data where they have a small multiplicity dependence where EPOS predicts a strong multiplicity dependence.

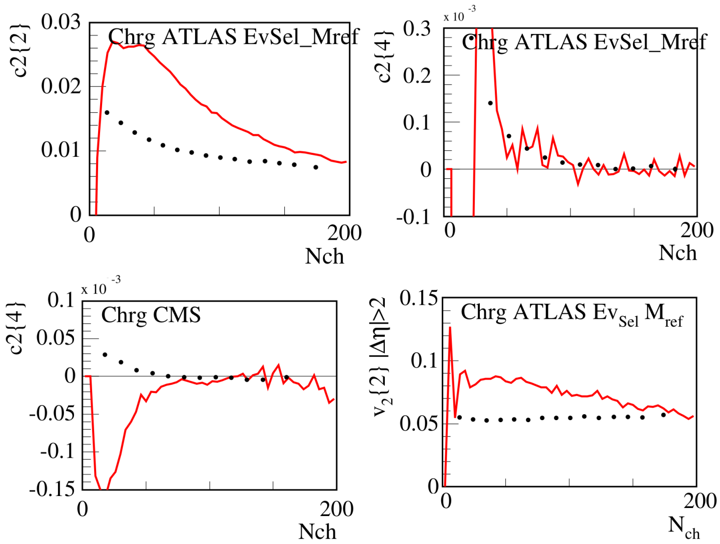

Figure 4.26: Multiplicity dependence about reference cumulants and anisotropic flow of charged particles using two or four-particle azimuthal correlations calculated by Q Cumulant methods for p-p collision at $\sqrt{s_{NN}}$ =13 TeV.

Finally, for pp collisions, we have the same behavior than Pb-p collisions excepted for $c_2\{4\}$ where we have a negative value for all multiplicities. We can assume than EPOS results at low multiplicity are totally wrong but not totally for high multiplicity. That means that EPOS predicts a fluid contribution on collectivity observables, this is coherent with our hydrodynamic model. We have the same conclusion concerning the multiplicity dependence of the integrated flow than Pb-p collisions.

We can conclude on the multiplicity dependence of anisotropic flow:

- the centrality and multiplicity dependence are coherent: we have less elliptic flow at low and high multiplicity than middle one using two or four-particle azimuthal correlations for ALICE data
- ATLAS data give a little dependence on multiplicity for smaller system sizes p-Pb and pp on elliptic flow
- EPOS can reproduce experimental data at very high multiplicity for Pb-Pb collisions
- however it cannot reproduce experimental data for lower multiplicity for all system sizes
- experimental data give a negative $c_2\{4\}$ for all system sizes with enough multiplicity but EPOS predicts a positive value of $c_2\{4\}$ for p-Pb collisions.

I will conclude this part on the system size dependence on the formation of a QGP with preliminary works on the complex observable of symmetric cumulants.

4.1.3 Standard Candles or Symmetric Cumulants

Same as previous section on the integrated flow, I start by the centrality dependence of this new observable. In the ALICE reference paper [243], they report the measurements of correlations between event-by-event fluctuations of amplitudes of anisotropic flow harmonics in Pb-Pb collisions at the center-of-mass energy per nucleon pair of $\sqrt{s_{NN}}$ =2.76 TeV. This is the purpose of the new observable using multiparticle cumulants in mixed harmonics: to measure the correlations between event-by-event fluctuations of amplitudes using different anisotropic flow harmonics.

The experimental data come from [243] of ALICE experiment. The comparison between experimental and theoretical data about the centrality dependence of correlation between event-by-event fluctuations of the elliptic and quadratic flow harmonics, as well as of anti-correlation between elliptic and triangular flow harmonics is presented.

The main analysis was performed with charged particles in the transverse momentum interval $0.2 < p_T < 5.0$ GeV/c and pseudorapidity region $|\eta| < 0.8$. The low p_T cut-off are chosen to reduce event-by-event biases from smaller reconstruction efficiency at lower p_T, while the high p_T cut-off was introduced to reduce the contribution to the anisotropies from jets and see if possible only anisotropies from fluid.

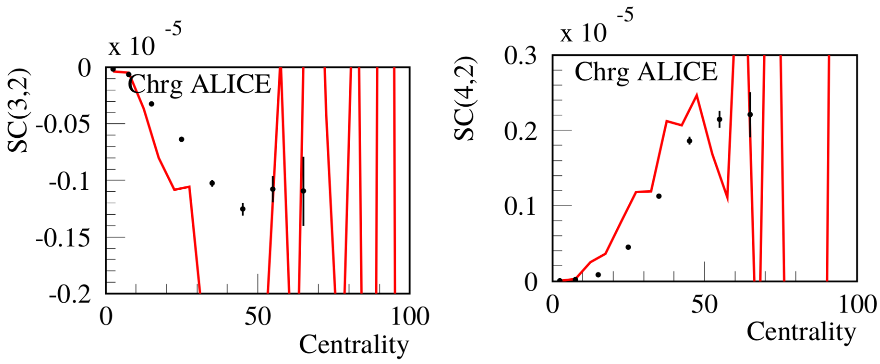

Figure 4.27: Centrality dependence on Symmetric Cumulant for Pb-Pb collision at $\sqrt{s_{NN}}$ =2.76 TeV.

The results suggest a correlation between the event-by-event fluctuations of the elliptic and quadratic flows **(SC(4,2))**, which means that finding v_2 larger than $\langle v_2 \rangle$ in an event enhances the probability to have v_4 larger than $\langle v_4 \rangle$ in this event. SC(4,2) is larger for peripheral collisions.

On the other hand, we have negative value between the event-by-event fluctuations of the elliptic and triangular flows **(SC(3,2))**. This result suggests that finding v_2 larger than $\langle v_2 \rangle$ in an event enhances the probability to have v_3 smaller than $\langle v_3 \rangle$ in this event. SC(3,2) seems larger negative at peripheral collisions but the statistical errors are too big to have a realistic conclusion.

We see that our model can reproduce the data qualitatively but not quantitatively. We have the same behavior about the centrality dependence, however we do not reproduce good quantitative value. For peripheral collisions, we need more statistics to have a conclusion.

We conclude by the fact: **EPOS seems to reproduce qualitatively the centrality dependence of symmetric cumulants observable for Pb-Pb collisions at $\sqrt{s_{NN}}$ =2.76 TeV**. This collision plays once again the role to check our analysis. This is because EPOS have been created to work on this collision and it provides already a lot of important results for Pb-Pb collisions at $\sqrt{s_{NN}}$ =2.76 TeV.

Now I show a direct comparison of different system sizes about the multiplicity dependence of symmetric cumulants. In CMS reference [244], they report the measurements of correlations between event-by-event fluctuations of amplitudes of anisotropic flow harmonics in Pb-Pb collisions at the center-of-mass energy per nucleon pair of $\sqrt{s_{NN}}$ =2.76 TeV, p-Pb with $\sqrt{s_{NN}}$ =5.02 TeV energy collision and pp with $\sqrt{s_{NN}}$ =13 TeV energy collision.

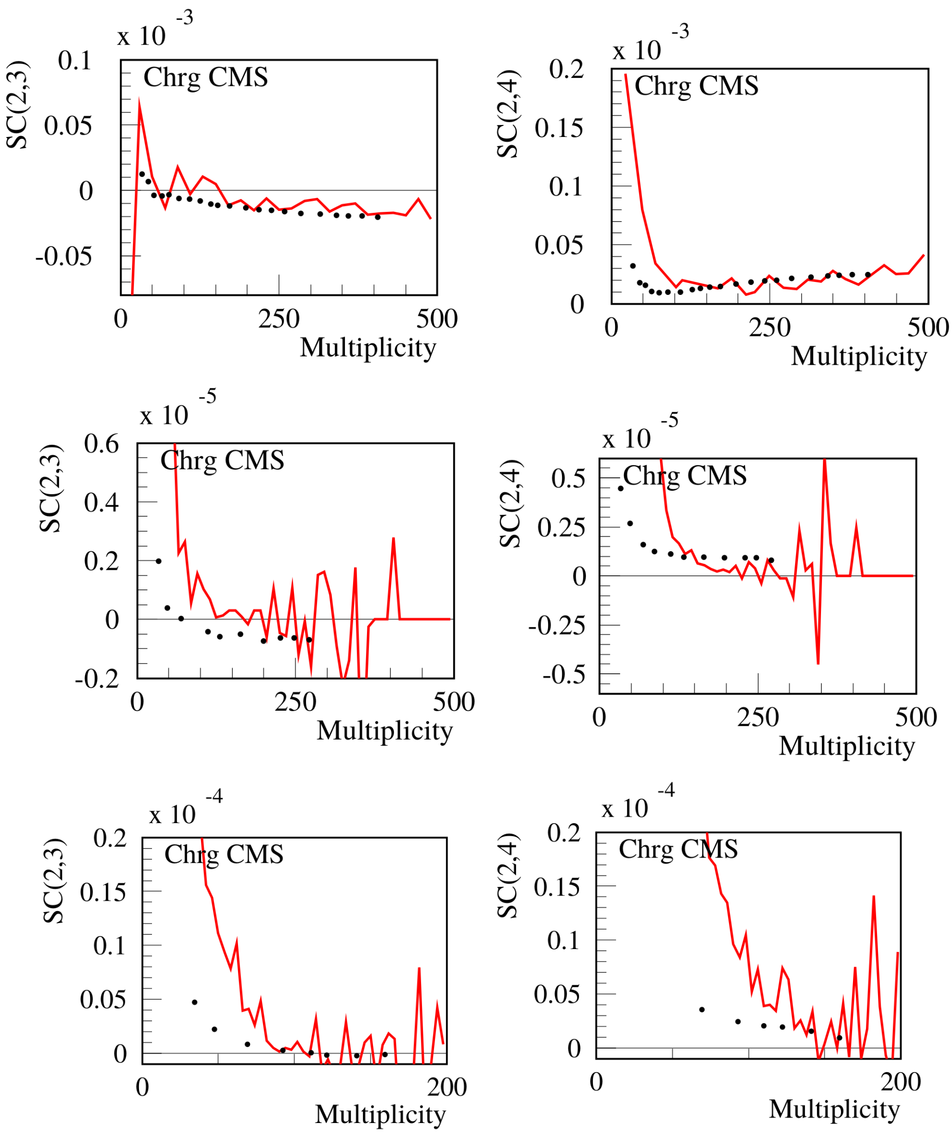

Figure 4.28: Multiplicity dependence on Symmetric Cumulant for Pb-Pb (above) and p-Pb (middle) collisions at $\sqrt{s_{NN}}$ =5.02 TeV and p-p (below) collisions at $\sqrt{s_{NN}}$ =13 TeV

The experimental data come from [244] of CMS experiment. The comparison between experimental and theoretical data about the centrality dependence of correlation between event-by-event fluctuations of the elliptic and quadrangular flow harmonics, as well as of anti-correlation between elliptic and triangular flow harmonics is presented for all system sizes.

Like the ALICE analysis, the main analysis of CMS was performed with charged particles in the transverse momentum interval $0.3 < p_T < 3.0$ GeV/c and pseudorapidity region $|\eta| < 2.4$. The reasons of these cuts are the same: the low p_T cut-off are chosen to reduce event-by-event biases from smaller reconstruction efficiency at lower p_T and the high p_T cut-off was introduced to reduce the contribution to the anisotropies from jets and see if possible only anisotropies from fluid.

For Pb-Pb collisions, the results suggest a correlation between the event-by-event fluctuations of the elliptic and quadratic flows **(SC(4,2))**, which means that finding v_2 larger than $\langle v_2 \rangle$ in an event enhances the probability to have v_4 larger than $\langle v_4 \rangle$ in this event. SC(4,2) is larger at small multiplicity for theoretical and experimental data. Even if the theory overestimates strongly SC(4,2) at small multiplicity.

On the other hand, we have negative value between the event-by-event fluctuations of the elliptic and triangular flows **(SC(3,2))** at large multiplicity. This result suggests that finding v_2 larger than $\langle v_2 \rangle$ in an event enhances the probability to have v_3 smaller than $\langle v_3 \rangle$ in this event. SC(3,2) seems larger negative at large multiplicity. The theory follows the data except at very low multiplicity where EPOS predicts a strong negative value, however this value can be a statistical error.

We see that our model can reproduce the data qualitatively and also quantitatively at large multiplicity. We have the same behavior about the multiplicity dependence.

For p-Pb collisions, the results suggest a correlation between the event-by-event fluctuations of the elliptic and quadratic flows **(SC(2,4))**, which means that finding v_2 larger than $\langle v_2 \rangle$ in an event enhances the probability to have v_4 larger than $\langle v_4 \rangle$ in this event. SC(2,4) is larger at small multiplicity. Obviously, SC(2,4) is smaller for p-Pb than Pb-Pb collisions. On the other hand, we see that we have the same behavior between the two system sizes. The theory has some difficulties to reproduce quantitatively the experimental data but our model reproduce the behavior.

On the other hand experimentally, we have negative value between the event-by-event fluctuations of the elliptic and triangular flows **(SC(2,3))** at large multiplicity. This result suggests that finding v_2 larger than $\langle v_2 \rangle$ in an event enhances the probability to have v_3 smaller than $\langle v_3 \rangle$ in this event. We have the same behavior and conclusion between SC(2,3) and SC(2,4) for experimental and theoretical data. Excepted about one thing, it is complicated to say if we have a negative value of SC(2,3) because of the statistical errors. We can have a negative value in same probability that we oscillate around zero.

We see that our model can reproduce the data qualitatively but not quantitatively for SC(2,4) but it is too early to conclude for SC(2,3).

For p-p collisions, the results suggest also a correlation between the event-by-event fluctuations of the elliptic and quadratic flows **(SC(2,4))**, which means that finding v_2 larger than $\langle v_2 \rangle$ in an event enhances the probability to have v_4 larger than $\langle v_4 \rangle$ in this event. SC(2,4) is larger at small multiplicity for theoretical and experimental data. Even if the theory overestimates strongly SC(2,4) at small multiplicity. SC(2,4) seems equivalent for p-Pb and pp collisions. We keep a positive value of SC(2,4) when we do not pay attention about statistical errors.

On the other hand, we have negative value between the event-by-event fluctuations of the elliptic and triangular flows **(SC(2,3))** at large multiplicity. This result suggests that finding v_2 larger than $\langle v_2 \rangle$ in an event enhances the probability to have v_3 smaller than $\langle v_3 \rangle$ in this event. Like the EPOS data of p-Pb collisions, we cannot conclude if we have a negative value of SC(2,3) because of statistical errors. We can have a negative value in same probability that we oscillate around zero.

We see that our model can reproduce the data qualitatively and also quantitatively at large multiplicity. We have the same behavior about the multiplicity dependence.

4.1.4 Conclusion

The LHC detectors provide a lot of data that we can examinate to do a synthesis about the system size dependence about the formation of a QGP. Of course, history choices give us a lot of data expecially for Pb-Pb collisions, on the other hand the study of small systems steps up and we will have access to a lot of data also for pp collisions, Quark Matter 2018 is a concrete evidence.

I separate the conclusion in three parts: i) conclusion about the experimental data, ii) conclusion about theoretical production, iii) what is about the system size dependence?

Starting with the Pb-Pb collisions, we can see some differentiation about baryon and meson using SP method: we have more mesons at low p_T and more baryons at high p_T. We observe a centrality and transverse momenta dependence for the anisotropic flow: the flow increases until $p_T \simeq 3-4$ GeV, it increases until $\simeq 50\%$, for more peripheral collision, the flow decreases slowly. We observe this characterization for all methods and for all orders n and k in $v_n\{k\}$. We saw also that the elliptic flow depends weaker of the pseudorapidity for all k in $v_2\{k\}$. However, we can see a little stronger elliptic flow at $\eta = 0$. The elliptic flow calculated using four-particle azimuthal correlations removes some nonflow effects as expected.

About the system size dependence, we can look at the last results of this section: multiplicity dependence on collectivity observables. In Pb-Pb collisions, we can see a positive $c_2\{2\}$ and negative $c_2\{4\}$ when multiplicity increases. For the p-Pb collisions, it seems more complicated to observe the same behavior. Depending of the experiment and analysis techniques, we can observe or not a negative $c_2\{4\}$ when multiplicity increases. And this is more complicated in the case of pp collisions where the value of $c_2\{4\}$ is too close of zero to say if it is negative or positive for all detectors. Using more complex and robust observable, the symmetric cumulants. We strongly see that SC(2,3) is negative for Pb-Pb and p-Pb collisions but we have the same problem than reference flow measurements to conclude about a negative value at high multiplicity for pp collisions.

I start the theoretical part by an important fact, in EPOS we create a fluid for all system sizes. This is important and we can see for all basic observables like yields or spectra that the core/fluid contribution is stronger than corona part. That means that not only we have a fluid but also it contributes stronger and it cannot be negligible for all collisions. This is, of course, a typical expectation of a fluid model but I think that it is important to demonstrate it directly.

The theoretical results of EPOS have good agreement for all kinds of observables for Pb-Pb collisions at $\sqrt{s_{NN}}$ =2.76 TeV or $\sqrt{s_{NN}}$ =5.02 TeV. This is not perfect, we have difficulties to reproduce data at high p_T and the statistical errors can hide the truth, for example some jet-matter interaction. However, we reproduce generally the behavior of all spectra and flow using all methods to calculate the anisotropic flow. We observe also, the separation between baryon and meson using SP, the same centrality, transverse momenta, pseudorapidity, multplicity dependence qualitatively.

About the system size dependence, we have some difficulties to conclude directly like experimental results. Of course, we have a positive $c_2\{2\}$ and negative $c_2\{4\}$ when multiplicity increases for Pb-Pb collisions. That means that the different algorithms to calculate the anisotropic flow work. However, we do not follow the experimental data (qualitatively and quantitatively) for smaller system sizes. EPOS seems to have less difficulties to reproduce experimental data at large multiplicity but cannot describe the data at low multiplicity. And we do not see a negative value of $c_2\{4\}$ when multiplicity increases even if we create a fluid during the p-Pb collisions, the value fluctuates aroud zero. On the other hand, we have more realistic results for pp collisions where we create a fluid. We have a strong negative value of $c_2\{4\}$ which is close to experimental data at high multiplicity for the comparison with CMS experiment. For symmetric cumulant, even if we have stronger positive value at low multiplicity of each calculated SC(n,m), we have the same behavior than experiment for SC(2,4). It is complicated to conclude about a negative value of SC(2,3) because our results fluctuate too much around zero.

My conclusion about the system size dependence for the formation of a QGP is that we are sure that we create a QGP for big system sizes. For smaller sizes, it is more complicated. We create a fluid theoretically for each system size, if we have a fluid experimentally, we must find same data, minimally qualitatively, and this is what we find! However, we must take in account all statistical errors and we have only integrated anisotropic observables for smaller system sizes. This is not enough to have a robust conclusion. We only can have assumptions about the probability to have a QGP or not.

The only thing that we can say is that we do not have a zero value of anisotropic flow for p-Pb and pp collisions. We have less ambiguity on the p-Pb collisions because we have a negative value on SC(2,3) for CMS experiment or a negative value of $c_2\{4\}$ when multiplicity increases for ATLAS experiment. On the other hand, we have just something that looks like a fluctuation around zero for collectivity observables which must be negative. The theoretical predictions about pp collisions do not follow directly the data. Generally, EPOS gives a good agreement with experimental data at high multiplicity but not enough to tell that EPOS predicts correctly a fluid for pp collisions.

Now that we see the system size dependence about the formation of a Quark Gluon Plasma, I present the energy dependence about the formation of a QGP using the BES program for experimental support.

4.2 Dependence of Energy

The experimental complex that we use for this analysis is generally the RHIC for its interesting BES program conducted at Brookhaven Narional Laboratory. The main purposes of the BES program are related to the QGP, thus, this is natural that we do the same analysis than BES program. Main goals of this project are to examine the Phase Diagram, to study the characteristics of the first-order phase transition between Hadron Gas and QGP phases of nuclear matter. The search of critical point between different phase transitions is another interesting topic that we do not study with EPOS. RHIC collides beam of Gold with such energies as: $\sqrt{s_{NN}} = 7.7,\ 11.5,\ 14,5\ 19.6,\ 27,\ 39,\ 62.4$ GeV. The variety of these energies provides covering at widest part of Phase Diagram of nuclear matter. The main goal of the BES program is to understand the QCD phase diagram. The BES program tries to look for the evidences of:

- critical point fluctuations
- signals of first-order phase transition
- turn-off the signatures of QGP

Using EPOS, only the third point is analysed. This is the first time that we use EPOS at these energies, consequently this is an interesting challenge to reproduce the experimental data of the new BES program. The question that we can try to answer is the following: **Do we have a QGP for all energies of the BES program?**

To answer this question, we use EPOS which is an hydrodynamic event generator where we can create a fluid for all energies between 7.7 and 64 GeV. If we have a good agreement between EPOS and BES data, that means that the hydrodynamic point of view for little AA collision energy is supported.

In this section, I compare with few observables the differences and similarities between little and high energies. I start by the basic observables to see what is the core (fluid) contribution to the particle production.

4.2.1 Basic Observables

Like the system size dependence's section, I start by basic observables because I think it is better to know how an event generator works for basic observables like different spectra before comparing the theory with the data on complex observable like anisotropic flow. The theoretical model has more credit if it can already reproduce the different spectra for all studied energies.

Spectra of particles

Transverse momenta spectra

The p_t spectra allow us to know the distribution of particles following their transverse momentum. We will see if the core contribution is important for all energies in the next page. This is also a starting point to compare the theoretical results with experimental data. In the same way as the system size dependence's section, I want to check if the core contribution is important for all energies. I start by plotting the p_t spectra of charged (anti)particles π, K and p like the system size dependence's section.

The experimental data come from the analysis in this reference [245].

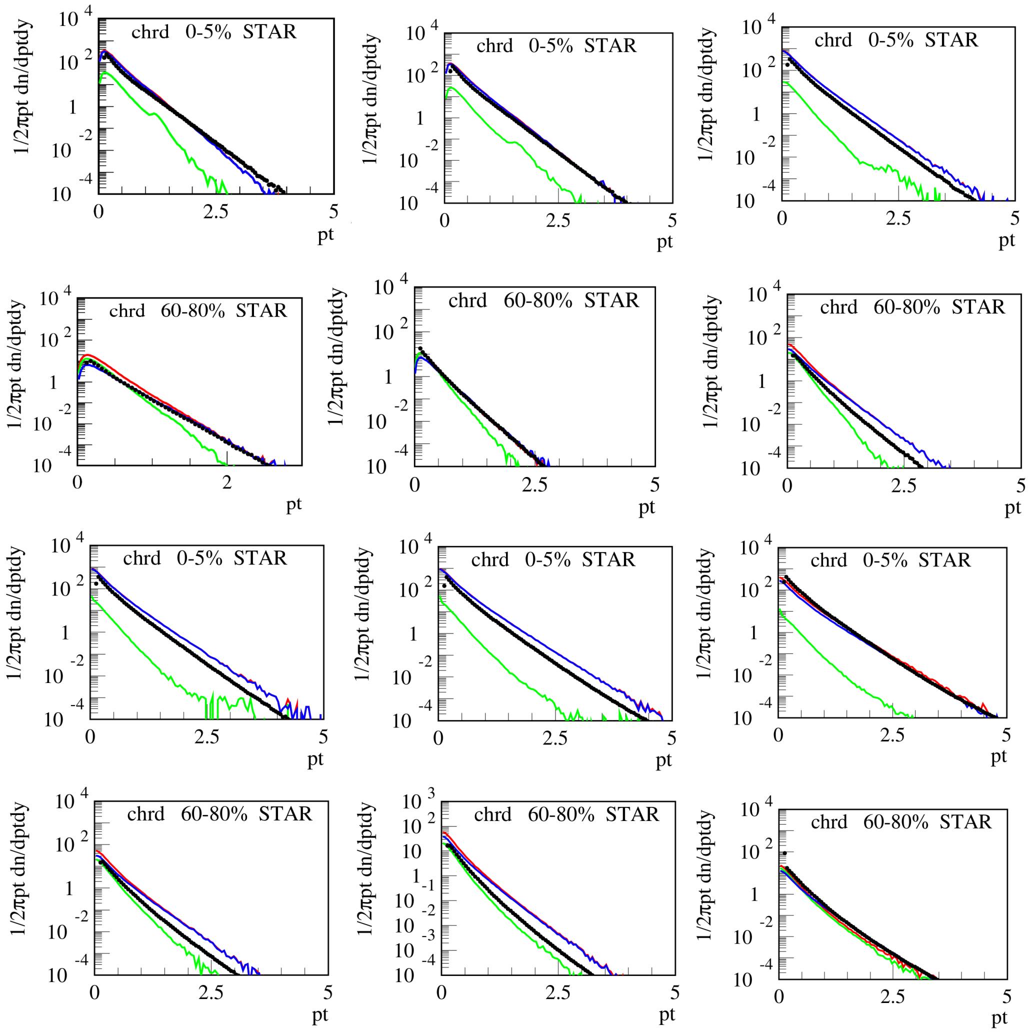

Figure 4.29: Transverse momentum spectra of charged particles for Gold-Gold collisions at different energies: (above) $\sqrt{s_{NN}}$ =7.7 (left) 11.5 (middle) 19.6 (right) for central and peripheral collisions. (below) $\sqrt{s_{NN}}$ =27 (left) 39 (middle) 62.4 (right) for central and peripheral collisions. The core part is plotted in blue and corona part is plotted in green.

If we start by the theoretical observations: we see that we produce a fluid even at $\sqrt{s_{NN}}$ =7.7 GeV. We also see that the core part contributes stronger than corona part. However, the corona part is not negligible and contributes strongly for peripheral collisions as expected. We have these behaviors for all energies. Consequently, we do not see any energy dependence for the moment.

For the comparison with the experimental data, we see that we do not reproduce easily the experimental data. We do not have the same shape and we do not have the exact same magnitude. However, we are not too bad if we take in account that we use EPOS for the first time at these energies. Consequently: different works will be done to fix these problems. **In particular about the initial system size and the exact time when we start the core-corona separation procedure**.

Finally, we see that EPOS reproduces experimental data better for the higher energy of BES program: $\sqrt{s_{NN}}$ =62.4 GeV. Now, I want to show which particles can give disagreement with data for the transverse momentum spectra. Consequently, I will plot the transverse momentum spectra for identified charged particles. The experimental data come from [246]:

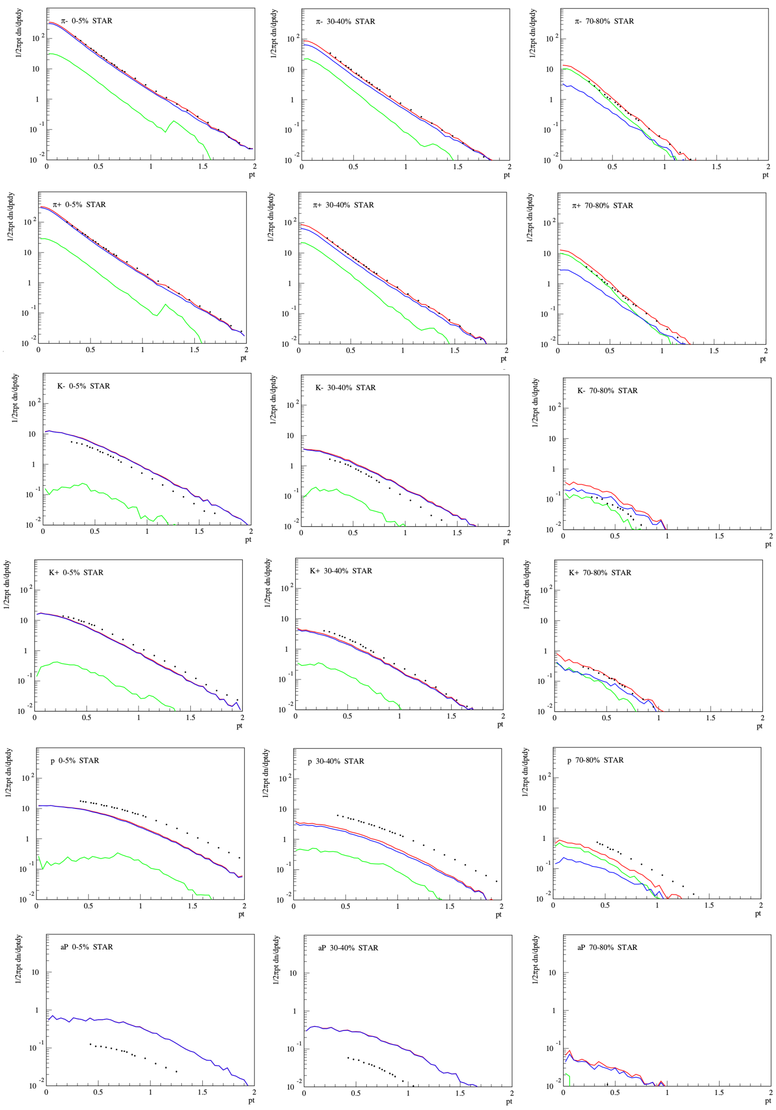

Figure 4.30: Transverse momentum spectra of identified particles for Gold-Gold collisions at $\sqrt{s_{NN}}$ = 7.7 GeV. For each particle, the transverse momentum spectra for central, mid and peripheral collisions are drawn. The core part is plotted in blue and corona part is plotted in green.

Before analyzing the different plots, I show here only the transverse momentum spectra of identified particles for Gold-Gold collisions at $\sqrt{s_{NN}}$ = 7.7 GeV because we have the exact same behavior for each energy between $\sqrt{s_{NN}}$ = 7.7-39 GeV. I will show the transverse momentum spectra of identified particles for Gold-Gold collisions at $\sqrt{s_{NN}}$ = 62.4 GeV later.

I start by the theoretical observations: like the transverse momentum spectra of charged particles (unidentified particles), we see that we produce a fluid for $\sqrt{s_{NN}}$ =7.7

GeV and it contributes strongly about the particle production. We do not see an energy dependence about transverse momentum spectra of particles.

For the comparison with the experimental data, we see that we have a good agreement for π (anti)particles and we almost reproduce the data for Kaons (anti) particles for central, mid and peripheral collisions. We do not have an agreement for protons (anti)particles, EPOS predicts less protons and more antiprotons than experiment. We see that the trend of theoretical prediction is not exactly the same than experimental points. Consequently, we have the same conclusion than before. Different works will be done to fix these problems. **In particular about the initial system size and the exact time when we start the core-corona separation**.

In the next page, I show results of the transverse momentum spectra of identified particles for Gold-Gold collisions at $\sqrt{s_{NN}}$ = 62.4 GeV. Sorry to plot the core and corona part in different colors as usual. I do not have more peripheral collision from the PHOBOS experiment. The experimental data from PHOBOS come from [247].

We see that we can almost reproduce all p_T spectra for all (anti)particles for all different centrality collisions. We see that the core part (in yellow here) contributes stronger than corona part (in blue here) for all centrality collisions. EPOS predicts generally more kaons, protons and pions than experiment.

For more peripheral collisions, we see that corona part contributes stronger than central collisions, this is the expected behavior because we have less multiplicity at peripheral collision. Consequently, the fluid must contribute less for peripheral collision. For the proton (anti)particle, the fluid contributes again strongly because we need more energy to create a more massive particle and this energy comes from the fluid in EPOS.

The trend of EPOS predictions seems much near experimental results at lower energies ($\sqrt{s_{NN}}$ = 7.7-39 GeV). This is because we approach the usual energy used by EPOS with more multiplicity.

Finally, we can see in two pages that EPOS can reproduce at low p_T the experimental data for the summation of particles and antiparticles of kaons, pions and protons[6].

[6] I call in the following, semi-identified particles because we do the summation between particles and antiparticles, consequently this is not totally identified.

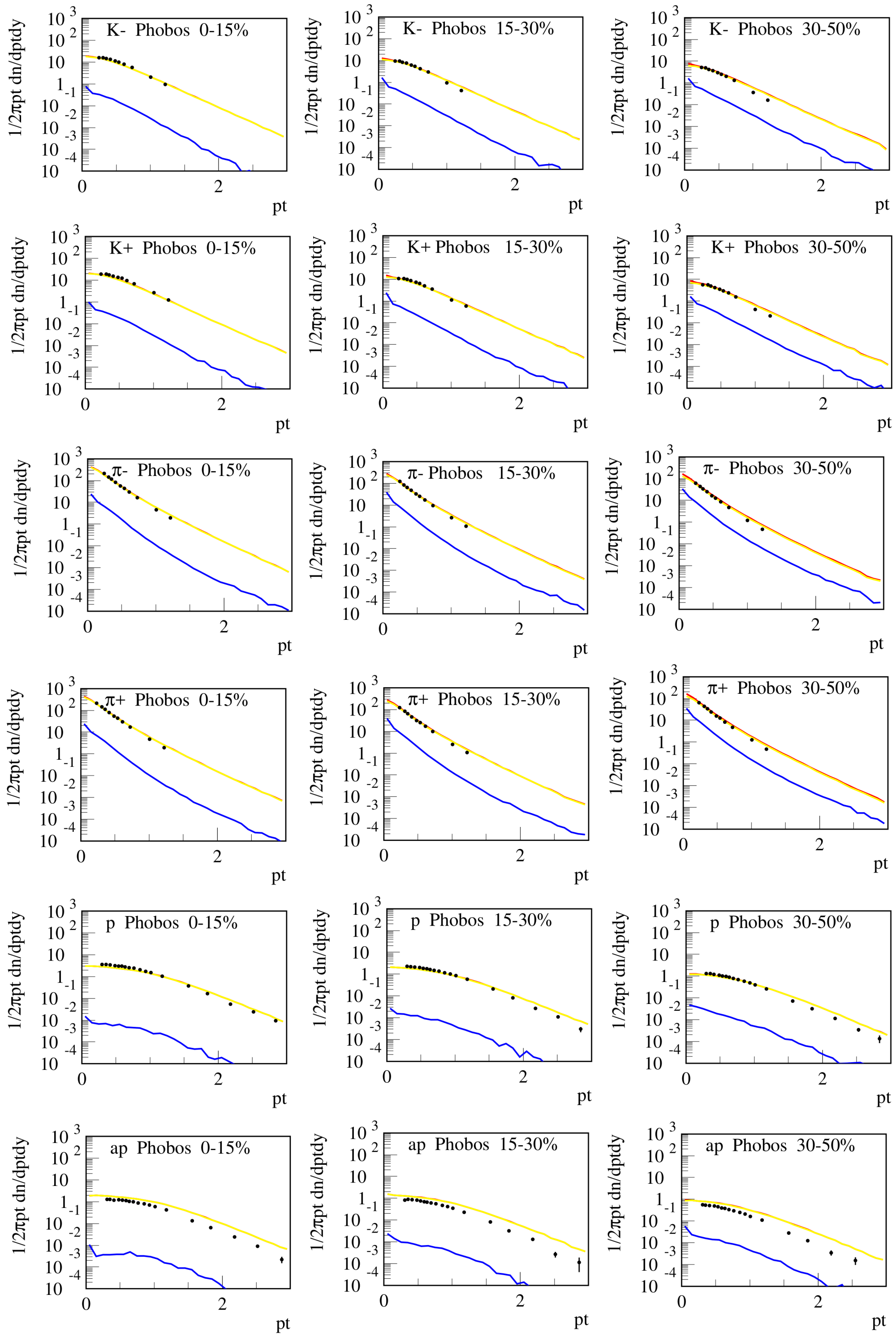

Figure 4.31: Transverse momentum spectra of identified particles for Gold-Gold collisions at $\sqrt{s_{NN}}$ = 62.4 GeV. For each particle, the transverse momentum spectra are plotted for different centrality collisions. The core part is plotted in yellow and corona part is plotted in blue.

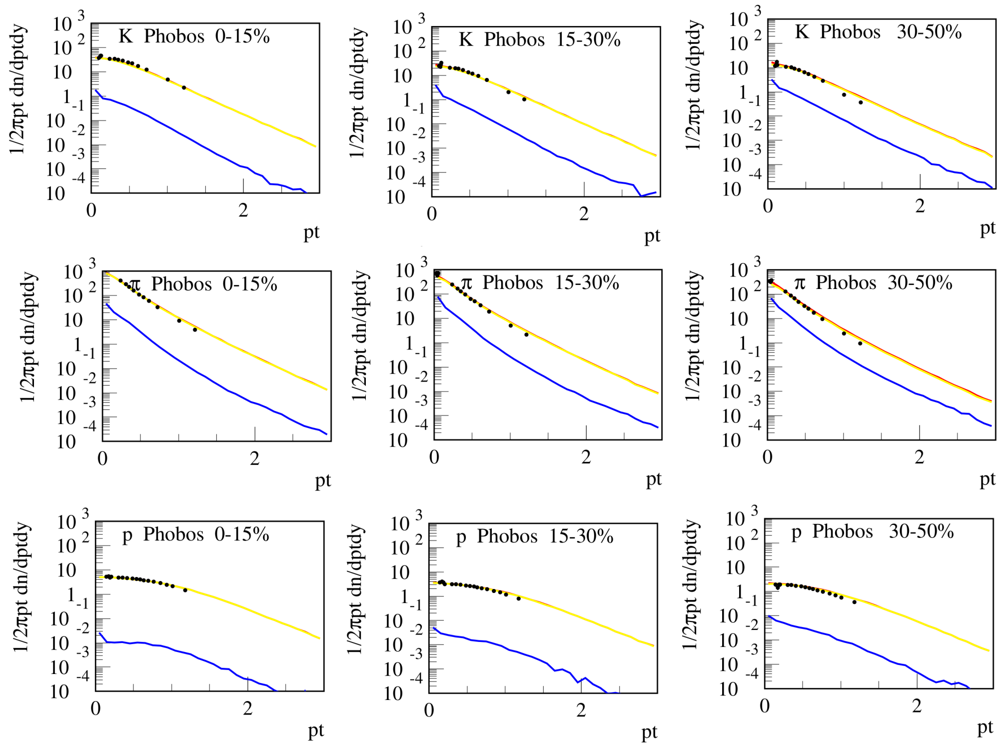

Figure 4.32: Transverse momentum spectra of semi-identified particles for Gold-Gold collisions at $\sqrt{s_{NN}} = 62.4$ GeV. For each particle, the transverse momentum spectra are plotted for different centrality collisions. The core part is plotted in yellow and corona part is plotted in blue.

For the moment, we do not see an energy dependence about the production of particles. To lighten the Ph.D thesis, I will not show the rapidity and pseudorapidity spectra because we see the exact same conclusion and I do not have data for all energies of BES. EPOS reproduces the same magnitude of particles qualitatively but not quantitatively for pseudorapidity spectra. I show an example here:

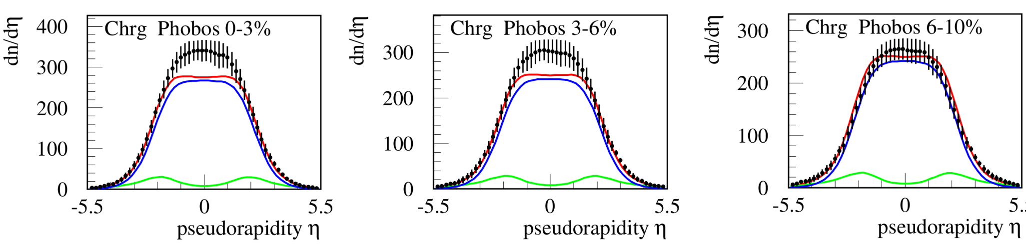

Figure 4.33: Pseudorapidity spectra of semi-identified particles for Gold-Gold collisions at $\sqrt{s_{NN}} = 39$ GeV. For each particle, the transverse momentum spectra are plotted for different centrality collisions. The core part is plotted in blue and corona part is plotted in green.

Even if we do not reproduce exactly the experimental data about different spectra of particle production, we have a strong contribution of fluid part. Consequently, this is legit to work on anisotropic flow observable for these energies. We will see if EPOS can reproduce the different experimental results and see if our hydrodynamic model can be used to predict collectivity results for the BES program.

4.2.2 Anisotropic Flow

Concerning the energy dependence, I have in almost all cases, same numbers of data for all energies. Consequently, we have enough data to correctly work on the energy dependence concerning BES energies. During all this section, I will give simultaneously results for all BES energies to have a complete vision about the anisotropic flow of these collisions.

The experimental results come from the first run of BES program and the analysis will continue when the second run of BES program will be effectuated. The science of energy dependence grows up with the construction and collaboration of Nuclotron-based Ion Collider fAcility (NICA) [248] and Facility for Antiproton and Ion Research (FAIR) [249]. The NICA heavy ion program is to study different ions (from p to Au) by scanning in impact parameter b and energy (in the range from 3 to 11 AGeV) and one of the different topics is the directed and elliptic flows for various hadrons. This task is directly a perspective to this thesis that I will discuss at the end of this chapter.

Like the previous section on the system size dependence, I will separate this section with the contribution of different observables on integrated and differential anisotropic flows.

4.2.2.1 Contributions in transverse momenta

I have access to a lot of experimental data about the transverse momenta dependence of the anisotropic flow and I will not show all results to not surcharge the manuscript.

I start with the transverse momentum dependence of the anisotropic flow calculated with the EP method. The experimental data come from this reference [208].

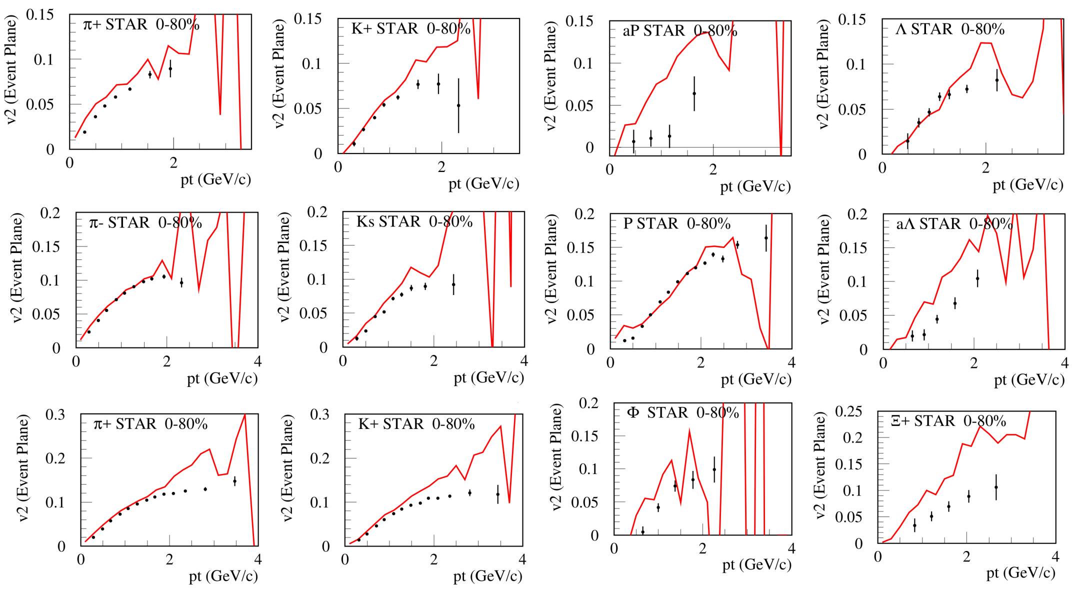

Figure 4.34: Differential flow of charged particles calculated by Event Plane method for Au-Au collision at $\sqrt{s_{NN}}$ =7.7 (above) 11.5 (middle) and 19.6 (below) GeV at minimum bias of STAR. EPOS results are in full line and experimental in dots.

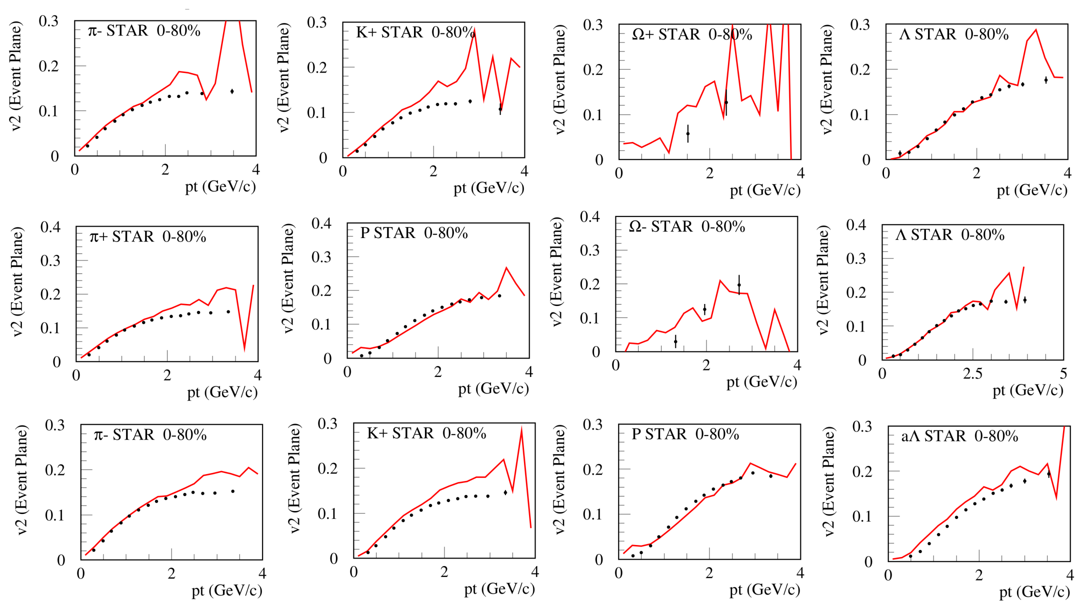

Figure 4.35: Differential flow of charged particles calculated by Event Plane method for Au-Au collision at $\sqrt{s_{NN}}$ =27 (above) 39 (middle) and 62.4 (below) GeV at minimum bias of STAR. EPOS results are in full line and experimental in dots.

Generally, the transverse momentum dependence of the anisotropic flow of baryons is located to the right and the transverse momentum dependence of the anisotropic flow of mesons to the left. The EPOS predictions are given using approximately 150 000 events for each energy excepted $\sqrt{s_{NN}} = 39$ GeV where we have approximately 800 000 events. We see that at this energy, the precision to reproduce experimental data is better than other energies.

Starting by the theoretical point of view: We see that EPOS can reproduce experimental data for almost all (anti)particles at low p_T. This is an excellent news because we did not expect that we can reproduce the differential flow with the spectra results. **The goal was to reproduce the different experimental data for $p_T < 2$ GeV and this is what we see!**

I show in these figures different particles than pions, kaons, protons to see the power prediction of EPOS for less usual particles. We see that EPOS reproduces better the results of usual particles (π, K and Λ) because we produce much more of these particles thus we have more statistics.

EPOS seems to have more difficulties to reproduce the antiparticles like $\bar{p}$ or $\bar{\Lambda}$[7]. EPOS overestimates generally the transverse momentum of the anisotropic flow for antiparticles. This is the moment to express that EPOS overestimates all differential flows with $p_T > 2$ GeV/c. However, EPOS can reproduce better the experimental data when the number of events increases, the results for Au-Au collisions at $\sqrt{s_{NN}} = 39$ GeV prove it.

[7] called aX for antiparticle X in the different plots

Concerning the experimental point of view, the first thing to see is that we have a non-zero value of anisotropic flow even for Au-Au collisions at $\sqrt{s_{NN}} = 7.7$ GeV.

The second thing is that we see a separation between the baryons (in the right side of the different figures) and the mesons (in the left side of the different figures). The anisotropic flow is higher at high p_T for baryons than mesons. I will plot later different figures containing mesons and baryons simultaneously.

On the other hand, I prefer to show the centrality dependence before reproducing the separation of mesons-baryons. This is a natural following of analysis after the reproduction of different transverse momentum contribution of anisotropic flow at minimum bias collisions to see what is the centrality dependence about this observable. The experimental data come from [209]:

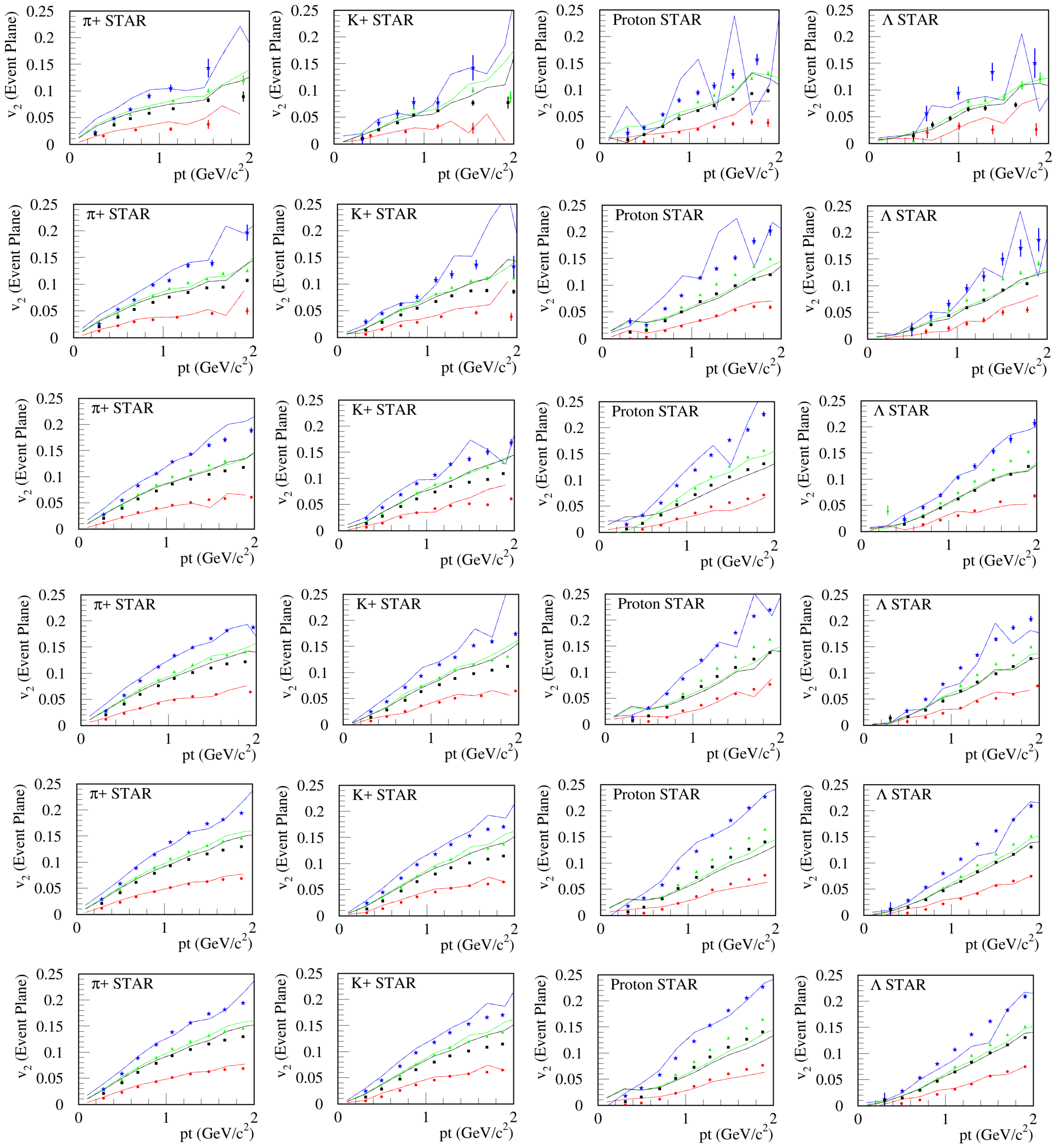

Figure 4.36: Differential flow of charged particles calculated by Event Plane method for Au-Au collision at $\sqrt{s_{NN}}$ =7.7 (above) to 62.4 (below) GeV for different centrality collisions: 0-80% in black, 0-10% in red, 10-40% in blue and 40-80 % in green. EPOS results are in full line and experimental in different types of dots.

We see that EPOS follows the experimental points for all energies at each range of centrality for all particles. The power prediction of EPOS is stronger at high energies. On the other hand, if we look at lower energies, this is also because we need more energies to product heavier particles (baryons), consequently, we have less statistics and a lower power prediction. We see for lighter particles (mesons) that even for $\sqrt{s_{NN}}$ =7.7 and 11.5 GeV, EPOS can reproduce the transverse momentum dependence of elliptic flow for each range of centrality.

The higher elliptic flow is for mid collisions (10-40 %), this is consistent with the system size results of Pb-Pb collisions. We have in both cases a non-zero value of elliptic flow for all values of p_T. We have also in both Pb-Pb and Au-Au cases the lower value of elliptic flow for central collisions.

All results are consistent with that we expected, that means that we see an energy dependence concerning the transverse momentum dependence of the elliptic flow for mesons and baryons: **the elliptic flow increases for baryons and mesons with the energy.** We see also a difference between the elliptic flow of particles and anti-particles. The difference is increasing with decreasing collision energy and is almost identical for all baryons. The difference is larger for baryons than mesons (theoretically and experimentally).

I show the results of the transverse momentum dependence of the anisotropic flow, yet, I show if we can observe the baryons-mesons separation of the elliptic flow at these energies. In other words, we will see if we can observe an elliptic flow dependence with the number of quark-constituent the particle. For this purpose, we do not work with the transverse momentum but with the transverse kinetic energy $m_T - m_0$ variable. This variable using the transverse mass of particles will be better to find some scaling properties on elliptic flow.

I show the different results in the next page, I do not show all results that I have calculated because this is not necessary to understand the message of these plots. The experimental data come from the same STAR reference [209] concerning elliptic flow stuffs for the first run of BES program. Important fact concerning all points of these figures: **I put in red information for protons, green for Λ, blue for π and black for Kaons**.

The first observation is that EPOS can better reproduce the experimental data for higher energies (as expected with the previous results). On the other hand, EPOS reproduces qualitatively the results for lower energies too. Our theoretical model seems to give a separation between baryons and mesons for all energies and each centrality range excepted for Au-Au collisions at $\sqrt{s_{NN}}$ =7.7 GeV. However, the high statistic errors prevent us to have a real conclusion at this collision energy. When we observe a baryons-mesons separation, the elliptic flow of baryons is higher than mesons.

EPOS has also more difficulties to reproduce the experimental results for antiparticles as expected by one observation of the previous results.

For higher collision energies than $\sqrt{s_{NN}}$ =7.7 GeV, we observe that we do not have systematically a baryons-mesons separation for antiparticles before the energy collisions of $\sqrt{s_{NN}}$ =27 GeV. For the particles, we observe a separation between the mesons and baryons since the energy collision of $\sqrt{s_{NN}}$ =7.7 GeV. As expected, the higher elliptic flow is for mid collisions in 10-40 % centrality range.

We observe thus an energy dependence concerning the baryons-mesons separation especially for the antibaryons and antimesons. Except at the lowest beam energies we observe a similar relative v_2 baryon-meson splitting for all centrality classes. The larger v_2 for most particles relative to antiparticles, already observed for minimum bias collisions, shows a clear centrality dependence, with the largest difference for the most central collisions.

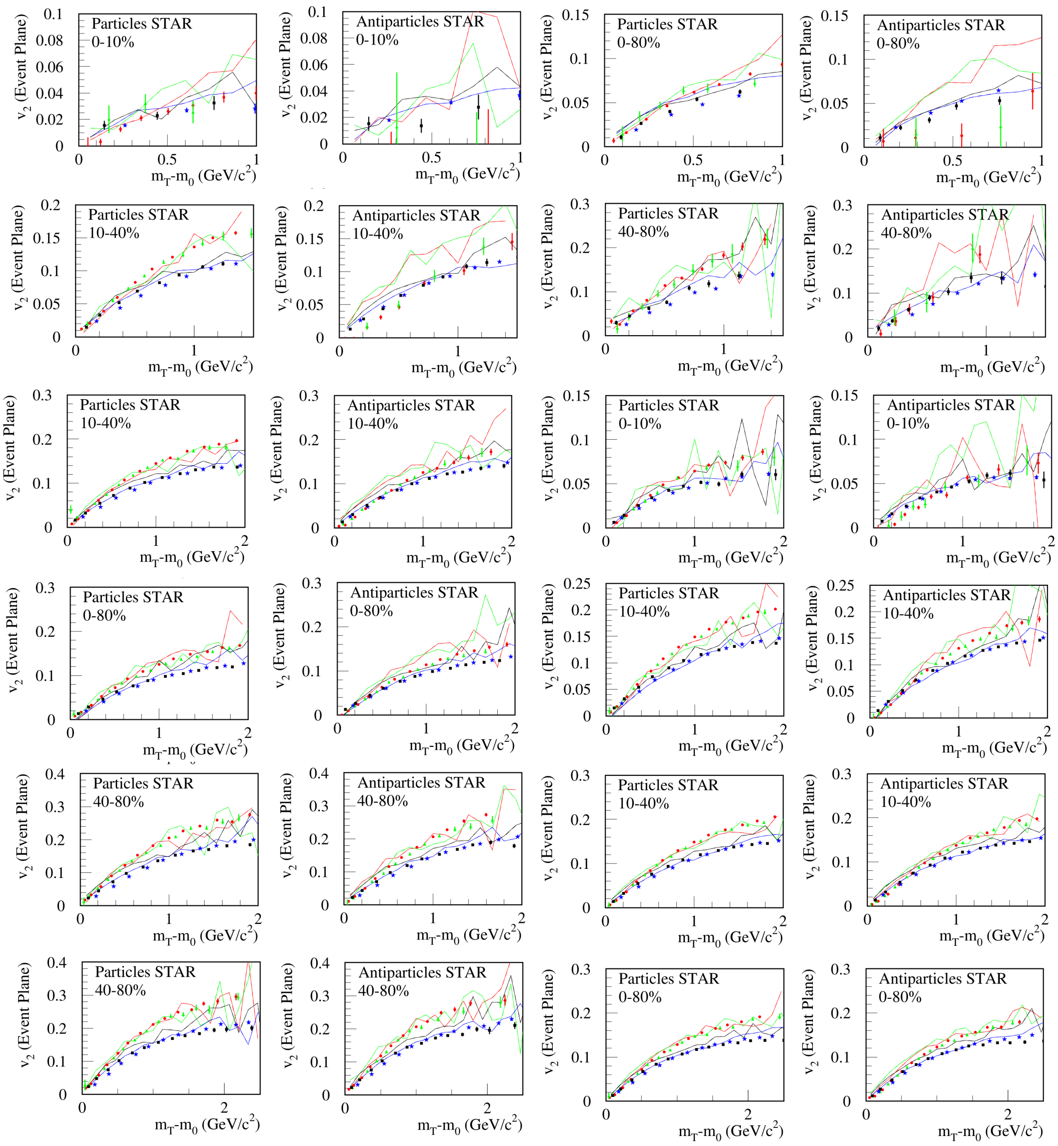

Figure 4.37: Differential flow of (anti)particles calculated by Event Plane method for Au-Au collision at $\sqrt{s_{NN}}$ =7.7 (above) to 62.4 (below) GeV at different centrality ranges. Protons are in red, Lambda in green, Pions in blue and Kaons in black. EPOS results are in full line and experimental in different types of dots.

We saw all that we can see for the first approach of the transverse momentum dependence using the EP method. Fortunately, STAR collaboration gives us also differential flow results using the QC method. I start by the centrality dependence of the two first orders of the elliptic flow using two or four-particle azimuthal correlations for the same energy collisions $\sqrt{s_{NN}}$ =39 GeV. The experimental data come from [250]. This analysis is the reason to have higher events for the energy collisions $\sqrt{s_{NN}}$ =39 GeV, it is better to have a lot of events to reduce the statistical errors using the QC method to calculate the differential flow over the transverse momentum.

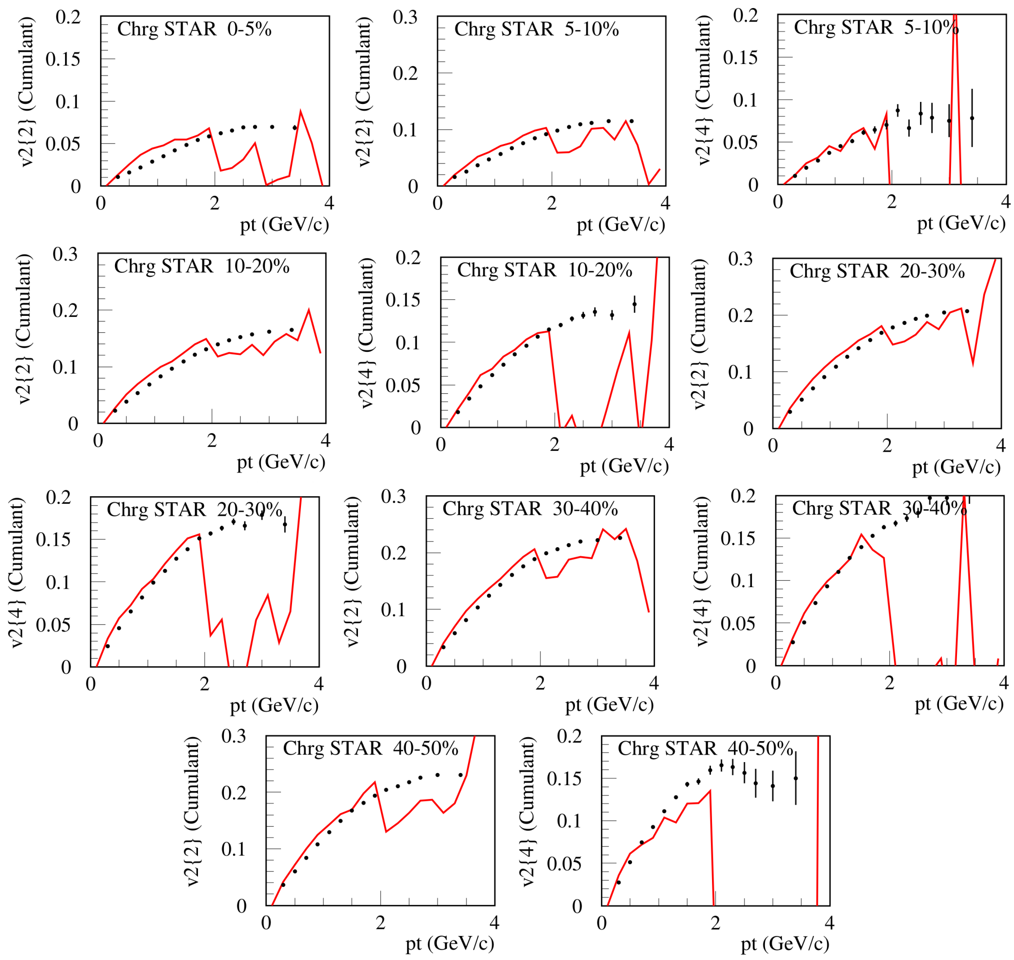

Figure 4.38: Differential flow of charged particles calculated using Q-Cumulant method with two or four-particle azimuthal correlations for Au-Au collision at $\sqrt{s_{NN}}$ =39 GeV at different centrality ranges.

We already did a comparison between the EP and QC methods in the system size dependence sections. Consequently, we assume that we have the same conclusion: the QC method seems to remove more nonflow correlations than the EP method when we use four-particle azimuthal correlations. We did not include the jet interaction with matter, consequently EPOS cannot reproduce data at $p_T > 2$ GeV. However, EPOS reproduces very well the data for $p_T < 2$ GeV for all orders of particle azimuthal correlation. The anisotropic flow increases when the centrality increases, this is the same observations than system size dependence analysis. We cannot conclude for a centrality higher than 40-50 % but we will see in the following of this thesis. The elliptic flow calculated with four-particle azimuthal correlations $v_2\{4\}$ is lower than $v_2\{2\}$, that means that the QC method removes well non-flow effects. EPOS follows the exact same evolution than experiment.

We can now look on the energy dependence about anisotropic flow versus the transverse momentum calculated by QC method.

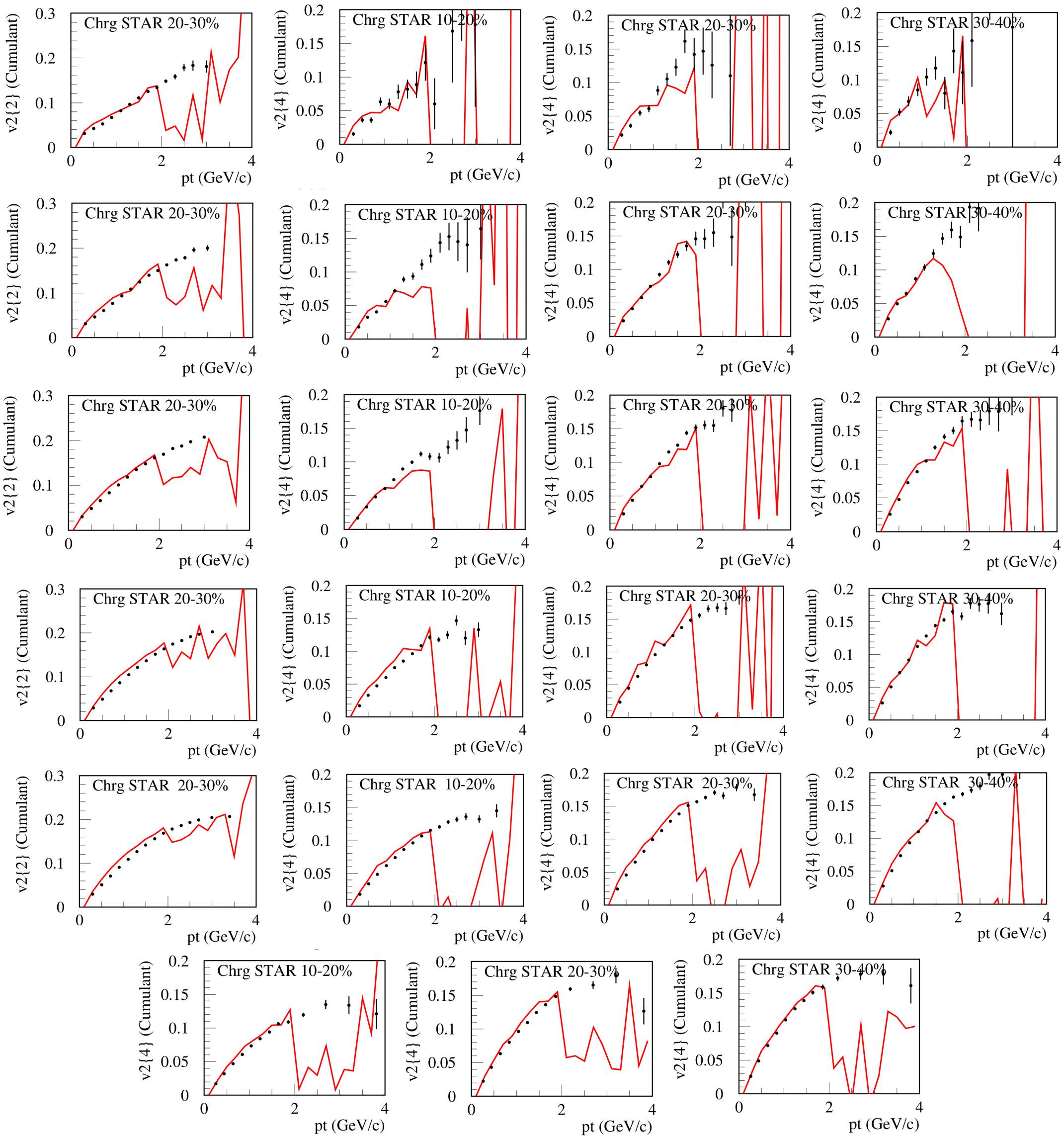

Figure 4.39: Differential flow of charged particles calculated using Q-Cumulant method with two (left) or four-particle (right) azimuthal correlations for Au-Au collision at $\sqrt{s_{NN}}$ =7.7 (above) to 62.4 (bottom) GeV at different centrality ranges.

Without surprise, we see that EPOS cannot reproduce data for $p_T > 2$ GeV and it follows the data for $p_T < 2$ GeV. $v_2\{2\}$ does not seem to evolve with respect to the energy, the $v_2\{2\}$ seems approximately the same and we do not see some different trends: for the moment $v_2\{2\}$ increases with p_T and we can observe a beginning of saturation for high $p_T > 3-4$ GeV. On the other hand, we observe a weak energy dependence for $v_2\{4\}$. We have a lower $v_2\{4\}$ for higher energy since $\sqrt{s_{NN}} = 27$ GeV where we observe the saturation for $p_t > 3$ GeV. However the low experimental statistics of high p_T data for $\sqrt{s_{NN}} < 19$ GeV prohibit a conclusion about the energy dependence. Finally, we observe directly the centrality dependence: $v_2\{4\}$ increases with the centrality for all energies, with experimental and theoretical data.

We observe consistent results between EP and QC:

- the anisotropic flow increases with transverse momentum up to 3 GeV, after we observe a saturation;
- EPOS reproduces the experimental data with $p_T > 2$ GeV for all charged particles and all centrality ranges $\Rightarrow$ Reproduction of the baryon-meson separation;
- the elliptic flow is the most lower at central collisions (0-10 %) and most higher at mid collisions (10-40 %) and seems similar between 40-80 % and 0-80 %

Now, we see the pseudorapidity dependence of the anisotropic flow and if EPOS can reproduce the data or not.

4.2.2.2 Contributions in (pseudo)rapidity

We saw that the pseudorapidity dependence for the elliptic flow is weak at high energies for LHC for each system size. We do the same analysis concerning the possible energy dependence of the elliptic flow versus pseudorapidity. The experimental data come from [250]. The elliptic flow is calculated at 10-40 % to have the most higher possible elliptic flow using centrality range. The comparison between EPOS and the experimental data is in the following Figure:

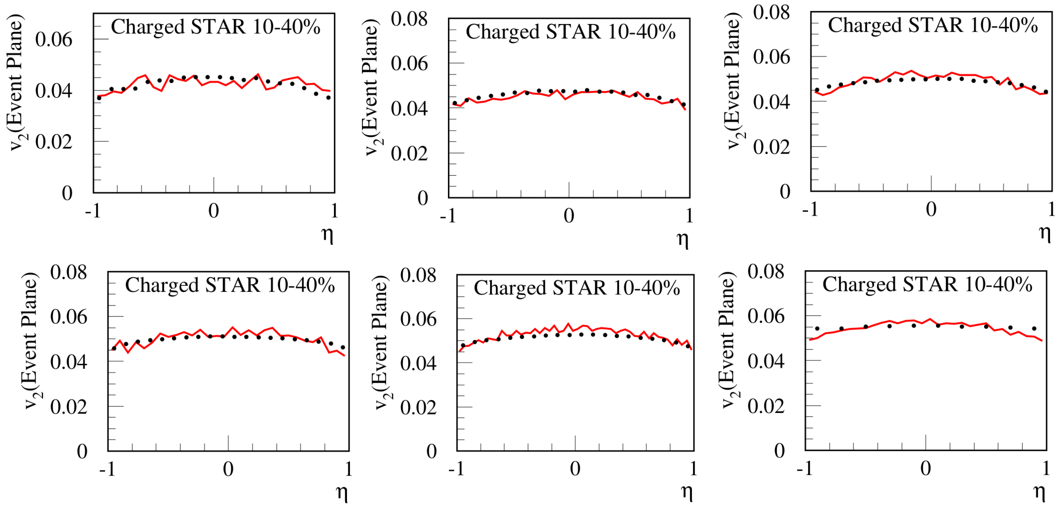

Figure 4.40: Differential flow of charged particles calculated using Event Plane method for Au-Au collision at $\sqrt{s_{NN}}$ =7.7 (above left) to 62.4 (bottom right) GeV at 10-40 % centrality range.

We see that EPOS can reproduce very well the pseudorapidity dependence of the elliptic flow calculated with the EP method. Concerning the pseudorapidity dependence, we see a weak dependence of the elliptic flow. The elliptic flow is higher for $\eta = 0$. We observe the same pseudorapidity dependence than high energies of LHC. We also see a little dependence with the energy: the elliptic flow increases weakly with the energy. However we do not see a drastic changing of the trend of the different elliptic flows increasing the energy: **if we have the same behavior, mustbe we have fluid experimentally for all energies**.

We will conclude the dependence of anisotropic flow by the possible centrality or multiplicity dependence in the next section.

4.2.2.3 Contributions in centrality

We have already seen some parts of the centrality dependence by studying the transverse momentum dependence of the elliptic flow. However we did not have a complete view of the centrality dependence of the elliptic flow and this is what we will do in this section. The experimental data come one more time from STAR [250].

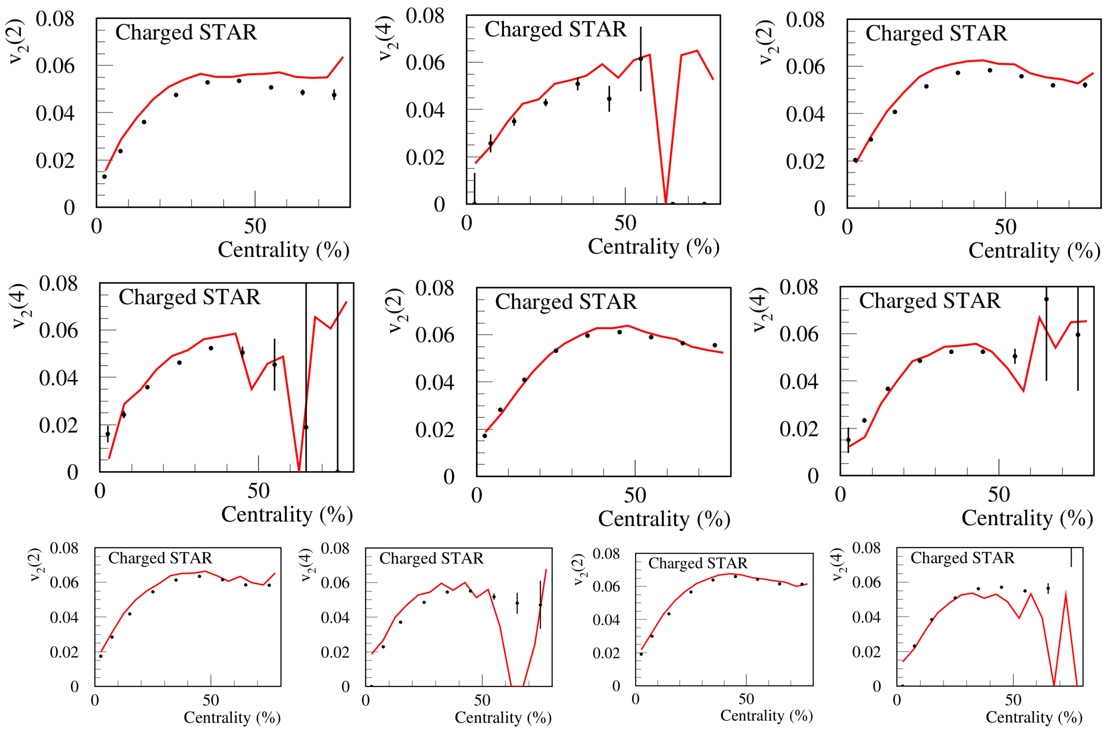

Figure 4.41: Integrated flow of charged particles calculated using Q-cumulant method using two and four-particle azimuthal correlations for Au-Au collision at $\sqrt{s_{NN}}$ =7.7 (above left) to 39 (bottom right) GeV.

In these plots, the most central collision is where we have 0% in centrality percentile and the most peripheral collision is where we have 100 % in centrality percentile. I show the results until 80 % because the experimental data stop to this centrality percentile. Here we see that the most higher elliptic flow is between 40-50 %, this is consistent with the previous results. We see a large centrality dependence of the elliptic flow. EPOS reproduces the experimental data for $v_2\{2\}$ and $v_2\{4\}$ even if we have some kinks at 65 % in centrality percentile. $v_2\{2\}$ and $v_2\{4\}$ seem almost equal for the whole centrality range, but $v_2\{4\}$ is lower than $v_2\{2\}$. EPOS reproduces better the data for high multiplicity events (or central collision) because that is why it was created initially.

The integrated elliptic flow depends weakly with the energy: **the elliptic flow increases slowly with the energy**. On the other hand, we see the same behavior of the elliptic flow for all energies. Consequently, using the hydrodynamical model of EPOS, **we can tell that we have a collectively expanding plasma for all energies**.

4.3 Physical Conclusion

In this section we try to answer this question: **Do we really have a "collectively expanding plasma" in all systems, big (PbPb) and small (pp), at high energies and low energies?** using the third version of the event generator EPOS.

To answer this question, I created a framework directly implemented in EPOS to calculate the collective anisotropic flow observable by different methods versus different integrated or differential variables. This section has also the aim to see the power prediction of EPOS in new range of energies and small system sizes.

I used my framework on big system sizes first to test the veracity of it when EPOS has already proved its efficiency, we saw that the framework works for all elliptic flow dependence. Then, we work on smaller system sizes to work on the system size dependence and try to see if we have a plasma for small system sizes at high energies of LHC run II.

For the system size dependence, we start by the different spectra to know how EPOS can reproduce the "basics" observables and how it can reproduce in a reasonable data/theory ratio, expecially at low p_T and high multiplicity. This observation done, we work on collectivity observable to work on the possible QGP formation at each system size. The free parameters are the same for all system size collisions: we create a fluid and we do not include the jet-matter interaction because the code is not stable enough.

The new EPOS framework was tested in AA collisions to calculated the anisotropic flow in different orders (v_2, v_3, v_4) versus different variables and EPOS reproduces the experimental data as expected. Concerning the system size dependence, EPOS cannot currently reproduce pA and pp data, however we see that the different results of EPOS are closer to experimental data at high multiplicity. Even creating a fluid at pA collisions, we do not find a negative value of $c_2\{4\}$ and this is curious to not find it while we find a strong negative value for pp collisions. We see a system size dependence on the value of the different elliptic flow: v_2 is larger for AA collisions than pA or pp and $c_2\{4\}$ is larger negative for AA collisions. However, $c_2\{4\}$ seems negative also for pp collisions but not significantly to conclude anymore.

We cannot conclude already on the possible existence of a collectively expanding plasma in small system at high energy. However, we see that creating a fluid even at pp, we can be close to experimental data at high multiplicities. In any case, we find a positive value of elliptic flow for charged particles in the different detectors of LHC and EPOS, we can conclude that the pp collisions contains collective characteristics that we will explore!

Concerning the energy dependence, we start also by the different spectra to know how EPOS works on this new range of energies. The free parameters are the same for all energy collisions: we created a fluid and we do not include the jet-matter interaction, an important point is that we work with chemical potential equal to zero. In the following, we will use the new EPOS framework to reproduce easily these results at chemical potential non equal to zero.

Unfortunately, EPOS does not seem to reproduce the basic observable of all Au-Au collisions for all energy collisions of the BES program: $\sqrt{s_{NN}}$ = 7.7, 11.5, 19.6, 27, 39, 62.4 GeV. The trend of spectra is different and the problem comes from the fluid which contributes almost totally to the particle production, the major problem comes when we want produced massive particle like proton. EPOS reproduces the experimental data for higher energy collision $\sqrt{s_{NN}}$ =62.4 GeV. On the other side, we observe the same theoretical behavior for all energies, for the moment we do not see an energy dependence with experimental and theoretical data.

The fluid contributes strongly to produce particle for all energies, this is the starting point to see the different kinematics variables contributions of the collectively anisotropic flow observable. We see that EPOS can reproduce the elliptic flow data creating a flow for each energy since $p_T < 2$ GeV for all centrality ranges. The model can reproduce experimental challenge like the baryons-mesons separations (not for low energy collision $\sqrt{s_{NN}}$ =7.7 GeV) . We see a little energy dependence, the elliptic flow of charged particles increases with the energy. We see also a difference between the elliptic flow of particles and anti-particles. The difference is increasing with decreasing collision energy and is almost identical for all identified baryons. We observe the same centrality dependence than other collisions in the LHC: the elliptic flow is higher at mid collisions (30-50 %) and lower at central collisions (0-20 %). The same behavior is observed for all kinematics variable dependence of the elliptic flow, even using fluid at all energies.

If we observe the same behavior for all energies, that means that we create a fluid for all energies. However we observe different behaviors at $\sqrt{s_{NN}}$ =7.7 and maybe 11.5 GeV where we do not observe exactly the baryon-meson separation for particle and anti-particle. Indeed we observe the baryon-separation with EPOS but not experimentally. If we conclude that we do not create a fluid experimentally for smaller energy collisions, the formation of the QGP is between $\sqrt{s_{NN}}$ =11.5 and 19.6 GeV. Consequently, we will work with the new energy collision of the BES program: $\sqrt{s_{NN}}$ =14.5 GeV to constrain more the possible energy collision to form a QGP.

CHAPTER 5

OUTLOOK AND PERSPECTIVES

In the last decade with the LHC era, large experimental data arise and the different theoretical models work to reproduce all observables of experimental data. The QGP plasma was confirmed using the LHC and its dedicated experiment ALICE produced a lot of data to characterize it. With the era of the LHC or QGP comes the era of hydrodynamic models. The different hydrodynamic models try to reproduce the collectivity observables and most of them manage to reproduce them. EPOS is a hydrodynamic model which tries to reproduce (in the frame of my Ph.D) soft and hard probes of the QGP, I focus on one soft observable: **the anisotropic flow**.

With the LHC era comes the study of its three main collisions: Pb-Pb, p-Pb or Pb-p and pp at different energies. At the beginning, the main collision of interest was the Pb-Pb collision to study the QGP of the production of massive particles, then we produced p-Pb collisions to study the cold nuclear matter, finally the pp collisions were produced to be a reference for the other collisions. However, very recently, some different results of pp collisions disturb the initial plan because the pp show characteristics of heavy ion physics even if the system was normally too small. Consequently, that change our point of view and we will study more the pp collisions in the future.

On the other hand, for lower energies of RHIC, the STAR experiment created the BES program in order to study the phase diagram of QCD using Au-Au collisions at different energies in function of the temperature and the density. The BES has three main goals: i) Can we see evidence of a Critical Point?, ii) Can we see evidence of a phase transition? iii) What is the evolution with $\sqrt{s_{NN}}$ of the medium that we produce?

The physical point of view of my Ph.D Thesis focuses on these two aspects: the study of the system size dependence (using LHC data) or energy dependence (using BES data) to answer this following question:

> **Do we really have a "collectively expanding plasma" in all systems, big (PbPb) and small (pp), at high energies and low energies?**

To perform the analysis on the system and energy dependence, I developed a new framework that can be easily used with EPOS and totally independent of further EPOS's developments. So we do not only got an overview of flow properties based on EPOS3.235

simulations, but for all future developments of EPOS, we may easily redo the analysis based on the tools. This is important, since based on the results of this analysis, there will be substantial updates of the model in particular at low energies and small system sizes. The framework was developed specifically for several methods to calculate the anisotropic flow: Event Plane, Scalar Product, Q-cumulants (each time using or not a gap to reduce non-flow contributions) or to calculate more complex observable: Symmetric Cumulants.

The results of my analysis are the following for the system size dependence:

A collectively expanding plasma is formed for high energy of LHC accelerator for AA collisions. EPOS agrees with almost all experimental data for Pb-Pb collisions at both energy collisions: $\sqrt{s_{NN}} = 2.76$ or 5.02 TeV.
It seems but not guaranteed that an expanding plasma is formed for p-Pb collisions because we do not have a zero value of elliptic flow. We have a negative value on SC(2,3) for CMS experiment or a negative value of $c_2\{4\}$ when multiplicity increases for ATLAS experiment. On the other hand, the different values of $c_2\{4\}$ versus the centrality look like a fluctuation around zero and not clearly a negative value. EPOS agrees with the experimental data when the multiplicity is large enough.
For the pp collisions it is more complicated to conclude. EPOS does not agree with experimental data for ansiotropic flow observable. Generally, EPOS gives a good agreement with experimental data at high multiplicity but not enough to tell that EPOS predicts correctly a fluid for pp collisions.

Concerning the energy dependence about the formation of a Quark Gluon Plasma, the results are the following:

The assumption is that if we observe the same behavior for all energies, that means that we create a fluid for all energies because it is expected to create a fluid at the energy collision of $\sqrt{s_{NN}}$ =62.4 GeV. However, we observe different behavior at $\sqrt{s_{NN}}$ =7.7 and maybe 11.5 GeV where we do not observe the baryon-meson separation for particle and anti-particle. Indeed we observe the baryon-separation with EPOS but not experimentally. If we conclude that we do not create a fluid experimentally for smaller energy collisions, the formation of the QGP is between $\sqrt{s_{NN}}$ =11.5 and 19.6 GeV.

Consequently, we will work with the new energy collision of the BES program: $\sqrt{s_{NN}}$ =14.5 GeV to constrain more the possible energy collision to form a QGP.

The two main goals of the Ph.D are effectuated. For the first goal: I moved forward the release of EPOS by simplifications for users mainly due to the creation of new tools to calculate the anisotropic flow directly using EPOS effectuated at the same time of the event generation and the centralization of all particle characteristics like decay, mass, width decay, charge, identification in the event generator etc... To study the energy and system size dependence, I analyzed anisotropic flow with EPOS for all kinds of systems (pp, AA), energies (LHC, RHIC, BES), and all kinds of flow "probes".

Based on these various flow observables,

- we find for big systems (AA) at RHIC and LHC energies good agreements with the data, which means that our scenario of an hydrodynamical expansion, based on initial conditions from our Gribov-Regge approach, is supported;
- we find also good agreements of flow observables at very high multiplicity in small (pp) systems at LHC energies, but large deviations at low multiplicity, which are not yet fully understood;
- we find for the lowest energies of the BES program pretty good agreements with the data for anisotropic observables but not at simple observable like pt or pseudorapidity spectra.

The perspectives of this work are already established:

- work on the energy collision $\sqrt{s_{NN}}$ =14.5 GeV of the BES program;
- in the BES energies, all the simulations are done using chemical potential equal to zero, this is not consistent with the experimental point of view of BES program, we will redo the analysis using non-zero value of chemical potential;
- we did not include the jet-matter interaction during the event generation, we will include this phenomenum;
- NICA will effectuate new data at lower energies than BES program, that will be a good opportunity to test EPOS at those energies;
- different works will be effectuated concerning the size of initial fluid to solve the problem of anisotropy at small system sizes.

APPENDIX A
BEYOND LHC ENERGIES

We have some ideas on the future colliders that we can construct. The main goal is to go beyond the LHC energies of course and increase the luminosity. I introduce naturally the first project: the High Luminosity Large Hadron Collider .

A.1 High Luminosity Large Hadron Collider

If I follow the article on the physics at the LHC Run-2 and Beyond [251], we will finish the Run 3 of the LHC at the end of the year 2023. We will install during 2 or 3 years some upgrade to increase drastically the luminosity of the LHC for the Run 4 and 5. The integrated luminosity must be 20 times larger than the current luminosity.

But we talk about a big upgrade of the LHC, what can be the future installation of next collider? We have some possibilities with those three participants: the Compact Linear Collider, the International Linear Collider and the Future Circular Collider.

A.2 Compact Linear Collider

The Compact Linear Collider is a future collider between positrons and electrons. We have currently a collaboration of more than 70 institutes from more than 30 countries around the world [252]. The main goal is to collide electrons and positrons at energies up to several TeV. Because these are some collisions between leptons and not hadrons, even if we poss the same order of energy, we will gain different perspectives to explore subatomic physics.

The Compact Linear Collider is not a circular collider as its name suggests but a linear collider. The method to accelerate particles is to use a two-beam concept to produce accelerating fields as high as 100 MeV per meter to reach a nominal total energy of 3 TeV. If you want more details about this possible future experiment, please see the website of the collaboration [252].

A.3 International Linear Collider

The International Linear Collider is the second idea for a future linear collider. The physicists have the same idea to collide electrons and positrons up to 500 GeV and more later at 1 TeV. This collider is 31 km long with two main linear accelarators of 11 km each and a central region of 5 km to place the detector in the beam collider [253].

The International Linear Collider is based on a high radio-frequency (few GHz) superconducting accelerating technology. The host country (to my knowledge) has not been chosen but if we construct this collider, the best proposed location can be Japan.

Because the International Linear Collider and the Compact Linear Collider are both proposals for future colliders with approximatively the same length, these two projects have been unified under the name of the Linear Collider Collaboration [254]. This is the best place to learn more deeply about those two future possible colliders.

A.4 Future Circular Collider

The last idea that I show (of course, we have other possibilities) is the Future Circular Collider. If this collider will be constructed, I am pretty sure that the name will be changed. The idea of the Future Circular Collider is simple but very expensive. We will do the the same thinking than when we constructed the LHC. We want to do the same things than the previous collider (for the LHC, this is the RHIC) but bigger and larger.

The Future Circular Collider will collide also hadrons and nuclei like the LHC but the collider must have approximately between 80 and 100 km in circumference and will reach a nominal energy of 100 TeV for protons collisions [255]. We have currently a collaboration of more than 100 institutes from more than 30 countries around the world.

The main goal of the proposal design is to study hadron collider with a center of mass energy up to 100 TeV for the study of physics at the highest possible energies. The LHC will be another accelerator of the CERN accelerator complex. But the Future Circular Collider could be a lepton collider too with a nominal energy up to 350 GeV. If you want more deeply details about this collider, please look on the website [255].

We have finished with the description of possible future colliders, I think that it is important to explain a little what can be the future of the subatomic physics because that can drive my future life in the physics even if I want to stay in theoretical physics.

A.5 EPOS Interest

Would my subject have an interest to perform this kind of study on these systems? A part of answer is because we do not have a parton structure in initial state of collisions and could we reach enough high energy density in final state?

One can find new discovery about a better control sample to turn on/off collectivity! All future experiments (High Luminosity LHC, CLC, ILC and FCC) could have an interest with EPOS to discuss about the control of collectivity by raising the multiplicity.

APPENDIX B

TOWARDS TO RELEASE OF EPOS

Contents

In this chapter, I will not talk a lot about physics. Indeed, the two main purposes of this Ph.D are:

1. simplify the way and create new tools to use EPOS to moving forward its release;
2. discussed about the possibility to have a "collectively expanding plasma" in all systems, big (PbPb) and small (pp), at high energies and low energies?

The chapter 5 will be dedicated to the second aim of this Ph.D with the discussion of the possibility to create a "collectively expanding plasma" experimentally using EPOS. This chapter is dedicated to the computing part upgrade of EPOS. I will not explain all little upgrades that I had implementate to use easier EPOS like upgrade for memory problem etc .. I will focus on the different towards that can be used and important for the next different upgrades of EPOS.

Concretely, in this chapter, I will show the different upgrades that give life to the most important tool for new users of EPOS. In the first section, I will focus on the first work on the reorganization of particles generated in EPOS to have the opportunity to create more particles with the event generator. This first work allow the possibility to include more particles not set in the event generator. Finally the significant number of particles and characteristics in EPOS give the idea to centralize concretely all particle's characteristics in only one table.

B.1 Towards the release of EPOS

B.1.1 Reorganization of particles

The first big changment implemented in EPOS is the creation of a new way to identify particles. Previously, some particles contain the same identification even if these particles are different. This is not a consistent work and we had to change the method to identify particles to permit the possibility to identify all particles.

We identify each hadrons by its constituants. To be simple the following about the epos identification of quarks is as following:

```
1  2   99   99   99    u
2  1   99   99   99    d
3  3   99   99   99    s
4  4   99   99   99    c
5  5   99   99   99    b
6  6   99   99   99    t
```

In this table, only the first and second columns are important to identify particles for this thesis. If we want identify a particle, for example a proton, we take its constituant: deux up quarks and one down quark. Consequently, we identify the proton by the **112X** code. The last X term is a number to identify high harmonics of uud baryons.

However, X can take only 10 different terms (0 to 9). Consequently, we add the possibility to switch the different number of quark componing to identify the different harmonics of particles. For example, for high resonances of mesons, we have:

```
        129    10215   99    99    99     pi2(1670)+
        212    217     99    99    99     rho3(1690)+
```

We switch, the term used to identify the quark constituant. To have more than 20 possibilities for mesons, we implemente the possibility to have this kind of identification *7XX* without breaking the different flavor constituant the mesons.

B.1.2 Centralization of particle's characteristics

The history of EPOS gives different tables to give the different characteristics of a particle (related to it mass, decay width, charge, etc...) and different table only to create particles:

1. early 90s: limited hadron set only use for string decay in VENUS model
2. 2000: 52 hadrons are used with the droplet decay (kind of first effective plasma version)
3. 2010: using hydrodynamics with an extended hadron set (in addition to the existing one)

All the code related to particle identification are completely restructured and extended to include a "complete" list of hadrons, easy to update in the future, transparent for (future) users and developers.

Now, all the particle characterizations are include in only one table with 14 columns with these properties:

```
!-------------------------------------------
! List of particle properties
!------------------------------------------
! column 1 : id_EPOS
! column 2 : id_PDG
! column 3 : id_QGSJET
! column 4 : id_GHEISHA
! column 5 : id_SIBYLL
! column 6 : Name of the particle
! column 7 : ifl1  !Quark flavors:
! column 8 : ifl2  !Baryons: ifl1,ifl2,ifl3
! column 9 : ifl3  !Mesons: ifl2,ifl3  Quarks: ifl3  Diquarks
    ifl1,ifl2
! columnn 10 : Counter (formely jspin variable)
! column 11 : Mass (in units of GeV/c^2)
! column 12 : Charge (in units of e)
! column 13 : Width (in units of GeV)
! column 14 : Multiplicity variable : 1 wrote particle+anti,
   2 : wrote just the particle
```

B.2 Framework for users to anisotropic flow calculation

We have different possibilities to use EPOS depending of user's interest:

1. just event simulation, output as "events" into root files: for users
2. online analysis, during simulation, with event storing: for developers
3. both

For developers, we have a proper language dedicated to do an analysis with EPOS in same time of the simulation. EPOS input works like a shell, with command lines. Thus we can "predefine" what kind of histogram we want in the end, as EPOS shell script, with very simple commands.

B.2.1 The optns files

This *shell language* is writed in a options files (called optns). We can write all optns include to generate events as following:

```
!-----------------------------------------------------
! example input file    ("!" is comment)
!-----------------------------------------------------
application hadron !hadron-hadron, hadron-nucleus, or nucleus
   -nucleus collision
set laproj 82  !projectile atomic number
set maproj 207 !projectile mass number
set latarg 82  !target atomic number
set matarg 207 !target mass number
set ecms 2760  !sqrt(s)_AA
set istmax 25
set ninicon 1 !number of initial conditions used for hydro
   evolution
set iranphi 1 !for internal use. if iranphi=1 event will be
   rotated such that
              !the impact parameter angle and the (n=2) event
    plane angle
              !(based on string segments) coincide. Particles
    rotated back at the end.
core full hydro x3ff       !hydro activated (to suppress:
   core off hydro x3ffoff)
hacas off                  !hadronic cascade not activated
set nfull 2 set nfreeze 10 !run nfullxnfreeze events (with
   always nfreeze events using the same hydro evolution)
set centrality 0           ! 0=min bias
```

Where we can choose all important characteristics about the collision like number of projectile atomic/mass number and target atomic/mass number easily.

Then, we can write directly which analysis we want to do in the same optns file including a proper language with a proper vocabulary already defined in the different subroutines of EPOS event generator. For example, if we want look the p_T spectra of particles, one can write the analysis as following:

```
write "!---------------------------------------"
write "!  pt distribution of pions             "
write "!---------------------------------------"

!defining a histogram for analysis during run

beginhisto
  histogram
    pt      !variable name (x-axis)
    numptl  !what is counted (yaxis)
    12      !normalisation (see below)
    0 20    !range for x variable
    100     !number of bins
  trigger iptl A+B+1 inf  !do not consdier spectators
  trigger rap -1 1        !rapidity range
  set hisfac 0.5          !overall normalization factor
  idcode 120  idcode -120 !define particle species (see EPOS id codes)
  noweak                  !no weak decays
endhisto

!write out final histogram

write "openhisto"                  !starts a histogram
write "name pi-pt"                 !some name
write "xrange 0 10"                !range for x-axis
write "yrange 5e-6 500"            !range for y-axis
write "htyp lin"                   !line type (see below)
write "xmod lin"                   !x-axis lin or log representation
write "ymod log"                   !y-axis lin or log representation
write ""txt "xaxis pt " ""         !text
write ""txt "yaxis dn/dptdy " ""
write ""txt "title  [p]"  ""
histoweight                        !provides event weight
writearray 3                       !provides histogram table
write "closehisto"                 !closes histogram
write "plot 0"                     !plots histogram
```

One purpose of my thesis is to extend this language to the anisotropic flow to prepare future results. Consequently, the next section introduces my work on it.

B.2.2 Using a optns files to calculate the anisotropic flow

I show only an example to calculate the anisotropic flow with the Event Plane (EP) method because Q-cumulants method is more complex to understand easily the way to calculate the anisotropic flow.

The complete example to calculate the anisotropic flow with the EP method is the following:

```
write "!-----------------------------------------------"
write "! v2 vs pT via event plane method       "
write "!-----------------------------------------------"

write "!    Calcul of R2 in the event plane method      "
beginhisto
  xps 11 -1 -0.05 0.05 1 0.15 5 1 1 2 2 1
  histogram
    egyevt                             !x-axis
    epxevt                             !y-axis
    2                                  !normalisation
    egy egy                            !range of x variable
    1                                  !number of bins
    trigger bimevt 0 bim80
endhisto

write "openhisto"
write "name rr2-00to80"
histoweight
writearray 2
write "closehisto"

write "!  Calcul of v2(np) in the event plane method     "
beginhisto
  xps 11 -1 -0.05 0.05 1 0.15 5 1 1 2 2 0
  histogram
    pt
    epx
    4
    0 4
    20
    trigger bimevt 0 bim80
    trigger iptl A+B+1 inf
    idcode 331               !phi particle
endhisto

write "openhisto"
write "name v2pt-ch-phi-00to80-ep"
histoweight
writearray 3
write "closehisto"

write "!  Plot of v2(EP) in the event plane method    "
write "openhisto"
```

```
write "xrange 0 3.5"
write "yrange -0.1 0.1"
write "xmod lin"
write "ymod lin"
write "{txt ""title [F]  STAR  0-80%"" }"
write "{txt ""xaxis pt (GeV/c)                    "" }"
write "{txt ""yaxis v2 (Event Plane)                 "" }"
write " calc rr2-00to80  ^ 0.50  ; -> 1 "
write "openhisto"
write "htyp lin"
write "calc v2pt-ch-phi-00to80-ep / $1 ; closehisto plot 0"
```

The first block is the following:

```
beginhisto
  xps 11 -1 -0.05 0.05 1 0.15 5 1 1 2 2 1
  histogram
    egyevt                                  !x-axis
    epxevt                                  !y-axis
    2                                       !normalisation
    egy egy                                 !range of x variable
    1                                       !number of bins
    trigger bimevt 0 bim80
endhisto
```

We have 11 inputs to calculate the R_n resolution of the Equation 3.3.32 or 3.3.34. We use the epxevt variable which called the epx subroutine with these 11 inputs:

```
!---------------------------------------------------------
      subroutine epx(n,ishift)  !'epx'
!---------------------------------------------------------
      ! input
      !   n = histogram number
      !   xpara(1,n)-xpara(4,n) ... etamin to etamax with gap
      !   xpara(5,n)-xpara(6,n) ... pmin to pmax
      !   xpara(7,n) rapidity max
      !   xpara(8,n) choice of weight wi
      !   xpara(9,n) n order of anisotropy v_n
      !   xpara(10,n) n order of event angle psi_n
      !   xpara(11,n) optimization variable 1 to calc, 0 just
    result
      !---------------------------------------------------------
```

In this subroutine, the output can be determined by the following lines:

```
    .
    .
      eta1=xpara(ishift+1,n)
      eta2=xpara(ishift+2,n)
      eta3=xpara(ishift+3,n)
      eta4=xpara(ishift+4,n)
      pmin=xpara(ishift+5,n)
      pmax=xpara(ishift+6,n)
      rapmax=xpara(ishift+7,n)
      iwi=nint(xpara(ishift+8,n))
      ivn=nint(xpara(ishift+9,n))
      inr=nint(xpara(ishift+10,n))
      icalc=nint(xpara(ishift+11,n))
    .
    .
              if(eta.gt.eta3.and.eta.lt.eta4)then
                a=polar(px,py)
                avcosnp=avcosnp+weight*cos(ivn*a)
                avsinnp=avsinnp+weight*sin(ivn*a)
              elseif(eta.lt.eta2.and.eta.gt.eta1)then
                a=polar(px,py)
                avcosnn=avcosnn+weight*cos(ivn*a)
                avsinnn=avsinnn+weight*sin(ivn*a)
              endif
     .
     .
     .
      ypara(1,n)=polar(avcosnn,avsinnn)/inr
      ypara(2,n)=polar(avcosnp,avsinnp)/inr
      ypara(3,n)=ivn
      ! output
      ! ypara(1-2,n) ... phi2neg, phi2pos
```

Finally, we have all options to calculate finally the denominator of the Eq 3.3.34. In the glossary of EPOS we can find the following calculation:

```
      elseif(inom.eq.540)then                              !'epxevt'
        phi2n=ypara(1,n)
        phi2p=ypara(2,n)
        ivn=ypara(3,n)
        x=cos(ivn*(phi2n-phi2p))
```

Consequently, we have the denominator of this equation:

$$\boxed{v_n = \frac{v_n^{\text{obs}}}{\mathcal{R}_{n,sub}} = \frac{\langle \cos[n(\phi_i - \Psi_n)] \rangle}{\sqrt{\langle \cos[n(\Psi_n^A - \Psi_n^B)] \rangle}}} \tag{B.2.1}$$

The second block is the following:

```
write "openhisto"
write "name rr2-00to80"
histoweight
writearray 2
write "closehisto"
```

where we only write the result of the x variable which contains the $\mathcal{R}_{n,sub}$ resolution variable. Now, we can calculate the numerator of the Equation 3.3.34: $v_n^{\rm obs}$. This is the purpose of the third block:

```
beginhisto
  xps 11 -1 -0.05 0.05 1 0.15 5 1 1 2 2 0
  histogram
    pt
    epx
    4
    0 4
    20
    trigger bimevt 0 bim80
    trigger iptl A+B+1 inf
    idcode 331                !phi particle
endhisto
```

Where we used also the epx subroutine, with the same outputs. However, we use the *epx* variable (in opposite of epxevt in the calculation of $\mathcal{R}_{n,sub}$). Consequently, we use another word in the glossary of EPOS with the following calculation:

```
      elseif(inom.eq.94)then  !'epx' ... event plane stuff
        phi=polar( p(1,lf) , p(2,lf) )
        pt=sqrt(p(2,lf)**2+p(1,lf)**2)
        eta=0
        ivn=ypara(3,n)
        if(p(3,lf).ne.0..and.pt.ne.0.)eta=sign(1.,p(3,lf))*
     *        alog((sqrt(p(3,lf)**2+pt**2)+abs(p(3,lf)))/pt)
        if(eta.gt.0)then
        phi2=ypara(1,n)    !phi2neg
        else
        phi2=ypara(2,n)    !phi2pos
        endif
        x=cos(ivn*(phi-phi2))
```

We can see that we calculate the numerator of this equation:

$$\boxed{v_n = \frac{v_n^{\rm obs}}{\mathcal{R}_{n,sub}} = \frac{\langle \cos[n(\phi_i - \Psi_n)]\rangle}{\sqrt{\langle \cos[n(\Psi_n^A - \Psi_n^B)]\rangle}}} \tag{B.2.2}$$

We obtain the final results by write the fraction of the numerator and the denominator in own optns file. This is what we do in this block:

```
write "openhisto"
write "xrange 0 3.5"
write "yrange -0.1 0.1"
write "xmod lin"
write "ymod lin"
write "{txt ""title [F]  STAR  0-80%"" }"
write "{txt ""xaxis pt (GeV/c)                    "" }"
write "{txt ""yaxis v2 (Event Plane)                  "" }"
write " calc rr2-00to80  ^ 0.50  ; -> 1 "
write "openhisto"
write "htyp lin"
write "calc v2pt-ch-phi-00to80-ep / $1 ; closehisto plot 0"
```

with the final line: *calc v2pt-ch-phi-00to80-ep / $1* is exactly the Equation 3.3.34.

Finally, we can measure the anisotropic using the EP method following this procedure:

1. calculate the denominator or the numerator using the *epxevt* or *epx* variable (respectively)
2. put in *xps* the 11 triggers following the experimental measure
3. write directly the fraction of these two variables
4. compare with the experimental results.

All the vocabulary and the subroutine associated to calculate the anisotropic flow with the Q-cumulants, Scalar Product, Event Plane and Symmetric Cumulants are written during my thesis. This word are effectuated in order to calculate the anisotropic flow in any order using the specific vocabulary of the specific method easily in an optns file.

B.3 Conclusion

I did two important upgrades for the EPOS's developments during my thesis. Firstly, all the code related to particle identification are completely restructured and extended to include a "complete" list of hadrons, easy to update, transparent for (future) users and developers

Secondly, to perform my analysis, I developped a framework that can already be easily used, independently of further EPOS's developments. This fact is very important, because results of this analysis will impact incoming updates of the model at little system sizes and low energies.

APPENDIX C

DETAILED STUDY OF MULTI-PARTICLE AZIMUTHAL CORRELATIONS

In Section 3.5.1, I showed how we can calculate the anisotropic flow using multi-particle azimuthal correlations. However, some demonstrations need to be explain to have a complete description of the method.

C.1 Cumulant of the four-particle correlation

I will start by demonstrate the Equation 3.5.10. The cumulant of the four-particle azimuthal distribution has been defined when the source is isotropic:

$$\begin{aligned}\langle\langle e^{in(\phi_1+\phi_2-\phi_3-\phi_4)}\rangle\rangle = {} & \langle e^{in(\phi_1+\phi_2-\phi_3-\phi_4)}\rangle \\ & - \langle e^{in(\phi_1-\phi_3)}\rangle\langle e^{in(\phi_2-\phi_4)}\rangle + \langle e^{in(\phi_1-\phi_4)}\rangle\langle e^{in(\phi_2-\phi_3)}\rangle\end{aligned} \tag{C.1.1}$$

Here, we want to evaluate the right-hand side of this equation when the source is no longer isotropic. In order to do that, we expand the four-particle distribution into connected parts. v_n is equal to $\langle e^{in\phi}\rangle$ by the Equation 3.5.1. Consequently the right-hand side of this equation leads to:

$$\begin{aligned}\langle e^{in(\phi_1+\phi_2-\phi_3-\phi_4)}\rangle - 2\times\langle e^{in(\phi_1-\phi_3)}\rangle^2 = {} & - v_n^4 + 2v_n^2\langle\langle e^{-in(\phi_3+\phi_4)}\rangle\rangle \\ & + \langle\langle e^{in(\phi_1+\phi_2)}\rangle\rangle\langle\langle e^{-in(\phi_3+\phi_4)}\rangle\rangle \\ & +4v_n\langle\langle e^{\pm in(\phi_1+\phi_2-\phi_3)}\rangle\rangle \\ & \langle\langle e^{in(\phi_1+\phi_2-\phi_3-\phi_4)}\rangle\rangle\end{aligned} \tag{C.1.2}$$

A good characteristic is that the direct two-particle correlations $\langle\langle e^{in(\phi_1+\phi_2)}\rangle\rangle$ are automatically removed. The difference between the isotropic case is that we keep only the connected part of the correlation (where all points are connected in the schematic point of view). In the isotropic case, we keep only $\langle\langle e^{in(\phi_1+\phi_2-\phi_3-\phi_4)}\rangle\rangle$.

It is time to know exactly the orders of magnitude of the different terms in the right hand of the Equation C.1.2. As already stated, all terms without the last vanish in the isotropic case. Indeed, $\langle\langle e^{\pm in(\phi_1+\phi_2-\phi_3)}\rangle\rangle$ and $\langle\langle e^{in(\phi_1+\phi_2)}\rangle\rangle$ are not invariant under the transformation $\phi_j \to \phi_j + \alpha$, where α is any angle.

Therefore, it seems reasonable to consider that these terms are proportional to v_n or v_{2n}, depending of the factor $e^{\pm in\alpha}$ or $e^{\pm 2in\alpha}$ appears under the previous transformation. Finally, we consider that for the connected k-particle correlations, they behave like $\mathcal{O}(1/N^{k-1})$. Consequently:

$$\langle\langle e^{in(\phi_1+\phi_2-\phi_3)}\rangle\rangle = \mathcal{O}\left(\frac{v_n}{N^2}\right) \qquad \langle\langle e^{\pm in(\phi_1+\phi_2)}\rangle\rangle = \mathcal{O}\left(\frac{v_{2n}}{N}\right) \tag{C.1.3}$$

The second term in the right-hand side of Equation C.1.2 is smaller than either the first of third terms. Finally, the order of magnitude of the right-hand of Equation C.1.1 is $v_n^4 + \mathcal{O}(v_{2n}^2/N^2 + 1/N^3)$. We have neglected v_n^2/N^2 since it is smaller than either v_n^4 or $1/N^3$. Transcript in an equation, we see:

$$\langle\langle e^{in(\phi_1+\phi_2-\phi_3-\phi_4)}\rangle\rangle = -v_n^4 + \mathcal{O}\left(\frac{1}{N^3} + \frac{v_{2n}^2}{N^2}\right) \tag{C.1.4}$$

C.2 Contribution of flow to the integrated cumulants

In this section, I will evaluate the contribution of flow to the cumulant $c_n\{2k\}$. For the case of EPOS, we have a perfect detector. I will show the generating function $\langle G_n(z)\rangle$ and, from it, the values of the cumulants.

We call Ψ_r the azimuthal angle of the reaction plane of a given event. The average over events can be performed in two steps: one first estimates the average over all events with the same Ψ_r; then one averages over Ψ_r. We denote by $\langle x|\Psi_r\rangle$ the average of a quantity x for fixed Ψ_r. With this notation, the definition of v_n gives:

$$v_n \equiv \langle e^{in(\phi-\Psi_r)}\rangle \quad \Rightarrow \quad \langle e^{in\phi_j}|\Psi_r\rangle = v_n e^{in\Psi_r} \tag{C.2.1}$$

Now using the Generating function defined as following (like 3.5.13 without weight of particles):

$$G_n(z) = \prod_{j=1}^{M}\left[1 + \frac{z^*\ e^{in\phi_j} + z\ e^{-in\phi_j}}{M}\right] \tag{C.2.2}$$

We can calculate the average of the generating function for a fixed reaction plane:

$$\langle G_n(z)|\Psi_r\rangle = \left[1 + \frac{z\ v_n\ e^{-in\Psi_r} + z^*\ v_n\ e^{in\Psi_r}}{M}\right]^M \tag{C.2.3}$$

Therefore, one must then average over Ψ_r:

$$\langle G_n(z)\rangle = \int_0^{2\pi}\langle G_n(z)|\Psi_r\rangle\frac{d\Psi_r}{2\pi} \tag{C.2.4}$$

Inserting the Equation C.2.3 in this expression, one obtains the following results:

$$\langle G_n(z)\rangle = \sum_{k=0}^{[M/2]}\frac{M!}{(M-2k)!(k!)^2}\left(\frac{v_n}{M}\right)^2|z|^{2k} \approx I_0(2v_n|z|) \tag{C.2.5}$$

The approximate result comes by the assumption of a large M, consequently $\frac{M!}{(M-2k)!} \approx M^{2k}$. Then, one may extend the sum over k to infinity. I_0 denotes the modified Bessel function of the first kind. The result depends only on $|z|$.

The generating function of the cumulants $C_n(z)$ is defined by:

$$C_n(z) = M\left(\langle G_n(z)\rangle^{1/M} - 1\right) = \sum_{k,l} \frac{z^{*k} z^l}{k!l!} \langle\langle e^{in\phi_1+\cdots+\phi_k-\phi_{k+1}-\cdots-\phi_{k+l})}\rangle\rangle \tag{C.2.6}$$

In this equation, cumulants with $k \neq l$ vanish for a perfect detector, since the generating function $C_n(z)$ depends only of $|z|$. The interesting cumulants are the diagonal terms with $k = l$, which are related to the flow. The denotation of these terms are $c_n\{2k\}$ defined by:

$$c_n\{2k\} = \langle\langle e^{in(\phi_1+\cdots+\phi_k-\phi_{k+1}-\cdots-\phi_{2k})}\rangle\rangle \tag{C.2.7}$$

Inserting the C.2.5 equation in the C.2.6, the generating function of cumulants now reads:

$$C_n(z) \approx M\left(I_0(2v_n|z|)^{1/M} - 1\right) \approx \ln I_0(2v_n|z|) \tag{C.2.8}$$

This equation can be expanded in power series. Comparing with C.2.6, the cumulants with $k \neq l$ vanish, as expected for a perfect detector, while the diagonal cumulants $c_n\{2k\}$ defined by the equation C.2.7 are related to v_n. From the measured $c_n\{2k\}$, one thus obtains an estimate of v_n, which is denoted by $v_n\{2k\}$. The lowest order are estimated as following:

$$\boxed{v_n\{2\}^2 = c_n\{2\}} \qquad \boxed{v_n\{4\}^4 = -c_n\{4\}} \qquad \boxed{v_n\{6\}^6 = \frac{c_n\{6\}}{4}} \tag{C.2.9}$$

Consequently, one obtains anisotropic flow:

$$\begin{array}{cc} \boxed{v_n\{2\} = \sqrt{c_n\{2\}}} & \boxed{v_n\{4\} = \sqrt[4]{-c_n\{4\}}} \\ \boxed{v_n\{6\} = \sqrt[6]{\frac{c_n\{6\}}{4}}} & \boxed{v_n\{8\} = \sqrt[8]{\frac{-c_n\{8\}}{33}}} \end{array} \tag{C.2.10}$$

C.3 Contribution of flow to the differential cumulants

In this section, I will evaluate the contribution of flow to the differential cumulants $d_{mn/n}\{2k+m+1\}$. We neglect nonflow correlations and assume a perfect detector using EPOS. Under these assumptions, we can compute the generating function of the cumulant $D_{p/n}(z)$. As the previous section, we first average over all events with a fixed orientation of the reaction plane ψ_r and over the POI of each single event:

$$\langle e^{ip\phi}|\psi_r\rangle = v'_p e^{ip\psi_r} \tag{C.3.1}$$

The generating function for differential cumulants is:

$$D_{p/n}(z) \equiv \frac{\langle e^{ip\Psi} G_n(z)\rangle}{\langle G_n(z)\rangle} = \sum_{k,l} \frac{z^{*k} z^l}{k!l!} \langle\langle e^{ip\Psi+in\phi_1+\cdots+\phi_k-\phi_{k+1}-\cdots-\phi_{k+l})}\rangle\rangle \tag{C.3.2}$$

Consequently, this equation becomes:

$$D_{p/n}(z) = \frac{\int_0^{2\pi} e^{ip\Psi_r}\langle G_n(z)|\Psi_r\rangle d\Psi_r/2\pi}{\langle G_n(z)\rangle} v'_p \tag{C.3.3}$$

The denominator is given by the equation C.2.5 and $\langle G_n(z)|\Psi_r\rangle$ by C.2.3. The numerator vanishes unless p is a multiple of n, i.e. $p = mn$ with m integer. Integrating over Ψ_r, one then obtains:

$$\int_0^{2\pi} e^{ip\Psi_r}\langle G_n(z)|\Psi_r\rangle d\Psi_r/2\pi = \sum_{k=0}^{(M+m)/2} \frac{M!}{(M-m-2k)!k!(2k+m)!}\left(\frac{v_n}{M}\right)^{2k+m} z^* z^{k+m} \tag{C.3.4}$$

Consequently, one obtains:

$$\int_0^{2\pi} e^{ip\Psi_r}\langle G_n(z)|\Psi_r\rangle d\Psi_r/2\pi \approx I_m(2v_n|z|)\left(\frac{z}{|z|}\right)^m \tag{C.3.5}$$

where we assumed that M is large, so that $\frac{M!}{(M-m-2k)!} \approx M^{2k+m}$, and we extend the sum over k to infinity. The final equation is:

$$D_{mn/n}(z) = \frac{I_m(2v_n|z|)}{I_0(2v_n|z|)}\left(\frac{z}{|z|}\right)^m v'_{mn} \tag{C.3.6}$$

Since this quantity depends only on $|z|$, the only nonvanishing cumulants in the previous equation are those with $l = k + m$. Consequently, the denotation of these relevant quantities is:

$$d_{mn/n}\{2k+m+1\} \equiv \Re\left[\langle\langle e^{in(m\psi+\phi_1+\cdots+\phi_k-\phi_{k+1}-\cdots-\phi_{2k+m})}\rangle\rangle\right] \tag{C.3.7}$$

These cumulants can give the differential flow, for a perfect detector like EPOS, this flow is given by:

$$\boxed{v'_{n/n}\{2\} = d_{n/n}\{2\}/v_n\{2\}} \qquad \boxed{v'_{n/n}\{4\} = -d_{n/n}\{4\}/v_n^3\{4\}}$$
$$\boxed{v'_{2n/n}\{3\} = d_{2n/n}\{3\}/v_n^2\{4\}} \qquad \boxed{v'_{2n/n}\{5\} = -d_{2n/n}\{5\}/(2v_n^4\{4\})} \tag{C.3.8}$$

APPENDIX D

RÉSUMÉ FRANÇAIS DE LA THÈSE

Cette annexe résume mes travaux de thèse, supervisés par Klaus Werner, portant sur la formation du Plasma de Quarks et de Gluons (PQG) : compréhension de la dépendance en énergie et en taille de système d'octobre 2015 en octobre 2018.

Mots clefs : Plasma de Quarks et de Gluons, Collisions d'ions lourds, EPOS-génerateur d'évenements, Corrélations angulaires, Ecoulement anisotropique, Simulations Monte Carlo.

Le PQG est un état de la matière hadronique prédit par la ChromoDynamique Quantique où les partons (quarks et gluons) sont déconfinés des hadrons initiaux. L'étude de cet état est un champ de recherche très actif et c'est dans ce cadre que cette thèse s'inscrit. L'étude du PQG ne peut s'effectuer directement dû à sa trop petite taille (10^{-15} m) et à son temps de vie trop court (10^{-31} s). Différentes sondes ont donc été proposées pour le caractériser. La sonde choisie pour cette thèse, de part ses nombreuses applications, est l'écoulement anisotropique.

L'écoulement anisotropique indique que la production de particules est anisotrope dans l'espace de Fourier (voir Eq 1.3.2). Cette production peut être privilégiée selon une ou plusieurs directions. Pour une direction privilégiée, l'écoulement se nomme écoulement directe, et pour deux directions privilégiées, nous l'appelons l'écoulement elliptique. Cette sonde est une observable complexe étant donné qu'il est possible de mesurer des anisotropies dans la production de particules n'ayant aucun lien avec la création de PQG. Plusieurs méthodes ont été créées pour éliminer ces biais et mesurer le plus possible les anisotropies directement liées aux écoulements anisotropiques induite par le PQG.

On observe des effets d'écoulement lors des collisions d'ions lourds (AA) aux hautes énergies du RHIC et du LHC mais aussi aux basses énergies du Beam Energy Scan (BES). Récemment, des effets d'écoulement ont également été observés lors des collisions de petits systèmes (pp). La problématique de cette thèse est : **Est-ce qu'un « plasma en expansion collectif » est créé dans tous les systèmes : grand (AA) ou petit (pp) des basses énergies du BES aux hautes énergies du RHIC et du LHC ?**

L'étude des différents ordres d'écoulement anisotropique (en particuler le second) sera traitée avec le générateur d'événements EPOS. EPOS est un générateur d'évènements dédié à l'étude des collisions d'ions lourds et proton-proton. EPOS est basé sur la théorie de Parton-Based-Gribov-Regge. Cette théorie consiste à inclure le modèle des partons dans la théorie de Gribov-Regge. Les interactions élémentaires sont vues comme un échange de pomerons entre partons pour la Parton-Based-Gribov-Regge et entre hadrons pour Gribov-Regge. Les conditions initiales à l'évolution hydrodynamique sont obtenues en suivant la séparation coeur couronne détaillée dans la section 2.4.2. Les fragments de cordes établis par les conditions initiales sont rangés dans deux zones différentes suivant leurs densités. Si la densité des fragments dépasse la densité critique ρ_0, ils seront comptabilisés dans le coeur hydrodynamique sinon dans la couronne. L'analyse de l'écoulement anisotropique a été effectuée avec EPOS pour tous les types de systèmes (pp,pA, AA), énergies (LHC, RHIC, BES) et pour tous les types de sondes d'écoulement.

Le point fort de ce modèle est lié à sa particularité de pouvoir être utilisé avec les mêmes conditions initiales pour tout type de collisions de particules. Les conditions de génération d'événements sont fixées peu importe le système ou l'énergie étudiée. Pour citer quelques conditions : aucunes interactions jet-matière, potentiel chimique fixé comme nul, équation d'état du fluide fixée, η/s fixé à 0.08, ρ_0 pour activer la possibilité d'avoir une création de fluide fixé. Pour effectuer les analyses en utilisant EPOS, j'ai développé une infrastructure (informatique) spécifique à l'analyse des écoulements anisotropiques utilisable indépendamment des futurs développements d'EPOS. Les résultats que j'ai apporté vont impacter les prochaines mises à jour du modèle à petite taille et pour les petits systèmes.

Ce résumé est séparé en quatre parties : apports pour le générateur d'événements, conclusions des résultats liés aux énergies du BES, conclusions des résultats liés aux énergies du LHC, et finalement ouverture sur les possibilités de travaux futurs.

D.1 Apports pour le générateur d'événements EPOS

Pour des raisons historiques, EPOS utilisait plusieurs tables de particules afin de les caractériser, créer, définir, etc... Un travail important a été effectué pour restructurer et centraliser toutes les données de particules en créant une liste *complète* de particules comprenant toutes les caractéristiques de celles-ci. Cette table est transparente et facile d'utilisation pour les futurs utilisateurs et développeurs.

Des travaux d'analyses théoriques ont été effectués pour plusieurs types de sondes d'écoulements ; pour la méthode du plan d'événements, des produits scalaires et des cumulants directs. Ces méthodes sont détaillées dans le Chapitre 3.

Pour simplifier, la méthode du plan d'événements vérifie s'il y a une anisotropie de particules liée à un plan d'événements défini. La méthode des produits scalaires vérifie s'il y a une anisotropie par rapport à une catégorie de particules de références. La méthode des cumulants directs mesure directement les écoulements anisotropiques en utilisant les corrélations azimutales de particules. On utilise les corrélations azimutales de plus de deux particules en éliminant les biais liés aux corrélations d'ordres inférieurs, plus on monte en nombre de particules liés aux corrélations d'écoulements, plus on élimine les biais.

J'ai développé des routines spécifiques à chaque méthode pour pouvoir calculer tout ordre d'écoulement (directe, elliptique, triangulaire ...). Il est possible d'utiliser nombre (pair) arbitraire de particules pour calculer leur corrélation azimutale (deux, quatre, six ou huit), pour tout les types de particules (chargées ou neutres) et finalement en utilisant ou non un gap en pseudorapidité pour réduire les effets d'auto-corrélations.

D.2 Résultats aux énergies du BES

Dans le cadre du collisionneur de particules RHIC situé au laboratoire national de Brookhaven aux Etats-Unis, un programme appelé Beam Energy Scan (BES) a été créé pour permettre d'effectuer un scan en énergie (comme son nom l'indique) de collisions Or-Or en ayant ces trois buts :

1. Trouver une preuve de la transition de phase hadronique.
2. Trouver un possible point critique.
3. Remarquer une évolution liée à l'énergie de collision sur le milieu créé (PQG).

Les collisions Or-Or effectuées vont de'une énergie de collisions dans le centre de masse $\sqrt{s_{NN}}$ de 7.7 GeV à 62.4 GeV. Toutes les énergies de collisions sont les suivantes : 7.7, 11.5, 19.6, 27, 39 et 62.4 GeV. Une étude d'une possible dépendance en énergie sur la création du PQG peut donc être effectuée en comparant les données théoriques d'EPOS avec les données expérimentales du programme BES.

Les résultats globaux sur l'analyse d'une possible dépendance en énergie sont les suivants (plus de détails dans la section 4.2 du Chapitre 4):

Premièrement, EPOS peut créer un fluide sous toutes les énergies de collisions du BES. En ce qui concerne les analyses sur les spectres de particules, EPOS ne reproduit pas les données expérimentales du BES, cependant nous remarquons un plus grand nombre de particules créées à partir d'un fluide que de particules créées par les jets pour toutes les énergies (voir Fig. 4.29). EPOS reproduit tous les écoulements intégrés et différentiels pour toutes les énergies lorsque l'impulsion transverse est inférieure à 2 GeV (exemple Fig. 4.34 et Fig. 4.35). L'observation expérimentale d'une séparation entre les baryons et les mésons est remarquée théoriquement pour toutes les énergies alors qu'elle n'est observée expérimentalement que pour les énergies supérieures à 11.5 GeV. **Nous observons donc une dépendance en énergie**. Une première naïve conclusion pourrait être que l'on créer un fluide (PQG) expérimentalement entre 11.5 et 19 GeV.

Les résultats favorisent la possibilité de notre scénario d'une expansion hydrodynamique, basée sur les conditions initiales de la théorie de Gribov-Regge pour les études d'écoulement anisotropique.

D.3 Résultats aux énergies du LHC

Le collisionneur de particules LHC, situé en Suisse à Genève a donné de grands résultats comme la découverte du Boson de Higgs. Il a été établi que les collisions d'ions lourds au LHC permettent d'étudier le PQG, les collisions de protons-nucléons (pA) permettent d'étudier la matière froide et les collisions protons-protons (pp) servent de référence pour mieux distinguer les aspects des collisions d'ion lourds (AA).

Récemment, des caractéristiques précédemment exclusives aux collisions d'ions lourds ont été remarquées pour les collisions pp à très haute multiplicité. Les collisions pp à très haute multiplicité qui sont considérés comme des collisions de petits systèmes présentent des aspects collectifs concernant la production de particules. Une nouvelle définition des petits systèmes s'impose alors : ce sont des systèmes *à priori* trop petits pour montrer des caractéristiques d'ions lourds mais avec lesquels nous pouvons en observer.

Grâce aux LHC, l'étude de la possible formation de PQG dépendant de la taille de systèmes initiaux collisionnant a pu être effectuée. Les trois tailles étant celles pour les collisions suivantes : Plomb-Plomb (Pb-Pb), Proton-Plomb (p-Pb) et Proton-Proton (p-p). Expérimentalement, le constat est que l'on a créé un PQG pour les hautes énergies et densité de collisions AA. La possibilité d'avoir cet état pour des collisions pp est en discussion. La dépendance en taille de système sur la création du PQG peut être effectuée en comparant les données théoriques d'EPOS avec les données expérimentales du LHC.

Les résultats globaux sur l'analyse de la dépendance en taille de système sont les suivants (plus de d'étails dans la section 4.1 du Chapitre 4) :

EPOS peut créer un fluide pour toutes les collisions car la densité critique des cordes ρ_0 peut être dépassée. En ce qui concerne les analyses sur les spectres de particules, EPOS reproduit les données expérimentales du LHC pour les trois tailles de système. Pour les trois types de collisions, nous remarquons une forte contribution du nombre de particules provenant de fluide. Cette contribution est proche de 100 % pour les collisions AA. Les données d'EPOS sont en accords avec les toutes les données expérimentales pour les collisions Pb-Pb aux deux énergies de collisions : 2.76 et 5.02 TeV. EPOS peut reproduire toutes les données expérimentales sur l'écoulement anisotropique intégré pour les hautes multiplicités et grand système, cependant il ne reproduit pas les données pour les petits systèmes. EPOS semble mieux reproduire les résultats lorsque l'on augmente la multiplicité de particules. **On peut en conclure que nous avons une nette dépendance en taille de système** mais il est trop tôt pour conclure une possible création de PQG pour les collisions pp avec les données actuelles.

Les résultats appuient la possibilité de création d'un PQG pour les grands systèmes mais des études supplémentaires doivent être fait pour établir une concrète conclusion pour les plus petits systèmes.

D.4 Perspectives

Les deux buts principaux de ma thèse ont été effectués. Le premier but étant d'avancer la sortie publique du générateur d'événements EPOS par des travaux de simplifications et de transparences pour les futurs utilisateurs. Ces travaux sont principalement liés, premièrement, à des créations de nouveaux outils pour calculer l'écoulement anisotropique en même temps que la génération d'événements avec EPOS et, deuxièmement, à une centralisation de toutes les caractéristiques des particules comme la masse, charge ou l'identification dans nos codes. Pour étudier la dépendance en énergie et en taille des systèmes de collisions, j'ai effectué des analyses sur l'écoulement anisotropique avec EPOS pour tout type de systèmes (pp, pA, AA), énergies (LHC, RHIC, BES) et pour tout type de sondes d'écoulements. Les premières conclusions que l'on peut établir avec mes travaux de thèse sont les suivantes :

1. EPOS peut reproduire les données expérimentales pour tous les grands systèmes pour les collisions du RHIC et du LHC. Ces résultats confirment le scénario d'une expansion hydrodynamique de notre modèle pour les grands systèmes.

2. Nous observons de petites déviations pour les observables d'écoulements pour les très hautes multiplicités pour les petits systèmes (pp) aux énergies du LHC, cependant nous observons une très grande déviation à basse multiplicité et qui n'est pas encore totalement compris.

3. En ce qui concerne les plus petites énergies, nous trouvons un bon accord pour les plus basses énergies de collisions du programme BES et EPOS pour les observables d'écoulements anisotropiques mais pas pour les observables simples telles que les spectres en impulsion transverse et de pseudorapidité.

Mes travaux de thèse ont pour vocation de préparer les résultats scientifiques des futures améliorations d'EPOS. Les perspectives de travail sont d'ores et déjà établies:

1. Une première conclusion a également été faite grâce à la première phase du programme BES : il se passe bien quelque chose entre les énergies de collisions de 11.5 et 19.6 GeV. Des premières collisions ont donc été effectuées aux énergies de 14.5 GeV, nous allons pouvoir faire les mêmes analyses sur l'écoulement anisotropique avec EPOS.

2. Nous avons généré des événements en fixant un potentiel chimique nul pour les énergies du BES, ce qui est en désaccord avec le point de vue expérimental. Nous devons refaire les analyses en ajoutant ces valeurs pour le potentiel chimique.

3. Les interactions jet-matière n'ont pas été inclus lors de la génération des événements, nous allons inclure ce phénomène.

4. Un nouvel accélérateur de particules va être créé à Dubna en Russie appelé Nuclotron based Ion Collider fAcility (NICA). Il y aura donc de nouvelles données expérimentales à plus basses énergies que le programme BES. Ce sera une bonne opportunité pour tester EPOS à ces énergies.

5. Différents travaux vont être effectués concernant la taille du fluide initial pour résoudre les problèmes de non concordance entre les données expérimentales et théoriques aux petits systèmes.

LIST OF FIGURES

LIST OF TABLES

BIBLIOGRAPHY

[1] G. Zweig. An SU(3) model for strong interaction symmetry and its breaking. Version 1. 1964. (Cited on page 6.)

[2] G. Zweig. Origin of the Quark Model. 1980. (Cited on page 6.)

[3] M. Gell-Mann. A Schematic Model of Baryons and Mesons. In Harald Fritzsch and Murray Gell-Mann, editors, *50 years of quarks*, pages 1–4. 2015. (Cited on page 6.)

[4] Harald Fritzsch and Murray Gell-Mann, editors. *50 years of quarks*. World Scientific, Hackensack, 2015. (Cited on page 6.)

[5] H. Fritzsch, Murray Gell-Mann, and H. Leutwyler. Advantages of the Color Octet Gluon Picture. *Phys. Lett.*, 47B:365–368, 1973. (Cited on page 6.)

[6] Jean-Philippe Uzan. The Fundamental constants and their variation: Observational status and theoretical motivations. *Rev. Mod. Phys.*, 75:403, 2003. (Cited on pages 7, 9, and 193.)

[7] Paul Dirac. Developments in atomic theory, December 1945. (Cited on page 8.)

[8] Enrico Fermi, editor. *Elementary Particles*. Yale University Press, 1951. (Cited on page 8.)

[9] S. N. Bose. Planck's law and light quantum hypothesis. *Z. Phys.*, 26:178–181, 1924. (Cited on page 8.)

[10] C. Patrignani et al. Review of Particle Physics. *Chin. Phys.*, C40(10):100001, 2016. (Cited on pages 8, 11, 12, 13, 14, 18, and 187.)

[11] P. J. E. Peebles and Bharat Ratra. The Cosmological constant and dark energy. *Rev. Mod. Phys.*, 75:559–606, 2003. (Cited on page 9.)

[12] Laurent Canetti, Marco Drewes, and Mikhail Shaposhnikov. Matter and Antimatter in the Universe. *New J. Phys.*, 14:095012, 2012. (Cited on page 10.)

[13] J Wess and B Zumino. Supergauge transformations in four dimensions. *Nucl. Phys. B*, 70(CERN-TH-1753. 1):39–50, 1974. (Cited on page 10.)

[14] Pierre Fayet. The Supersymmetric Standard Model. *Adv. Ser. Direct. High Energy Phys.*, 26:397–454, 2016. (Cited on page 10.)

[15] H. Miyazawa. Baryon Number Changing Currents. *Prog. Theor. Phys.*, 36(6):1266–1276, 1966. (Cited on page 10.)

[16] Hironari Miyazawa. Spinor Currents and Symmetries of Baryons and Mesons. *Phys. Rev.*, 170:1586–1590, 1968. (Cited on page 10.)

[17] Peter Freund, editor. *Introduction to Supersymmetry*. Cambridge University Press, 1986. (Cited on page 10.)

[18] Jean-Loup Gervais and B. Sakita. Field Theory Interpretation of Supergauges in Dual Models. *Nucl. Phys.*, B34:632–639, 1971. (Cited on page 10.)

[19] D. V. Volkov and V. P. Akulov. Is the Neutrino a Goldstone Particle? *Phys. Lett.*, 46B:109–110, 1973. (Cited on page 10.)

[20] J Wess and B Zumino. Supergauge transformations in four dimensions. 70:39–50, 02 1974. (Cited on page 10.)

[21] Pierre Ramond. Dual Theory for Free Fermions. *Phys. Rev.*, D3:2415–2418, 1971. (Cited on page 10.)

[22] Pierre Fayet and J. Iliopoulos. Spontaneously Broken Supergauge Symmetries and Goldstone Spinors. *Phys. Lett.*, 51B:461–464, 1974. (Cited on page 10.)

[23] Pierre Fayet and S. Ferrara. Supersymmetry. *Phys. Rept.*, 32:249–334, 1977. (Cited on page 10.)

[24] Pierre Fayet. Spontaneously Broken Supersymmetric Theories of Weak, Electromagnetic and Strong Interactions. *Phys. Lett.*, 69B:489, 1977. (Cited on page 10.)

[25] Stephen P. Martin. A Supersymmetry primer. 1997. [Adv. Ser. Direct. High Energy Phys.18,1(1998)]. (Cited on page 11.)

[26] Gerard Jungman, Marc Kamionkowski, and Kim Griest. Supersymmetric dark matter. *Phys. Rept.*, 267:195–373, 1996. (Cited on page 11.)

[27] Barton Zwiebach, editor. *A First Course in String Theory*. Cambridge University Press, 2009. (Cited on page 11.)

[28] Melanie Becker, Katrin Becker and John Schwarz, editors. *String Theory and M-theory: A Modern Introduction*. Cambridge University Press, 2007. (Cited on page 11.)

[29] H. Bohr and H. B. Nielsen. Hadron production from a boiling quark soup A thermodynamical quark model predicting particle ratios in hadronic collisions. *Nuclear Physics B*, 128:275–293, September 1977. (Cited on page 12.)

[30] Francesco Sannino. α_s at LHC: Challenging asymptotic freedom. In *Proceedings, High-Precision α_s Measurements from LHC to FCC-ee: Geneva, Switzerland, October 2-13,2015*, pages 11–19, 2015. (Cited on page 13.)

[31] H. D. Politzer. Reliable Perturbative Results for Strong Interactions? *Physical Review Letters*, 30:1346–1349, June 1973. (Cited on pages 14 and 17.)

[32] D. J. Gross and F. Wilczek. Ultraviolet Behavior of Non-Abelian Gauge Theories. *Physical Review Letters*, 30:1343–1346, June 1973. (Cited on pages 14 and 17.)

[33] T. D. Lee and G. C. Wick. Vacuum Stability and Vacuum Excitation in a Spin 0 Field Theory. *Phys. Rev.*, D9:2291–2316, 1974. (Cited on page 14.)

[34] H. A. Grunder, C. W. Leemann, and F. B. Selph. Relativistic Heavy Ion Accelerators. In *Proceedings, 10th International Conference on High-Energy Accelerators, HEACC 1977, v.1-2: Protvino, USSR, July 11–17, 1977*, pages 321–338, 1977. (Cited on page 14.)

[35] http://cerncourier.com/cws/article/cern/28470. (Cited on pages 14 and 70.)

[36] https://www.bnl.gov/rhic/. (Cited on pages 14, 42, and 43.)

[37] Mark G. Alford, Andreas Schmitt, Krishna Rajagopal, and Thomas Schäfer. Color superconductivity in dense quark matter. *Rev. Mod. Phys.*, 80:1455–1515, 2008. (Cited on page 14.)

[38] John C. Collins and M. J. Perry. Superdense Matter: Neutrons Or Asymptotically Free Quarks? *Phys. Rev. Lett.*, 34:1353, 1975. (Cited on pages 14 and 18.)

[39] N. Cabibbo and G. Parisi. Exponential Hadronic Spectrum and Quark Liberation. *Phys. Lett.*, 59B:67–69, 1975. (Cited on page 14.)

[40] P. Steinberg. Relativistic Heavy Ion Physics: Results from AGS to RHIC. *ArXiv Nuclear Experiment e-prints*, October 2002. (Cited on page 15.)

[41] B. Müller, J. Schukraft, and B. Wysłouch. First Results from Pb+Pb Collisions at the LHC. *Annual Review of Nuclear and Particle Science*, 62:361–386, November 2012. (Cited on pages 15 and 16.)

[42] Jaroslav Adam et al. Centrality dependence of the charged-particle multiplicity density at midrapidity in Pb-Pb collisions at $\sqrt{s_{NN}} = 5.02$ TeV. *Phys. Rev. Lett.*, 116(22):222302, 2016. (Cited on page 15.)

[43] J. D. Bjorken. Highly Relativistic Nucleus-Nucleus Collisions: The Central Rapidity Region. *Phys. Rev.*, D27:140–151, 1983. (Cited on pages 15 and 16.)

[44] Chiho Nonaka and Masayuki Asakawa. Modeling a Realistic Dynamical Model for High Energy Heavy Ion Collisions. *PTEP*, 2012:01A208, 2012. (Cited on pages 15 and 187.)

[45] Particle data group, http://pdg.lbl.gov/. (Cited on page 18.)

[46] Yasuyuki Akiba. Quest for the quark–gluon plasma—hard and electromagnetic probes. *PTEP*, 2015(3):03A105, 2015. (Cited on pages 18 and 19.)

[47] C.O. Escobar. Photoproduction of large transverse momentum mesons and production of large-pt photons and leptons in proton-proton collisions. *Nuclear Physics B*, 98(1):173 – 188, 1975. (Cited on page 18.)

[48] M. M. Aggarwal et al. Observation of direct photons in central 158-A-GeV Pb-208 + Pb-208 collisions. *Phys. Rev. Lett.*, 85:3595–3599, 2000. (Cited on page 18.)

[49] L. Apanasevich et al. Measurement of direct photon production at Tevatron fixed target energies. *Phys. Rev.*, D70:092009, 2004. (Cited on page 18.)

[50] M. Werlen et al. A New determination of α_s using direct photon production cross-sections in pp and $\bar{p}p$ collisions at $S^{(1/2)} = 24.3$-GeV. *Phys. Lett.*, B452:201–206, 1999. (Cited on page 18.)

[51] D. L. Adams et al. Measurement of single spin asymmetry for direct photon production in p p collisions at 200-GeV/c. *Phys. Lett.*, B345:569–575, 1995. (Cited on page 18.)

[52] A. L. S. Angelis et al. Direct Photon Production at the CERN ISR. *Nucl. Phys.*, B327:541–568, 1989. (Cited on page 18.)

[53] M. Bonesini et al. Production of High Transverse Momentum Prompt Photons and Neutral Pions in Proton Proton Interactions at 280-GeV/c. *Z. Phys.*, C38:371, 1988. (Cited on page 18.)

[54] C. De Marzo et al. A Measurement of Direct Photon Production at Large Transverse Momentum in $\pi^- p$, $\pi^+ p$ and pp Collisions at 300-GeV/c. *Phys. Rev.*, D36:8, 1987. (Cited on page 18.)

[55] S. Abachi et al. Isolated photon cross-section in the central and forward rapidity regions in $p\bar{p}$ collisions at $\sqrt{s} = 1.8$ TeV. *Phys. Rev. Lett.*, 77:5011–5015, 1996. (Cited on page 18.)

[56] E. Anassontzis et al. High p(t) Direct Photon Production in p p Collisions. *Z. Phys.*, C13:277–289, 1982. (Cited on page 18.)

[57] F. Abe and M. G. et all. Albrow. Precision measurement of the prompt photon cross section in $p\bar{p}$ collisions at $\sqrt{s} = 1.8$ tev. *Phys. Rev. Lett.*, 73:2662–2666, Nov 1994. (Cited on page 18.)

[58] S. S. Adler et al. Mid-rapidity direct-photon production in p^+p collisions at $\sqrt{s} =$ 200-GeV. *Phys. Rev.*, D71:071102, 2005. (Cited on page 18.)

[59] A. Adare et al. Enhanced production of direct photons in Au+Au collisions at $\sqrt{s_{NN}} = 200$ GeV and implications for the initial temperature. *Phys. Rev. Lett.*, 104:132301, 2010. (Cited on page 19.)

[60] Paul Sorensen. Highlights from Heavy Ion Collisions at RHIC and the Acoustics of the Little Bangs. 2012. (Cited on page 19.)

[61] B. I. Abelev et al. Identified baryon and meson distributions at large transverse momenta from Au+Au collisions at s(NN)**(1/2) = 200-GeV. *Phys. Rev. Lett.*, 97:152301, 2006. (Cited on pages 19, 20, and 187.)

[62] John Adams et al. Pion, kaon, proton and anti-proton transverse momentum distributions from $p + p$ and $d+$ Au collisions at $\sqrt{s_{NN}} = 200$GeV. *Phys. Lett.*, B616:8–16, 2005. (Cited on page 19.)

[63] J. Adams et al. Identified hadron spectra at large transverse momentum in p+p and d+Au collisions at s(NN)**(1/2) = 200-GeV. *Phys. Lett.*, B637:161–169, 2006. (Cited on page 19.)

[64] P. Abreu et al. pi+-, K+-, p and anti-p production in Z0 —> q anti-q, Z0 —> b anti-b, Z0 —> u anti-u, d anti-d, s anti-s. *Eur. Phys. J.*, C5:585–620, 1998. (Cited on page 19.)

[65] Rudolph C. Hwa and C. B. Yang. Recombination of shower partons at high p(T) in heavy ion collisions. *Phys. Rev.*, C70:024905, 2004. (Cited on page 19.)

[66] R. J. Fries, Berndt Muller, C. Nonaka, and S. A. Bass. Hadron production in heavy ion collisions: Fragmentation and recombination from a dense parton phase. *Phys. Rev.*, C68:044902, 2003. (Cited on page 19.)

[67] Betty Bezverkhny Abelev et al. Production of charged pions, kaons and protons at large transverse momenta in pp and Pb–Pb collisions at $\sqrt{s_{NN}}$ =2.76 TeV. *Phys. Lett.*, B736:196–207, 2014. (Cited on page 20.)

[68] Betty Bezverkhny Abelev et al. K_S^0 and Λ production in Pb-Pb collisions at $\sqrt{s_{NN}}$ = 2.76 TeV. *Phys. Rev. Lett.*, 111:222301, 2013. (Cited on page 20.)

[69] K. Aamodt et al. Strange particle production in proton-proton collisions at sqrt(s) = 0.9 TeV with ALICE at the LHC. *Eur. Phys. J.*, C71:1594, 2011. (Cited on page 20.)

[70] G. Agakishiev et al. Strangeness Enhancement in Cu+Cu and Au+Au Collisions at $\sqrt{s_{NN}} = 200$ GeV. *Phys. Rev. Lett.*, 108:072301, 2012. (Cited on page 20.)

[71] Huichao Song and Ulrich W. Heinz. Suppression of elliptic flow in a minimally viscous quark-gluon plasma. *Phys. Lett.*, B658:279–283, 2008. (Cited on page 20.)

[72] Huichao Song and Ulrich W. Heinz. Causal viscous hydrodynamics in 2+1 dimensions for relativistic heavy-ion collisions. *Phys. Rev.*, C77:064901, 2008. (Cited on page 20.)

[73] Huichao Song and Ulrich W. Heinz. Multiplicity scaling in ideal and viscous hydrodynamics. *Phys. Rev.*, C78:024902, 2008. (Cited on page 20.)

[74] Huichao Song, Steffen A. Bass, and Ulrich Heinz. Elliptic flow in 200 A GeV Au+Au collisions and 2.76 A TeV Pb+Pb collisions: insights from viscous hydrodynamics + hadron cascade hybrid model. *Phys. Rev.*, C83:054912, 2011. [Erratum: Phys. Rev.C87,no.1,019902(2013)]. (Cited on page 20.)

[75] K. Werner. Lambda-to-Kaon Ratio Enhancement in Heavy Ion Collisions at Several TeV. *Phys. Rev. Lett.*, 109:102301, 2012. (Cited on page 20.)

[76] R. J. Fries, Berndt Muller, C. Nonaka, and S. A. Bass. Hadronization in heavy ion collisions: Recombination and fragmentation of partons. *Phys. Rev. Lett.*, 90:202303, 2003. (Cited on page 21.)

[77] B. Hippolyte. Bulk matter physics and its future at the Large Hadron Collider. *Eur. Phys. J.*, C62:237–242, 2009. (Cited on page 21.)

[78] J. Adams et al. Measurements of transverse energy distributions in Au + Au collisions at s(NN)**(1/2) = 200-GeV. *Phys. Rev.*, C70:054907, 2004. (Cited on pages 21 and 22.)

[79] K. Adcox et al. Measurement of the mid-rapidity transverse energy distribution from s(NN)**(1/2) = 130-GeV Au + Au collisions at RHIC. *Phys. Rev. Lett.*, 87:052301, 2001. (Cited on pages 21 and 22.)

[80] Jaroslav Adam et al. Measurement of transverse energy at midrapidity in Pb-Pb collisions at $\sqrt{s_{NN}} = 2.76$ TeV. *Phys. Rev.*, C94(3):034903, 2016. (Cited on page 22.)

[81] S. S. Adler et al. Transverse-energy distributions at midrapidity in p+p , d+Au , and Au+Au collisions at $\sqrt{s_{NN}} = 62.4$–200 GeV and implications for particle-production models. *Phys. Rev.*, C89(4):044905, 2014. (Cited on page 22.)

[82] Raimond Snellings. Elliptic Flow: A Brief Review. *New J. Phys.*, 13:055008, 2011. (Cited on pages 22 and 24.)

[83] Iu. A. Karpenko, P. Huovinen, H. Petersen, and M. Bleicher. Estimation of the shear viscosity at finite net-baryon density from $A+A$ collision data at $\sqrt{s_{NN}} = 7.7 - 200$ GeV. *Phys. Rev.*, C91(6):064901, 2015. (Cited on page 24.)

[84] C. Adler et al. Azimuthal anisotropy and correlations in the hard scattering regime at RHIC. *Phys. Rev. Lett.*, 90:032301, 2003. (Cited on page 24.)

[85] J. Adams et al. Azimuthal anisotropy in Au+Au collisions at s(NN)**(1/2) = 200-GeV. *Phys. Rev.*, C72:014904, 2005. (Cited on page 24.)

[86] Zhao Feng, Guang-Ming Huang, and Feng Liu. Anisotropic flow of Pb+Pb $\sqrt{s_{NN}}$ = 5.02 TeV from a Multi-Phase Transport Model. *Chin. Phys.*, C41(2):024001, 2017. (Cited on page 24.)

[87] I. M. Dremin. Soft and hard processes in QCD. *JETP Lett.*, 81:307–310, 2005. [Pisma Zh. Eksp. Teor. Fiz.81,391(2005)]. (Cited on page 25.)

[88] T. Matsui and H. Satz. J/ψ Suppression by Quark-Gluon Plasma Formation. *Phys. Lett.*, B178:416–422, 1986. (Cited on page 25.)

[89] Betty Bezverkhny Abelev et al. Centrality, rapidity and transverse momentum dependence of J/ψ suppression in Pb-Pb collisions at $\sqrt{s_{NN}}$=2.76 TeV. *Phys. Lett.*, B734:314–327, 2014. (Cited on page 25.)

[90] Zaida Conesa Del Valle. *Performance of the ALICE muon spectrometer. Weak boson production and measurement in heavy-ion collisions at LHC.* PhD thesis, SUBATECH, Nantes, 2007. (Cited on page 25.)

[91] Yun-peng Liu, Zhen Qu, Nu Xu, and Peng-fei Zhuang. J/psi Transverse Momentum Distribution in High Energy Nuclear Collisions at RHIC. *Phys. Lett.*, B678:72–76, 2009. (Cited on page 25.)

[92] Xingbo Zhao and Ralf Rapp. Medium Modifications and Production of Charmonia at LHC. *Nucl. Phys.*, A859:114–125, 2011. (Cited on page 25.)

[93] A. Emerick, X. Zhao, and R. Rapp. Bottomonia in the Quark-Gluon Plasma and their Production at RHIC and LHC. *Eur. Phys. J.*, A48:72, 2012. (Cited on page 25.)

[94] David d'Enterria. Jet quenching in QCD matter: From RHIC to LHC. *Nucl. Phys.*, A827:356C–364C, 2009. [,513(2009)]. (Cited on page 26.)

[95] R. Stock et al., editor. *Relativistic Heavy Ion Physics*, volume 23 of Landolt-Bornstein of *Numerical Data and Functional Relationships in Science and Technology*. Springer Berlin Heidelberg, Hackensack, 2010. (Cited on page 26.)

[96] R. Baier, Yuri L. Dokshitzer, Alfred H. Mueller, S. Peigne, and D. Schiff. Radiative energy loss of high-energy quarks and gluons in a finite volume quark - gluon plasma. *Nucl. Phys.*, B483:291–320, 1997. (Cited on page 27.)

[97] Surasree et al. Mazumder. Gluon bremsstrahlung by heavy quarks - its effects on transport coefficients and equilibrium distribution. *Phys. Rev.*, D89(1):014002, 2014. (Cited on page 27.)

[98] J. Adams et al. Evidence from d + Au measurements for final state suppression of high p(T) hadrons in Au+Au collisions at RHIC. *Phys. Rev. Lett.*, 91:072304, 2003. (Cited on pages 27 and 28.)

[99] Jaroslav Adam et al. Measurement of jet quenching with semi-inclusive hadron-jet distributions in central Pb-Pb collisions at $\sqrt{s_{NN}} = 2.76$ TeV. *JHEP*, 09:170, 2015. (Cited on page 27.)

[100] Serguei Chatrchyan et al. Studies of jet quenching using isolated-photon+jet correlations in PbPb and *pp* collisions at $\sqrt{s_{NN}} = 2.76$ TeV. *Phys. Lett.*, B718:773–794, 2013. (Cited on page 27.)

[101] Serguei Chatrchyan et al. Study of high-pT charged particle suppression in PbPb compared to *pp* collisions at $\sqrt{s_{NN}} = 2.76$ TeV. *Eur. Phys. J.*, C72:1945, 2012. (Cited on page 28.)

[102] Georges Aad et al. Measurement of charged-particle spectra in Pb+Pb collisions at $\sqrt{s_{NN}} = 2.76$ TeV with the ATLAS detector at the LHC. *JHEP*, 09:050, 2015. (Cited on page 28.)

[103] Betty Abelev et al. Centrality Dependence of Charged Particle Production at Large Transverse Momentum in Pb–Pb Collisions at $\sqrt{s_{NN}} = 2.76$ TeV. *Phys. Lett.*, B720:52–62, 2013. (Cited on page 28.)

[104] S. S. Adler et al. Absence of suppression in particle production at large transverse momentum in S(NN)**(1/2) = 200-GeV d + Au collisions. *Phys. Rev. Lett.*, 91:072303, 2003. (Cited on page 28.)

[105] B. B. Back et al. Centrality dependence of charged hadron transverse momentum spectra in d + Au collisions at S(NN)**1/2 = 200 GeV. *Phys. Rev. Lett.*, 91:072302, 2003. (Cited on page 28.)

[106] I. Arsene et al. Transverse momentum spectra in Au+Au and d+Au collisions at s**(1/2) = 200-GeV and the pseudorapidity dependence of high p(T) suppression. *Phys. Rev. Lett.*, 91:072305, 2003. (Cited on page 28.)

[107] John Adams et al. Experimental and theoretical challenges in the search for the quark gluon plasma: The STAR Collaboration's critical assessment of the evidence from RHIC collisions. *Nucl. Phys.*, A757:102–183, 2005. (Cited on pages 28 and 188.)

[108] Jaroslav Adam et al. Centrality dependence of the nuclear modification factor of charged pions, kaons, and protons in Pb-Pb collisions at $\sqrt{s_{NN}} = 2.76$ TeV. *Phys. Rev.*, C93(3):034913, 2016. (Cited on page 29.)

[109] Betty Abelev et al. J/ψ suppression at forward rapidity in Pb-Pb collisions at $\sqrt{s_{NN}} = 2.76$ TeV. *Phys. Rev. Lett.*, 109:072301, 2012. (Cited on page 29.)

[110] R.J. Van de Graaff. *Phys. Rev.*, 38(1):919 A, 1931. (Cited on page 30.)

[111] Cern, the lhc experiment. http://home.cern/topics/large-hadron-collider. (Cited on page 33.)

[112] Oliver S. Bruning, P. Collier, P. Lebrun, S. Myers, R. Ostojic, J. Poole, and P. Proudlock. LHC Design Report Vol.1: The LHC Main Ring. 2004. (Cited on page 33.)

[113] O. Buning, P. Collier, P. Lebrun, S. Myers, R. Ostojic, J. Poole, and P. Proudlock. LHC Design Report. 2. The LHC infrastructure and general services. 2004. (Cited on page 33.)

[114] M. Benedikt, P. Collier, V. Mertens, J. Poole, and K. Schindl. LHC Design Report. 3. The LHC injector chain. 2004. (Cited on page 33.)

[115] G. Aad et al. The ATLAS Experiment at the CERN Large Hadron Collider. *JINST*, 3:S08003, 2008. (Cited on page 34.)

[116] S. Chatrchyan et al. The CMS Experiment at the CERN LHC. *JINST*, 3:S08004, 2008. (Cited on page 34.)

[117] K. Aamodt et al. The ALICE experiment at the CERN LHC. *JINST*, 3:S08002, 2008. (Cited on page 34.)

[118] A. Augusto Alves, Jr. et al. The LHCb Detector at the LHC. *JINST*, 3:S08005, 2008. (Cited on page 34.)

[119] Alice - a large ion collider experiment. http://aliceinfo.cern.ch/Public/Welcome.html. (Cited on page 35.)

[120] K Aamodt and et al. Abrahantes Quintana. The ALICE experiment at the CERN LHC. A Large Ion Collider Experiment. *JINST*, 3:S08002. 259 p, 2008. Also published by CERN Geneva in 2010. (Cited on page 35.)

[121] Joao Pequenao. Computer generated image of the whole ATLAS detector. Mar 2008. (Cited on page 35.)

[122] Atlas - detector & technology. https://atlas.cern/discover/detector. (Cited on page 35.)

[123] Christian Lippmann. Particle identification. *Nucl. Instrum. Meth.*, A666:148–172, 2012. (Cited on page 36.)

[124] Y. Aoki, Z. Fodor, S. D. Katz, and K. K. Szabo. The QCD transition temperature: Results with physical masses in the continuum limit. *Phys. Lett.*, B643:46–54, 2006. (Cited on pages 38 and 39.)

[125] Y. Aoki, Szabolcs Borsanyi, Stephan Durr, Zoltan Fodor, Sandor D. Katz, Stefan Krieg, and Kalman K. Szabo. The QCD transition temperature: results with physical masses in the continuum limit II. *JHEP*, 06:088, 2009. (Cited on page 38.)

[126] A. Bazavov et al. The chiral and deconfinement aspects of the QCD transition. *Phys. Rev.*, D85:054503, 2012. (Cited on page 38.)

[127] Shinji Ejiri. Canonical partition function and finite density phase transition in lattice QCD. *Phys. Rev.*, D78:074507, 2008. (Cited on page 38.)

[128] E. S. Bowman and J. I. Kapusta. Critical points in the linear σ model with quarks. *Phys. Rev. C*, 79:015202, Jan 2009. (Cited on page 38.)

[129] M. M. Aggarwal et al. An Experimental Exploration of the QCD Phase Diagram: The Search for the Critical Point and the Onset of De-confinement. 2010. (Cited on page 38.)

[130] J. Cleymans, H. Oeschler, K. Redlich, and S. Wheaton. Comparison of chemical freeze-out criteria in heavy-ion collisions. *Phys. Rev. C*, 73:034905, Mar 2006. (Cited on page 39.)

[131] L. Adamczyk et al. Energy Dependence of Moments of Net-proton Multiplicity Distributions at RHIC. *Phys. Rev. Lett.*, 112:032302, 2014. (Cited on pages 39, 40, and 188.)

[132] L. Adamczyk et al. Beam-energy dependence of charge separation along the magnetic field in Au+Au collisions at RHIC. *Phys. Rev. Lett.*, 113:052302, 2014. (Cited on pages 39 and 188.)

[133] Y. Aoki, G. Endrodi, Z. Fodor, S. D. Katz, and K. K. Szabo. The Order of the quantum chromodynamics transition predicted by the standard model of particle physics. *Nature*, 443:675–678, 2006. (Cited on page 39.)

[134] M. M. et al. Aggarwal. Higher moments of net proton multiplicity distributions at rhic. *Phys. Rev. Lett.*, 105:022302, Jul 2010. (Cited on page 40.)

[135] P. Garg, D. K. Mishra, P. K. Netrakanti, B. Mohanty, A. K. Mohanty, B. K. Singh, and N. Xu. Conserved number fluctuations in a hadron resonance gas model. *Phys. Lett.*, B726:691–696, 2013. (Cited on page 40.)

[136] M. Bleicher et al. Relativistic hadron hadron collisions in the ultrarelativistic quantum molecular dynamics model. *J. Phys.*, G25:1859–1896, 1999. (Cited on pages 40, 71, and 75.)

[137] Dirk H. Rischke, Yaris Pursun, Joachim A. Maruhn, Horst Stoecker, and Walter Greiner. The Phase transition to the quark - gluon plasma and its effects on hydrodynamic flow. *Acta Phys. Hung.*, A1:309–322, 1995. (Cited on page 40.)

[138] J. Brachmann, S. Soff, A. Dumitru, Horst Stoecker, J. A. Maruhn, W. Greiner, L. V. Bravina, and D. H. Rischke. Antiflow of nucleons at the softest point of the EoS. *Phys. Rev.*, C61:024909, 2000. (Cited on page 40.)

[139] Studying the phase diagram of qcd matter at rhic,`https://drupal.star.bnl.gov/STAR/system/files/BES_WPII_ver6.9_Cover.pdf`. (Cited on pages 40 and 41.)

[140] L. Van Hove. Multiplicity Dependence of p(T) Spectrum as a Possible Signal for a Phase Transition in Hadronic Collisions. *Phys. Lett.*, 118B:138, 1982. (Cited on pages 40 and 42.)

[141] L. Ahle et al. Excitation function of K+ and pi+ production in Au + Au reactions at 2/A-GeV to 10/A-GeV. *Phys. Lett.*, B476:1–8, 2000. (Cited on page 41.)

[142] L. Ahle et al. An Excitation function of K- and K+ production in Au + Au reactions at the AGS. *Phys. Lett.*, B490:53–60, 2000. (Cited on page 41.)

[143] L. Ahle et al. Particle production at high baryon density in central au+au reactions at 11.6a gev/c. *Phys. Rev. C*, 57:R466–R470, Feb 1998. (Cited on page 41.)

[144] L. Ahle et al. Kaon production in Au + Au collisions at 11.6-A-GeV/c. *Phys. Rev.*, C58:3523–3538, 1998. (Cited on page 41.)

[145] J. L. Klay et al. Longitudinal flow from 2-A-GeV to 8-A-GeV Au+Au collisions at the Brookhaven AGS. *Phys. Rev. Lett.*, 88:102301, 2002. (Cited on page 41.)

[146] J. Barrette et al. Proton and pion production in Au + Au collisions at 10.8A-GeV/c. *Phys. Rev.*, C62:024901, 2000. (Cited on page 41.)

[147] S. V. Afanasiev et al. Energy dependence of pion and kaon production in central Pb + Pb collisions. *Phys. Rev.*, C66:054902, 2002. (Cited on page 41.)

[148] Betty Abelev et al. Centrality dependence of π, K, p production in Pb-Pb collisions at $\sqrt{s_{NN}} = 2.76$ TeV. *Phys. Rev.*, C88:044910, 2013. (Cited on page 41.)

[149] Broad range hadron magnetic spectrometers experiment at rhic. http://www4.rcf.bnl.gov/brahms/WWW/. (Cited on page 43.)

[150] Phenix - a physics experiment at rhic. http://www.phenix.bnl.gov/. (Cited on pages 43 and 44.)

[151] Phobos - home detector internal search. https://www.bnl.gov/phobos/. (Cited on page 43.)

[152] The star experiment at relativistic heavy ions collider, brookhaven national laboratory. https://www.star.bnl.gov/. (Cited on pages 43 and 44.)

[153] C. Aidala et al. The PHENIX Forward Silicon Vertex Detector. *Nucl. Instrum. Meth.*, A755:44–61, 2014. (Cited on page 44.)

[154] L. Adamczyk et al. Global Λ hyperon polarization in nuclear collisions: evidence for the most vortical fluid. *Nature*, 548:62–65, 2017. (Cited on page 44.)

[155] Torbjorn Sjostrand. Introduction to monte carlo event generators. 26 July - 4 August 2010. (Cited on page 49.)

[156] Alphago. https://deepmind.com/research/alphago/. (Cited on page 49.)

[157] René Carmona, Pierre Del Moral, Peng Hu, and Nadia Oudjane. An introduction to particle methods with financial applications. In René A. Carmona, Pierre Del Moral, Peng Hu, and Nadia Oudjane, editors, *Numerical Methods in Finance*, pages 3–49, Berlin, Heidelberg, 2012. Springer Berlin Heidelberg. (Cited on page 49.)

[158] Intergovernmental Panel on Climate Change. *Climate Change 2013 – The Physical Science Basis: Working Group I Contribution to the Fifth Assessment Report of the Intergovernmental Panel on Climate Change*. Cambridge University Press, 2014. (Cited on page 49.)

[159] Torbjörn Sjöstrand, Stefan Ask, Jesper R. Christiansen, Richard Corke, Nishita Desai, Philip Ilten, Stephen Mrenna, Stefan Prestel, Christine O. Rasmussen, and Peter Z. Skands. An Introduction to PYTHIA 8.2. *Comput. Phys. Commun.*, 191:159–177, 2015. (Cited on page 52.)

[160] http://home.thep.lu.se/~torbjorn/Pythia.html. (Cited on page 52.)

[161] http://home.thep.lu.se/~leif/Pythia7/Welcome.html. (Cited on page 52.)

[162] http://home.thep.lu.se/~leif/ThePEG/. (Cited on pages 52 and 53.)

[163] https://herwig.hepforge.org/. (Cited on page 53.)

[164] Johannes Bellm et al. Herwig 7.0/Herwig++ 3.0 release note. *Eur. Phys. J.*, C76(4):196, 2016. (Cited on page 53.)

[165] M. Bahr et al. Herwig++ Physics and Manual. *Eur. Phys. J.*, C58:639–707, 2008. (Cited on page 53.)

[166] http://www.montecarlonet.org/index.php?p=Projects/ariadne. (Cited on page 53.)

[167] https://indico.cern.ch/event/74601/contributions/2082515/attachments/1046556/1491687/CERN10b.pdf. (Cited on page 53.)

[168] http://home.thep.lu.se/~leif/talks/SLAC14.pdf. (Cited on page 53.)

[169] K Werner. Strings, pomerons and the venus model of hadronic interactions at ultrarelativistic energies. *Physics Reports*, 232(2):87 – 299, 1993. (Cited on pages 54, 57, 70, and 73.)

[170] G. Soyez. *Deep Inelastic Scattering at Small x*. PhD thesis, Liege U., 2004. (Cited on page 54.)

[171] Marcel Froissart. Asymptotic behavior and subtractions in the mandelstam representation. *Phys. Rev.*, 123:1053–1057, Aug 1961. (Cited on pages 56 and 57.)

[172] V. N. Gribov. A REGGEON DIAGRAM TECHNIQUE. *Sov. Phys. JETP*, 26:414–422, 1968. [Zh. Eksp. Teor. Fiz.53,654(1967)]. (Cited on page 56.)

[173] V. N. Gribov. Glauber corrections and the interaction between high-energy hadrons and nuclei. *Sov. Phys. JETP*, 29:483–487, 1969. [Zh. Eksp. Teor. Fiz.56,892(1969)]. (Cited on page 56.)

[174] V. N. Gribov and I. Ya. Pomeranchuk. Complex orbital momenta and the relation between the cross-sections of various processes at high-energies. *Sov. Phys. JETP*, 15:788L, 1962. [Phys. Rev. Lett.8,343(1962)]. (Cited on page 56.)

[175] V N. Gribov and I Ya. Pomeranchuk. Properties of the elastic scattering amplitude at high energies. 38:516–528, 10 1962. (Cited on page 56.)

[176] K. Werner, F. M. Liu, S. Ostapchenko, and T. Pierog. A New string model: NEXUS 3. *Acta Phys. Hung.*, A21:279–285, 2004. (Cited on page 57.)

[177] Richard P. Feynman. Very high-energy collisions of hadrons. *Phys. Rev. Lett.*, 23:1415–1417, 1969. [,494(1969)]. (Cited on page 58.)

[178] J. D. Bjorken and E. A. Paschos. Inelastic electron-proton and γ-proton scattering and the structure of the nucleon. *Phys. Rev.*, 185:1975–1982, Sep 1969. (Cited on page 58.)

[179] David J. Gross and Frank Wilczek. Ultraviolet behavior of non-abelian gauge theories. *Phys. Rev. Lett.*, 30:1343–1346, Jun 1973. (Cited on page 59.)

[180] H. J. Drescher, M. Hladik, S. Ostapchenko, T. Pierog, and K. Werner. Parton based Gribov-Regge theory. *Phys. Rept.*, 350:93–289, 2001. (Cited on pages 61, 72, and 73.)

[181] Benjamin Guiot. *Production de charms et de photons prompts avec le générateur d'évènements EPOS*. PhD thesis, 2014. Thèse de doctorat dirigée par Werner, Klaus Constituants élémentaires et physique théorique Nantes, Ecole des Mines 2014. (Cited on pages 64, 71, and 74.)

[182] Sarah Porteboeuf. *Study of hard processes in proton-proton and nucleus-nucleus collisions*. Theses, Université de Nantes, September 2009. (Cited on pages 64 and 73.)

[183] Bo Andersson, G. Gustafson, G. Ingelman, and T. Sjostrand. Parton Fragmentation and String Dynamics. *Phys. Rept.*, 97:31–145, 1983. (Cited on page 65.)

[184] X. Artru and G. Mennessier. String model and multiproduction. *Nucl. Phys.*, B70:93–115, 1974. (Cited on page 65.)

[185] Sergey Ostapchenko. Status of QGSJET. *AIP Conf. Proc.*, 928:118–125, 2007. (Cited on page 70.)

[186] Corsika – an air shower simulation program,https://www.ikp.kit.edu/corsika/. (Cited on page 70.)

[187] Till Bergmann, R. Engel, D. Heck, N. N. Kalmykov, Sergey Ostapchenko, T. Pierog, T. Thouw, and K. Werner. One-dimensional Hybrid Approach to Extensive Air Shower Simulation. *Astropart. Phys.*, 26:420–432, 2007. (Cited on page 70.)

[188] T. Pierog and K. Werner. EPOS Model and Ultra High Energy Cosmic Rays. *Nucl. Phys. Proc. Suppl.*, 196:102–105, 2009. (Cited on page 70.)

[189] T. Pierog, Iu. Karpenko, J. M. Katzy, E. Yatsenko, and K. Werner. EPOS LHC: Test of collective hadronization with data measured at the CERN Large Hadron Collider. *Phys. Rev.*, C92(3):034906, 2015. (Cited on page 70.)

[190] K. Werner, Iu. Karpenko, T. Pierog, M. Bleicher, and K. Mikhailov. Event-by-Event Simulation of the Three-Dimensional Hydrodynamic Evolution from Flux Tube Initial Conditions in Ultrarelativistic Heavy Ion Collisions. *Phys. Rev.*, C82:044904, 2010. (Cited on page 71.)

[191] Iurii Karpenko. *Développement d'approches hydrodynamique et hydrocinétique aux collisions noyau-noyau ultra-relativistes.* PhD thesis, 2010. Thèse de doctorat dirigée par Werner, Klaus et Sinyukov, Yu Physique nucléaire Nantes 2010. (Cited on pages 71 and 73.)

[192] K. Werner, B. Guiot, Iu. Karpenko, and T. Pierog. Analysing radial flow features in p-Pb and p-p collisions at several TeV by studying identified particle production in EPOS3. *Phys. Rev.*, C89(6):064903, 2014. (Cited on page 71.)

[193] K Werner, B Guiot, Iu Karpenko, and T Pierog. New developments in epos: Parton saturation. 458:2020–, 08 2013. (Cited on page 71.)

[194] K. Werner, Iu. Karpenko, T. Pierog, M. Bleicher, and K. Mikhailov. Evidence for hydrodynamic evolution in proton-proton scattering at 900 GeV. *Phys. Rev.*, C83:044915, 2011. (Cited on page 75.)

[195] H. Sorge. Highly sensitive centrality dependence of elliptic flow: A novel signature of the phase transition in QCD. *Phys. Rev. Lett.*, 82:2048–2051, 1999. (Cited on page 78.)

[196] Ekkard Schnedermann, Josef Sollfrank, and Ulrich W. Heinz. Thermal phenomenology of hadrons from 200-A/GeV S+S collisions. *Phys. Rev.*, C48:2462–2475, 1993. (Cited on page 78.)

[197] S. Voloshin and Y. Zhang. Flow study in relativistic nuclear collisions by Fourier expansion of Azimuthal particle distributions. *Z. Phys.*, C70:665–672, 1996. (Cited on pages 79 and 87.)

[198] Jean-Yves Ollitrault. Anisotropy as a signature of transverse collective flow. *Phys. Rev.*, D46:229–245, 1992. (Cited on page 81.)

[199] J. Barrette et al. Observation of anisotropic event shapes and transverse flow in Au + Au collisions at AGS energy. *Phys. Rev. Lett.*, 73:2532–2535, 1994. (Cited on page 81.)

[200] J. Barrette et al. Energy and charged particle flow in a 10.8-A/GeV/c Au + Au collisions. *Phys. Rev.*, C55:1420–1430, 1997. [Erratum: Phys. Rev.C56,2336(1997)]. (Cited on page 81.)

[201] C. Alt et al. Directed and elliptic flow of charged pions and protons in Pb + Pb collisions at 40-A-GeV and 158-A-GeV. *Phys. Rev.*, C68:034903, 2003. (Cited on page 81.)

[202] K. H. Ackermann et al. Elliptic flow in Au + Au collisions at (S(NN))**(1/2) = 130 GeV. *Phys. Rev. Lett.*, 86:402–407, 2001. (Cited on page 81.)

[203] Huichao Song, Steffen A. Bass, Ulrich Heinz, Tetsufumi Hirano, and Chun Shen. 200 A GeV Au+Au collisions serve a nearly perfect quark-gluon liquid. *Phys. Rev. Lett.*, 106:192301, 2011. [Erratum: Phys. Rev. Lett.109,139904(2012)]. (Cited on page 81.)

[204] Chun Shen and Ulrich Heinz. The road to precision: Extraction of the specific shear viscosity of the quark-gluon plasma. *Nucl. Phys. News*, 25(2):6–11, 2015. (Cited on page 81.)

[205] Arthur M. Poskanzer and S. A. Voloshin. Methods for analyzing anisotropic flow in relativistic nuclear collisions. *Phys. Rev.*, C58:1671–1678, 1998. (Cited on pages 81, 85, and 87.)

[206] Sergei A. Voloshin, Arthur M. Poskanzer, Aihong Tang, and Gang Wang. Elliptic flow in the Gaussian model of eccentricity fluctuations. *Phys. Lett.*, B659:537–541, 2008. (Cited on page 83.)

[207] E. Butkov. *Mathematical Physics*. Addison-Wesley Series in Advanced Physics, 1968. (Cited on page 83.)

[208] L. Adamczyk et al. Elliptic flow of identified hadrons in Au+Au collisions at $\sqrt{s_{NN}} = 7.7$-62.4 GeV. *Phys. Rev.*, C88:014902, 2013. (Cited on pages 86 and 149.)

[209] L. Adamczyk et al. Centrality dependence of identified particle elliptic flow in relativistic heavy ion collisions at $\sqrt{s_{NN}}$=7.7–62.4 GeV. *Phys. Rev.*, C93(1):014907, 2016. (Cited on pages 86, 151, and 152.)

[210] Nicolas Borghini, Phuong Mai Dinh, and Jean-Yves Ollitrault. A New method for measuring azimuthal distributions in nucleus-nucleus collisions. *Phys. Rev.*, C63:054906, 2001. (Cited on pages 89, 91, 92, and 100.)

[211] Nicolas Borghini, Phuong Mai Dinh, and Jean-Yves Ollitrault. Flow analysis from multiparticle azimuthal correlations. *Phys. Rev.*, C64:054901, 2001. (Cited on pages 89, 91, 92, and 100.)

[212] Nicolas Borghini, Phuong Mai Dinh, and Jean-Yves Ollitrault. Flow analysis from cumulants: A Practical guide. In *International Workshop on the Physics of the Quark Gluon Plasma Palaiseau, France, September 4-7, 2001*, 2001. (Cited on pages 89, 91, 92, and 100.)

[213] Ante Bilandzic, Raimond Snellings, and Sergei Voloshin. Flow analysis with cumulants: Direct calculations. *Phys. Rev.*, C83:044913, 2011. (Cited on pages 89, 92, 97, 100, and 102.)

[214] Ante Bilandzic, Christian Holm Christensen, Kristjan Gulbrandsen, Alexander Hansen, and You Zhou. Generic framework for anisotropic flow analyses with multiparticle azimuthal correlations. *Phys. Rev.*, C89(6):064904, 2014. (Cited on pages 89, 92, 97, and 110.)

[215] You Zhou, Xiangrong Zhu, Pengfei Li, and Huichao Song. Investigation of possible hadronic flow in $\sqrt{s_{NN}} = 5.02$ TeV $p-Pb$ collisions. *Phys. Rev.*, C91:064908, 2015. (Cited on page 104.)

[216] R. S. Bhalerao, N. Borghini, and J. Y. Ollitrault. Genuine collective flow from Lee-Yang zeroes. *Phys. Lett.*, B580:157–162, 2004. (Cited on pages 106, 107, and 108.)

[217] R. S. Bhalerao, N. Borghini, and J. Y. Ollitrault. Analysis of anisotropic flow with Lee-Yang zeroes. *Nucl. Phys.*, A727:373–426, 2003. (Cited on pages 106, 107, and 108.)

[218] N. Bastid et al. First analysis of anisotropic flow with Lee-Yang zeroes. *Phys. Rev.*, C72:011901, 2005. (Cited on page 106.)

[219] Chen-Ning Yang and T. D. Lee. Statistical theory of equations of state and phase transitions. 1. Theory of condensation. *Phys. Rev.*, 87:404–409, 1952. [,151(1952)]. (Cited on page 106.)

[220] T. D. Lee and Chen-Ning Yang. Statistical theory of equations of state and phase transitions. 2. Lattice gas and Ising model. *Phys. Rev.*, 87:410–419, 1952. [,157(1952)]. (Cited on page 106.)

[221] N. Borghini and J. Y. Ollitrault. Directed flow at RHIC from Lee-Yang zeroes. *Nucl. Phys.*, A742:130–143, 2004. (Cited on page 108.)

[222] Giuliano Giacalone, Li Yan, Jacquelyn Noronha-Hostler, and Jean-Yves Ollitrault. Symmetric cumulants and event-plane correlations in Pb + Pb collisions. *Phys. Rev.*, C94(1):014906, 2016. (Cited on page 110.)

[223] Jaroslav Adam et al. Correlated event-by-event fluctuations of flow harmonics in Pb-Pb collisions at $\sqrt{s_{\rm NN}} = 2.76$ TeV. *Phys. Rev. Lett.*, 117:182301, 2016. (Cited on page 110.)

[224] Vardan Khachatryan et al. Observation of Long-Range Near-Side Angular Correlations in Proton-Proton Collisions at the LHC. *JHEP*, 09:091, 2010. (Cited on page 114.)

[225] Georges Aad et al. Observation of Long-Range Elliptic Azimuthal Anisotropies in $\sqrt{s}$ =13 and 2.76 TeV pp Collisions with the ATLAS Detector. *Phys. Rev. Lett.*, 116(17):172301, 2016. (Cited on page 114.)

[226] Vardan Khachatryan et al. Measurement of long-range near-side two-particle angular correlations in pp collisions at $\sqrt{s}$ =13 TeV. *Phys. Rev. Lett.*, 116(17):172302, 2016. (Cited on page 114.)

[227] Serguei Chatrchyan et al. Observation of long-range near-side angular correlations in proton-lead collisions at the LHC. *Phys. Lett.*, B718:795–814, 2013. (Cited on page 114.)

[228] Betty Abelev et al. Long-range angular correlations on the near and away side in p-Pb collisions at $\sqrt{s_{NN}} = 5.02$ TeV. *Phys. Lett.*, B719:29–41, 2013. (Cited on page 114.)

[229] Roel Aaij et al. Measurements of long-range near-side angular correlations in $\sqrt{s_{\rm NN}} = 5$TeV proton-lead collisions in the forward region. *Phys. Lett.*, B762:473–483, 2016. (Cited on page 114.)

[230] K. Werner, Iu. Karpenko, and T. Pierog. "ridge" in proton-proton scattering at 7 tev. *Phys. Rev. Lett.*, 106:122004, Mar 2011. (Cited on page 115.)

[231] Nicolò Jacazio. Production of identified charged hadrons in Pb–Pb collisions at $\sqrt{s_{NN}} = 5.02$ TeV. *Nucl. Phys.*, A967:421–424, 2017. (Cited on pages 117 and 118.)

[232] Private Communication Ivan Ravasenga. (Cited on page 117.)

[233] Serguei Chatrchyan et al. Study of the production of charged pions, kaons, and protons in pPb collisions at $\sqrt{s_{NN}} =$ 5.02 TeV. *Eur. Phys. J.*, C74(6):2847, 2014. (Cited on page 117.)

[234] Jaroslav Adam et al. Pseudorapidity and transverse-momentum distributions of charged particles in proton–proton collisions at $\sqrt{s} = 13$ TeV. *Phys. Lett.*, B753:319–329, 2016. (Cited on pages 118 and 119.)

[235] Georges Aad et al. Charged-particle distributions in $\sqrt{s} = 13$ TeV pp interactions measured with the ATLAS detector at the LHC. *Phys. Lett.*, B758:67–88, 2016. (Cited on page 118.)

[236] Vardan Khachatryan et al. Pseudorapidity distribution of charged hadrons in proton-proton collisions at $\sqrt{s} = 13$ TeV. *Phys. Lett.*, B751:143–163, 2015. (Cited on page 119.)

[237] Jaroslav Adam et al. Centrality dependence of the pseudorapidity density distribution for charged particles in Pb-Pb collisions at $\sqrt{s_{\rm NN}} = 5.02$ TeV. *Phys. Lett.*, B772:567–577, 2017. (Cited on page 119.)

[238] Betty Bezverkhny Abelev et al. Elliptic flow of identified hadrons in Pb-Pb collisions at $\sqrt{s_{\rm NN}} = 2.76$ TeV. *JHEP*, 06:190, 2015. (Cited on page 120.)

[239] Georges Aad et al. Measurement of flow harmonics with multi-particle cumulants in Pb+Pb collisions at $\sqrt{s_{\rm NN}} = 2.76$ TeV with the ATLAS detector. *Eur. Phys. J.*, C74(11):3157, 2014. (Cited on pages 121, 127, and 131.)

[240] Jaroslav Adam et al. Anisotropic flow of charged particles in Pb-Pb collisions at $\sqrt{s_{\rm NN}} = 5.02$ TeV. *Phys. Rev. Lett.*, 116(13):132302, 2016. (Cited on pages 125 and 132.)

[241] Betty Bezverkhny Abelev et al. Multiparticle azimuthal correlations in p -Pb and Pb-Pb collisions at the CERN Large Hadron Collider. *Phys. Rev.*, C90(5):054901, 2014. (Cited on pages 134 and 136.)

[242] Morad Aaboud et al. Measurement of multi-particle azimuthal correlations in pp, p+Pb and low-multiplicity Pb+Pb collisions with the ATLAS detector. *Eur. Phys. J.*, C77(6):428, 2017. (Cited on pages 135 and 136.)

[243] Jaroslav Adam et al. Correlated event-by-event fluctuations of flow harmonics in Pb-Pb collisions at $\sqrt{s_{\rm NN}} = 2.76$ TeV. *Phys. Rev. Lett.*, 117:182301, 2016. (Cited on page 138.)

[244] Albert M Sirunyan et al. Observation of Correlated Azimuthal Anisotropy Fourier Harmonics in pp and $p+Pb$ Collisions at the LHC. *Phys. Rev. Lett.*, 120(9):092301, 2018. (Cited on pages 139 and 140.)

[245] Stephen P. Horvat. Measurement of beam energy dependent nuclear modification factors at STAR. *J. Phys. Conf. Ser.*, 446:012017, 2013. (Cited on page 144.)

[246] L. Adamczyk et al. Bulk Properties of the Medium Produced in Relativistic Heavy-Ion Collisions from the Beam Energy Scan Program. *Phys. Rev.*, C96(4):044904, 2017. (Cited on page 145.)

[247] B. B. Back et al. Identified hadron transverse momentum spectra in Au+Au collisions at s(NN)**(1/2) = 62.4-GeV. *Phys. Rev.*, C75:024910, 2007. (Cited on page 146.)

[248] http://nica.jinr.ru/. (Cited on page 149.)

[249] https://fair-center.eu/index.php?id=1. (Cited on page 149.)

[250] L. Adamczyk et al. Inclusive charged hadron elliptic flow in Au + Au collisions at $\sqrt{s_{NN}}$ = 7.7 - 39 GeV. *Phys. Rev.*, C86:054908, 2012. (Cited on pages 154, 156, and 157.)

[251] Andreas Hoecker. Physics at the LHC Run-2 and Beyond. In *2016 European School of High-Energy Physics (ESHEP 2016) Skeikampen, Norway, June 15-28, 2016*, 2016. (Cited on page 165.)

[252] Compact linear collider. http://clic-study.web.cern.ch/. (Cited on page 165.)

[253] International linear collider. https://www.linearcollider.org/ILC. (Cited on page 166.)

[254] Linear collider collaboration. https://www.linearcollider.org/. (Cited on page 166.)

[255] Future circular collider study. https://fcc.web.cern.ch/Pages/default.aspx. (Cited on page 166.)

GLOSSARY

AA Collision between two nuclei. 18, 19, 28, 48, 53, 70–72, 74, 114, 115, 134, 135, 143, 158, 162

Ariadne A QCD parton shower mergin with DIPSY to provide result both at pp and AA collisions. Ariadne is the name of the daughter of Minos and Pasiphaë in the Greek Mythology. 52–54

Au-Au Collision between two gold nuclei. 3, 29, 115, 150–152, 159, 161

e^+e^- Collision between one electron and one positron. 52, 53

e^+p Collision between one electron and one proton. 52, 53, 58, 59

EPOS 2 The second version of EPOS, the event generator based on Parton Based Gribov Regge Theory with an event-by-event hydrodynamic implemented. 70, 71

EPOS 3 The third version of EPOS, the event generator based on Parton Based Gribov Regge Theory with a viscous hydrodynamic expansion and a parton saturation implemented. 70–72, 75

EPOS LHC This is a version of EPOS developped in same time that EPOS2 using tuned with LHC accelerator. 70, 71

HERA Particle Accelera at DESYin Hamburg aim to measure CP violation in the decays of heavy B-mesons. 52, 53

Herwig A general purpose event generator coupled with ThePEG to be a complete event generator.. 52, 53

hh Collision between two hadrons. 53, 56

NeXuS The event generator based on Parton Based Gribov Regge Theory precursor of EPOS. 57, 70, 75

p $\bar{p}$ Collision between one proton and one anti-proton. 52, 56

p-Pb Collision between one proton and one lead nucleus. 74, 114, 116, 117, 119, 134, 136, 137, 139–142, 161, 162

pA Collision between one proton and one nucleus. 71, 72, 115, 158

Pb-p Collision between one proton and one lead nucleus. 118, 120, 137, 161

Pb-Pb Collision between two lead nuclei. 71, 115–121, 125, 126, 132–142, 152, 161, 162

PHOBOS Phobos is a moon of Mars, which was the name of the original proposed detector. Studies heavy-ion collisions at Brookhaven. 43, 146

pp Collision between two protons. 19, 25, 28, 29, 48, 52, 53, 56, 58, 59, 70–72, 74, 114–117, 119, 120, 134, 135, 137, 139, 141, 142, 158, 161, 162, 188

Pythia A general purpose event generator and the Lund Monte Carlo generator based on the parton model. Pythia is the name of the high priestess of the Temple of Apollo at Delphi in the Greek Mythology. 52–54, 65

Regge Theory The theory created before the QCD theory using Reggeon to describe a fundamental interaction between hadrons.. 54, 55, 57

Tevatron Circular accelerator in the Fermilab, it holds the second highest energy particle collider in the world. 18, 52, 70

Venus The event generator based on Gribov Regge Theory precursor of NeXus itself precursor of EPOS. 57, 70, 75

ACRONYMS

AGS Alternating Gradient Synchrotron. 15, 41–43, 81

ALICE A Large Ion Collider Experiment. 20, 22, 27, 34–36, 41, 44, 110, 125, 133–138, 140, 161, 188

ATLAS A Toroidal LHC ApparatuS. 34–37, 125, 127, 131, 136, 137, 142, 162, 188

BBCs Beam-Beam Counters. 45

BES Beam Energy Scan. 3, 38–40, 42, 44, 46, 114, 142, 143, 145, 148, 149, 152, 159, 161–163, 188, 193

BNL Brookhaven National Lab. 14

BRAHMS Broad RAnge Hadron Magnetic Spectrometers. 43

BSM Beyond the Standard Model. 10, 36, 37, 53

CKM Cabibbo Kobayashi Maskawa. 7

CMS Compact Muon Solenoid. 25, 27, 34, 36, 37, 139, 140, 142, 162, 188

DGLAP Dokshitzer Gribov Lipatov Altarelli Parisi. 12, 13, 62, 72, 75

DIS Deep Inelastic Scattering. 58

EC Electromagnetic Calorimeter. 45

EoS Equation of State. 40, 71, 78

EP Event Plane. 4, 79, 81, 82, 84, 85, 87, 89, 90, 93, 111, 112, 121, 123, 124, 126, 127, 129, 131, 132, 149, 153, 154, 156, 162, 172, 176

EPOS Energy conserving multiple scattering Partons, parton ladders, and strings Off-shell remnants Saturation. 3, 4, 20, 42, 46, 48, 54, 57, 60, 63, 65, 66, 69–71, 73, 75, 76, 78–81, 87, 93, 94, 96, 98, 103, 106, 111, 112, 114–117, 119–123, 125–129, 131–137, 139–146, 148, 150, 152, 154–159, 161–163, 166, 168–170, 174–176, 178–180

FAIR Facility for Antiproton and Ion Research. 149

GFC Generating Function Cumulant. 96, 97, 101, 103, 104, 106, 107, 109, 112

GRT Gribov-Regge Theory. 48, 56–58, 61, 64, 70, 76

HERWIG Hadron Emission Reactions With Interfering Gluons. 53, 54

LEP Large Electron-Positron. 52, 53

LHC Large Hadron Collider. 3, 14–16, 18–20, 27, 29, 30, 33, 34, 36–38, 41, 42, 44–46, 52–54, 70, 71, 81, 114, 115, 120, 141, 156, 158, 159, 161–163, 165, 166

LHCb Large Hadron Collider beauty. 34

LYZ Lee-Yang Zeroes. 106–110, 112

NICA Nuclotron-based Ion Collider fAcility. 149, 163

PBGRT Parton-Based-Gribov-Regge Theory. 4, 48, 54, 56, 60–64, 70–73, 75, 76

PHENIX Pioneering High Energy Nuclear Interaction eXperiment. 18, 29, 41, 43, 44, 188

POI Particles of Interest. 89, 95, 101–103, 105, 108, 109, 179

pQCD perturbative Quantum ChromoDynamics. 13, 18, 31, 53, 55, 62, 71

PS Proton Synchrotron. 33, 34

QC Q-cumulants. 4, 97, 102–107, 109, 110, 112, 121–124, 126–129, 131–133, 153–156, 162, 172, 176

QCD Quantum ChromoDynamics. 3, 6–8, 12–14, 18, 38, 39, 43, 44, 46, 53, 55, 56, 143, 161, 187

QED Quantum ElectroDynamics. 8, 12

QFD Quantum FlavourDynamics. 8

QFT Quantum Field Theory. 6, 10, 12, 59–61

QGP Quark Gluon Plasma. 3, 6, 12–19, 22–26, 29, 30, 34–38, 40, 43–46, 61, 81, 111, 114, 118, 120, 137, 141–143, 158, 159, 161, 162, 187

RHIC Relativistic Heavy Ion Collider. 3, 14, 15, 19, 20, 22, 28–30, 38, 39, 41–44, 46, 70, 81, 106, 114, 115, 143, 161–163, 166, 188

RP Reference Particles. 89, 95, 97, 101–103, 105

SC Symmetric Cumulants. 4, 110–112, 162, 176

SLAC Stanford Linear Accelerator Center. 58

SM Standard Model. 6–12, 60, 187, 193

SP Scalar Product. 4, 87, 89, 90, 93, 111, 112, 120, 141, 142, 162, 176

SPS Super Proton Synchrotron. 14, 18, 28, 33, 34, 41, 42, 70, 81, 106

STAR Solenoidal Tracker At RHIC. 19, 40, 41, 43–45, 86, 152, 153, 157, 161, 188

SUSY Supersymmetry. 10–12

ThePEG Toolkit for High Energy Physics Event Generation. 52, 53

TOF Time Of Flight. 45

TPC Time Projection Chamber. 45

UrQMD Ultrarelativistic Quantum Molecular Dynamics. 24, 40, 71, 75, 187

UNIVERSITE BRETAGNE LOIRE / MATIERE MOLECULES ET MATERIAUX

UNIVERSITÉ DE NANTES

Titre : Formation du Plasma de Quarks et de Gluons : compréhension de la dépendance en taille de système et en énergie

Mots clés : Plasma de Quarks et de Gluons, Collisions d'ions lourds, EPOS-génerateur d'évenements, Corrélations angulaires, Ecoulement anisotropique, Simulations Monte Carlo

Résumé : La ChromoDynamique Quantique (CDQ) décrit les interactions entre les partons. Ces partons sont confinés dans les hadrons, cependant la CDQ prédit un nouvel état de la matière où les partons sont déconfinés des hadrons : Le Plasma de Quarks et de Gluons (PQG). L'étude du PQG est un axe de recherche challengeant puisque l'on observe expérimentalement les hadrons et non les partons. Dans cette thèse, j'étudie les anisotropies des angles azimutaux de la production de particule qui est directement liée à l'anisotropie du fluide. Cette anisotropie, due à une anisotropie spatiale initiale, donne des informations sur les propriétés du PQG et son expansion. qui est directement liée à l'anisotropie du fluide. On observe des effets « d'écoulement » lors des collisions d'ions lourds (AA) aux hautes énergies du RHIC et du LHC mais également aux basses énergies du Beam Energy Scan (BES).

Récemment, des effets d'écoulement ont été également observés lors des collisions de petits systèmes (pp). La problématique de cette thèse est : Est-ce qu'un « plasma en expansion collectif » est créé dans tous les systèmes : grand (AA) ou petit (pp) des basses énergies du BES aux hautes énergies du LHC ? EPOS est un générateur d'évènements dédie à l'étude des collisions d'ions lourds et proton-proton. J'analyse l'écoulement anisotropique avec EPOS pour tous types de systèmes (pp, AA), énergies (LHC, RHIS, BES), pour tous types de « sondes » d'écoulement. Pour effectuer mon analyse, j'ai développé un framework facilement utilisable indépendamment des futurs développements d'EPOS. C'est très important car les résultats de mon analyse vont impacter sur les prochaines mises à jour du modèle à petite taille de système et à basse énergie.

Title : Formation of Quark-Gluon-Plasma: Understanding the energy and system size dependence

Keywords : Quark-Gluon Plasma, Heavy Ion Collisions, EPOS-event generator, Azimuthal Correlations, Anisotropic Flow, Monte Carlo Simulations

Abstract : Quantum ChromoDynamics (QCD) describes the interaction between partons (nuclear matter's degrees of freedom). These partons are usually confined into hadrons, however QCD predicts that a new state of matter exists where partons are deconfined from hadrons: the Quark Gluon Plasma (QGP). The QGP is formed in high energy heavy ion collisions. QGP study is exiting and theoretically challenging research field mainly because instead of partons, hadrons are observed. In this thesis, I study anisotropies in the azimuthal angle of particle production, which is directly related to the fluid's anisotropy. The fluid anisotropy is the response of the system to some initial space anisotropy and provides information on the properties of the QGP and its expansion. As in heavy ion (AA) collisions at high energies of RHIC and LHC, "flow-like" effects are hinted at Beam Energy Scan (BES) low energies.

Very recently, unexpected "flow-like features" have also been observed in small systems like proton-proton (pp). In this thesis, I try to answer the following question: Is there a "collectively expanding plasma" in all systems : big (PbPb) or small (pp), from BES low energies to LHC higher energies? EPOS is an event generator dedicated to the study of proton-proton and heavy ion collisions. I analyze anisotropic flow with EPOS for all kind of systems (pp, AA), energies (LHC, RHIC, BES), and all kinds of flow "probes". To perform my analysis, I developped a framework that can already be easily used, independently of further EPOS's developments. This fact is very important, because results of this analysis will impact incoming updates of the model at little system sizes and low energies.